STABLE ISOTOPE STRATIGRAPHY OF DEEP-SEA CORES FROM THE SOUTHWEST PACIFIC REGION: ASPECTS OF LATE QUATERNARY PALAEOCEANOGRAPHY

A thesis submitted for

the degree of

Doctor of Philosophy

by

Alison Macauley Cuthbertson M.Sc.(First Class Hons.)

School of Science

University of Waikato

1988

This thesis is dedicated to my mother, Daphne Cuthbertson, and to my fiancé Alan Whitton, who have provided every support and encouragement.

ABSTRACT

$^{18}O/^{16}O$ and $^{13}C/^{12}C$ ratios of calcareous planktonic and benthic foraminifera from the Late Quaternary section of deep-sea sediment cores from the Tasman Sea and Southwest Pacific Ocean have been determined in this study. The core sites cover a latitudinal range from the equator to 49°S, and samples were provided by the Ocean Drilling Program and the New Zealand Oceanographic Institute. In most cases the cores were sampled at 10cm intervals. Generally, attention has been focused on the latest Quaternary (stages 1 to 5) glacial-interglacial oscillations of the $\delta^{18}O$ and $\delta^{13}C$ record, and aspects of their palaeoceanographic significance. Some longer sequences of core were also studied.

Of the Southwest Pacific Ocean cores, 594 yielded the most detailed record for the past 130ky. Located just south of the Subtropical Convergence it has proved particularly sensitive to substage climatic fluctuations. In addition the high sedimentation rate (averaging ~13cm/ky) has reduced smoothing by bioturbation. Core 594 has yielded one of the most detailed isotopic records available world-wide for stages 1 to 6. Concurrent carbonate analysis by Cooke (1988) has revealed a similarly detailed carbonate record whose rises and falls are more or less synchronous with the isotopic record.

To the west of New Zealand Core 593 was analysed to 44m sub-bottom depth and a clear record of isotopic fluctuations back to the 55/56 stage boundary was obtained.

Sites 593 and 594 have thus provided useful isotopic reference curves for the Southwest Pacific region.

Consistent changes in the planktonic $\delta^{13}C$ record of some of the cores may reflect variations in $CaCO_3$ productivity linked to cyclical glacial-interglacial fluctuations.

Glacial benthic $\delta^{13}C$ results support a decreased volume of NADW production. Resumption of NADW flow is marked in many cases by a transient drop in $\delta^{13}C$ values before rising to interglacial values as the relatively stagnant, isotopically lighter water is "flushed" from Deep Water flow paths. AABW appears to dominate during glacial periods. A northern shift of the Subtropical Convergence east of New Zealand is suggested (and supported by micropalaeontological data; Cooke, 1988), with a more restricted shift in the Tasman Sea.

Interglacial Deep Waters appear to be dominated during interglacial times by AABW, whilst NADW is dominant in the Tasman Sea. Planktonic $\delta^{13}C$ results suggest a more southerly position of the Subtropical Divergence in the Tasman Sea during interglacial periods.

Lead-lag relationships in the $\delta^{18}O$ signal between surface and bottom-dwelling foraminifera over Termination I_A reveal a pattern of meltwater circulating first to the surface waters at higher latitudes, and to bottom waters at lower latitude sites. A modification of the meltwater "lid" is proposed, with the lid extending only partially across the ocean surface, and not into equatorial regions.

ACKNOWLEDGEMENTS

I wish to gratefully acknowledge the assistance of my principal supervisors Dr Chris Hendy and Assoc. Prof. Cam Nelson, who have provided guidance and encouragement.

I would like to thank Penny Cooke for her carbonate data, SEM photographs, micropalaeontological help, and most especially for the mud washing.

Thanks are also extended to the Deep Sea Drilling Project, the New Zealand Oceanographic Institute, and in particular to Dr Lionel Carter, whose assistance was invaluable.

Thankyou to Skelte Anema for helping me come to grips with word processing, and to the electronics technicians for keeping the mass spectrometer on its feet.

Dr Ray Littler provided advice on statistical matters, which was much appreciated, Helen Pridmore has helped with administrative details, and Dr Alan Hogg provided a job when it was needed most.

Finally, I would like to thank the University Grants Committee for funding this project.

CONTENTS

	Title page.	i
	Dedication.	ii
	Abstract.	iii
	Acknowledgements.	v
	Contents.	vi
	List of figures.	ix
	List of tables.	xiv
Section no.	Section title.	Page no.
CHAPTER ONE	An Introductory Review	1
1.1	The importance of palaeoclimatic studies.	1
1.2	The oceanic record.	2
1.3	Stable isotope ratios from calcite.	7
1.4	Instrumentation.	10
1.5	The oxygen signal in the ocean.	12
1.6	Orbital fluctuations and climatic changes.	20
1.7	The carbon isotopic signal.	24
1.8	Preservation of $CaCO_3$ in deep-sea sediments.	29
1.9	Species selection and equilibrium assumptions.	31
1.10	Salinity.	33
1.11	Climatic modelling.	35
1.12	The last deglaciation.	38
CHAPTER TWO	Oceanographic and Climatic Background to the Region of Study.	47
2.1	Oceanographic setting.	47
2.1.1	Water masses around New Zealand.	47
2.1.2	Oceanic fronts in the New Zealand region.	53
2.1.3	Circulation of currents around the New Zealand landmass.	59
2.2	Climatic Setting.	61
2.2.1	The present-day climate of New Zealand.	61
2.2.2	Climatic record of New Zealand for the Late Quaternary.	65

2.2.3 Correlation of on-land records to deep-sea records. 69
2.3 Oceanic sediment investigations in the southwest Pacific. 72

CHAPTER THREE Sampling and Experimental Techniques. 78
3.1 Drill site locations. 78
3.2 Samples. 81
3.2.1 Sample Collection. 81
3.2.2 Sample preparation (initial treatment). 82
3.3 Vacuum roasting. 88
3.4 Preparation of CO_2 sample. 90
3.5 Orthophosphoric acid. 92
3.6 The mass spectrometer. 92
3.7 Per mille deviations. 94
3.8 Standards. 97
3.9 Experimental problems. 99
3.9.1 Acid deterioration. 99
3.9.2 Instrumental difficulties. 100
3.9.3 Calculation problems. 103

CHAPTER FOUR Presentation of Data. 105
4.1 DSDP cores. 105
4.2 NZOI cores. 127

CHAPTER FIVE Discussion of Results. 134
5.1 Discussion of $\delta^{18}O$ results. 134
5.1.1 Assignment of stage boundaries. 134
5.1.2 Stratigraphic comparisons. 168
5.1.3 The Holocene. 189
5.1.4 Comparison between last glacial $\delta^{18}O$ with Holocene $\delta^{18}O$ values. 194
5.1.5 Glacial to interglacial extremes. 198
5.1.6 The last interglacial (stage 5e). 200
5.1.7 Synchroneity of the benthic and planktonic $\delta^{18}O$ records of 594. 202

5.2 A discussion of aspects of the $\delta^{13}C$ results. 210
5.2.1 Changes from the last glacial to present day. 210
5.2.2 The last interglacial. 217
5.2.3 $\delta^{13}C$ differences between sites to the west and east of New Zealand. 219
5.3 Carbonate results. 220

CONCLUSIONS 224
Summary and Synthesis. 224

APPENDIX ONE
Stratigraphic logs (where available) for the DSDP and NZOI cores analysed in this study. 230

APPENDIX TWO
Graphs of the $\delta^{18}O$ record of Termination I_A. 258

REFERENCES 264

LIST OF FIGURES

Figure no. Description. Page no.

CHAPTER ONE

1.1. A generalised palaeotemperature curve showing the system of numbering glacial and interglacial stages. 14

1.2a. A reference curve for the changing $\delta^{18}O$ of sea water over the last 130ky. 19

b. Estimated changes in deep-water temperature over the last climatic cycle. 19

1.3. Sea level estimates, with the sea level record of New Guinea terraces. 21

1.4. Numbering of glacial and interglacial stages in a composite $\delta^{18}O$ record back to stage 63. 21

1.5. An "ideal" isotopic record derived from variations in the eccentricity, obliquity and precession of the Earth's orbit. 23

1.6. Inorganic reactions of CO_2 between the atmosphere, the ocean, and the sediment. 24

1.7. A reconstruction of the differences between modern sea-surface temperatures, and estimated sea-surface temperatures of the last glacial maximum. 34

1.8. $\delta^{18}O$ records of the stage 2 to 1 transition, showing two distinct terminations. 40

1.9. Four different views of the timing of the last deglaciation. 40

1.10. Stacked benthic and planktonic $\delta^{18}O$ plots, showing the shape of the record of the last deglaciation, with three proposed terminations. 42

1.11. A summary regional sea level curve for eastern Australia and New Zealand, based on an episodic transgression model. 42

CHAPTER TWO

2.1. Temperature and salinity relationships around the New Zealand landmass. 46

2.2. Zonal and meridional flow of the water masses of the Southern Ocean. 46

2.3. The northward spread of Antarctic Bottom Water. 48

2.4. Bottom Water temperatures at the ocean floor in the New Zealand region. 50

2.5. The circulation of North Atlantic Deep Water. 51
2.6. Depth of the core of Antarctic Intermediate Water in the New Zealand region. 52
2.7. Salinity of the core of Antarctic Intermediate Water in the New Zealand region. 54
2.8. Salinity of the waters at 200m depth in the New Zealand region. 55
2.9. Temperature of the waters at 200m depth in the New Zealand region. 56
2.10. North-south section from temperature and salinity data across the Subtropical Convergence at 177°S. 58
2.11. General circulation of the waters, and positions of the major fronts in the Southwest Pacific Ocean and Tasman Sea. 60
2.12. Major topographical features affecting the circulation of waters around New Zealand. 62
2.13. A map of New Zealand showing the locations of place names mentioned in the text. 64
2.14. Late Neogene stage classifications in New Zealand. 66
2.15. Stratigraphic nomenclature for the North Island, correlated with the deep-sea $\delta^{18}O$ record. 70
2.16. The location of Deep Sea Drilling Project sites in the Tasman and Southwest Pacific region. 73
2.17. The locations of cores Z2101 to Z2112. 75

CHAPTER THREE

3.1. Physiographic diagram of core sites sampled in this thesis. 80
3.2. Picking tray used in the selection of foraminiferal samples by microscope. 83
3.3. SEM photograph of *Uvigerina* spp. 85
3.4. SEM photograph of *Globigerina bulloides* d'Orbigny. 85
3.5. SEM photograph of *Globigerina sacculifera*. 86
3.6. SEM photograph of *Globigerina ruber*. 86
3.7. Vacuum furnace tube for the roasting of foraminiferal samples. 87
3.8. Piccolo tube for holding sample vials upright in the furnace. 87
3.9. $CO_{2(g)}$ generation line, contained within an oven at 50°C. 89
3.10. Gas sample collection line, with cold traps for the removal of water. 91

3.11. Printout from the HX-20 control unit of the mass spectrometer. 93

3.12. Plot of the δ45 and δ46 mass ratios of CO_2 generated from NBS-19. 102

CHAPTER FIVE

5.1a. SPECMAP $\delta^{18}O$ stack.
b. 594 benthic $\delta^{18}O$ record.
c. 594 planktonic $\delta^{18}O$ record. 135

5.2a. M12 392 benthic $\delta^{18}O$ record.
b. 594 benthic $\delta^{18}O$ record.
c. V19-30 benthic $\delta^{18}O$ record. 137

5.3a-e. Stable isotope record of 594, with $\%CaCO_3$. 139

5.4a-e. Stable isotope record of Q200, with $\%CaCO_3$. 141

5.5a-e. Stable isotope record of Q217, with $\%CaCO_3$. 141

5.6a-e. Stable isotope record of Q219, with $\%CaCO_3$. 143

5.7a-e. Stable isotope record of Q580, with $\%CaCO_3$. 143

5.8a-e. Stable isotope record of Q585, with $\%CaCO_3$. 145

5.9a-e. Stable isotope record of Q858, with $\%CaCO_3$. 145

5.10a. SPECMAP $\delta^{18}O$ stack.
b. 593 planktonic $\delta^{18}O$ record.
c. 593 benthic $\delta^{18}O$ record. 147

5.11a. V28-239 planktonic $\delta^{18}O$ record.
b. DSDP 502 planktonic $\delta^{18}O$ record.
c. DSDP 593 planktonic $\delta^{18}O$ record.
d. DSDP 593 benthic $\delta^{18}O$ record. 149

5.12. 593 planktonic (a) and benthic (b) $\delta^{18}O$ records back to 22m. 150

5.13. 593 planktonic (a) and benthic (b) $\delta^{18}O$ records back to 43m. 151

5.14. 593 planktonic (a) and benthic (b) $\delta^{13}C$ records back to 43m. 152

5.15a-d. Stable isotope record of 586. 153

5.16a-d. Stable isotope record of 588. 153

5.17a-e. Stable isotope record of 589, with $\%CaCO_3$. 155

5.18a-d. Stable isotope record of 590. 157

5.19a-d. Stable isotope record of 591A. 157

5.20a-e. Stable isotope record of Z2108, with $\%CaCO_3$. 159

5.21a-d. Stable isotope record of 592 (low resolution). 161

5.22a-d. Stable isotope record of 592 (high resolution). 162

5.23. Summary of the sub-bottom depths to stage boundaries in each of the cores. 166

5.24. Mean glacial and interglacial sedimentation rates at each of the sites studied. 167

5.25. Isotopic palaeoevents identified in the V19-29 benthic $\delta^{18}O$ record. 170

5.26. A proposed isotopic taxonomy for the 594 benthic $\delta^{18}O$ record (version #1). 172

5.27. Orbitally based chronostratigraphy of a stacked $\delta^{18}O$ record. 177

5.28. 594 benthic δ^{18} data plotted on a timescale derived from Martinson et al. (1984). (Based on isotopic taxonomy version #1). 179

5.29. A second proposed isotopic taxonomy for the 594 benthic $\delta^{18}O$ record. 181

5.30. 594 benthic $\delta^{18}O$ data plotted on a timescale derived from Martinson et al. (1984). (Based on isotopic taxonomy version #2). 183

5.31. Numbering of 593 planktonic $\delta^{18}O$ isotope stages back to the 55/56 stage boundary. 187

5.32. Map showing isotopically derived Holocene surface water temperatures, with modern measured temperatures. 192

5.33. Map showing isotopically derived Holocene bottom water temperature, with modern measured temperatures. 193

5.34. Stage 5 and stage 1 bottom water temperatures derived from the benthic $\delta^{18}O$ record. 201

5.35. Stage 5 and stage 1 surface water temperatures dericved from the planktonic $\delta^{18}O$ record. 203

5.36. Locations of the cores for which lead-lag relationships have been determined. 206

5.37. The leading $\delta^{18}O$ signal over Termination I_A at various locations world-wide. 206

5.38a. Mean $\delta^{13}C$ values for the last interglacial.

b. Mean Holocene $\delta^{13}C$ values.

c. Last interglacial $\delta^{13}C$ anomaly. 216

CONCLUSIONS

6.1 A diagrammatic summary of aspects of the palaeoceanography of the Late Quaternary in the New Zealand region, comparitive to present day conditions. 229

APPENDIX ONE

I.1 Photographs of core 594. 248

I.2 Photographs of core 594B. 250

LIST OF TABLES

CHAPTER ONE

1.1. Sedimentary variables and their environmental significance. 4

1.2. Residence time of water in natural reservoirs. 12

CHAPTER TWO

2.1. Subdivisions of the Haweran Stage (N.Z. Late Quaternary). 67

CHAPTER THREE

3.1. Locations of DSDP Sites 586-594. 79

3.2. Site locations of NZOI cores. 81

3.3. The mass distribution of carbon and oxygen isotopes in natural CO_2. 96

3.4. Calibration of NBS-19. 98

3.5. NBS-19 cf. WLS. 98

3.6. Variation of NBS-19 δ46 values with increasing age of H_3PO_4. 100

CHAPTER FOUR

4.1. DSDP Core 586 $\delta^{18}O$ and $\delta^{13}C$ results. 106

4.2. DSDP Core 588 $\delta^{18}O$ and $\delta^{13}C$ results. 107

4.3. DSDP Core 589 $\delta^{18}O$ and $\delta^{13}C$ results, with $\%CaCO_3$. 108

4.4. DSDP Core 590 $\delta^{18}O$ and $\delta^{13}C$ results. 111

4.5. DSDP Core 591A $\delta^{18}O$ and $\delta^{13}C$ results. 112

4.6a. DSDP Core 592 $\delta^{18}O$ and $\delta^{13}C$ results (high resolution). 113

b. DSDP Core 592 $\delta^{18}O$ and $\delta^{13}C$ results (low resolution). 114

4.7. DSDP Core 593 $\delta^{18}O$ and $\delta^{13}C$ results. 115

4.8. DSDP Core 594 $\delta^{18}O$ and $\delta^{13}C$ results, with $\%CaCO_3$. 123

4.9. NZOI Core Q200 $\delta^{18}O$ and $\delta^{13}C$ results, with $\%CaCO_3$. 127

4.10. NZOI Core Q217 $\delta^{18}O$ and $\delta^{13}C$ results, with $\%CaCO_3$. 128

4.11. NZOI Core Q219 $\delta^{18}O$ and $\delta^{13}C$ results, with $\%CaCO_3$. 129

4.12. NZOI Core Q580 $\delta^{18}O$ and $\delta^{13}C$ results, with $\%CaCO_3$. 130

4.13. NZOI Core Q585 $\delta^{18}O$ and $\delta^{13}C$ results, with $\%CaCO_3$. 131

4.14. NZOI Core Q858 $\delta^{18}O$ and $\delta^{13}C$ results, with $\%CaCO_3$. 131

4.15. Core Z2108 $\delta^{18}O$ and $\delta^{13}C$ results, with $\%CaCO_3$. 132

CHAPTER FIVE

5.1. Depths and ages of stage boundaries in Core 594, with sedimentation rates for each stage. 140

5.2. Proposed stage boundaries, depths and sedimentation rates for Q200. 142

5.3. Proposed stage boundaries and sedimentation rates for Q217. 144

5.4. Proposed stage boundaries for 593, with sedimentation rates. 148

5.5. Proposed stage boundaries for 586, with sedimentation rates. 154

5.6. Proposed stage boundaries for 588, with sedimentation rates. 156

5.7. Proposed stage boundaries for 590, with sedimentation rates. 158

5.8. Proposed stage boundaries for 591A, with sedimentation rates.160

5.9. Proposed stage boundaries for Z2108, with sedimentation rates. 160

5.10. Positions of the stage boundaries in 592, with sedimentation rates. 163

5.11. Summary of the sub-bottom depths of the stage boundaries in each core, and the derived sedimentation rates for each stage. 164

5.12. Dates and depths of events numbered in Figure 5.26. 180

5.13. Dates and depths of events numbered in Figure 5.29. 186

5.14. A comparison of modern measured temperatures with isotopically derived Holocene temperatures, taking into account differences in salinity between the sites. 190

5.15. A comparison of Holocene $\delta^{18}O$ values, with glacial $\delta^{18}O$ values for each of the sotes studied. 195

5.16. A comparison of glacial to interglacial extremes recorded at each of the sites. 197

5.17. Benthic $\delta^{18}O$ values for stages 1 to 6 at each of the sites studied, with isotopically derived water temperatures for stage 1 and 5. 199

5.18. Planktonic $\delta^{18}O$ values for stages 1 to 6 at each of the sites studied, with isotopically derived water temperatures for stage 1 and 5. 199

5.19. Lead-lag relationships in $\delta^{18}O$ records of Termination I_A, from a variety of deep-sea cores. 206

5.20. Lead-lag relationships in the $\delta^{18}O$ record of 594. 209

5.21. A summary of mean glacial and interglacial $\delta^{13}C$ values for benthic and planktonic foraminifera over the available record. 212

5.22. A summary of the glacial/interglacial $\delta^{13}C$ differences for planktonic and benthic foraminifera. 213
5.23. Holocene planktonic $\delta^{13}C$ values, modern reactive phosphorus levels and primary productivity. 215
5.24. A comparison of Holocene and 5e benthic $\delta^{13}C$ values. 217
5.25. Summary of mean $\delta^{18}O$ and $\delta^{13}C$ values for benthic and planktonic foraminifera at Site 594 over stage 5. 218
5.26. Total sedimentation rate, $CaCO_3$ content and carbonate sedimentation rate at Site 594, for stages 1 to 6. 221

Chapter One

AN INTRODUCTORY REVIEW

1.1 The Importance of Palaeoclimatic Studies

Every year climate-related disasters forcefully remind us that human society is extremely vulnerable to climatic change. Any long-term alteration of current climatic trends would seriously affect the present balance of population and food production. Iceland provides a clear example of the vulnerability of some regions of the earth to even relatively minor climatic alterations (Bryson, 1974). He notes that in the late 1950s the mean warm-half-year temperature in Iceland was 7.65°C, and the Icelandic farmers were able to grow 4.33 metric tonnes of hay per hectare, with the application of 2.83kg of nitrogen fertilizer per hectare. In 1966 and 1967 fertilizer application had risen to 4.83kg per hectare, yet hay yield had dropped to only 3.22 tonnes; this was attributed to a drop in the mean temperature to 6.83°C. In other words, a drop in mean temperature of only 0.82°C markedly overshadowed any increase in crop yield that might otherwise have been expected from the extra fertilizer.

There is ample evidence to show that past climates were vastly different to those of today (Frakes, 1979). Morphological features of the European Alps (Goldthwaite, 1975) give clear evidence of past glaciation in regions no longer glaciated. Pollen and fossil evidence (e.g., Frenzel, 1968; Kershaw, 1973) likewise indicate dramatic vegetational change in response to changing temperatures. Hence there can be no reason to suppose that our modern climate is in any way the norm, and every reason to expect that it will one day be vastly different, and will continue to change as it has in the past.

Simplistic extrapolations of short-term temperature trends without any considerations of mechanisms or global processes were found to be inappropriate earlier this century when the warming trend of the 1890s to 1940s was reversed (Gribben, 1978). Speculation on an ice-free Arctic by the end of the century was seen to be a naive response to immediate physical evidence with no consideration of whether it indicated a short-term or long-term trend (Hecht, 1985).

In order to more effectively predict future changes, any records of past temperatures would be of great value. However, because human records only go back for a comparatively short length of time (e.g., Manley, 1975), it is necessary to seek physical evidence of fluctuating temperatures in an attempt to determine both the extent and the time-scale of change. An understanding of the relationship between ocean surface temperatures, circulation, incoming solar radiation, insolation and air temperatures is essential for sensible climatic prediction. In addition, the increased impact of humans on their environment since the industrial revolution must be considered. The fate of fossil fuel CO_2 in the atmosphere has become of particular concern in recent years (e.g., Pastor and Post, 1988), as has the destruction of the ozone layer (e.g., Crutzen and Arnold, 1986). Any realistic proposal for the mechanisms which drive our changing climate would have to involve the interactions of all these factors.

1.2 The Oceanic Record

It has long been recognised that the world's oceanic sediments contain a record from which previous climatic conditions might be interpreted. Deep sea sediments collected during the first sampling operations in 1872 (voyage of H.M.S. *Challenger*) up until World War II

produced a sufficient quantity of material for scientists to recognise the difference in nature of surface sediments (from present-day interglacial conditions) compared to subsurface sediments (attributed to previous glacial conditions). Thus the importance of obtaining large numbers of cores over a wide geographical area, to give a global view of climatic change, was quickly realised. United States government funding in the 1950s led to a vast expansion in the amount of core material available, but technological limitations of coring methods meant that these were mostly short (a few metres long) piston cores. In 1966 the Deep Sea Drilling Project (DSDP) vessel *Glomar Challenger* employed the then newly developed rotary drill technique to obtain much longer cores, but this process still badly disturbed the unconsolidated late Quaternary sediments. Development of the hydraulic piston corer in the late 1970s finally enabled relatively undisturbed, long cores to be recovered (Warme et al., 1981). The DSDP was specifically designed to provide an extensive scientific data base from large numbers of long cores from the world's oceans, and much of this thesis is based on core materials supplied by them from the Southwest Pacific region. In addition to the long cores, a very much larger number of short piston cores have been collected by oceanographic institutes around the world, some of which have also been sampled in this study.

There are several types of climatic indicators that can be measured in deep sea sediments. Stein and Sarnthein (1984) summarised the sedimentary variables and their environmental significance, and their table is reproduced here as Table 1.1.

Table 1.1. Sedimentary variables and their environmental significance (from Stein and Sarnthein, 1984, table 1).

Environmental interpretation: / Signals: Sedimentary variables	Polar ice sheets and global sea level	Sea surface temperature	Water masses	Upwelling (coastal and equatorial)	Local paleo-productivity	Deep water (temperatures advection and circulation	$CaCO_3$ dissolution	Aridity, offland winds	At least ephemeral fluvial runoff (semiarid to humid conditions)	Meridional trade winds (dust provenance: Atlas and Angola)	Zonal winds (SAL) (dust provenance: Sahel and South-Sahara)	Paleo-wind strength	ITCZ-position	Land vegetation
$\delta^{18}O$ (benthos)	Q					S								
$\delta^{18}O$ (plankton)	S	N												
$\Delta\delta^{18}O$ (benthos vs plankton)		S		S										
$\delta^{13}C$ (benthos)				S	S	S								
$\delta^{13}C$ (plankton)							N							
Foram. fragmentation							S							
Foram. assemblages		S	S	N										
% $CaCO_3$, flux rates					(N)	N	S							
Hiatus						N								
% opal				(N)	N				(N)					
Aeolian sand turbidites								Q						
Plant fibres									S					N
Excess of clay fract.									Q					
Terr. flux rates									N			N		N
Kaolinite											S		N	
Chlorite, illite										S				
Stained quartz										–	S			
Pollen assemblages										Q			S	Q
Terr. grain size												Q	S	

Q = quantitative, S = semi-quantitative, N = non-quantitative proxy data, – = absent, (N) special caution needed with interpretation.

Some of the major climatic indicators are briefly discussed here.

1. Micropalaeontological record

(a) Faunal assemblages of foraminifera: It has long been recognised that a close relationship exists between faunal assemblages and environmental conditions (Murray, 1897). From this it was inferred (Phillippi, 1910) that the fossilised remains of planktonic foraminifera in deep sea cores would give information on past climates. Work by Schott (1935) on the influence of temperature on species distributions of material from the *Meteor* expedition

(1925-1927) was of great importance. He attributed the existence of *Globorotalia menardii* in sediments above deposits where *G. menardii* was not present to a post-glacial change in climatic conditions. This early work has been corroborated by subsequent research and the link between palaeoclimatology and planktonic foraminiferal variations is accepted. Such studies assume no change in the environmental tolerances of species through time (and hence evolutionary stability within their environs), enabling analogies to be drawn between the climatic preferences of modern species and their fossilised counterparts. Some first and last appearance levels of species can result from changes in climate, with a species no longer found in one region surviving in more favoured environments elsewhere. The application of regression equations relating modern planktonic census data to oceanic properties (transfer functions) has been comprehensively described by Imbrie and Kipp (1971).

Ericson and Wollin (1954) noted that the coiling of foraminifera to the left or the right in modern species is dependent on geographic location, and that the boundary lines between sinistral and dextral coiling provinces shift with changing climate.

(b) Radiolaria: These are an important planktonic species in palaeoceanographic studies. They are widely distributed in the world's oceans and are able to be recovered from regions of the Pacific where planktonic foraminifera have not been preserved (Moore, 1978). However, three main problems with radiolaria do exist. (i) The abundance of *Cyclodophora davisiana* (Morley and Hays, 1979) in glacial conditions with no analogous existence in modern times. (ii) The large numbers of rare radiolaria. (iii) Their depth habitat is such that they respond to subsurface conditions.

(c) Diatoms: These tend to be not generally found (Heath, 1974) except in highly fertile regions of the Pacific, and to date have been of limited use for palaeoclimatic studies.

(d) Coccoliths: These have been used mostly for biostratigraphic zoning since, as a micropalaeontological tool, they present several problems: Evolutionary changes within species have resulted in there being no precise modern analogue for Late Quaternary species existing as recently as 10ky B.P. (Hecht, 1985). In addition they are environmentally insensitivity (Okada and M^{c}Intyre, 1977). However, recent work has shown that it is possible to produce a sensible stable isotope stratigraphy (Anderson and Steinmetz, 1983; Nelson et al.,1986) using polyspecific samples from nannofossil oozes.

2. Pollens

Since early this century it has been known that modern climatic conditions are reflected in vegetational distribution (e.g., Köppen, 1900). Pollen preserved within sediments may thus be used to map former vegetational patterns with associated implications of climatic change. Pollen records are particularly useful as they fill the data gap between the long-term marine record and short-term terrestrial tree-ring data; pollen records may be resolved to 300-500 years (Webb, 1982). Modern data that reflect the present climatic gradient may be used to calibrate pollen data from cores.

3. Sedimentary record

Areas which receive extensive input of terrestrial sediment are of great interest, as they can provide a record of successive on-land glaciations that may be directly correlated to the glacial periods determined through oxygen isotope analyses. (The significance of oxygen isotope ratios is discussed in Section 3.1).

The preservation and dissolution of $CaCO_3$ within the sediments may also give important information and is well reviewed in Volat et al. (1980). Variations in $CaCO_3$ content may be successfully correlated to climatic fluctuations induced by changes in the Northern Hemisphere ice sheets (e.g., Nelson et al., 1986). In addition $CaCO_3$ content may also reflect productivity fluctuations in calcitic organisms, although conflicting conclusions of high or low productivity during interglacial periods can make interpretation difficult (see Section 5.3).

4. Stable isotopes

This thesis concentrates largely on the stable isotope signal derived from foraminifera, whose significance is discussed in the next section.

1.3 Stable Isotope Ratios from Calcite

Neutral oxygen contains three stable isotopes with the following abundances (Garlick, 1969):

^{16}O	99.763%
^{17}O	0.0375%
^{18}O	0.1995%

Since ^{18}O has a higher abundance and a greater mass difference when compared with ^{16}O, than has ^{17}O compared with ^{16}O, and since all of the factors that contribute to separation are common to the three isotopes, it is usual to determine $^{18}O/^{16}O$ as the oxygen stable isotope ratio. No additional information would be obtained from the technically more difficult measurement of either $^{18}O/^{17}O$ or $^{17}O/^{16}O$ ratios.

The analytical technique employed also produces the $^{13}C/^{12}C$ ratios, and these have been included for completeness, although their significance for palaeoclimatic studies is still not as clearly understood as the $^{18}O/^{16}O$ information. Advances in our understanding of $^{13}C/^{12}C$ ratios are discussed in Section 1.7.

Urey (1947) undertook theoretical studies on the thermodynamic properties of oxygen isotopes in the CO_2-H_2O-$CaCO_3$ system and suggested that carbonates precipitated from the same aqueous solution, but at different temperatures, should have a different ^{18}O content. Urey recognised the significance of this theory for practical marine palaeoclimatology.

Subsequent experimental work was conducted by M^{c}Crea (1950) who succeeded in inorganically precipitating $CaCO_3$ from solution. This inorganic $CaCO_3$ had the same isotopic composition as shells that had grown in that solution. Consequently he was able to "grow" $CaCO_3$ at various temperatures and thus investigate the effect of temperature on isotopic composition. An equation relating the temperature of formation to the isotopic composition of $CaCO_3$ and the water was thus produced. M^{c}Crea further proposed that, within certain restrictions, palaeotemperatures could be determined for calcite samples of biological origin (discussed in Section 1.5).

M^{c}Crea's (1950) investigation of the methods of acid decomposition of $CaCO_{3(s)}$ to $CO_{2(g)}$ for analysis by mass spectrometer is also of great significance. Several factors must be considered in choosing an appropriate acid for $CaCO_3$ decomposition.

1) The following reaction scheme

$$3CaCO_3 + 2H_3PO_4 = 3CO_2 + 3H_2O + Ca_3(PO_4)_2$$

shows that only $\frac{2}{3}$ of the oxygen originally present in the carbonate is liberated to CO_2. This "splitting" must occur reproducibly.

2) The gas produced must be isotopically representative of the $CaCO_3$ from which it was formed.

3) Insoluble precipitates produced by some acids on reaction with $CaCO_3$ can slow or stop the reaction by forming a protective coating. Acids which form such by-products are unsuitable.

4) By-product gases (e.g., $NO_{2(g)}$ from reaction of HNO_3) that have the same m/e (ratio of mass to energy) as CO_2 wil effectively block the detection of CO_2.

5) There can be no exchange of oxygen between the reacting acid and CO_2 (as occurs in the case of H_2SO_4).

As a result of M^{c}Crea's work H_3PO_4 was found to be a suitable acid for CO_2 generation, best meeting the criteria required. M^{c}Crea's technique involved degassing both the sample and the 100% H_3PO_4 for 24h and then reacting them under agitation at 25°C. He allowed the reaction to continue for 4h before condensing the CO_2 formed. However, this method left the CO_2 and H_2O in contact with each other for a considerable length of time and allowed exchange of oxygen between the two. Moreover, Emiliani (1966) noted that variations in sample grain size will lead to variations in isotopic composition, the more finely ground samples being enriched in ^{16}O by $0.2^{o}/_{oo}$. These differences have been attributed to a differing speed of reaction (Fritz and Fontes, 1966; Walters et al.,1972). Later work has usually been based on higher reaction temperatures of 50°C (after Shackleton and Opdyke, 1973) which allows a very fast reaction between the calcite and the H_3PO_4. Since the reaction of very small samples is quickly completed at 50°C no grain size effect is noticed. The immediate condensation and separation of the CO_2 and H_2O is also carried out to minimise exchange (Shackleton and Opdyke, 1973; Mathews et al., 1980). "On-line" systems, where the CO_2 production line is attached to the

mass spectrometer, allow immediate analysis of product gases and minimise fractionation due to gas manipulation.

Coplen et al. (1983) specify a density range of 1.90-1.92g/ml for the H_3PO_4 which corresponds to 103-105% H_3PO_4.

Recent work by Wachter and Hayes (1985) has suggested that systematic errors arising from exchange between the CO_2 and the H_3PO_4 could be further reduced by a still higher reaction temperature of 75°C, giving a faster reaction and so less time for exchange. This would involve a review of mineral-specific fractionation (CO_2 vs. $CaCO_3$) at the higher temperature.

1.4 Instrumentation

There are several methods by which isotopic abundances can be determined, but the most effective of these are mass spectrometric measurements. The principles of a mass spectrometer are quite straightforward. A beam of electrons is produced by heating a filament (usually tungsten or rhenium). Collimation of the beam occurs as it passes through a weak magnetic field. The sample is introduced into the source region so that the gas collides with the electron beam as it is passed between parallel plates; positive ions are produced from this collision. An electric field draws the ions through a slit in one of the parallel plates and they are then accelerated by passing between another plate parallel to the first two. All singly charged ions thus have the same kinetic energy after passing through the electric field.

Since $\frac{1}{2}mv^2=eV$ relates energy to mass and velocity it may be seen that lighter ions will travel with a higher velocity than heavier ions.

The ions are subject to a strong magnetic field perpendicular to the direction of motion. They are thus forced to travel in an arc, the radius of which is determined by their mass and energy. Analysis of a beam of a particular mass is then possible when it passes through a defining slit on the analyser exit plate. A precision mass spectrometer of this type was developed by Nier (1940).

Since $^{18}O/^{16}O$ ratios are measured with respect to $^{18}O/^{16}O$ ratios in a reference gas (see Section 3.7) it is clearly advantageous to measure both the sample and the reference ratios simultaneously, as they would then be subject to virtually identical conditions. This was the motivation for modifications by Nier et al. (1947) to the original high precision mass spectrometer to include a null-reading double-collector balancing circuit.

M^{c}Kinney et al. (1950) further modified Nier's system with a dual gas feed to the analyser, consisting of an all-metal, solenoid-operated, changeover valve. The changeover valve maintains a stable gas flow by channeling away gas not being analysed through a balanced diffusion pump "bleed" system. Rapid standard/reference comparisons were then possible. More sophisticated electronic componentry was used to stabilise the signal. Electronic corrections to overcome the "pressure effect" (a seeming variation of isotope ratio actually due to ion beam intensity variations) were also made to the signal amplifier.

Shackleton (1965) defined further refinement of these systems to produce the Micromass - a machine capable of measuring very small differences of oxygen and carbon isotope ratios with a precision of $\pm 0.01^{o}/_{oo}$ in extremely small gas volumes (~0.1ml CO_2).

The technical specifications of the Micromass used for data production in this thesis are given in Section 3.6.

1.5 The Oxygen Signal in the Ocean

From M^{c}Crea's (1950) work on the CO_2-H_2O-$CaCO_3$ system it was apparent that the $CaCO_3$ oxygen isotope content would depend not only on the temperature of deposition, but also on the isotopic composition of the water from which it was formed. Ocean waters do not have a constant $^{18}O/^{16}O$ ratio. The total water balance of the earth involves the storage of water in various reservoirs (Table 1.2).

Table 1.2. Residence time of water in natural reservoirs. (From UNESCO, 1978).

Reservoir	Volume (km^3)	Residence time (period of renewal)
Ocean	1 338 000 000	2 500y
Ground water (not Antarctica)	33 930 000	1 400y
Soil moisture	16 500	1y
Surface water	380 410	Rivers 16d Lakes 17y Marshes 5y
Atmosphere	12 900	8d
Glacier and permanent snow cover	48 128 200	Polar 9 700y* Mountains 1 600y

*Values for the residence time of water in the ice sheets vary greatly from 10s of thousands (determined from annual ice discharge in this case) to 200ky for Antarctic ice (Shumsky, 1964) depending on the location of the ice sheet.

As water is transported between these reservoirs fractionation occurs as a result of preferential evaporation and precipitation of the lighter and heavier isotopes, respectively. As a consequence, the greater the temperature change during the process of evaporation-precipitation, the greater the fractionation. Thus ice accumulating in the centre of the ice sheets can be depleted by up to ~60°/$_{oo}$ (e.g., Lorius, 1974; Dansgaard, 1981) in ^{18}O compared to ocean surface waters.

The residence time of these reservoirs is also important as the oceans renew all of their water over approximately 2 500y, but ice sheets have residence times of many tens of thousands of years. During the last 2my the volume of the ice sheets has fluctuated greatly, and as a result the quantity of ^{16}O stored within them has changed sufficiently to have caused significant changes in the $^{18}O/^{16}O$ ratio of all other water reservoirs.

$^{18}O/^{16}O$ ratios of calcite are thus reflections of both temperature of formation and sea water composition, and the differentiation of these two factors in the isotopic signal makes the derivation of precise palaeotemperatures very difficult, as some sort of estimate of the past isotopic composition of the water is required.

Epstein (1951) measured $^{18}O/^{16}O$ ratios (by use of M^{c}Crea's acid-extraction technique) of marine invertebrates grown in a known temperature environment, and so derived a palaeotemperature scale for organically precipitated $CaCO_3$. He then derived palaeotemperature equations relating $^{18}O/^{16}O$ ratios to temperature:

$$T=16.5-4.3(\delta^{18}O_c-\delta^{18}O_w)+0.14(\delta^{18}O_c-\delta^{18}O_w)^2$$

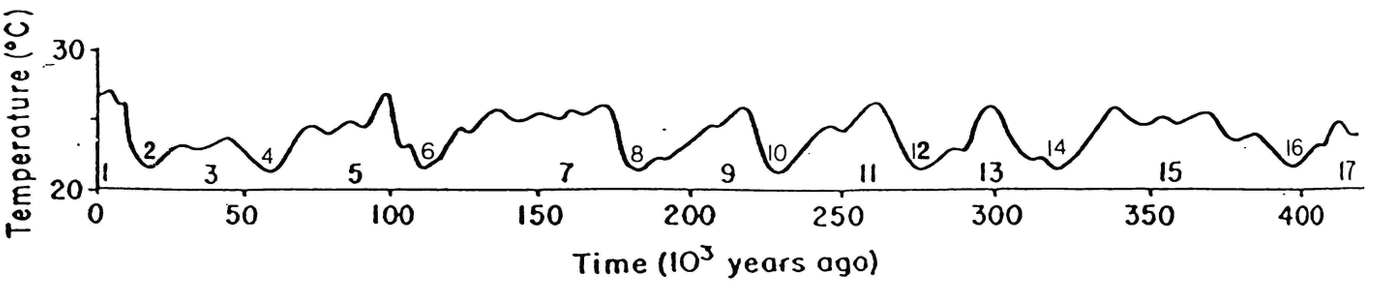

Figure 1.1. A generalised palaeotemperature curve (for the surface water of the central Caribbean) showing the system of numbering glacial and interglacial stages. (From Emiliani, 1966, fig. 6).

where c=calcite, w=water (Epstein et al., 1953). Per mille deviations from a standard, represented by the "δ" symbol, are defined in Section 3.7.

The temperature equations derived by Epstein were subsequently applied by other workers, predominantly to calcareous planktonic foraminifera from deep sea cores. Corrections to Epstein's assumptions of past ice volume compositions have been made as more information has become available. The equation was also later modified by Craig (1957, 1961) to account for ^{17}O content and instrumental inaccuracies.

Emiliani (1955) was the first worker to use such palaeotemperature equations to produce a generalised palaeotemperature curve for foraminifera from deep sea cores. This curve was based on planktonic foraminifera in the Caribbean Sea. He noted cyclical variations from periods of high to low temperatures and interpreted these quasi-periodic fluctuations in terms of cyclical variations in the Quaternary climate. Subsequent work on numerous cores (Emiliani, 1958) revealed similar fluctuations in other records. Emiliani (1966) assigned numbers to the cyclic peaks and dips in the $^{18}O/^{16}O$ record, with glacial periods (high $\delta^{18}O$ values) being given even stage numbers and interglacial periods (low $\delta^{18}O$ values) being given odd stage numbers. This method of nomenclature is now standard and makes inter-core comparisons easier (Figure 1.1).

In order to interpret $\delta^{18}O$ fluctuations in terms of changing surface temperature by use of Epstein's palaeotemperature equation (1951), Emiliani proposed a value for the isotopic composition of sea water. This was based on a depression of sea level of 100m during glacial periods (from apparent past shore lines on continental shelves) and on an ice sheet composition of $-15^{o}/_{oo}$ (based on modern precipitation over previously glaciated regions). With a mean world

sea level of 3.8km this led to a calculated change of $+0.39^{o}/_{oo}$ attributed to ice volume changes (from 100/3800 X$15^{o}/_{oo}$). Since some cores obtained by this time displayed glacial/interglacial changes of $1.5\text{-}2.0^{o}/_{oo}$ it was thus assumed for much of the 1950s and early 1960s that the $\delta^{18}O$ signal must be predominantly influenced by changes in sea surface temperature.

Shackleton (1967) proposed a test for Emiliani's assumptions by arguing that the oceanic bottom waters, which currently have temperatures of 0°C to 2°C, should not show significant temperature changes between glacial and interglacial stages. Organisms dwelling in these waters, such as benthic foraminifera, should only show change in their $^{18}O/^{16}O$ ratios as a response to changes in the composition of sea water. Prior to this suggestion very few analyses had been attempted on benthic foraminifera because their low abundance in most sediments made it impracticable to pick the very large sample size required by existing mass spectrometers. In collaboration with Shackleton, V.G.Micromass developed a M^{c}Kinney-Nier type mass spectrometer with an extremely small inlet system. Using this mass spectrometer Shackleton and Opdyke (1973) showed that the benthic foraminifera displayed the same shape $\delta^{18}O$ versus depth curve as planktonic foraminifera, but with a glacial/interglacial amplitude of $1.6^{o}/_{oo}$. Hence Shackleton and Opdyke concluded that almost all of the change in the $\delta^{18}O$ values observed by Emiliani in planktonic foraminifera was derived from changes in the $^{18}O/^{16}O$ ratio of sea water.

The time-scale of Emiliani's cores was also questioned. Emiliani (1966) had proposed 17 glacial and interglacial stages from the present to about 425ky B.P., with a cyclicity of ~100ky. Inter-core comparison was achieved from first and last appearance levels of

pelagic foraminifera, temperature-dependent morphological features and variations in coiling ratios. Emiliani's timescale was thus derived from correlation between the cores and continental events, by a comparison of $^{230}Th/^{238}U$ ages of marine molluscan shells from interglacial Alaskan deposits, and $^{231}Pa/^{230}Th$ dating of temperature maxima deposits in the cores. A good agreement was found with dates for interglacial stages 5, 7, and 9 given as 96, 171, and 218ky B.P., respectively. $^{40}K/^{40}Ar$ dating, however, showed a temperature maximum in stage 15 at a date normally associated with on-land glacial deposits (354-370ky B.P.). Broecker and Ku (1969) criticised Emiliani's estimation of uranium content in his cores. Uranium content is necessary to correct for the amounts of parent-supported ^{231}Pa and ^{230}Th, and the discrepancy between Emiliani's estimation and Broecker and Ku's was sufficient to affect the supposed dating of the core. Broecker and Ku proposed that plotting the logarithm of a series of $^{230}Th/^{231}Pa$ ratios against depth, using a line of best fit to determine sedimentation rates and hence ages, would be more accurate. A determination of the sedimentation rate in core V12-122, ^{14}C dating, and evidence from upraised marine terraces in Barbados showing high sea levels at 125ky B.P. (Broecker et al., 1968; Broecker and van Donk, 1970), indicated that Emiliani's timescale was too short by ~25%. Four major warm periods were instead proposed starting at about 11, 127, 225, and 300ky B.P.

The development and calibration of biostratigraphy and palaeomagnetic stratigraphy by $^{40}K/^{40}Ar$ dating (Ericson and Wollin, 1968; Cox, 1969) further supported a revised timescale. The last magnetic reversal (Brunhes/Matuyama) has proved particularly useful, having been dated at 730ky B.P. (Mankinen and Dalrymple, 1979) and occurs immediately below the isotope stage 19/20 boundary.

Emiliani (1970) proposed revised calculations for variations due to changing ice volumes based on a drop of 130m in sea level, but still rejected values for the Pleistocene ice sheet composition of $-30^{o}/_{oo}$ (Dansgaard and Tauber, 1969) and used $-9^{o}/_{oo}$ as the value of additional ice. Subsequent measurements of -30 to $-35^{o}/_{oo}$ for ice in Greenland (Dansgaard et al., 1971) and -50 to $-55^{o}/_{oo}$ in Antarctica (Johnson et al., 1972) indicate that this figure should have been larger. Mix and Ruddiman (1984) have extensively reviewed the problems inherent in an estimation of ice sheet composition. Not only must the average isotopic composition have varied with both size and latitudinal position of the ice sheet, but differences also exist in the $^{18}O/^{16}O$ ratios of steady state as opposed to growing ice sheets.

Later development of transfer functions (Imbrie and Kipp, 1971; Imbrie et al., 1973) also supported largely ice volume dominated changes in $\delta^{18}O$ values as glacial/interglacial sea surface temperature changes in low latitudes were too small to dominate the signal.

More recent work has shown that Shackleton's assumption (1967) of a constant global deep water temperature was not correct. Evidence from marine terraces (e.g., Dodge et al., 1983) has shown a large discrepancy between measured sea levels and those expected from the benthic $\delta^{18}O$ signal. Chappell and Shackleton (1986) have concluded that this discrepancy is due to changing temperatures in the abyssal ocean. They propose a step-like cooling in the deep waters beginning ~115ky B.P., that was reversed ~11ky B.P.

Labeyrie et al. (1987) have taken the $\delta^{18}O$ signal of benthic foraminifera from the Norwegian Sea (an area where bottom water temperature changes are assumed to have been minimal, as it has been the site of active Deep Water formation right through the last interglacial and early glacial period) as representing only sea water

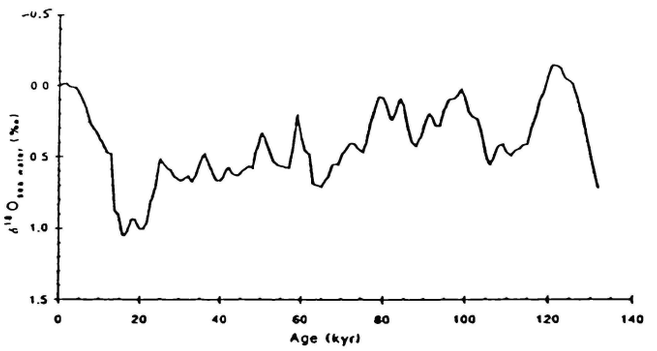

Figure 1.2a. A reference curve for the changing $\delta^{18}O$ of sea water over the last 130ky. (From Labeyrie et al., 1987, fig. 5).

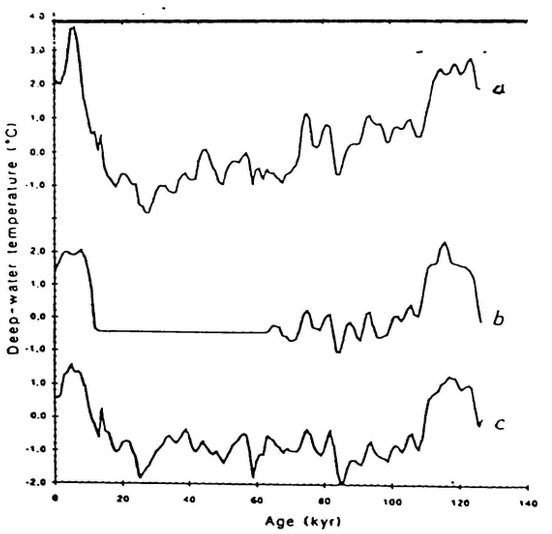

Figure 1.2b. Estimated changes in deep-water temperature over the last climatic cycle in (a) the Atlantic Ocean (b) the Equatorial Pacific Ocean and (c) the Indian Ocean. (From Labeyrie et al., 1987, fig. 6).

$\delta^{18}O$ changes. Comparison between this and the V19-30 record (from Shackleton et al., 1983) shows a major cooling in the deep Pacific Ocean water of ~2°C at the 5e/d transition (~110ky B.P.). As the water temperature in the Deep Pacific was probably constant during glaciation (Duplessy et al., 1980), Labeyrie et al. (1987) proposed using the isotope record of V19-30 to derive a reference curve of mean global $\delta^{18}O$ changes in sea water composition, over the glacial period 12-65ky B.P. This was combined with the Norwegian Sea $\delta^{18}O$ record for periods of Deep Water formation, 0-12 and 65-135ky B.P., to derive a reference curve for the past 130ky (Figure 1.2a). This reference curve was then subtracted from the benthic foraminiferal records under consideration to give an estimate of changing deep water temperatures (Figure 1.2b).

Shackleton (1987) presented a comparison of two oxygen isotope records with detailed records of sea level changes, and so generated a combined record which may be a better record of ice volume change (Figure 1.3).

Williams et al. (1988) have recently proposed an extension to the numbering of glacial and interglacial Stages from the 6/7 boundary back to stage 63 (at 1.88my B.P.) in the Pliocene (Figure 1.4).

1.6 Orbital Fluctuations and Climatic Changes

Despite subsequent criticism of Emiliani's timescale and signal interpretation his early work remains of great importance as it showed the very marked cyclicity of the $\delta^{18}O$ signal for the first time.

This was particularly important as it provided strong supporting evidence for Milankovitch's (1938) astronomical theory of climatic change which postulated that the distribution of heat around the earth

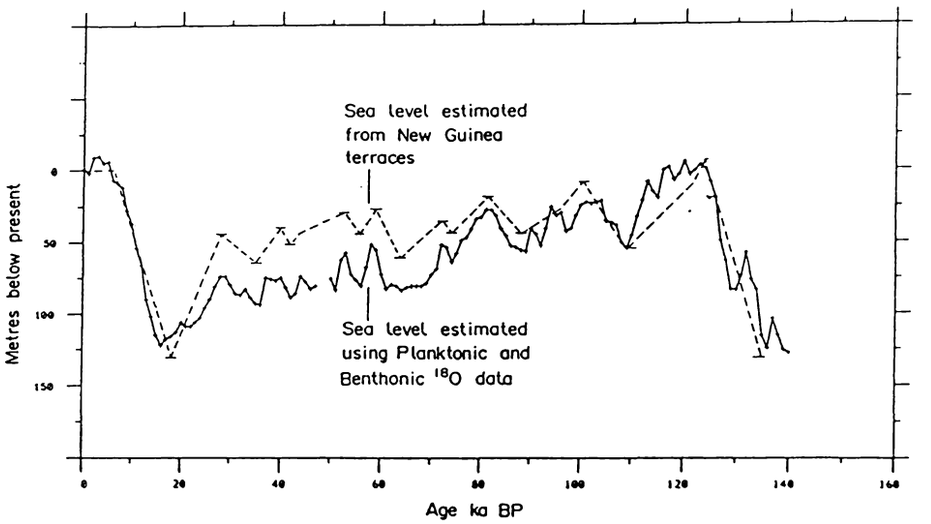

Figure 1.3. Sea level estimates derived by Shackleton et al. (1987), with the sea level record of New Guinea terraces. (From Shackleton et al., 1987, fig. 5).

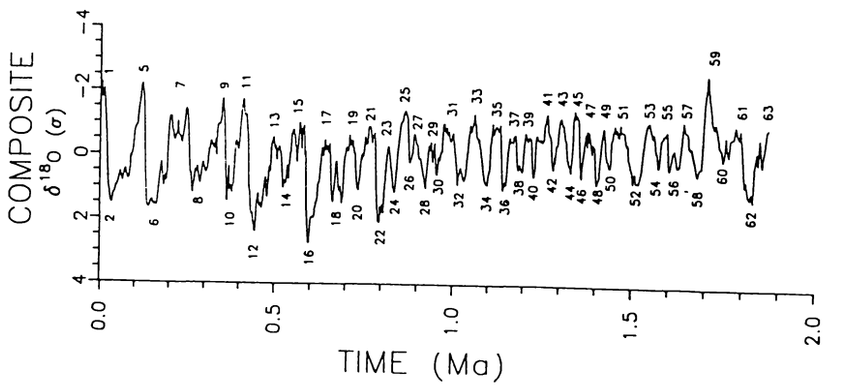

Figure 1.4. Numbering of glacial and interglacial stages in a composite $\delta^{18}O$ record back to stage 63, 1.88my B.P. (From Williams, 1988, fig. 15).

was controlled by changes in the earth's orbital parameters. These parameters were:

1. Precession of the equinoxes.
2. Eccentricity of orbit.
3. Obliquity of the ecliptic.

Milankovitch proposed that these factors controlled the size of the continental ice sheets, and that one would expect the $\delta^{18}O$ signal to reflect such variations. If these orbital parameters were the cause of climatic variation then the periodicities of the climatic fluctuations should match the combined periodicities of the orbital fluctuations. The major orbital frequencies are given as 23ky (precession), 41ky (obliquity), and 100ky (eccentricity). The revised timescale of Emiliani's cores allowed a good match between the $\delta^{18}O$ signal cyclicity and the orbital frequencies and became the standard to which other Pleistocene events have been calibrated (Hecht, 1985). Comparison of various types of organic data from the Pleistocene showed that the principal periodicities of the Pleistocene $\delta^{18}O$ record match the periodicities of the earth's eccentricity, obliquity and precession cycles (Broecker et al.,1968; Shaw and Donn, 1968). Critical adjustments by Hays et al. (1976) to the timescale of the last 400ky finally confirmed the importance of the orbital frequency rhythms in the $\delta^{18}O$ signal.

This work was taken a stage further by Imbrie et al. (1984) who have produced a so-called "ideal" isotope curve (Figure 1.5), with proposed dates for stage boundaries based on orbital fluctuation frequencies. Thus by the use of spectral analysis which matches the periodicities in the isotopic record with the orbital periodicities, within the constraints of ages definitely known (from ^{14}C dating, magnetic reversals, micropalaeontological data, etc.), it is possible

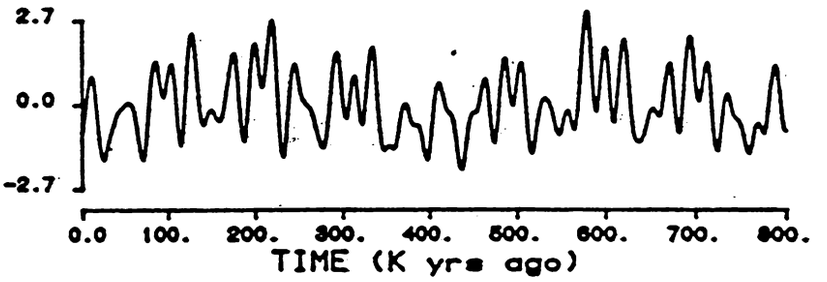

Figure 1.5. An "ideal" isotopic record derived from variations in the eccentricity, obliquity and precession of the Earth's orbit. (From Imbrie et al., 1984, fig. 2).

to obtain a timescale for the $\delta^{18}O$ record from deep sea cores (e.g., Black et al., 1988).

1.7 The Carbon Isotopic Signal

The $\delta^{13}C$ record from deep sea cores has not received the attention given to the $\delta^{18}O$ signal because of difficulties in interpretation. These difficulties largely arise from the fact that carbon is involved in a variety of organic and inorganic fractionations.

The inorganic equilibration reactions between the atmosphere, the ocean, and the sediment layer are outlined in Figure 1.6.

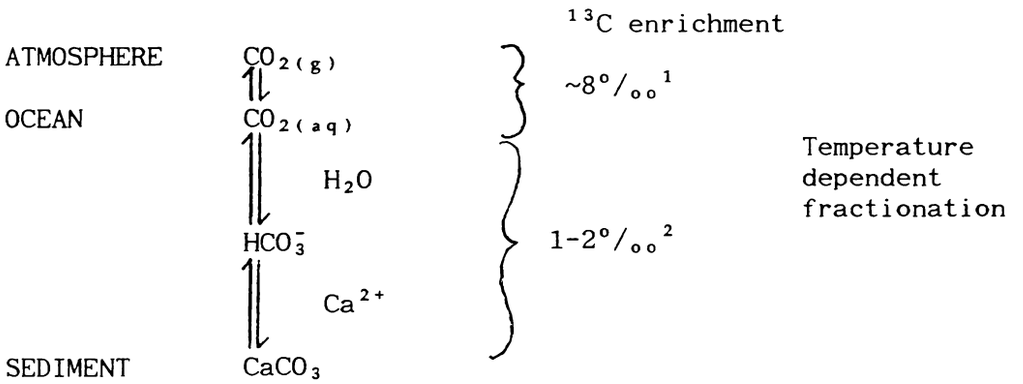

Figure 1.6. Inorganic reactions of CO_2 between the atmosphere, the ocean, and the sediment.
[1] *In* Hoefs (1973) p.25.
[2] Rubinson and Clayton (1969).

Kinetic fractionation during the exchange of CO_2 results in an enrichment of ^{13}C in the HCO_3^-. The temperature dependence of the ^{13}C content of calcite is also of importance. Calcite precipitated at 25°C is enriched in ^{13}C by 0.9°/₀₀ (Rubinson and Clayton, 1969), whereas calcite precipitated at 2°C is enriched by 1.7°/₀₀. The $\delta^{13}C$ content of the dissolved inorganic carbon is thus dependent on a variety of factors, including production of CO_2 in the water column, the rate of

upwelling of CO_2 from deep waters, equilibrium with the atmosphere, oxidation of organics, and carbonate dissolution.

Biological reactions must also be considered. During photosynthesis in the reaction

$$CO_2 + H_2O = CH_2O + O_2,$$

$^{12}CO_2$ is preferentially "fixed" into the primary photosynthesis products. Since not all of the dissolved CO_2 is fixed, a portion of the unreacted ^{13}C-enriched dissolved CO_2 is eliminated from photosynthesising organisms into the ocean water. This has become a useful measure of sea surface productivity (e.g., Kroopnick et al., 1977) where low CO_2 demand results in a higher fractionation (CH_2O can be depleted in ^{13}C by ~17°/$_{oo}$), whereas in periods of high productivity (and hence high CO_2 demand) no ^{13}C is eliminated, and an enrichment in the CH_2O is even possible.

Sackett et al. (1965) reported the temperature dependence of the carbon isotopic composition of planktonic marine sediments, where an enrichment of ^{12}C was noted in surface waters at 2°C (cf. waters at ~25°C in the Atlantic). A greater fractionation of carbon isotopes at lower temperatures during photosynthesis was proposed to account for this. Van Donk (1970) was one of the first workers to study the $\delta^{13}C$ record of planktonic foraminifera. His samples, taken from the Caribbean, revealed no consistent relationship between $\delta^{13}C$ and climate. Shackleton (1977), working in the Atlantic, and Berger and Killingley (1977) in the Pacific, likewise found very little glacial to interglacial change in the $\delta^{13}C$ record. It must be noted that the residence time of carbon in the sea is ~200ky whereas the mean duration of a single glacial or interglacial episode is ~50ky; hence neither ΣCO_2 or ^{13}C content is significantly altered during the course of a single glacial or interglacial event.

Kroopnick (1974) noted that in the present day ocean the $\delta^{13}C$ of dissolved inorganic carbon varies from $+2^{o}/_{oo}$ to $-0.5^{o}/_{oo}$ at the surface, with bottom waters varying between $-0.2^{o}/_{oo}$ and $+0.2^{o}/_{oo}$. This would imply higher $\delta^{13}C$ values in surface dwelling plankton compared with those of benthic foraminifera that have grown in deeper, cooler conditions. The $\delta^{13}C$ content of the dissolved inorganic carbon will itself vary in accordance with several factors (outlined earlier).

Several workers have proposed using $\delta^{13}C$ values of planktonic foraminifera, which are known to vary with temperature, to determine depth habitat. Hence a palaeo-$\delta^{13}C$ profile and palaeothermocline for the water column could be derived. However, problems exist (discussed in Section 1.9) in non-equilibrium species-dependent fractionation. Since the $\delta^{13}C$ record reported by Kroopnick et al. (1973) indicates a maximum shift of $3^{o}/_{oo}$, and since under equilibrium conditions this would correspond to $25°C/^{o}/_{oo}$ - which would clearly give an impossible temperature change for the water - it was deduced that equilibration between calcite and dissolved inorganic carbon cannot be involved. Instead, it was proposed that the $\delta^{13}C$ signal reflected growth habitat, productivity (see later in this section), and the rate of vertical mixing. Kroopnick et al. (1973) further suggested that following the $\delta^{13}C$ record by nannofossil analysis could prove useful as nannofossils do not display species-dependent fractionation (although this view is not universally accepted), and some nannofossil analysis has been done (e.g., Dudley and Nelson, 1988). "Vital effects" must also play an important role in governing $\delta^{13}C$, as HCO_3^- (which constitutes 97% of the ΣCO_2) and dissolved CO_3^{2-} are both dependent on organic reactivity, and are important sources of carbon. In addition, the presence of symbiotic algae in spinose planktonic

foraminifera will result in the inclusion of photosynthetically fractionated carbon. Further complications arise as large and small tests of monospecific planktonic foraminifera can show up to $1^{o}/_{oo}$ difference in $\delta^{13}C$.

At high latitudes planktonic foraminifera record a very different carbon isotope record than they do at low latitudes (Mix and Fairbanks, 1985; Labeyrie et al., 1985), the significance of which is not yet understood.

Benthic foraminifera occupy a more static layer in the ocean (cf. planktonic foraminifera) at the sediment/water interface. The $CO_{2(aq)}$ content of this layer is affected considerably by the oxidation and dissolution of organic material, and can be quite depleted in ^{13}C. Shackleton (1977) was the first worker to systematically study $\delta^{13}C$ values in benthic foraminifera. He found lower $\delta^{13}C$ values during peak glacial times, in comparison to peak interglacial values. This was attributed by Shackleton to decreased forest cover during glacial periods, where a 33% reduction of carbon stored in forests and soils (where the $\delta^{13}C$ is $-26^{o}/_{oo}$) resulted in a lowering of the ocean-atmosphere carbon pool by $0.7^{o}/_{oo}$. It has also been speculated (Niitsuma and Ku, 1977) that the $\delta^{13}C$ variations are due to the production and destruction of shelf sediments (with a $\delta^{13}C$ of $-21^{o}/_{oo}$), and the transference of these sediments to the deep sea floor.

Extensive work by Kroopnick (1980) as part of the GEOSECS (Geochemical Ocean Sections) programme on the distribution of the $\delta^{13}C$ of the total dissolved inorganic carbon in the Atlantic suggested that the dominant influence on distribution is physical circulation, and noted that the oxidation of organic matter (with a $\delta^{13}C$ of $\sim -23^{o}/_{oo}$) to CO_2 provides a marker to distinguish various water masses. As a

water mass ages, oxidation of organic matter adds ^{12}C preferentially to the CO_2 reservoir. Hence a ^{12}C enrichment results along deep water flow paths, and a difference of $1^{o}/_{oo}$ between Pacific Ocean waters and their source in the Atlantic may be measured (Kroopnick, 1974, 1980). The geographic distribution of changing $\delta^{13}C$ is hence dependent on circulation patterns. *In situ* $CaCO_3$ dissolution (to CO_2 with a $\delta^{13}C$ value of $2^{o}/_{oo}$) is also an important factor. Following Kroopnick's work on global $\delta^{13}C$ distribution, Curry and Lohman (1982) used carbon isotopic changes in benthic foraminifera to follow glacial abyssal circulation patterns, by comparing numerous $\delta^{13}C$ records from various cores. They assumed that changes in ^{13}C that occurred synchronously (within ocean mixing time) were the result of changes in the flux of terrestrial carbon, whereas individual core differences could be attributed to changes in abyssal circulation. A lowering of North Atlantic Deep Water production during the last glacial period was deduced, which modified the abyssal circulation of the Vema Channel region in the eastern equatorial Pacific.

Analysis of air bubbles in polar ice cores (reported by Delmas et al., 1980; Neftel et al., 1982) suggested a low atmospheric CO_2 content during the last glacial. Broecker (1982) attempted to model this in terms of photosynthesis in the ocean and its preferential removal of ^{12}C from the surface carbon pool. Enrichment of ^{13}C would occur at times of high phosphorus content (the limiting nutrient of photosynthesis). Shackleton et al. (1983) used Broecker's approach to obtain a record of atmospheric CO_2 from the $\delta^{13}C$ of both planktonic and benthic foraminifera in core V19-30, and provided independent confirmation of the decreased CO_2 concentration in the glacial-age atmosphere.

$^{13}C/^{12}C$ ratios may thus be seen to provide potentially important information for palaeoceanographic studies, but our understanding of their significance is far from perfect. For this reason, and because $\delta^{13}C$ results are easily obtained in conjunction with $\delta^{18}O$, $\delta^{13}C$ values have been recorded in this thesis for each of the cores studied.

1.8 Preservation of $CaCO_3$ in Deep Sea Sediments

Coring operations to recover preserved calcareous foraminiferal-bearing sediments cannot be conducted over all regions of the world's oceans, as the preservation of calcitic tests is limited by the position of the lysocline. The bottom waters of the ocean are known to be undersaturated in calcite, whereas the surface waters are generally supersaturated. This arises from several factors:

1. High bottom water pressures alter the equilibrium constant controlling carbonate dissolution (Pytkowicz, 1968).
2. Metabolically produced CO_2 from bottom-dwelling organisms increase the pCO_2 (Li et al., 1969).
3. Bottom water is formed in high latitude seas from the sinking of very cold, dense brines with a high CO_2 solubility which means that the pCO_2 of bottom waters increases as they warm during circulation.
4) A decrease of the $CaCO_3$ content in the sediment due to dilution by terrigenous sediments and siliceous-biogenic particles.

All of these factors lead to increased carbonate solubility.

The carbonate compensation depth (CCD), which occurs in the zone between the supersaturated surface waters and the undersaturated bottom waters , is generally defined as the depth below which the amount of $CaCO_3$ is <10% (Lisitzin, 1972). The lysocline is generally a few hundred metres above the CCD and is defined (by Berger, 1968) as

the depth range where the dissolution of planktonic foraminiferal tests increases rapidly. A redefinition (Berger, 1971) of a lysocline zone with the lysocline level as its upper boundary means that the lysocline marks the shallowest depth at which any solution-caused change in foraminiferal tests may be detected. The CCD shallows progressively away from the regions of deep water formation as the deep waters accumulate CO_2 during circulation (resulting in an increased pCO_2, and hence greater dissolution of $CaCO_3$). Deep waters flow south through the Atlantic Ocean from the Norwegian Sea, joining the westward circulation around Antarctica with the cold waters from the Ross and Weddell Seas, and then spiral north into the Pacific (see Figure 2.5). Hence in the North Atlantic the CCD is 5.5km deep at 30°N, and only 3km deep at 50°N in the Pacific (Berger, 1976).

Preserved calcareous foraminifera suitable for oxygen isotope studies may thus be found only above the lysocline, which means only in cores taken from raised areas of the ocean floor, as the average depth of the ocean is ~3.8km.

The assumption that increasing sub-bottom core depth implies increasing age of sediments is made, although this assumes no reworking of sediments after deposition. Areas subject to strong turbidity currents, earthquakes, and other disturbances, are thus unsuitable for sampling.

Bioturbation also results in sediment disturbance, although these have been shown to have little effect on the timescale resolution of high sedimentation rate cores (Shackleton and Opdyke, 1976).

1.9 Species Selection and Equilibrium Assumptions

Suitable species for isotopic studies must fulfill several requirements:

1. That they be of reasonable and persistent abundance.
2. That they may be "picked" physically with relative ease.
3. That their depth habitat (in the case of planktonic species) is in the mixed layer of the ocean that has the same oceanographic characteristics as the surface water.
4. That they deposit their shells either at isotopic equilibrium with sea water, or with a known deviation from equilibrium.

The last point raises some considerable difficulties. Duplessy et al. (1970) reported isotopic fractionation in some species of benthic foraminifera. Shackleton (1974) found that *Uvigerina* spp. deposit $CaCO_3$ near isotopic equilibrium within the temperature range 0.8-7.0°C, and hence are a suitable benthic species for analysis. Where *Uvigerina* is not present, *Cibicides* spp. can be a suitable substitute since, although not growing in isotopic equilibrium with sea water, they have a known depletion value for $\delta^{18}O$ of $0.64^{o}/_{oo}$, and of $-0.90^{o}/_{oo}$ for $\delta^{13}C$, with respect to *Uvigerina* spp. (Shackleton and Opdyke, 1973), and hence appropriate adjustments may be made for interspecies comparison.

In the case of planktonic foraminifera, however, the suitability of various species remains confused due to a number of conflicting and contradictory studies of isotopic equilibrium and disequilibrium. Emiliani (1954) reported that different species of foraminifera in the same core level had differing oxygen isotopic compositions. This was interpreted as indicating that different species of foraminifera deposited their shell material at different depths in the water column; the deeper the colder. Emiliani assumed that the calcitic

tests were deposited in equilibrium with sea water and obtained good agreement for comparison between experimental determinations of depth habitats (from oxygen isotopes) and samples collected from nets at various depths in the water column. Since the determined stratification and *in situ* collection agreed so well, it was tacitly accepted by subsequent workers that the assumption of isotopic equilibrium in planktonic foraminifera was in all cases valid. More recent work suggests that this was not correct.

Van Donk (1970) produced data that suggested disequilibrium existed in planktonic foraminifera. Shackleton et al. (1973) detail studies of planktonic foraminifera taken from plankton tows within the isothermal layer of the ocean. Since not all the species in the tow sample had the same isotopic composition they suggested that disequilibrium must occur in planktonic species.

Vergnaud Grazzini (1976) likewise supported non-equilibrium values, and also pointed out that for any given species the deviation from isotopic equilibrium is greater in the living plankton tow specimen than in the sedimented specimen. Subsequent work has not been consistent however. Kahn and Williams (1981) report considerable deviations from equilibrium for *Globigerina bulloides* from sediment traps off Bermuda, but Durazzi (1981) found no evidence for disequilibrium among a variety of species, including *G. bulloides*, in North Atlantic core tops. Curry and Mathews (1981) found deviations in some species of planktonics, but found *G. bulloides* to be substantially at oxygen isotopic equilibrium with surface water conditions.

Erez and Honjo (1981) noted also from a comparison of plankton tows to sediment traps that skeletal deposition continues below the photic zone leading to heavier $\delta^{18}O$ values as the temperature in these

zones is colder and the symbiotic algae less active. (Symbiotic algae may partially affect disequilibrium by the incorporation of isotopically lighter metabolic CO_2 into the test. They are present in most spinose species, although there is conflicting evidence as to their presence or absence in *G. bulloides*). Hence the oxygen isotopic composition of planktonic foraminifera should best be interpreted as representing an integrated isotopic ratio for a few hundred metres of the sea water column.

The disequilibrium of carbon is far greater than that of oxygen, as carbon has a small pool (mostly of dissolved carbonate) and tends to interact with various metabolic processes.

It is clear that interpretation of the $^{18}O/^{16}O$ ratios as palaeotemperatures should be done with caution as the separation and importance of various other factors such as depth migration, horizontal advection, and seasonality are not yet thoroughly understood.

In addition to processes affecting the isotopic composition of living specimens, care needs to be taken that post-depositional changes to the shell material have not occurred. Such changes may result from the deposition of calcite on the tests after death (overgrowths) and the inclusion of very much smaller grained carbonates within the chambers of the foraminifera. Avoidance of these problems essentially depends on the skill of the analyst.

1.10 Salinity

Interpretation and comparison of stable isotope signals must also involve a consideration of the salinity of the surrounding water masses.

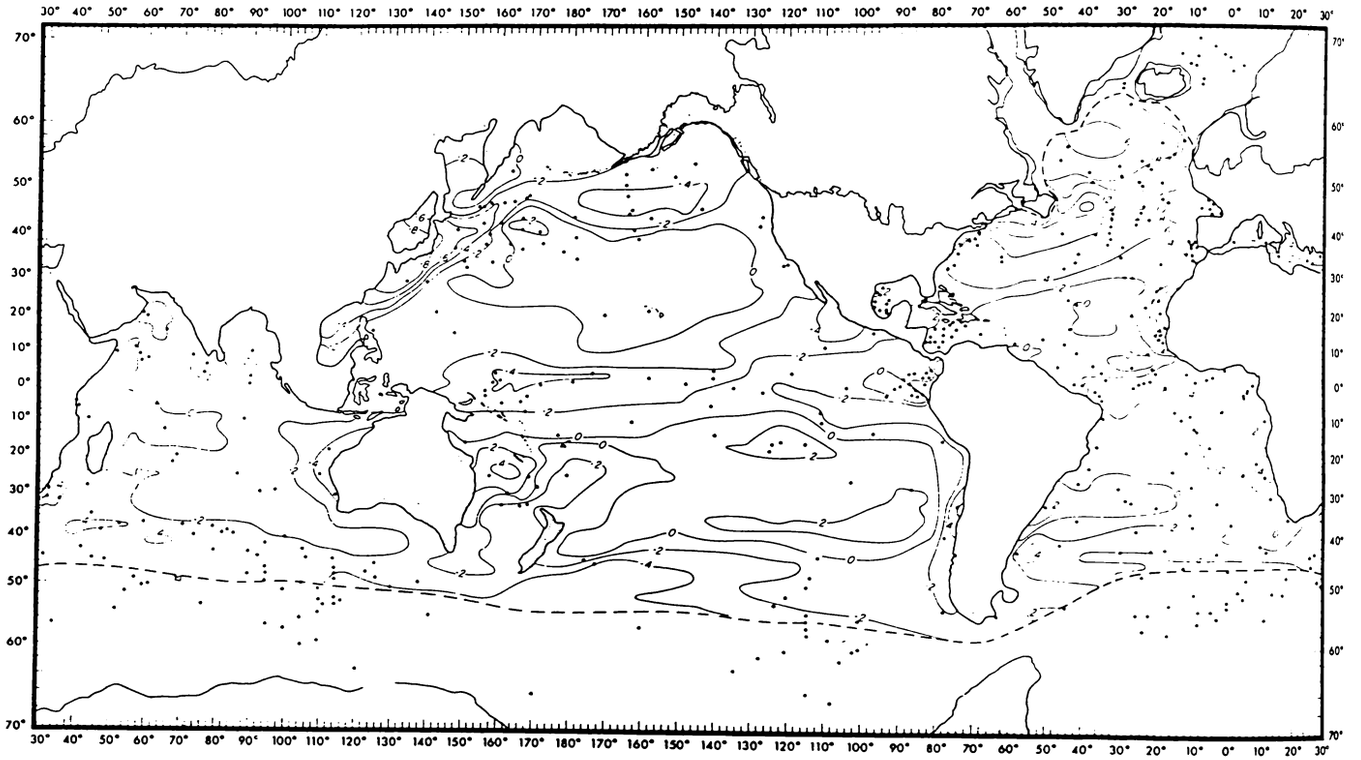

Figure 1.7. A reconstruction of the difference between modern sea-surface temperatures, and estimated sea-surface temperatures of the last glacial maximum, 18ky B.P. (in °C). (From CLIMAP, 1982, fig. 8).

Craig and Gordon (1965) note that surface waters have a linear relationship between $\delta^{18}O$ and salinity of $0.5^{o}/_{oo}$ $\delta^{18}O$ per $^{o}/_{oo}$ salinity. In low latitude regions, where evaporation exceeds continental run-off and precipitation, ^{16}O is preferentially evaporated with an average $\delta^{18}O$ of $-17^{o}/_{oo}$. Transport of this vapour to high latitude regions, where precipitation exceeds evaporation, results in water of decreased salinity and with a low $\delta^{18}O$ content. Deviations from this linear relationship in polar regions are explained in terms of salt enrichment during sea-ice formation.

1.11 Climatic Modelling

In order to obtain a clearer picture of climatic changes over the past million years - and in particular where that change has been recorded in deep sea sediments - a consortium of scientists was organised in 1971, under the title CLIMAP (Climate Long-Range Mapping and Prediction), to study climatic data sets and create a model of palaeoclimatic and palaeoceanographic conditions at certain key times. The first of these reconstructions concentrated on the last glacial maximum, 18ky B.P., with an oceanographic reconstruction based on data from 450 ocean cores (CLIMAP Project Members, 1976, 1982). They reported colder average winter temperatures in the Tasman and South Pacific surface waters due to marked cooling along the South Equatorial Current (Figure 1.7). Maximum cooling was found at 6°S and 46°S. The major gyres of the ocean circulation continued, but were altered in shape, size, and position. Burkle (1983) has shown that the Antarctic gyral systems were intensified during glacial periods.

Prell et al. (1980) have suggested an intensified West Australia Current 18ky B.P., resulting from the deflection of part of the West Wind Drift northwards along the Australian coast.

Inferences about the nature and structure of deep waters are tenuous, but the compression of thermal gradients and the increased surface transport indicate a more rapid turnover of surface and intermediate waters.

Streeter and Shackleton (1979) followed the variation in abundance of *Uvigerina peregrina* over the past 150ky and noted its abundance during times of reduced NADW production and a more northerly position of the polar front in the North Atlantic. Ice cover and stratification of the Norwegian Sea during the last ice age prevented the formation of deep water from this source. The North Atlantic itself could not be a source of deep water until sufficiently dense water could form in the middle of the cyclonic gyre north of the polar front (CLIMAP Project Members, 1976). Duplessy et al. (1980) have shown that the North Atlantic acted as a sink for surface waters, with a cold deep water mass at least 1.3°C colder than modern times.

The evidence of better mixed, cooler near-surface waters, combined with evidence of a change in production of NADW, and an inference of a greater conservation of heat beneath the sea ice at high latitudes, are suggestive of a much smaller thermal contrast between the surface and bottom waters of 18ky B.P. (i.e. a steepening of the temperature gradient) compared with that of the present day ocean. The study of microfossil distributions in the North Pacific undertaken by Moore et al. (1980) indicates an intensified circulation 18ky B.P., with warm tropical waters contained within gyre centres.

The final study undertaken by CLIMAP centred on a reconstruction of the last interglacial ocean 122ky B.P., at a time of similar sea

surface temperatures to the modern day, with comparable global ice volumes. It was noted that the agreement in relative timing between planktonic and benthic foraminiferal $\delta^{18}O$ curves suggested that local temperatures did not markedly alter the phasing of the global ice volume signal - even though surface and/or shallow subsurface parts of the Southern Hemisphere Ocean were generally leading the global ice volume response into and out of the interglaciation. Quantification of lead-lag relationships tied to orbital frequency was suggested for future study.

Mapping by Romine (1982) of a number of Quaternary time slices shows marked changes in oceanic circulation patterns occurring a few thousand years in advance of increased ice sheet growth. This would imply that atmospheric changes in the Pacific occurred prior to, and influenced, polar and continental ice sheet growth in the Northern Hemisphere.

A review of the sensitivity and response time of natural systems, including foraminifera in deep sea sediments, has been published by Wright (1984). He notes that global synchroneity of the $\delta^{18}O$ record within ocean mixing times (~500y - Stuiver et al., 1983) is to be expected. However, a lag in the recording of an onset of colder conditions must be expected as glacial advance itself lags behind the climatic change that initiated the growth of the ice sheets. In addition the growth of ice sheets takes time to register in the $\delta^{18}O$ signal as they build up slowly. In interglacial periods water stored as glacial ice cannot immediately return to the ocean (latent heat factor) and so a time lag is inevitable. Deglacial response times are further confused as the timing of the transference of the signal to the ocean varies according to the cause of the deglaciation (e.g., a reduction in snow fall, rather than an increase in ablation, will

result in a considerable time lag before the change in ice volume is seen in the ocean $\delta^{18}O$ record).

1.12 The Last Deglaciation

Isotopic analyses of foraminifera from many oceanic cores show that a rapid change in $\delta^{18}O$ occurs between ~18ky and 10ky B.P., with an amplitude of 1.5-2.0°/$_{oo}$. This contrasts with the relatively gradual increase in $\delta^{18}O$ from over the previous 100ky, giving a "sawtooth" appearance to $\delta^{18}O$ records (Broecker and van Donk, 1970). During the 1970s this shape was interpreted as being the result of a slow build-up of ice in the Quaternary continental ice sheets followed by rapid deglaciation. The sequence was repetitive with eight or nine such events being recorded during the last million years, of which only the last has left evidence which is widely preserved on land and within the range of ^{14}C dating. As a result, much effort is being expended on obtaining information on the nature of this last deglaciation.

Comparison of records from different high latitude locations and different environments poses a few problems which need to be reconciled. Continental pollen and vegetational records largely show responses to temperature changes which in turn are linked to the altitude of the snow lines and the areal extent of ice sheets in that specific location. Palynologists in Europe have long recognised two pulses of warming during the last deglaciation, the "Bølling" and the "Allerød", separated by a cooling pulse, the "Younger Dryas" (e.g., De Geer, 1957).

Palaeontologists see differing assemblages of planktonic foraminifera which respond to temperature and salinity changes in

oceanic surface waters (Imbrie and Kipp, 1971). Isotopic analysis of core material also shows changes due to variations in temperature and salinity, with salinity apparently playing a dominant role - the effect of salinity being amplified by the release of meltwaters from the ice sheets. These records tend to be dominated by the volume of the major ice sheets. However, since ice sheets are anisotropic and since deglaciation could occur by a variety of mechanisms, such as down-drawing through ice streams, calving of marine ice sheets, or gradual shrinkage, there is no direct linear correlation between $\delta^{18}O$ and ice volume (Mix and Ruddiman, 1984). A further complication is added by the way in which the additional meltwaters are mixed into the oceans, as this cannot be regarded as instantaneous in comparison to the accumulation rate in deep sea sediments. An example of this has been observed in the Orca Basin (Gulf of Mexico) where the Mississippi River has carried meltwater from the southern margin of the Laurentide ice sheet, causing a rapid addition of isotopically light melt water (Emiliani et al., 1975; Kennett et al., 1975). Known as a meltwater spike, it overwhelms the background $\delta^{18}O$ signal which reflects the entire ocean composition, and becomes a signal for local deglaciation. Leventer et al. (1982) have presented a detailed $\delta^{18}O$ record of the Orca Basin which suggested a two-part meltwater spike dated at 16.5-15ky B.P. and 14.5-12.2ky B.P.

During the 1970s it was largely accepted that the abrupt glacial to interglacial change that marked the end of the last glaciation (designated a "termination" by Broecker and van Donk, 1970) was characterised by a smooth sigmoidal $\delta^{18}O$ signal centred around 11ky B.P. The record of this termination is frequently lost in deep sea cores as bioturbation disturbs the top few centimetres of

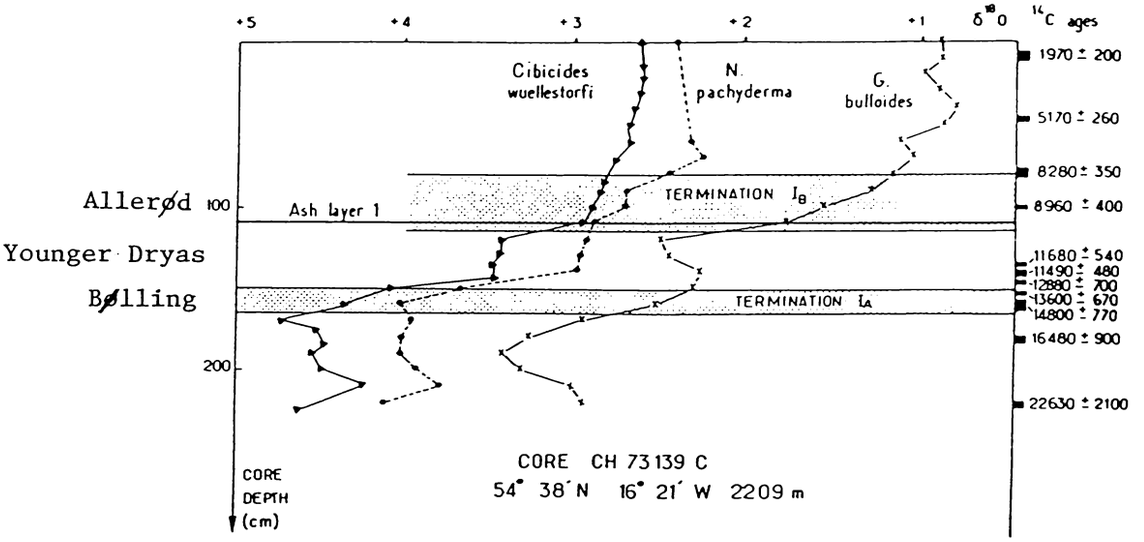

Figure 1.8. $\delta^{18}O$ records of the stage 2 to 1 transition, showing two distinct terminations. (From Duplessy et al., 1981, fig. 3).

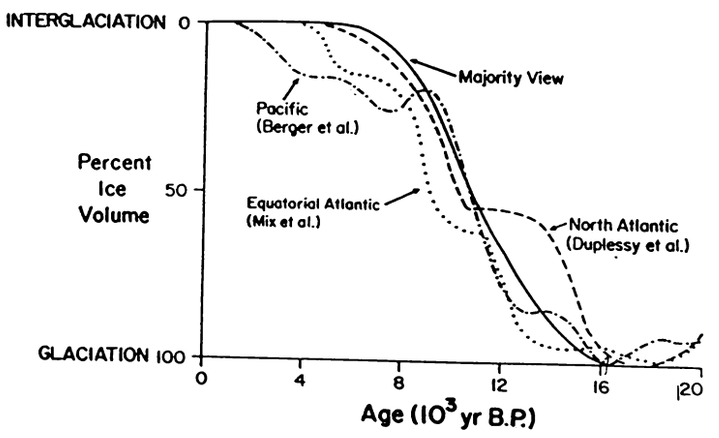

Figure 1.9. Four different views of the timing of the last deglaciation. (From Mix and Ruddiman, 1985, fig. 1).

sediment, and so recent climatic events become blurred within the sedimentary record.

However, from analysis of four high sedimentation rate cores (in which bioturbation smoothing is minimised) in the North Atlantic, Duplessy et al. (1981) presented evidence that challenged the idea of a smooth one-step termination. They noted that the isotopic record of all four cores presented similar features; a general $\delta^{18}O$ decrease from stage 2 to stage 1 that occurred in a step-wise fashion, with a plateau (or increase - depending on species analysed) occurring before the $\delta^{18}O$ decreased to present day values (Figure 1.8). They referred to the first of these terminations as I_A and the second as I_B, and concluded that the Younger Dryas cold event could be a short term response to European continental deglacial warming as cold polar waters spread southwards. I_A was ^{14}C dated from 15.5 to 13.3ky and I_B from 10 to 8.28ky B.P. This implied a pause in the $\delta^{18}O$ decrease at just the point where it was assumed to be the period of fastest change.

Berger et al. (1982) presented a smoothed, stacked, record of Pacific $\delta^{18}O$ values that showed a slight pause dated as 12-11ky, inferred to be equivalent to the Younger Dryas, but not two definite steps. The flattening of the Pacific curves at ~9ky B.P. to present day values may imply that these records miss the later part of the ice volume record, or that the detail has been lost in the smoothing technique (Figure 1.9). Problems with ^{14}C dating (of contamination, redistribution, bioturbation, and dissolution) have caused controversy over the dating of I_A.

Duplessy (in Ruddiman and Duplessy, 1985) noted that the benthic signal tends to lead planktonic records in the Atlantic and Indian Oceans by a few hundred years. Shackleton (in Ruddiman and Duplessy,

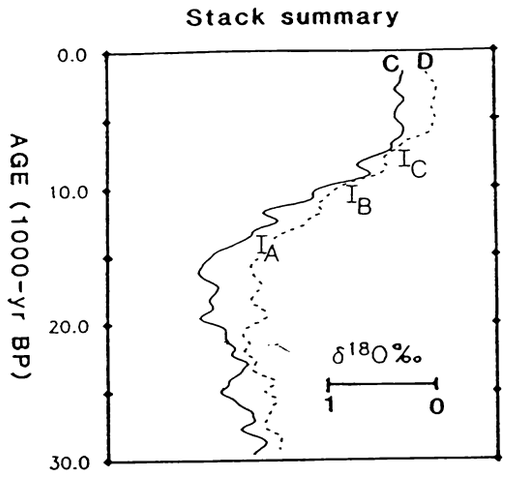

Figure 1.10. Stacked benthic (C) and planktonic (D) $\delta^{18}O$ plots, showing the shape of the record of the last deglaciation, with three proposed terminations. (From Mix and Ruddiman, 1985, fig. 5).

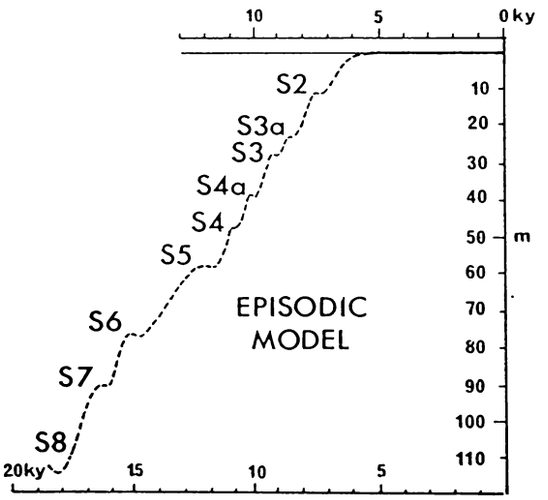

Figure 1.11. A summary regional sea-level curve for eastern Australia and New Zealand, based on an episodic transgression model. (From Carter et al., 1986, fig. 7c).

1985) also noted a benthic lead in the Pacific core V19-30 which suggested that the arrival of the $\delta^{18}O$ meltwater signal is immediately recorded in the deep ocean and retarded in low latitude surface waters. This would imply rapid transfer of cold, isotopically light, glacial meltwater to the bottom waters of the oceans, with later upwelling to the surface waters.

Mix and Ruddiman (1985) studied 24 tropical Atlantic cores constrained by 77 ^{14}C dates, and so obtained a stacked record of termination I. They note the appearance of three termination steps I_A (14-12ky B.P.), I_B (10-9ky B.P.), and I_C (8-6ky B.P.). Although these are close to the statistical limits of detection, the appearance of three steps in individual records would suggest that they are real (Figure 1.10).

High resolution seismic profiles from the northeast of Australia, and to the east of the South Island of New Zealand (Carter et al., 1986) support an episodic deglaciation between 18 and 6.5ky B.P., with time constraints provided partly by radiocarbon dating, but principally from regional stratigraphy. Carter et al. (1986) found significant post-glacial shorelines from 18, 17, 15, 12, 11, 9.5, 9, 7.5, and 6.5ky B.P. They concluded that some of these shorelines were the result of local isostatic or tectonic factors, but those shorelines with large sedimentary wedges were likely to be world-wide features. In particular the size of the 12ky B.P. sedimentary wedge (shoreline S5 in Figure 1.11) coincides with similar significant shorelines seen elsewhere (in North and South America, the Mediterranean and the Arctic). This may be correlated with the inferred post-glacial regression after Termination I (Younger Dryas). The summary regional sea-level curve, with probable shoreline pauses,

based on an episodic model of transgression presented by Carter et al. (1986) is shown in Figure 1.11.

A comparison of North Atlantic isotopic, micropalaeontological and pollen records (Duplessy et al., 1981) shows that there was a rapid deglaciation that started before the maximum caloric summer insolation at 11ky B.P., which would imply that decreasing ice sheet size is not directly attributable to orbital changes. In addition, the duration of the steps in termination I is too short to be reasonably explained in terms of Milankovitch's orbital theory. Some sort of feed-back mechanism, driven by the earth's climatic system, in conjunction with orbital forcing seems more likely. Several feed-back mechanisms to account for rapid deglaciation have been proposed. Increasing concentrations of atmospheric CO_2 have been measured both indirectly (Shackleton and Pisias, 1985) using $\delta^{13}C$ in marine sediments, and directly from pCO_2 of ice cores (Lorius et al., 1985). Ice core data from Antarctica correlate well with the Shackleton and Pisias method, with atmospheric pCO_2 starting to rise ~200ky B.P. and contributing to early forcing. Rapid ice calving to the ocean or proglacial lakes could accelerate melting begun by insolation changes (e.g., Andrews, 1984; Pollard, 1984). It has also been suggested that disintegration of floating Antarctic ice shelves (on resumption of production and circulation of relatively warmer NADW to circumpolar Antarctic regions) would have rapidly changed ocean isotopic ratios - although contributing no sea level change (Johnson and Andrews, 1986). Delayed bedrock rebound (in Ruddiman and Duplessy, 1985) could keep partially melted ice sheets at lower altitudes, in contact with warm air, and so accelerate melting. Downdraw of ice sheet centres via unstable ice streams (Denton and Hughes, 1981) would increase the rate of deglaciation. The possibility of moisture starvation as sea ice

cover expands has also been investigated (Ruddiman and M^{c}Intyre, 1981) and must be considered in conjunction with downdraw and ice calving. However, moisture starvation is not likely to have played a major role in deglaciation by stage I_B as the North Atlantic had warmed to modern values by then, with the exception of the Labrador Sea (Ruddiman and Duplessy, 1985).

Mix and Ruddiman (1985) have proposed that the steps in the termination record are due to a thinning of the ice sheets - which is recorded in the $\delta^{18}O$ signal - that is not recorded in the areal data from North America and Scandinavia, which show unabated, smooth retreats. They suggest that the stepwise signal resulted from several calving and downdraw events. In addition they note the time lag of ~2ky between estimates of volumetric deglaciation and isotopic evidence of deglaciation. This ties in well with previous work (Mix and Ruddiman, 1984) suggesting that lower latitude ("warmer", and therefore less depleted) ice sheets (i.e. British, Laurentide and Scandinavian) melt before high latitude ice sheets. This is also consistent with Ruddiman and M^{c}Intyre's (1981) suggestion that insolation changes vary greatly in spectral nature with latitude, thus there is a varying volumetric response depending on geographical location.

Chapter Two

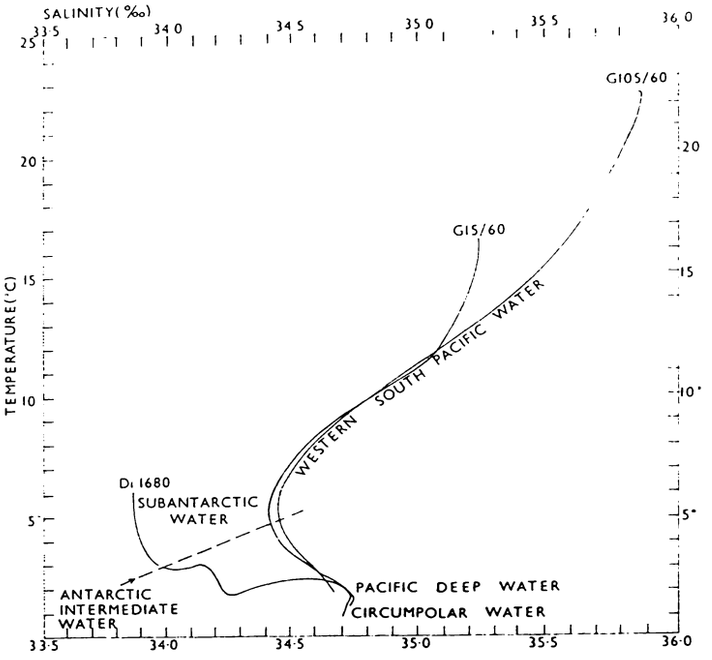

Figure 2.1. Temperature and salinity relationships around the New Zealand landmass. (From Ridgway, 1969, fig. 6).

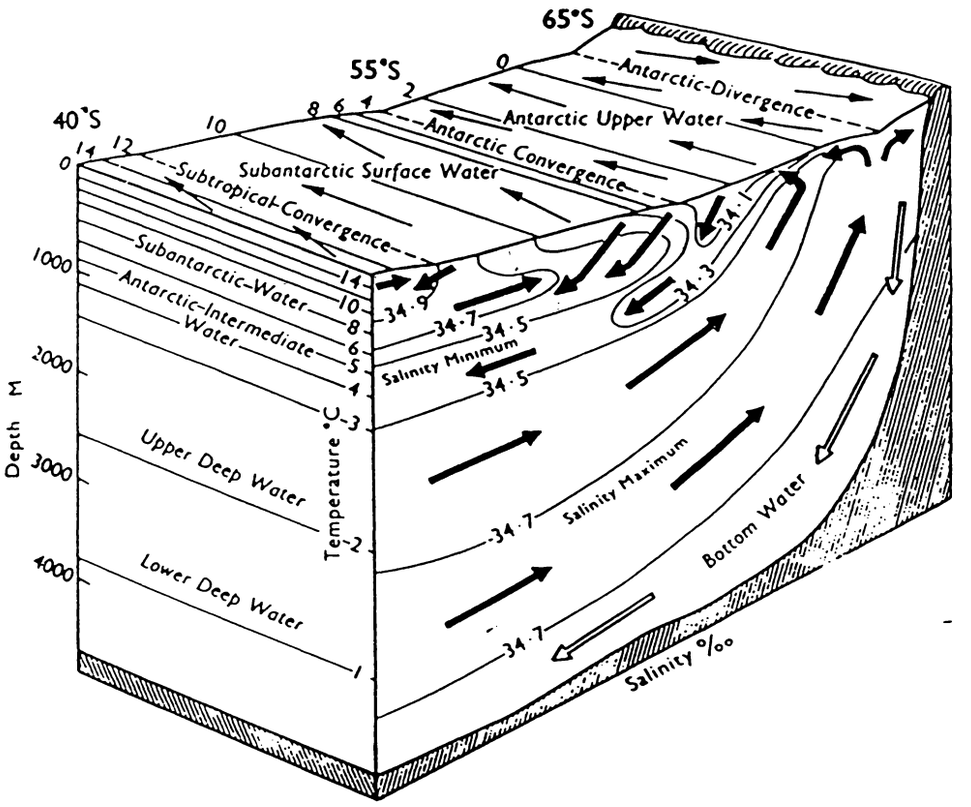

Figure 2.2. Zonal and meridional flow of the water masses of the Southern Ocean. (From Brodie, 1965, fig. 33).

OCEANOGRAPHIC AND CLIMATIC BACKGROUND TO THE REGION OF STUDY

2.1 Oceanographic Setting

2.1.1 Water Masses Around New Zealand

Oceanic deep waters acquire distinctive characteristics of temperature and salinity depending on the region in which they have been formed. The retention of these properties over long periods of time and vast distances allows monitoring and identification of different water masses, and hence permits determination of deep oceanic circulation. At any one location several different water masses may contribute to the water column, each occupying a particular level depending on its respective density. An illustration of the temperature and salinity relationships which allow the identification of various water masses is shown in Figure 2.1. This indicates the inhomogeneity of oceanic waters and the importance of identifying the water mass in which a sample site lies, as this affects the growing conditions of calcareous foraminifera.

There are five main water masses in the vicinity of New Zealand (Figure 2.2):

1. Bottom Waters

The majority of Bottom Waters are formed in polar regions where cooling and formation of sea ice increases the density of surface waters to the point where they sink and flow beneath all other waters. In order to acquire maximum density they must form in regions of low continental run-off (to minimise dilution) and where there is a shallow basin to accumulate cold winter brines. These criteria are met in the Norwegian Sea and in the Weddell and Ross Seas of Antarctica. Winter cooling and sinking of the extremely dense waters of the

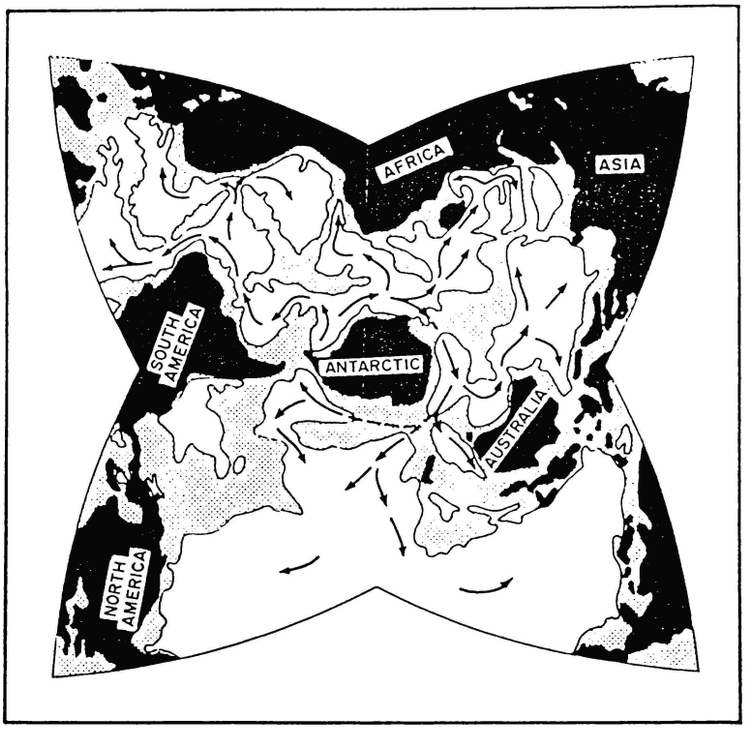

Figure 2.3. The northward spread of Antarctic Bottom Waters. (From Tchernia, 1980, fig. 4.16).

Weddell Sea (σ_t 27.9, Ridgway, 1969) leads to the formation of cold (~1°C, Ridgway, 1969) Antarctic Bottom Waters which flow eastwards around Antarctica and northward into the Atlantic, Indian, and Pacific Oceans. This northward spreading is greatly influenced by sea-floor topography and the rotation of the earth, and is represented diagramatically in Figure 2.3. Bottom water temperatures at the ocean floor in the vicinity of New Zealand are shown in Figure 2.4 (Ridgway, 1979a).

2. Deep Waters

The Deep Waters flow above the Bottom Waters and originate in the surface waters of the North Atlantic Ocean. North Atlantic Deep Water (NADW) is formed, at present, by the overflow of both highly saline North Atlantic water and less saline Arctic water from the Norwegian Sea east of Greenland. Once these waters have spilled over the ridge running from Greenland to the British Isles, they flow south through the Atlantic, where they are modified by high salinity Mediterranean waters, across the Indian Ocean and finally into the Pacific Ocean. These Deep Waters are slightly less dense and warmer (1-2°C, Ridgway, 1969) than the Bottom Waters over which they flow. A salinity maximum of ~34.75°/$_{oo}$ is reached at a depth of 3000m, and the waters may be further stratified into Upper and Lower Deep Water on this basis. The patterns of circulation of NADW are represented in Figure 2.5.

3. Antarctic Intermediate Water

Upwelling of the less saline Pacific Deep Waters at the Antarctic Divergence (Figure 2.2), and their eventual cooling and resinking, results in the formation of extremely low salinity (34.3-34.4°/$_{oo}$ at 700m) Antarctic Intermediate Waters (AIW) (Heath, 1972). The depth of the core of AIW in the vicinity of New Zealand is shown in Figure 2.6 (Ridgway, 1979b). Figure 2.6 will be referred to in Chapter 5 for

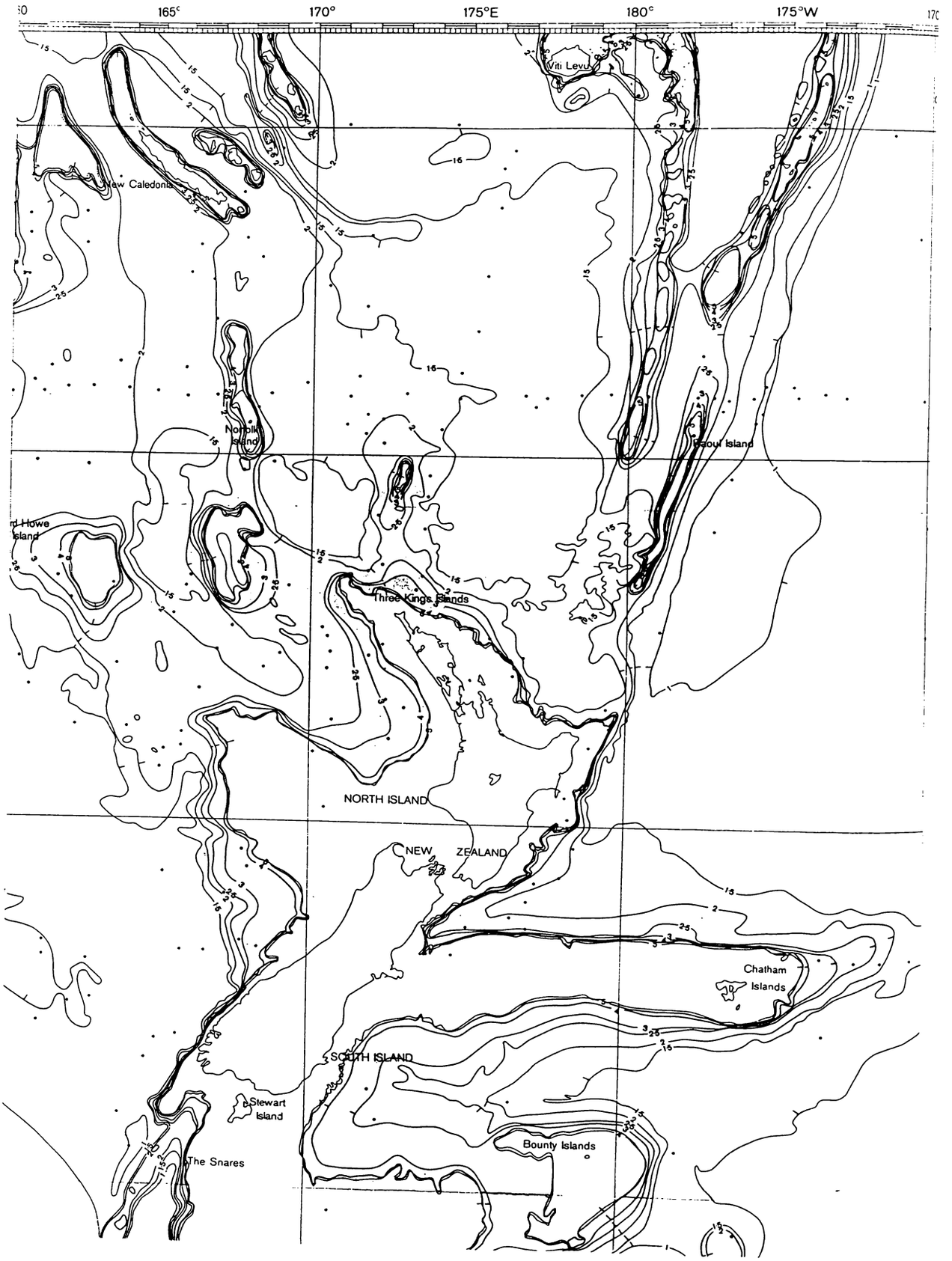

Figure 2.4. Bottom Water temperatures at the ocean floor in the New Zealand region. (From Ridgway, 1979a).

Figure 2.5. The circulation of North Atlantic Deep Water. (From van Arx, fig. 7.15).

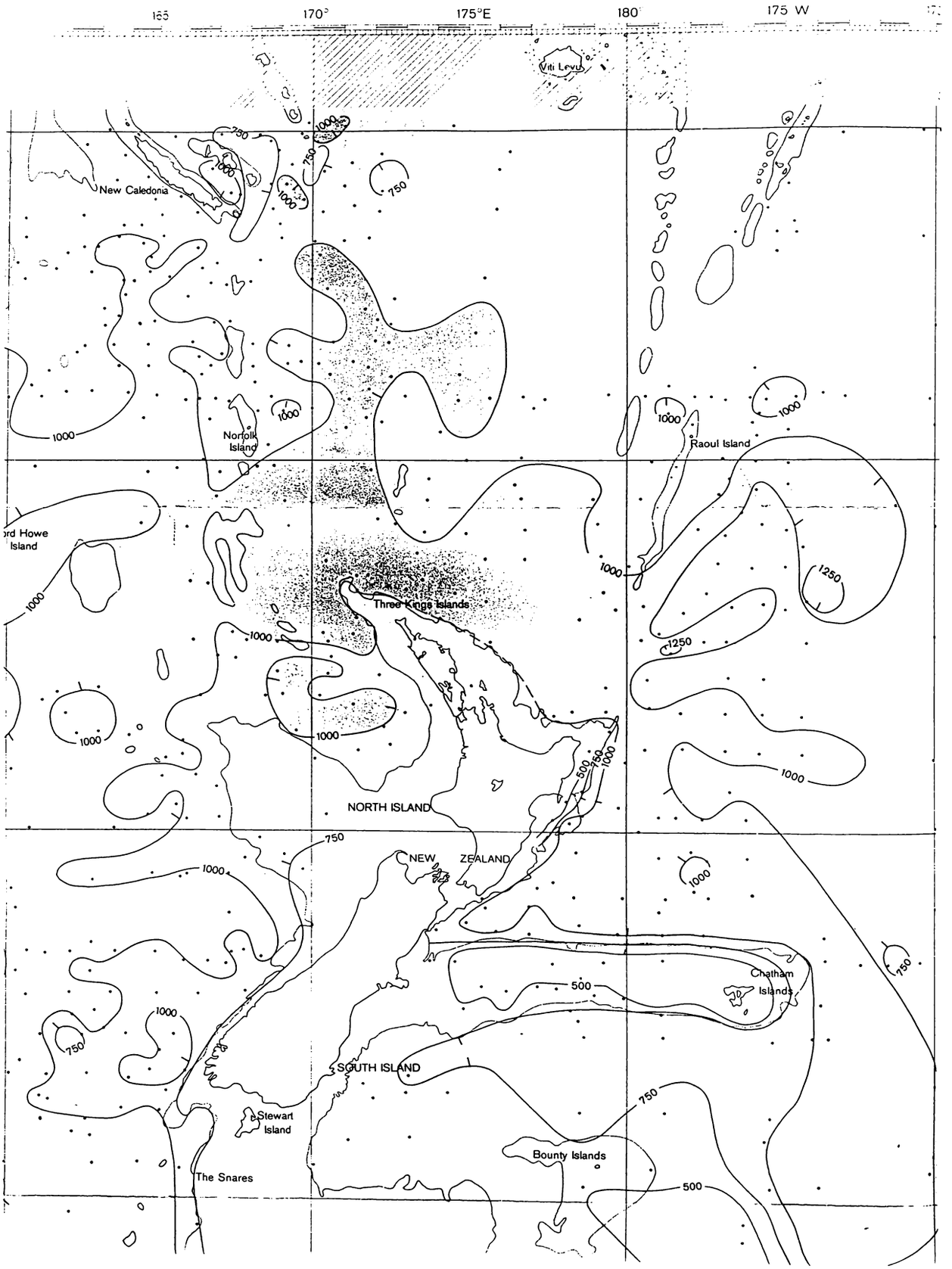

Figure 2.6. Depth of the core of Antarctic Intermediate Water in the New Zealand region.(From Ridgway, 1979b).

determinig the body of water in which the sample sites lie that were investigated in this study. Salinity of the core of AIW around New Zealand is shown in Figure 2.7 (Ridgway, 1979c).

4. Subantarctic Surface Water

These waters are influenced by surface currents (described in Section 2.3) and are characterised by relatively low salinity and temperature. Flow depths may be determined from Figure 2.6, as the surface waters flow above the core of AIW. M^{c}Cartney (1977) has suggested designating the thick subsurface layer of nearly isothermal water to the north of the Subantarctic Front as Subantarctic Mode Water.

5. Subtropical Surface Waters

These originate in the central Pacific Ocean. They are derived in the New Zealand region from the East Australian Current, which is fed by the westward flowing South Equatorial Current.

2.1.2 Oceanic Fronts in the New Zealand Region

The boundaries between major changes in ocean water characteristics are known as fronts. Three major fronts exist in the Southwest Pacific between 30°S and 60°S (their locations are shown in Figure 2.11). Two of these fronts are of particular interest as they lie directly across sample sites. These are the Tasman Front and the Subtropical Convergence. Isohalines and isotherms across these fronts may be seen in the charts in Figures 2.8 and 2.9 respectively (Ridgway, 1979d and e).

1. The Tasman Front (Subtropical Divergence)

The Tasman Front marks the boundary of regions of different flow dynamics and is not a water mass boundary. It was formerly called the Mid-Tasman Convergence (Stanton, 1969) as it was thought to represent

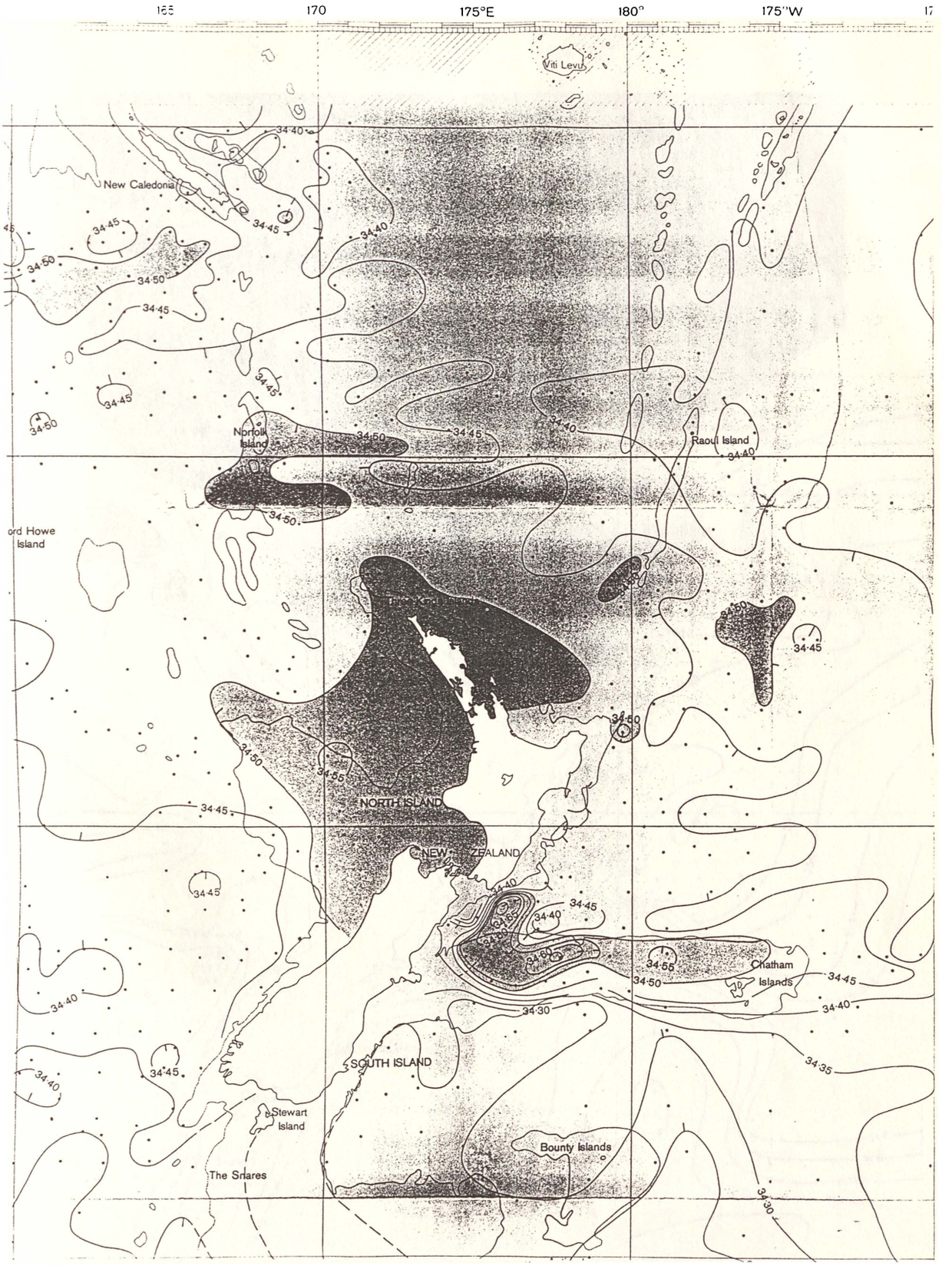

Figure 2.7. Salinity of the core of Antarctic Intermediate Water in the New Zealand region. (From Ridgway, 1979c).

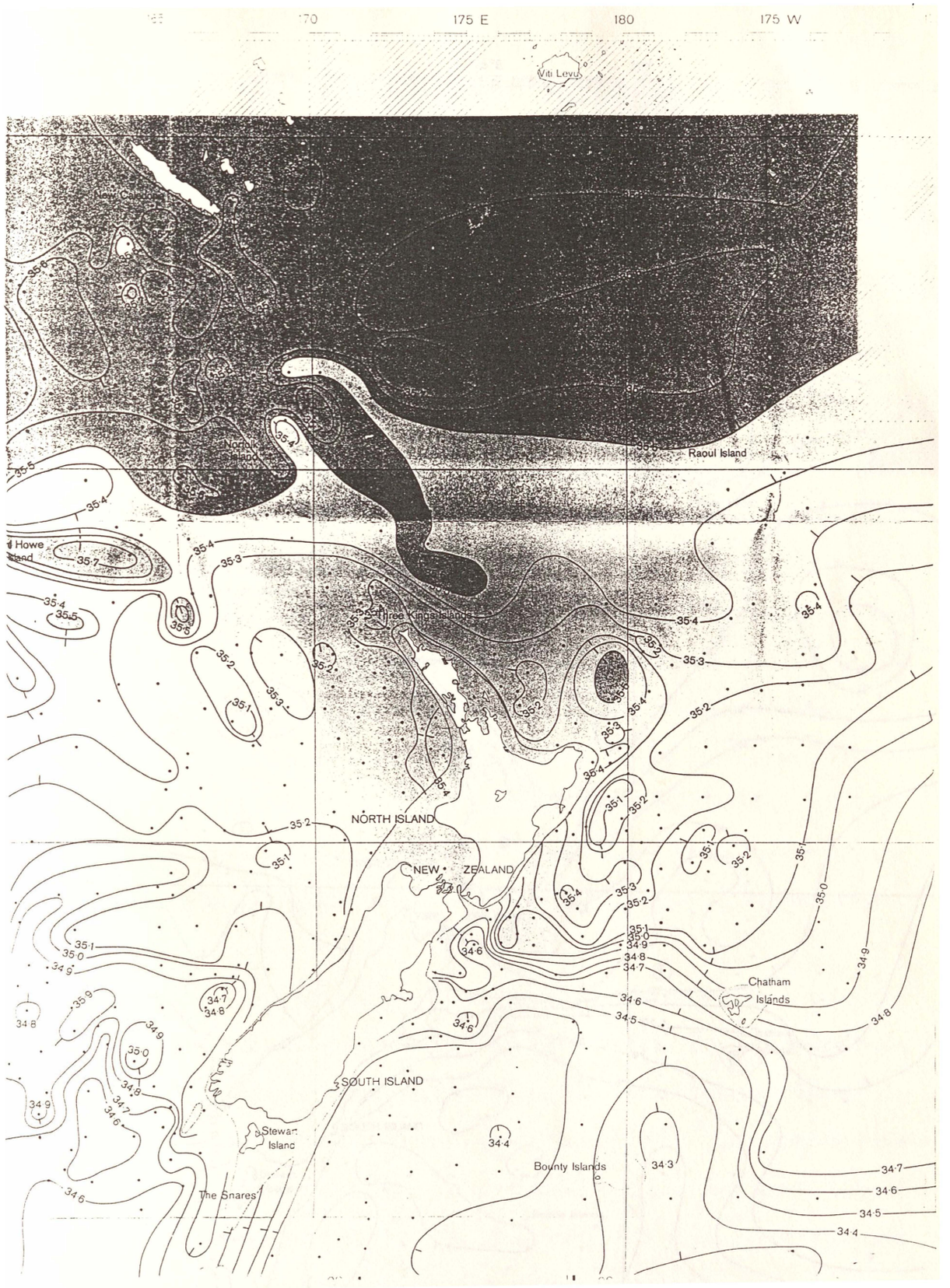

Figure 2.8. Salinity of the waters at 200m depth in the New Zealand region. (From Ridgway, 1979d).

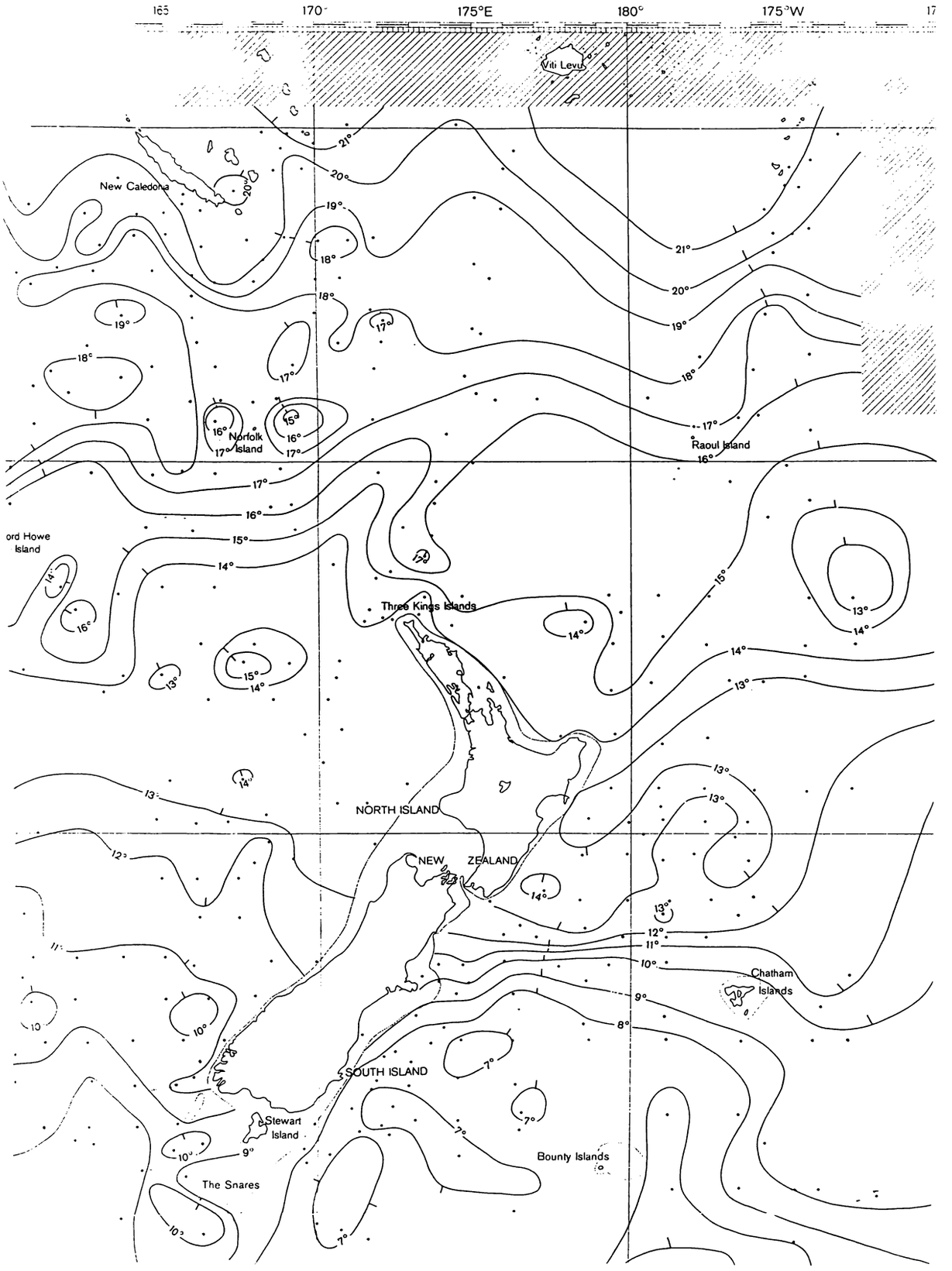

Figure 2.9. Temperature of the waters at 200m depth in the New Zealand region. (From Ridgway, 1979e).

the meeting of waters that had moved across the Tasman Sea by a southern route, and waters that had crossed it directly. However, accumulated evidence (eg., Denham and Crooks, 1976; Stanton, 1979; Andrews et al., 1980) suggests that it is a zonal jet connecting the East Australian Current to the flow east of New Zealand. Variations in the position of the Tasman Front are probably due to changes in the East Australian Current. The Deep Sea Drilling Project Sites 590 and 591A (examined in this study) are positioned slightly to the north and south respectively of this front (see Figure 3.1) and are of interest as they are influenced by both warm sub-tropical and temperate water masses.

3. The Subtropical Convergence

The meeting of warm, saline, Subtropical Waters to the north and cooler, less saline Subantarctic Water to the south is marked by the Subtropical Convergence. It is continuous around southern New Zealand, although along the east coast of the South Island it is known as the Southland Front. The Southland Front marks the region of high horizontal gradients of salinity and temperature between the Subtropical Water inshore and the Subantarctic Water offshore (Heath, 1977).

To the east the position of the convergence is determined by the shallow waters of the Chatham Rise, which restricts the southward flow of the warmer waters. Consequently there is little seasonal change in the position of the Subtropical Convergence over the Chatham Rise compared to the seasonal latitudinal changes of as much as 6° in the open ocean (Deacon, 1937). The Chatham Rise also restricts the projection of a high-salinity subsurface tongue southwards. The horizontal scale of the tongue is 100-200km south of the shallower section of the Rise, increasing to 350km east of Chatham Island

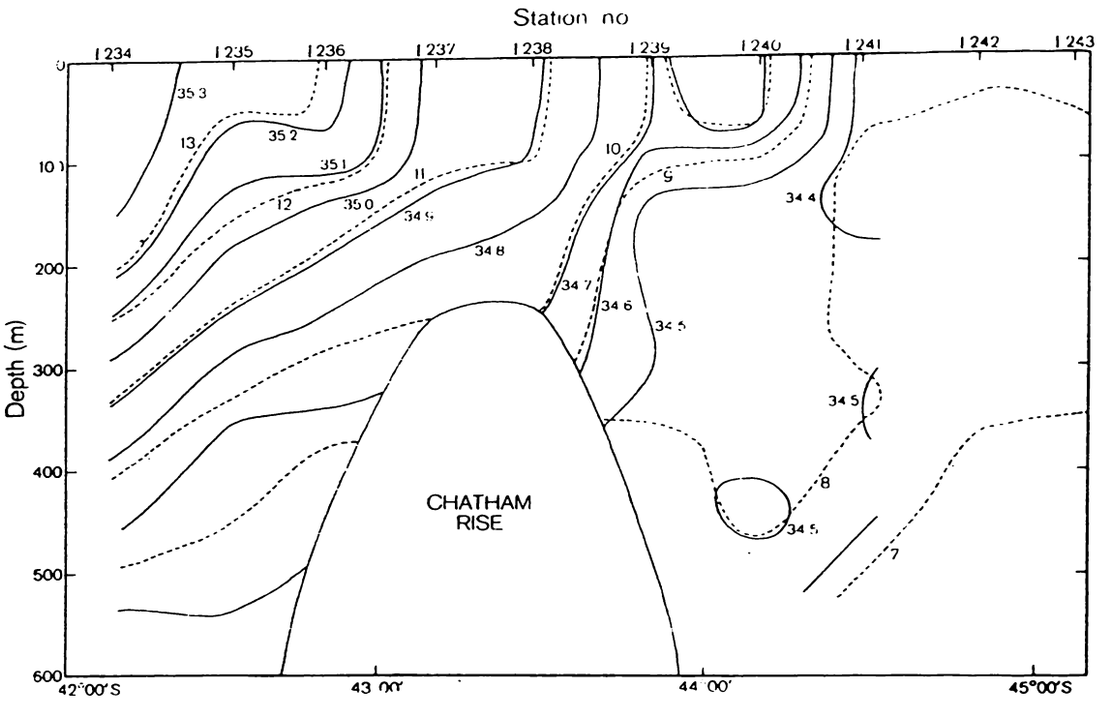

Figure 2.10. North-south section from temperature and salinity data across the Subtropical Convergence at 177°E. (From Gilmore and Cole, 1979, fig. 2).

(Ridgway, 1975), but it extends for 3000km on the open west coast of New Zealand.

The large horizontal gradients of both temperature and salinity in the waters above the Chatham Rise are shown in Figure 2.10.

2.1.3 Circulation of Currents around the New Zealand Landmass

New Zealand lies across a major flow of surface waters travelling eastward, which have originated from the East Australian Current. The waters of the East Australian Current flow southwards to between 31°S and 34°S. Part of the waters then continue south as anticyclonic eddies to Tasmania, where they meet the northeast flowing West Wind Drift at the Subtropical Convergence. The remaining body of water turns eastward and flows directly across the Tasman (Figure 2.11).

The presence of a landmass across this flow causes it to divide. Topographical features which influence this division are shown in Figure 2.12.

Waters flowing to the south of the Challenger Plateau pass through Fouveaux Strait and join the north-flowing Southland Current. The Southland Front separates these waters over the Campbell Plateau from low salinity Subtropical Waters which have flowed across the Snares Shelf. The Southland Current flows northwards along the eastern continental shelf of the South Island (Heath, 1972) and through the Mernoo Saddle. Only waters at depths of >800m do not pass through the saddle, waters above this depth are forced upwards (the Saddle has a maximum depth of 580m). A cool, low salinity tongue extends north from the Saddle. The Southland Front is the eastern side of the tongue and the Subtropical Convergence the western side (Heath, 1972). Some of the Southland Current waters flow into Cook Strait, the rest diverge seawards between Kaikoura and Cook Strait. Eventually the Southland

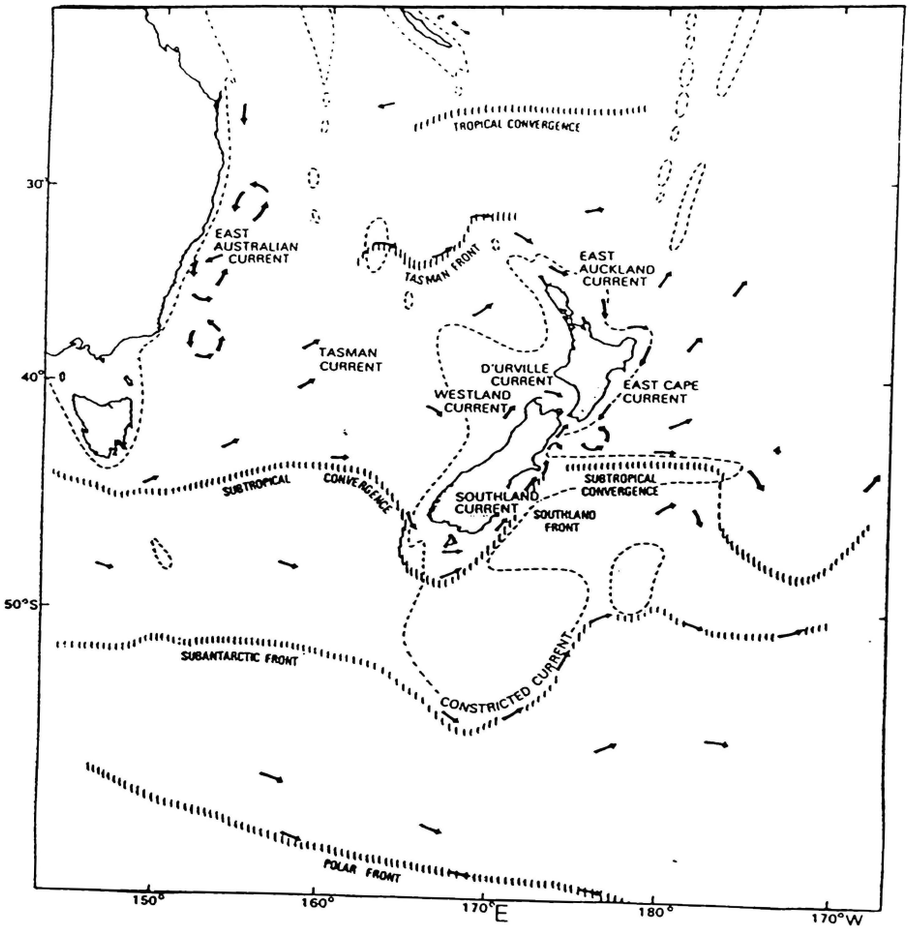

Figure 2.11. General circulation of the waters, and positions of the major fronts in the Southwest Pacific Ocean and Tasman Sea. (From Heath, 1985, fig. 2).

Current turns and combines with the East Cape Current. The combined waters flow south to Cape Palliser, then to the east and north where they finally form part of the East Cape Current system. (A reference map of New Zealand, showing place names mentioned in the text, is presented in Figure 2.13).

To the north of Cook Strait the waters of the Westland Current (flowing north along the west coast of the South Island) form the D'Urville Current which flows into Cook Strait. These mix with waters from the East Cape Current and the Southland Current and flow eastward to join the seaward bound part of the Southland Current.

The East Auckland Current is formed from the eastern flow across the Tasman to the north of New Zealand. This flows southeast along the east coast of the North Island between North Cape and East Cape (Barker and Kibblewhite, 1965). To the north of 37°S the flow turns northwards, with the more southerly water flowing around East Cape and forming the East Cape Current. A warm saline tongue extends southwards of East Cape (Heath, 1973), at the southern end of which is a permanent eddy at about 41°S, 178°E.

2.2 Climatic Setting

2.2.1 The Present-Day Climate of New Zealand

Physical Influences

The New Zealand landmass (267 000km^2 in area) stretches for 1 930km from north to south. From west to east it is only 400km at the widest point; consequently the whole country is well exposed to oceanic influences - no part being further than 130km from the sea (Maunder, 1970).

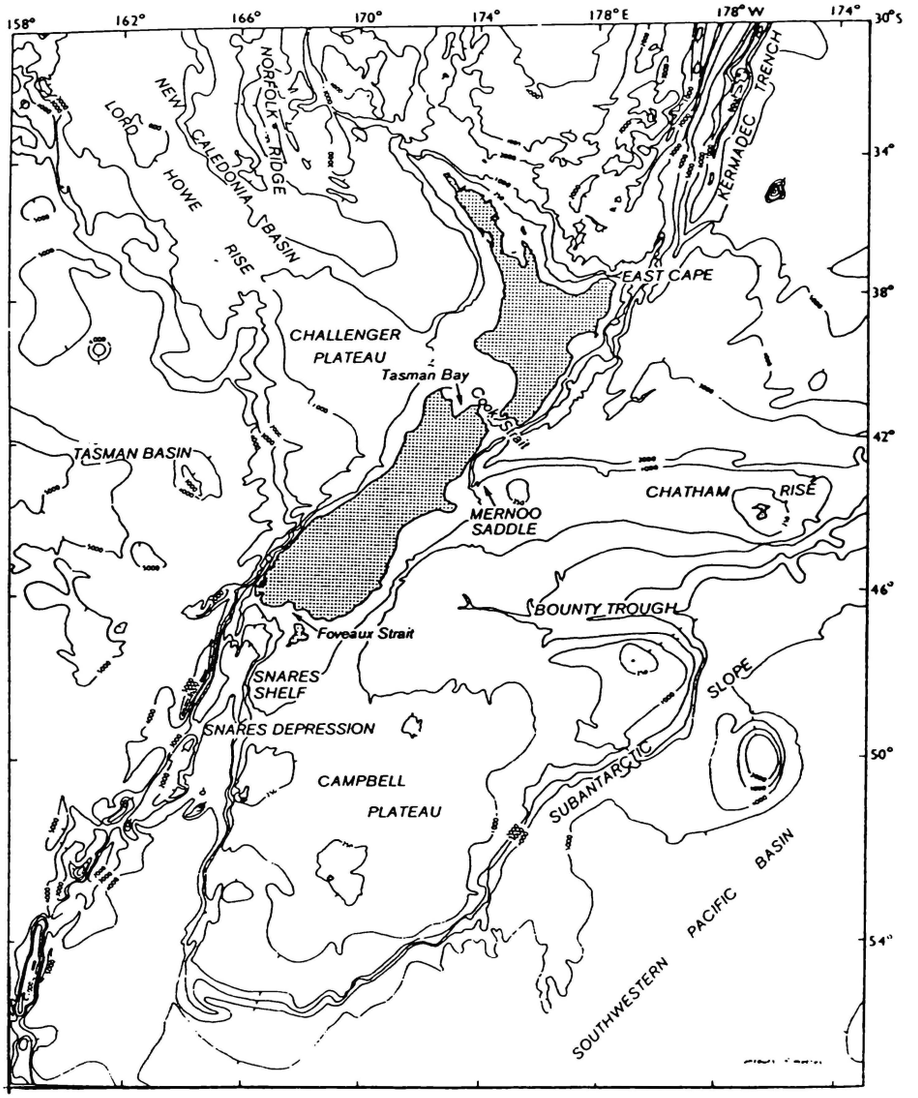

Figure 2.12. Major topographical features affecting the circulation of waters around New Zealand. (From Heath, 1985, fig. 11).

High mountain ranges cause considerable disturbance in the atmosphere and seldom allow the formation of continuous cloud cover. Hence there is a high percentage of bright sunshine (Kidson, 1950). The orientation of the main mountain ranges along a line of 220° is particularly significant as it serves as a block to the passage of wind across the country. During southwesterly conditions one coast is exposed and the other sheltered - small deviations in air flow direction can rapidly change which coast is sheltered, with consequent rapid changes in weather. The chain of mountains also results in a sharp west/east rainfall gradient; the average precipitation in Fiordland to the west is ~6 000mm/y, compared with 330mm/y in Central Otago to the east.

New Zealand is very isolated and surrounded by a vast body of water. The air masses reaching New Zealand are considerably modified by their long sea passage. "Polar" air from the south becomes "cool maritime", and "tropical dry" and "tropical moist" from the north becomes "temperate maritime". This modification of air masses results in a range of temperatures from highest to lowest (up to 1967)of 58°C (Maunder, 1970), with the maximum of 38.4°C being recorded at Ashburton.

Dynamics

In the Australasian region there is a continuous eastward migration of anticyclones at approximately weekly intervals (Robertson, 1967). These anticyclones cross the Tasman Sea to the east-northeast (relative to their Australian location) over the summer from October to March. From April to August they move east-southeast. To the west of the anticyclones the flow (usually from the north or northwest) of warm maritime air brings mild, humid, cloudy conditions.

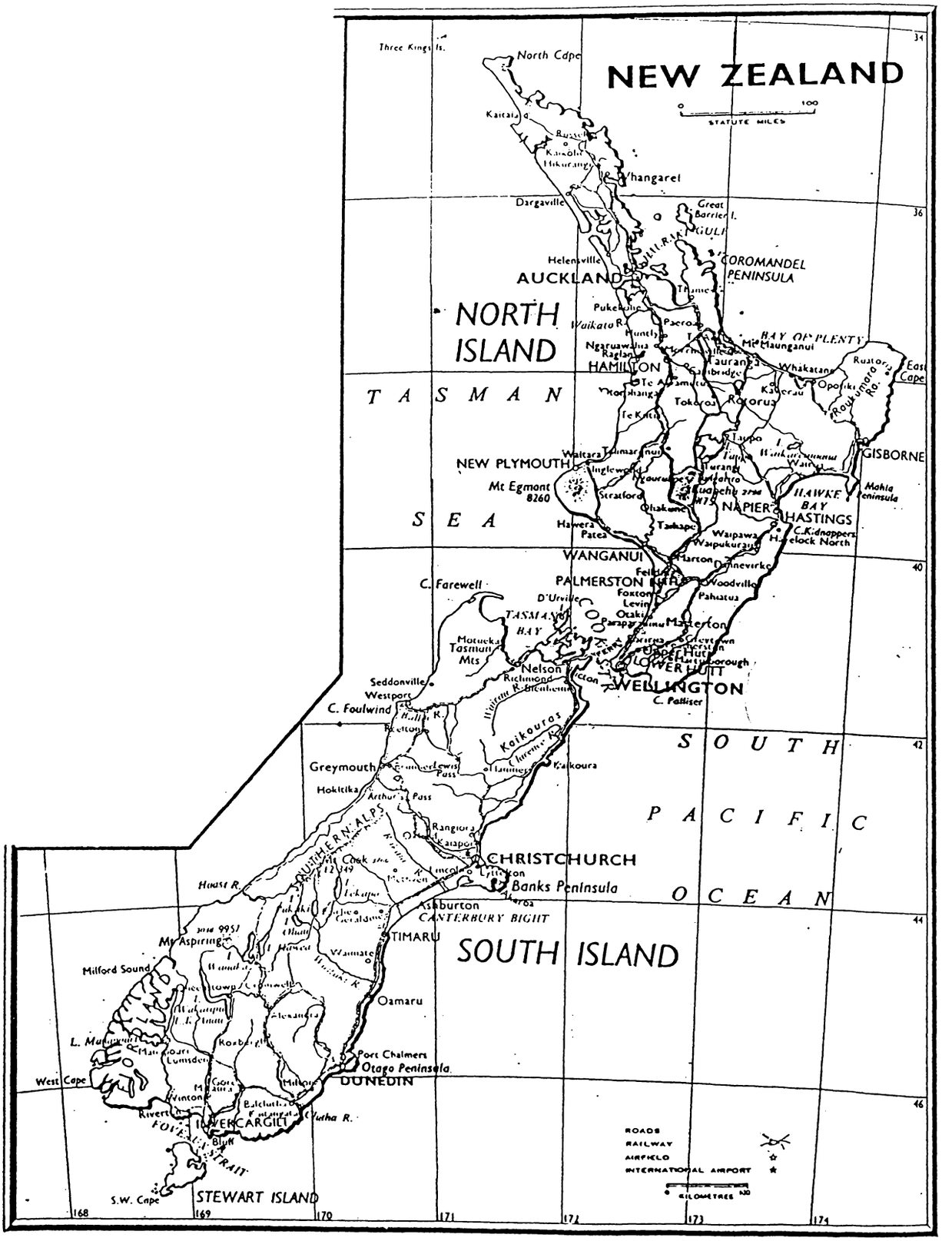

Figure 2.13. A map of New Zealand showing locations of place names mentioned in the text. (Adapted from Kennedy, 1974).

On the eastern side the flow is generally of cool maritime air from the south or southwest, with cool humid air resulting in widespread drizzle. In general, anticyclones bring settled weather with light winds.

Low pressure troughs are experienced between anticyclones as the cool, moist westerly to southerly airstreams from each preceding anticyclone are replaced by the mild, moist northwesterly airstream from the following one. It is the confluence of these contrasting airstreams that results in troughs.

The upper level flow in New Zealand (3-15km) is from the west, maximised in a jet stream near 13.7km elevation between 25-30°S (60m/sec in the winter and 26m/sec in the summer - Gabites, 1953a). Temperature gradients in the troposphere from north to south are steeper in winter (>1°C/degree of latitude between 25-30°S) than in summer (~0.5°C/degree of latitude - Gabites, 1953b). Much of New Zealand's worst weather is associated with pools of cold air (depressions) in the upper levels of the atmosphere.

The climate of New Zealand can generally best be described as humid and temperate with glaciers confined only to the Southern Alps (South Island) except for one small summit glacier on Mount Ruapehu (central North Island).

2.2.2 Climatic Record of New Zealand for the Late Quaternary

Climatic conditions during the Quaternary have been determined from a variety of physical data, including glacial deposits, periglacial features, geomorphic evidence of depressed snow lines, palynology, and sea-level changes.

Figure 2.14 and Table 2.1 have been included here to clarify the nomenclature and dates of subdivisions of the New Zealand Quaternary.

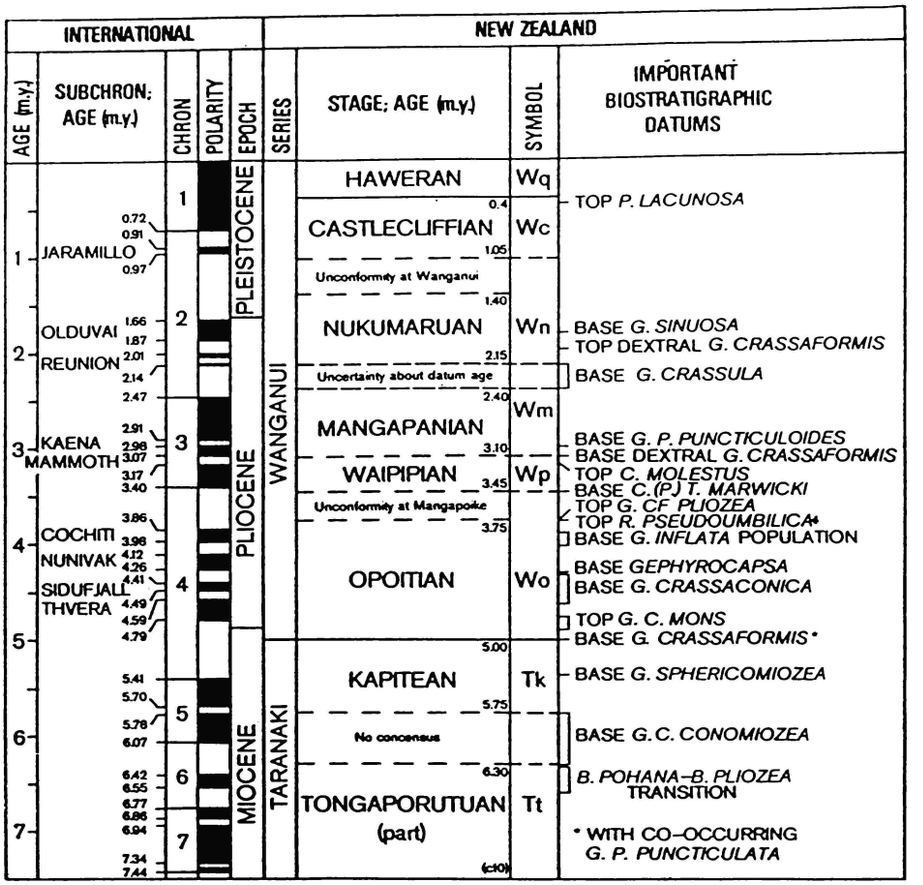

Figure 2.14. Late Neogene stage classifications in New Zealand. (From Edwards, 1987, fig. 2).

Figure 2.14 (Edwards, 1987) shows the Haweran Stage (formerly the Haweran Series) extending back 0.4my into the Quaternary. The Haweran may be further subdivided into Aranuian, Otiran, Oturian, Waimean, Terangian, Waimaungan, Waiwheran, and Porikan (Table 2.1). Of these subdivisions only that time covered by the Aranuian, Otiran, Oturian, and Waimean periods has been looked at in the majority of cores analysed. These subdivisions extend back to the 5/6 stage boundary.

Table 2.1. Subdivisions of the Haweran Stage (N.Z. Upper Quaternary).

Stage	Sub-stage	ky B.P.
Haweran	Aranuian (interglacial)	14
	Otiran (glacial)	70
	Oturian (interglacial)	130
	Waimean (glacial)	
	Terangian (interglacial)	250
	Waimaungan (glacial)	
	Waiwheran (interglacial)	
	Porikan (glacial)	500

The glacial record of New Zealand has received considerable attention. During the Late Quaternary glaciers extended down all of the main valleys of the Southern Alps, which at times of maximum expansion united along the western base of the Southern Alps to form aprons of piedmont ice. Outwashes gravel from the various advances resulted. In the absence of interglacial deposits, the time elapsed between successive glaciations may be determined by considering the degree of weathering and erosion that occurred between glacial advances (Suggate, 1978). Since the stratigraphic relations of glacial and interglacial deposits are best known in Westland, this is the area

from which the standard series of glacials for New Zealand has been established. Westland is particularly sensitive to climatic variations as the high, steep, western face of the Southern Alps is exposed to sources of abundant moisture, and the glaciers are fast-flowing with rapid turn-over budgets. Variations in precipitation and ablation affect the glaciers considerably. For example a 2-3°C drop in temperature is sufficient to produce the same results (of glacier expansion) as a 5-7°C drop to the east of the Alps (Maunder, 1970).

Although extensive glacial deposits occur on both sides of the Alps, correlation of these has proved difficult partly because the preservation of glacial deposits retaining depositional morphology is dependent on rate and timing of uplift (Suggate, 1985). In most cases only four Late Quaternary glaciations can be distinguished. The youngest of these, the Otiran, contains at least three advances; older Kumara-2, younger Kumara-2 (22.3-18ky B.P.) and Kumara-3 (17-14ky B.P.) (Radiocarbon dates are from Suggate (1965) and Suggate and Moar (1970)). It has generally been held that the New Zealand Late Quaternary glacial sequence is comparable to that seen in the Northern Hemisphere (Suggate, 1978).

The snow line in New Zealand during the cool maximum of the Otiran glaciation is estimated to have been lower by ~1 200m on average from its present position (currently ~2 000m in the southwest South Island to 3 700m on Mount Ruapehu in the North Island - Willet, 1950).

Prevailing winds between southwesterly and northwesterly quarters appear to have been dominant during the Otiran glacial periods: East Canterbury loess deposits indicate deposition largely from the northwest, and evidence from glaciers suggests a buildup by precipitation largely from the west or northwest (Gage, 1965). The weak glaciation of the Kaikoura Ranges close to the

northeast/southwest extending "east" coast also suggests a lack of snow nourishment from the east or south during glacial periods.

Quaternary glacial deposits in New Zealand have characteristics suggestive of a plentiful supply of water during glacial advances resulting in relatively small moraines (compared with those in strongly continental settings). Erratic sequences of deposits along the sides of glaciated valleys suggest complex cyclic weather patterns, where low-pressure troughs could bring heavy rain and result in unseasonal ablation of the glaciers. Although mean temperatures may have dropped by 6°C (Willet, 1950), spells of above freezing weather must have occurred during glacial winters (Gage, 1966).

2.2.3 Correlation of On-land Records to Deep-Sea Records

Coastal deposits and landforms indicative of changed sea levels have been preserved in some regions of New Zealand. Kamp (1978) was the first to demonstrate a correlation between palaeoceanographic oxygen isotope stages and New Zealand on-land sequences. Beu and Edwards (1984) showed a correlation between isotope stages 7a-25 defined in core V28-239 (isotope data from Shackleton and Opdyke, 1976; revised time scale of curve from Gardner, 1982) and on-land marine sequences from the Castlecliffian sequence exposed west of Wanganui. Disconformities were interpreted as being the result of glacio-eustatic sea level drops. Most of the sequence was deposited during interglacial periods. Changes in sedimentation rates in the sequence were judged to be reflective of a change from off-shore to near-shore depositional sites. Correlation between the on-land deposits and V28-239 was achieved by considering a number of tie points provided by:

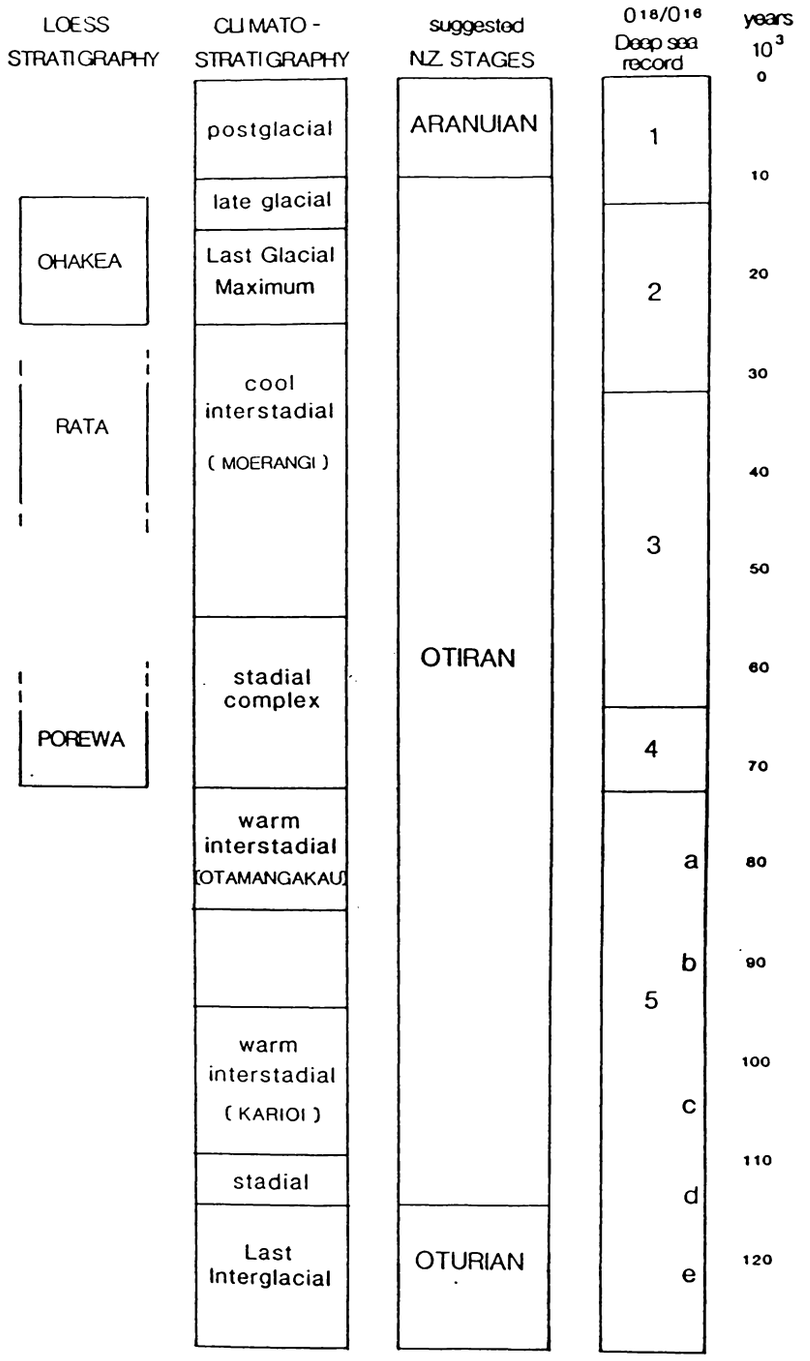

Figure 2.15. Stratigraphic nomenclature for the North Island, correlated with the deep-sea $\delta^{18}O$ record. (From M^{c}Glone, 1985, fig. 4).

1. Biostratigraphic data.
2. The Brunhes/Matuyama magnetic polarity boundary (19/20 isotope stage boundary).
3. Fission-track dating of tephras.

Correlation of the lower resolution sampling of DSDP 594 (at 30cm intervals) to V28-239 and the Wanganui Terraces was presented by Cuthbertson (1985).

Marine terraces exposed on the South Taranaki coastline have also been dated and correlated with offshore data and interpreted to match each of the interglacial isotope stages from 11 to 17 (Pillans, 1983).

Pollen analysis by M^{c}Glone (1985) of sediments in the North Island have displayed complex vegetational changes which may be related to the deep sea oxygen isotope record (Figure 2.15). Isotope stage 5 (130-70ky B.P.) has been recognised with three warm forested episodes and two cool climate episodes (characterised by partially treeless landscapes). The Otiran stage (~115-10ky B.P.) has also been recognised as being characterised by cool climates and treeless shrub and grass landscapes. A long shrubland-dominated Moerangi interstadial (~55-25ky B.P.) equivalent to stage 3 has been noted with forestation in some regions. Rapid forest expansion after the treeless glacial maximum (25-14ky B.P.) occurred until full forest cover was established ~10ky B.P. M^{c}Glone suggested a stratigraphic nomenclature for the southern North Island, with correlation to the Late Quaternary deep sea record, and confined the classification of the last interglacial to stage 5e (Oturian) only, as this was the last period for which vegetational distribution was comparable to that of the present day.

Edwards (1987) has published an extensive review on the integration of biostratigraphic, magnetostratigraphic, and oxygen

isotopic events for the Late Neogene of New Zealand. This is of particular interest as the oxygen isotope marine stratigraphy is largely provided by analysis of sequences from DSDP Site 284 (Kennett et al., 1974). Site 284 was re-cored by DSDP during Leg 90 as Site 593 (Kennett et al., 1986), which has been extensively isotopically analysed both in this study (back to 42m sub-bottom depth) and by P.S.Head (D.Phil., in prep., University of Waikato) beneath 42m sub-bottom depth.

2.3 Oceanic Sediment Investigations in the Southwest Pacific

Quaternary marine sediments from the southwest Pacific are available from several sources. A number of locations in New Zealand experienced rapid uplift during the Quaternary, so that thick sequences of Early to Middle Quaternary marine sediments are exposed in Hawkes Bay, Wairarapa and Wanganui (Beu and Edwards, 1984). Useful as these sequences are, they suffer from a number of disadvantages for oxygen isotope stratigraphic studies. This is because they often display unconformities resulting from fluctuating sea levels, they may be influenced by low ^{18}O terrestrial run-off, and they are also prone to post-depositional changes such as cementation and weathering.

Available cores for the analysis of off-shore sediments in the New Zealand region have largely been derived from three sources:

1. The eleven cruises of the N.S.F. oceanographic research vessel *Eltanin* (1962 to 1972) took piston cores from 180° to 95°E and from ~34° to 78°S through the Tasman Sea and the South Pacific from New Zealand to the Ross Sea.

2. The N.S.F. Deep Sea Drilling Project used the research vessel *Glomar Challenger* which ran three cruises in the New Zealand region.

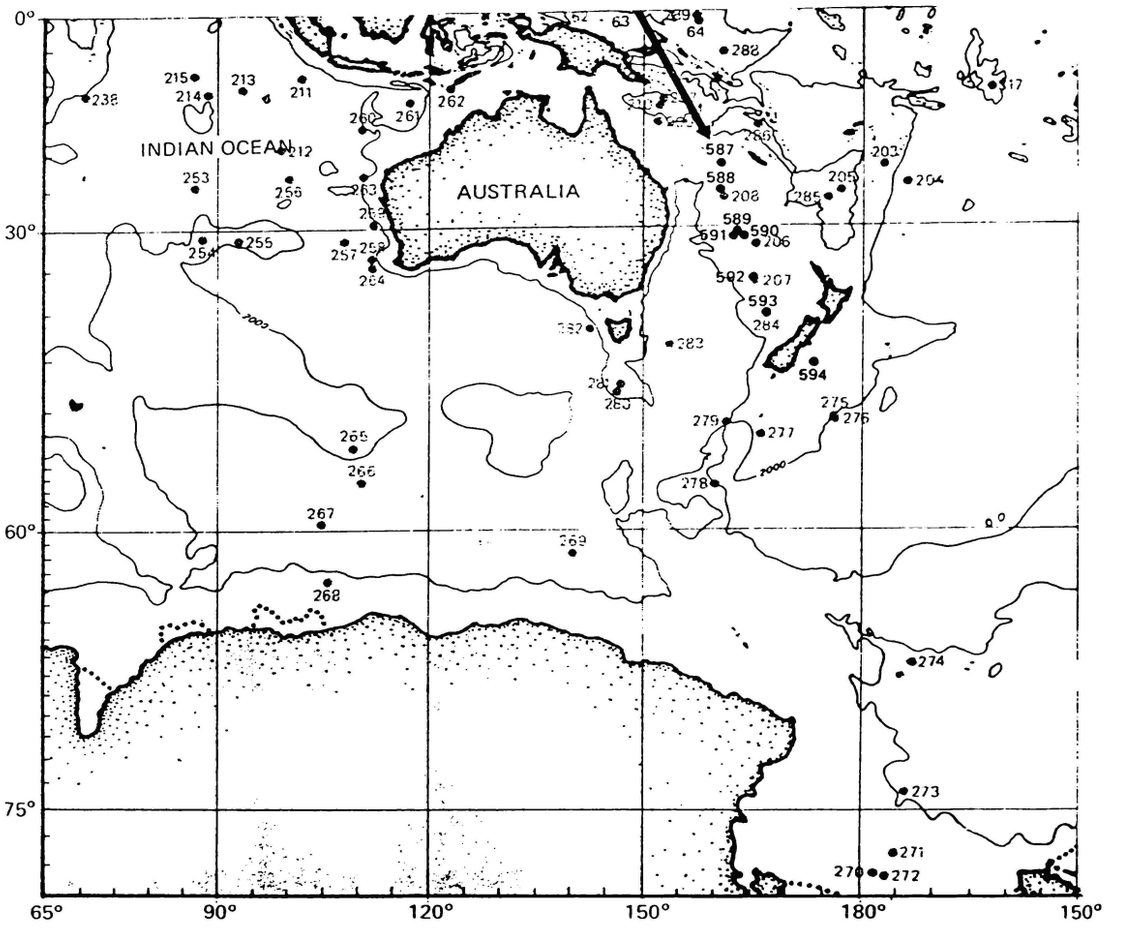

Figure 2.16. The locations of Deep Sea Drilling Project sites in the Tasman and Southwest Pacific region. (From Kennett et al., 1986).

The first two of these, Leg 21 in 1971-72 (Cores 206,207 and 208) and Leg 29 in 1973 (Cores 275-281, 283 and 284) used conventional rotary drilling techniques, which recovered lithified sediments to considerable depths, but resulted in very poor recovery of the overlying unconsolidated sediments. (Site locations are shown in Figure 2.16). The third cruise (Leg 90, 1982-83) used the then newly developed hydraulic piston corer to recover these sediments relatively intact.

3. The New Zealand Oceanographic Institutes research vessel *Tangaroa* has obtained many short to medium length piston cores from New Zealand waters.

Some piston cores from the Tasman Basin have also been recovered by the r.v. *Oceanographer*, a U.S. coastguard and geodetic survey ship, on a passage between Sydney and Auckland.

However, compared to the vast quantity of work carried out on Late Quaternary deep-sea sediments in most ocean basins, relatively little work has been done in the Southwest Pacific region.

Micropalaeontological work was conducted by Eade and van der Linden (1970) on twelve deep-sea cores taken from the northern Tasman Sea by the r.v. *Oceanographer*, including Z2108 which is analysed in this study. Six cores taken to the west of the Dampier Ridge (shown in Figure 2.17) were characterised by low percentage carbonates and a high proportion of clastic material. The six cores to the east of Dampier Ridge were all dominantly calcareous in nature. Sedimentation rates calculated for this region were found to be low (1-5.5cm/ky), but doubled during the last glacial.

Shackleton and Kennett (1975) obtained a detailed palaeoclimatic sequence from stable isotope studies of DSDP Sites 277, 279 and 281. Their aim was to examine the earlier development of the Antarctic ice

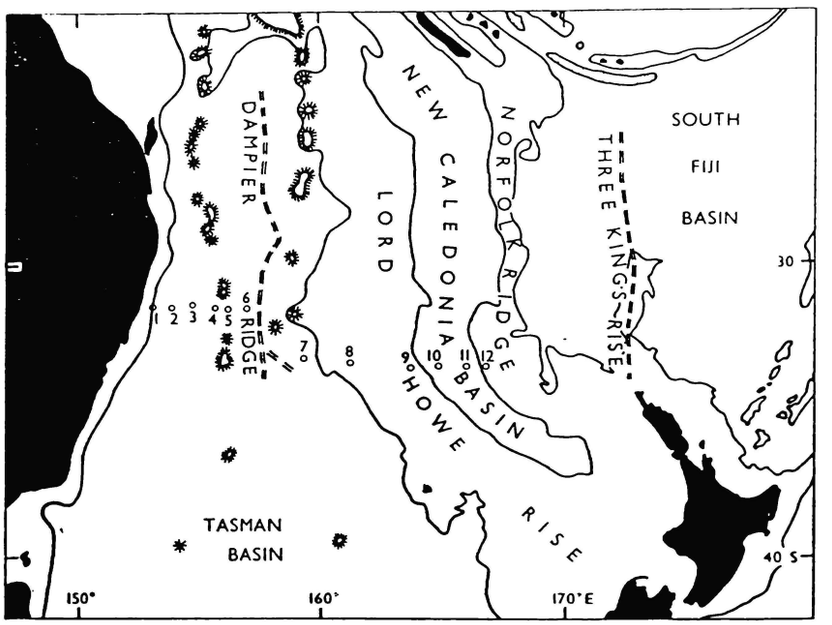

Figure 2.17. The locations of cores Z2101 to Z2112 (nos. 1 to 12) (ex *Oceanographer*) examined by Eade and van der Linden (1971, fig. 1).

sheet and the related deep-temperature structure of the ocean. Isotope changes in the benthic foraminifera *Uvigerina* during the Tertiary were inferred to reflect mainly ice volume changes in polar regions.

Site 284 oxygen and carbon isotope values were examined by Kennett et al. (1979). The oxygen isotope compositions of three species of planktonic foraminifera (*G. quinqueloba*, *G. bulloides* and *Neogloboquadrina*) and one of benthic foraminifera (*Uvigerina*) were shown to display a ranking consistent with palaeo-depth habitat.

Luz (1977) did extensive work on the statistical analysis of planktonic foraminifers. He examined the tops of 78 South Pacific cores in order to derive a transfer function to relate sea-surface temperatures to foraminiferal assemblages. Luz derived a palaeotemperature record of the past 150ky and estimated sea surface temperatures for the last glacial maximum. He found the greatest change between glacial and present-day conditions, and hence the most sensitive region to climatic change, to be at 50°S. Malmgren and Kennett (1981) examined the morphological changes in planktonic foraminifera, since changes in shape measurements may offer a method of stratigraphic correlation between the temperate South Pacific sequences. Changes in these sequences were later examined by Srinivasan and Kennett (1983) over the Oligocene-Miocene transition in South Pacific cores.

Cruises 1063 and 1097 of the r.v. *Tangaroa* collected a large number of piston cores from the Pacific Ocean off the east coast of the South Island. 36 of these cores were studied by Griggs et al. (1983), involving core desciption, textural and microfaunal analysis and carbon-dating of foraminiferal-rich sediment. Griggs et al. found that during low sea level glacial periods South Island east coast rivers delivered vast volumes of sediments to the shelf edge.

Micaceous hemipelagic deposits, consisting mainly of siliceous remains, dominated the sediments of the deep adjacent basins. Increased dissolution of planktonic foraminifera made them rare, with cool-water forms predominating. Higher sea levels during interglacials led to decreased sedimentation in the deep basin, and the retreating of glaciers left deposits in glacial lakes and on the plains. A foraminiferal-rich pelagic sediment was deposited. Late Quaternary marine sedimentation adjacent to southeast New Zealand was thus shown to be dominated by palaeoclimatic influences controlling terrigenous sediment input, dissolution, biogenic productivity and planktonic microfossil migration. Cores Q200, Q217 and Q219 (isotope values presented in this thesis) were among those studied by Griggs et al. for which glacial/interglacial boundaries were assigned on the basis of colour and coarse-fraction changes. These boundaries will be discussed and compared with the isotope boundaries in Chapter 5.

Work to date on DSDP Site 594 (Cuthbertson, 1985; Nelson et al., 1986) has revealed similar pelagic/hemipelagic sedimentation cycles dependent on climate, as were found by Griggs et al., extending back to (and beyond) the Brunhes/Matuyama palaeomagnetic boundary. Site 594 also displayed a correlation between $CaCO_3$ content and climatic conditions. Alpine glaciation in the South Island was shown to be in phase with the major fluctuations of the Pleistocene ice sheets. Site 594 has been resampled at higher resolution, and the stable isotope ratios are presented in Chapter 4.

Chapter Three

SAMPLING AND EXPERIMENTAL TECHNIQUES

3.1 Drill Site Locations

Oceanic sediments for this study were available from two sources: (a) Short piston cores collected (or held) by the New Zealand Oceanographic Institute (NZOI), from New Zealand waters. (b) Long cores of Quaternary sediments collected by the DSDP.

The DSDP have organised a number of cruises designed to provide palaeoceanographic information from continuous sequences with relatively high sedimentation rates, to enable high resolution stratigraphies to be determined. These have included Leg 68 (Carribean, Gulf of Panama), Legs 72-76 (South Atlantic), Leg 85 (eastern equatorial Pacific), and Leg 87 (northwest Pacific). During December 1982/January 1983 a further cruise in this sequence was undertaken. This was Leg 90 which concentrated on the southwest Pacific region.

A sequence of eight middle to late Cenozoic cores (Site numbers 587-594) of high quality were successfully recovered from a series of holes drilled in a transect from 21°S to 45°S. A further site (Site 586) had been drilled on the northern extremity of the ship's traverse during Leg 89. (Site 586 had also previously been occupied during Leg 30 and drilled as Site 289, but this was prior to the development of hydraulic piston core techniques and so was re-drilled at an adjacent site to provide better quality Cenozoic sequences. Site 588 likewise had previously been cored as Site 208 during Leg 21). The inclusion of Site 586 provided a complete traverse of the southwest Pacific from the equator to 45°S.

A number of platforms extending latitudinally across the sea bed makes the southwest Pacific an ideal location for shallow water drilling, as they enable the carbonate sediment rain to be intercepted before it falls below the lysocline and undergoes dissolution in the bottom waters. Site 586 is located on the Ontong-Java Plateau, Sites587-592 are on the Lord Howe Rise, with Site 593 on the Challenger Plateau and Site 594 on the Chatham Rise (Figure 3.1).

The availability of a series of high quality long cores through the Quaternary and located along a traverse from 45°S to the equator (Table 3.1) has provided the impetus for this study of the climatic history of the southwest Pacific. Carbonate preservation within the cores is such that they provide ideal material for an oxygen isotope stratigraphy (Kennett et al., 1986).

Table 3.1. Locations of DSDP Sites 586-594 (Kennett et al., 1986) (depicted in Figure 3.1).

DSDP Site No.	Location	Water Depth (m)
586	00°29.84'S;158°29.89'E	2208
587	21°11.08'S;161°19.99'E	1101
588	26°06.70'S;161°13.60'E	1533
589	30°42.72'S;163°38.39'E	1391
590	31°10.02'S;163°21.51'E	1299
591A	31°35.06'S;164°26.92'E	2131
592	36°28.40'S;165°26.53'E	1098
593	40°30.47'S;167°40.47'E	1068
594	45°31.41'S;174°56.88'E	1204

In order to provide a more complete picture of the water masses in this region seven further cores were analysed from the NZOI collection

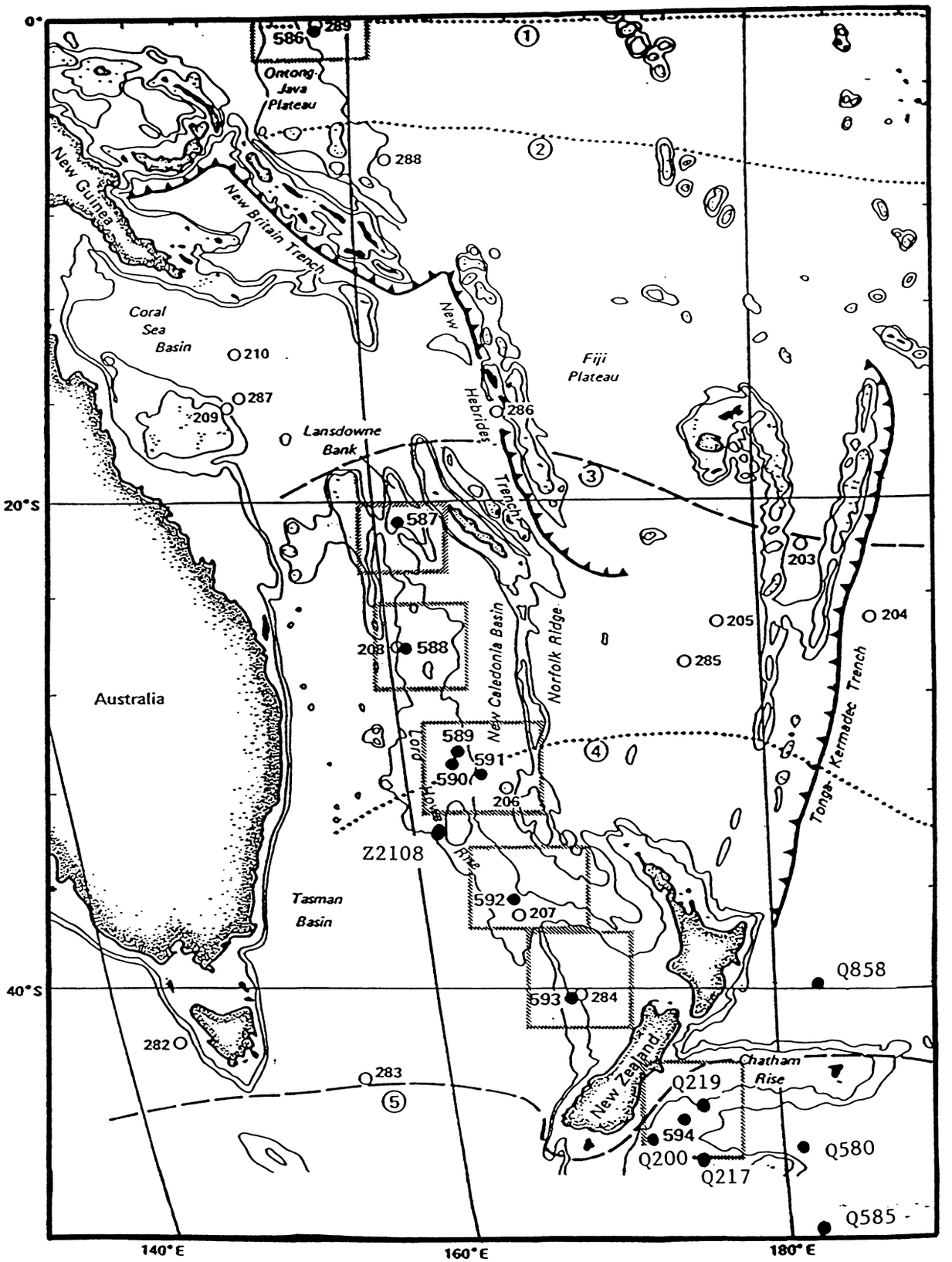

Figure 3.1. Physiographic diagram (adapted from Kennett et al., 1986, p.4) of core sites sampled in this thesis. Numbers 1 to 5 mark major water mass boundaries: 1)Equatorial Divergence. 2)Southern Tropical Divergence. 3)South Tropical Convergence. 4)Subtropical Divergence. 5)Subtropical Convergence. The contour line marks 1000 fathoms.

in Wellington. These are short piston cores recovered from the r.v. *Tangaroa* (with the exception of Z2108, which was collected by the r.v. *Oceanographer* (see Section 2.3)). These cores, and their site locations, are listed in Table 3.2.

Table 3.2. Site locations of NZOI cores (see also Figure 3.1).

Site No.	Year[1]	Location	Water Depth (m)
Z2108[2]	1967	33°22.6'S;161°36.8'E	1448
Q858	1983	39°49.6'S;178°03.5'W	3735
Q219	1979	45°00.9'S;174°59.2'E	1122
Q200	1979	45°59.7'S;172°01.5'E	1370
Q580	1980	46°12.2'S;179°00.0'W	3964
Q217	1979	46°27.9'S;175°04.0'E	1936
Q585	1980	49°42.2'S;177°55.5'W	4354

[1]Refers to year of coring.
[2]Cored by U.S. Geodetic Survey, samples held at NZOI.

3.2 Samples

3.2.1 Sample Collection

Shipboard sampling of the Quaternary section of DSDP cores from Leg 90 was done on board *Glomar Challenger* by the shipboard scientists, including Dr. C.S.Nelson (University of Waikato). About 10cc plugs were taken from the cores at 20-40cm intervals. These plugs were sealed in polythene bags until use. All samples were assigned a sample number in accordance with DSDP convention (i.e., core number-section number-depth in section). Each section within the core being 1.5m long. For example, a sample designated as 3-2-120 means the sample has been taken from 120cm down the 2nd section of core number 3 at a given site location. The site numbers run consecutively from the

first site drilled in 1968. The first hole drilled at a site bears only the site number, subsequent holes are given the site number and a letter. e.g., 594, 594A, 594B, etc. Further high resolution samples were provided by the DSDP on request.

NZOI samples were taken at 10cm intervals from cores held in storage in Wellington, and were handled in an identical fashion to the DSDP samples.

The DSDP cores chosen for analysis were to provide a complete picture of $\delta^{18}O$ changes occurring in the New Zealand region during the Late Quaternary. As Site 594 had already provided an exceptionally detailed record of these changes (Cuthbertson, 1985), attention was focused on the NZOI sites to the east of New Zealand in the vicinity of Site 594.

3.2.2 Sample Preparation (Initial Treatment)

All samples for analysis were treated in exactly the fashion described below in order to minimise variations in results due to inconsistencies in experimental procedure.

Method

$\frac{1}{2}$ to $\frac{3}{4}$ of the sample plug was placed in a wide-necked 50ml flask. 40ml of pH 9.4 buffer solution was then added. This solution was prepared by dissolving 4g of $NaHCO_3$ and 1-3g of Na_2CO_3 (the pH is adjusted to 9.4 by the Na_2CO_3 addition) in 20l of distilled water, as described by Hay (1977). pH 9.4 allows the best dispersion of clays, and enables them to be most easily eliminated from the sample. In addition, dissolution of the foraminiferal tests is minimised.

The sample and solution were gently agitated for 10-15min on an auto-shaker to aid disaggregation, and then left soaking overnight. (Some samples proved difficult to sieve and were left soaking for

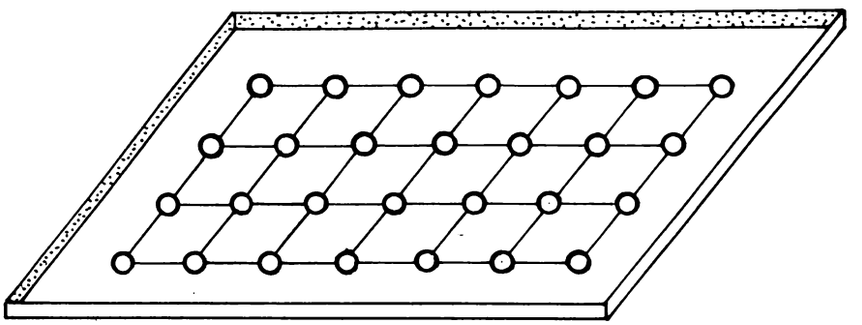

Figure 3.2. Picking tray used in the selection of foraminiferal samples by microscope (actual size 8 X 5 X 0.25cm).

several days as necessary). The next day samples were washed through a 63μm-mesh sieve with the buffer solution. The <63μm mud fraction (or silt + clay) was left to settle, and the supernatant liquid removed by suction. The remaining 50ml volume suspension was washed into a glass jar and stored at 4°C for percentage mud and S.E.M. nannofossil analysis.

The >63μm fraction was washed with distilled water back into the 50ml flask and probed in a sonic bath for 10sec. The samples were then re-sieved to remove the fine material (of <63μm) released in this fashion. The remaining >63μm fraction was then washed onto filter paper, rinsed, and dried at room temperature. The dried samples were weighed and the percent sand determined.

The >63μm samples were then sieved through a 125μm-mesh sieve, and the >125μm fraction was weighed to determine "coarse" sand content. This coarse fraction was spread over a picking tray and placed under a microscope. (The picking tray was a flat piece of metal, painted matt black for easier viewing, with raised sides and holes at regular intervals across the surface (Figure 3.2). This allowed the foraminifera to be dropped through to the sample bottle fixed below the microscope stage. 10-20 specimens of the benthic foraminifer *Uvigerina* spp. (Figure 3.3) were then picked for isotopic analysis (*Uvigerina perigrina* was the preferred species, and species very similar in structure). Since planktonic foraminifera have less shell than the heavier, bottom-dwelling benthics, 30-35 *Globigerina bulloides* d'Orbigny (Figure 3.4) were picked for the planktonic sample. A uniform size (250-350μm) of this species was sought, since they float in the ocean at a depth that is dependent on their weight (Ramsay, 1977). Where *Uvigerina* spp., and *G.bulloides* were not present (in cores taken from the more northern sites, 586 and 588) two

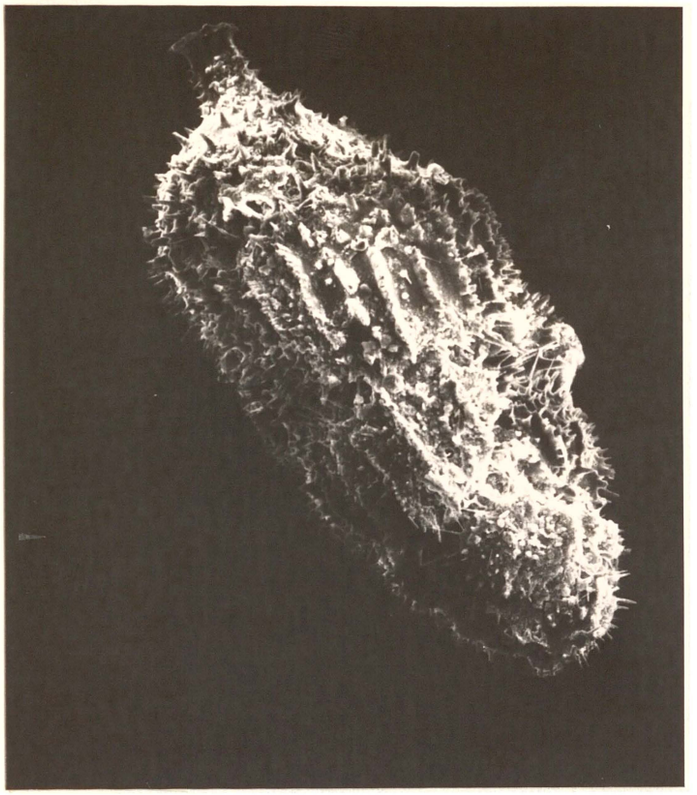

Figure 3.3. Scanning electron microscope (SEM) photograph of *Uvigerina* spp.

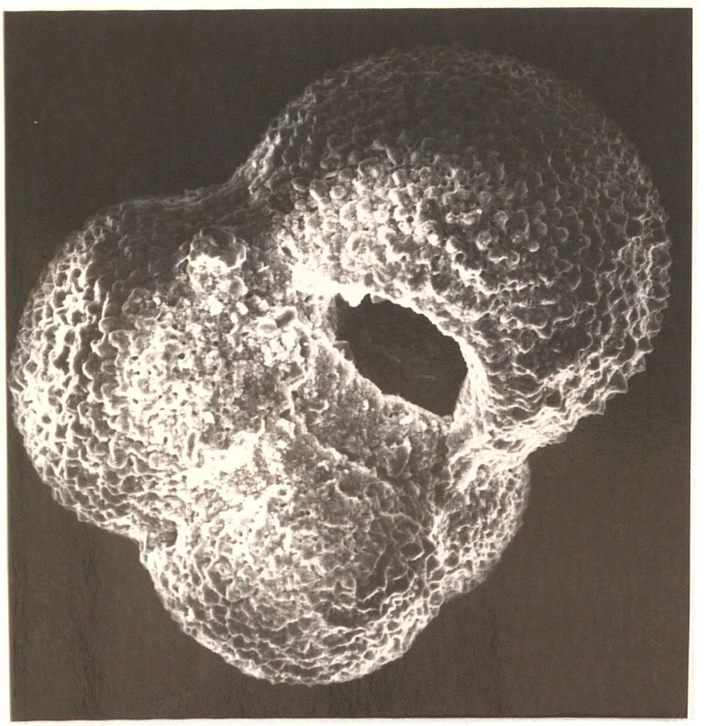

Figure 3.4. SEM photograph of *Globigerina bulloides* d'Orbigny.

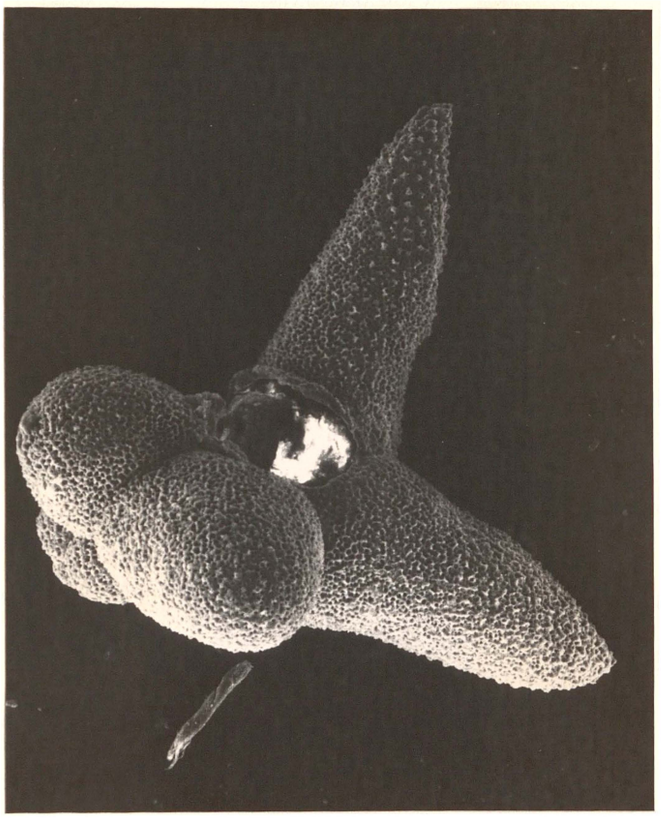

Figure 3.5. SEM photograph of *Globigerina sacculifera*.

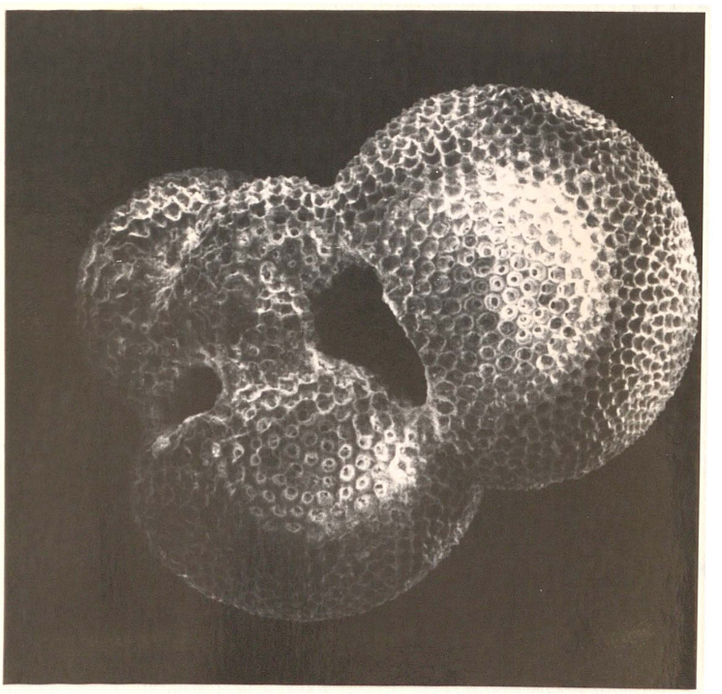

Figure 3.6. SEM photograph of *Globigerina ruber*.

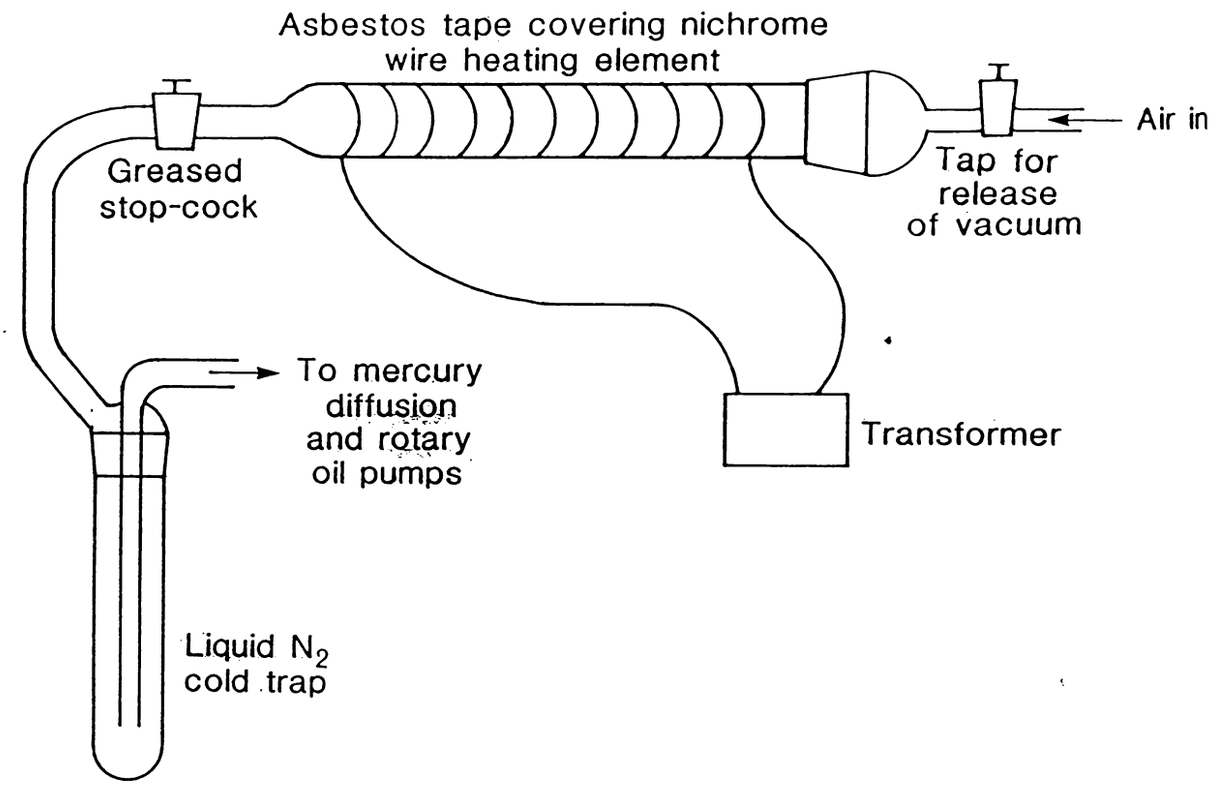

Figure 3.7. Vacuum furnace tube for the roasting of foraminiferal samples.

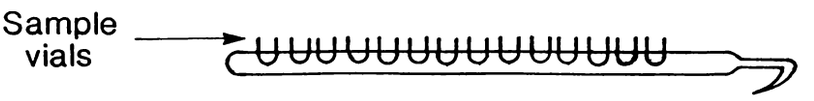

Figure 3.8. Piccolo tube for holding samples vials upright in the furnace.

planktonic species were picked. These were *Globigerina sacculifera* (Figure 3.5) and *Globigerina ruber* (Figure 3.6).

After picking, all samples were washed with methanol and probed ultrasonically for 1min to remove any extraneous material, and then left until the methanol had completely evaporated. The clean samples were finally checked under the microscope, where unwanted material and unsuitable specimens were removed, and the foraminifera recounted. They were then stored in small glass bottles until analysis.

3.3 Vacuum Roasting

Residual organic contaminants were removed from the purified foraminiferal samples by vacuum roasting at 400°C. This treatment may not have been essential in all cases, but a standardised treatment of samples was desirable.

The roasting tube consisted of a pyrex cylinder wound around with nichrome wire, to form the heating element, and then covered with several layers of asbestos insulation paper (after Burns, 1980) (Figure 3.7).

The samples were placed in small glass vials, which were held by a hollow glass tube with holes in it, called a piccolo (Figure 3.8). The piccolo had a hook at one end to facilitate extraction from the furnace tube. The glass stopper was sealed with high vacuum silicon grease and the tap to the air was closed. The entire system was then evacuated to ~1μm Hg for 15min and then the heating element was turned on. Samples were roasted for $2\frac{1}{2}$h and then allowed to cool under vacuum.

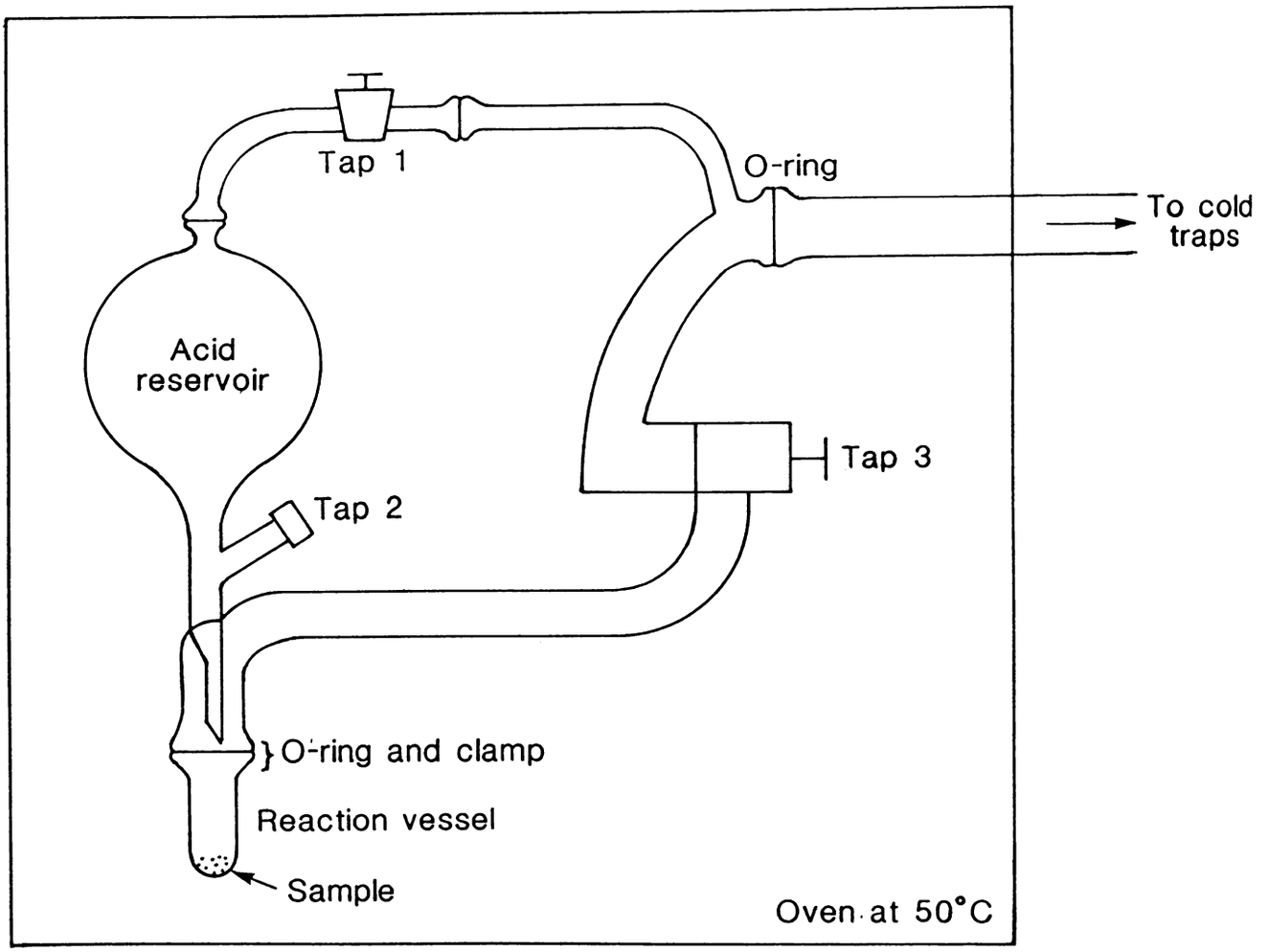

Figure 3.9. $CO_{2(g)}$ generation line, contained within an oven at 50°C.

3.4 Preparation of the CO_2 Sample

The system used for CO_2 generation was a modified version of that employed by Burns (1980), who based his design on Shackleton (1965a, 1965b). Shackleton described a method of production of CO_2 gas from very small samples by reaction with 100% H_3PO_4 (see discussion in Section 1.3).

The equipment used is shown schematically in Figures 3.9 and 3.10. Burns' original design involved ten reaction vessels attached to the reaction line manifold. This, however, led to problems of isotopic fractionation varying with the position of the sample down the line. The line was redesigned with only one reaction vessel operating at a time, and then further modified to duplicate this set-up with an equal length of tubing in each of the two lines. With this modification the line satisfied the requirements for handling small volumes of CO_2:

1. Complete CO_2 collection.
2. No isotopic exchange.
3. No contamination of samples (by air, water, grease, pump oil etc.).

Moreover, the two lines operated with staggered timing allowed for production of CO_2 as quickly as the mass spectrometer could analyse the previous sample gas, and so was very efficient.

The CO_2 production part of the line was contained within an oven kept at 50°C, as described by Shackleton (1965a). This was constructed on a trolley for easy removal from the vicinity of the mass spectrometer. The cold traps were immersed in dewars containing 50:50 ethanol:propanol mixed with liquid nitrogen and kept between -90°C and -110°C.

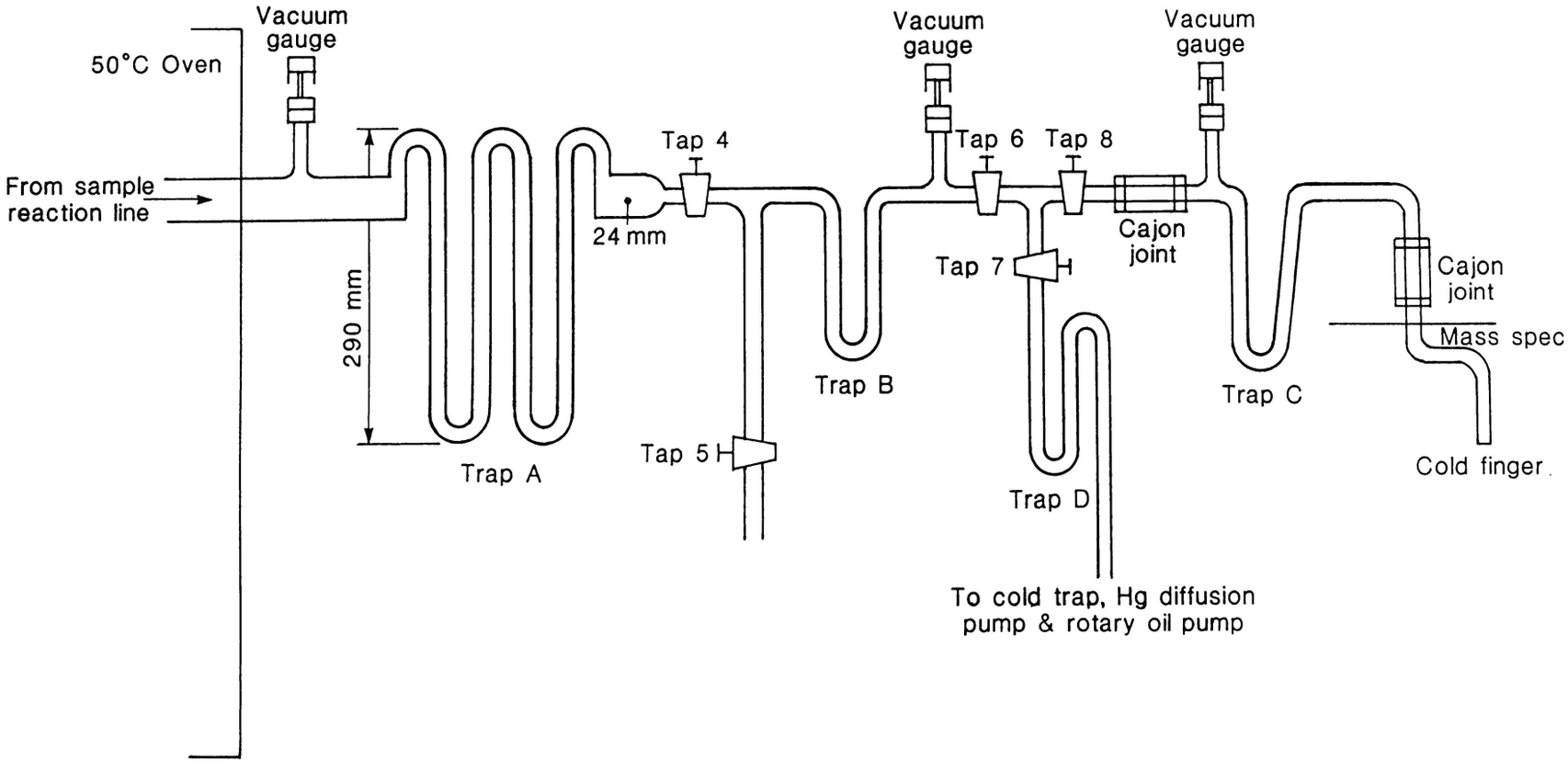

Figure 3.10. Gas sample collection line, with cold traps for the removal of water.

3.5 Orthophosphoric acid

The orthophosphoric acid was prepared by the following method (after Duplessy - pers. commun., 1983): 100-200ml of 80% H_3PO_4 (B.D.H. Analar grade) was put in the bowl of a rotary evaporator and the system evacuated using a rotary oil pump. The presence of a large cold trap surrounded with liquid nitrogen helped to remove water as it was driven off. The acid was heated progressively to 200°C over 6h, and was then left overnight at room temperature. The next day it was again heated at 200°C for 6h, and then for 1 further hour at 220°C. This acid was cooled under vacuum and then poured into the acid reservoir of the reaction line. An outline of certain problems encountered with the use of this acid is presented in Section 3.9.

3.6 The Mass Spectrometer

Since the completion of Burns' (1980) experimental work, modifications have been carried out on the original Micromass 602c mass spectrometer (manufactured by V.G. Micromass Ltd., England). (For detailed operating instructions see Cuthbertson, 1985).

The Micromass 602c is a 90° sector magnetic deflection instrument, with a 6cm radius. The gas is introduced to the mass spectrometer through a double batch inlet system with balanced capillary leaks. It then flows through an all-metal solenoid-operated changeover valve, of the type described by M^{c}Kinney et al. (1950), to the ion source. A balanced flow is maintained by bleeding away the gas not being analysed.

TS63 M46

Raw data:

	Major (nA)	Ratio (ppm)
R	1.28797	10402
S	1.28281	10415
R	1.28148	10400
S	1.27382	10415
R	1.27557	10398
S	1.27140	10415
R	1.26998	10397
S	1.26605	10412
R	1.26468	10397
S	1.26091	10410
R	1.25925	10395
S	1.25522	10410

Delta values (per mil)

1	1.358
2	1.487
3	1.576
4	1.498
5	1.426
6	1.436
7	1.414
8	1.376
9	1.409
10	1.477

Mean delta	1.446	mil
2 sigma 10	0.001	
Ref ratio	10398	ppm

M45

Raw data:

	Major (nA)	Ratio (ppm)
R	0.76535	29827
S	0.76507	29849
R	0.76311	29826
S	0.76290	29846
R	0.76073	29826
S	0.76082	29843
R	0.75819	29824
S	0.75837	29844
R	0.75563	29823
S	0.75626	29841
R	0.75269	29820
S	0.75397	29841

Delta values (per mil)

1	-5.949
2	-5.999
3	-6.051
4	-6.093
5	-6.102
6	-6.043
7	-6.017
8	-6.053
9	-6.038
10	-5.976

Mean delta	-6.032	/mil
2 sigma 10	0.006	
Ref ratio	29824	ppm

Figure 3.11. Printout from the HX-20 control unit of the mass spectrometer.

Twin Farraday plate collectors allow the enrichment of a gas of unknown isotopic composition to be related directly to that of a known standard.

The 602c at Waikato University has been modified by the replacement of the amplifiers and the addition of an Epson HX-20 control unit to bring it up to 602e specifications. The HX-20 is programmed to take ratio data from sample and reference gases over twelve operations of the changeover valve. It then prints out pressure and ratio data for the twelve changeovers and automatically calculates the ten delta values obtained from these changeovers, and the mean per mille deviation. An example of the type of printout obtained is shown in Figure 3.11.

3.7 Per Mille Deviations

$^{13}C/^{12}C$ and $^{18}O/^{16}O$ ratios are reported as per mille ($^{o}/_{oo}$) deviations (δ values) from a standard. Hence for a sample A with isotopic ratio R, compared with a standard of isotopic ratio R_{std}, the mass spectrometer would normally be giving:

$$\delta_{std}\ A = \frac{R - R_{std}}{R_{std}} \times 1000$$

where a positive delta value is indicative of an enrichment, and a negative value a depletion, in the heavier isotope with respect to the standard.

However, the employment of a mobile trolley carrying the reaction line meant that, in order to avoid a long connection between the reaction line and the mass spectrometer, the sample gas had to be introduced to what was normally the reference side of the mass

spetrometer. Since this resulted in the mass spectrometer being operated "backwards" the HX-20 was calculating δ values from:

$$\delta_{std}\ A = \frac{R_{std} - R}{R} \times 1000$$

This meant that the signs of the δ values were opposite to what they would have been had the mass spectrometer been set up in the usual fashion, hence adjustments were made accordingly. A difference in the per mille deviation result also occurred, but since the sample and reference ratio values were similar the difference was only small, and even in extreme cases where δ45 or δ46 reached $5^{o}/_{oo}$ the error was only $0.02^{o}/_{oo}$, which was not significant - being less than the standard deviation of the NBS-19 value (discussed in Section 3.8).

The mass distribution of carbon and oxygen isotopes in natural CO_2 is shown in Table 3.3. It may be seen that to measure the $^{13}C/^{12}C$ ratio the mass spectrometer must compare the mass 45 and mass 45+44 ion beams, and for the $^{18}O/^{16}O$ ratio mass 46 and mass 45+44 must be compared.

Table 3.3. The mass distribution of carbon and oxygen isotopes in natural CO_2 (from M^{c}Crea, 1950).

Mass	Contributing species	Individual abundance	Relative abundance of given mass
44	$^{12}C^{16}O_2$	0.9842	0.9842
45	$^{13}C^{16}O_2$	$1.095X10^{-2}$	0.01172
	$^{12}C^{16}O^{17}O$	$7.7X10^{-4}$	
46	$^{12}C^{16}O^{18}O$	$4.025X10^{-3}$	0.00403
	$^{13}C^{16}O^{17}O$	$1.6X10^{-6}$	
	$^{12}C^{17}O_2$	$1.5X10^{-7}$	
47	$^{13}C^{16}O^{18}O$	$4.48X10^{-5}$	$4.63X10^{-5}$
	$^{12}C^{17}O^{18}O$	$1.6X10^{-6}$	
	$^{13}C^{17}O_2$	$1.7X10^{-9}$	
48	$^{12}C^{18}O_2$	$4.12X10^{-6}$	$4.13X10^{-6}$
	$^{13}C^{17}O^{18}O$	$1.8X10^{-8}$	
49	$^{13}C^{18}O_2$	$4.6X10^{-8}$	$4.6X10^{-8}$
All	All	1.0000	1.0000

A number of corrections must be made to the δ45 and δ46 values to obtain the $\delta^{13}C$ and $\delta^{18}O$ values. This is partly because the ion beams of mass 45 and mass 46 are composed of a variety of different isotopic ions, and also because the double collector system measures both mass 45 and mass 44 on the minor collector, when set up on mass 46. In addition, the final $\delta^{13}C$ and $\delta^{18}O$ results are required relative to the PDB standard (discussed in Section 3.8) for which a conversion equation is needed. The equations used for this thesis have been derived by Burns (1980), based on work by Mook (1968) and Grinstead

(1977). Adjustments have been made to allow for the different international standard used (Burns used NBS-20).

The equations are:

$$\delta^{18}O_{PDB} = 0.999\ \delta 46 + 0.0098\ \delta 45 - 0.80$$

$$\delta^{13}C_{PDB} = 1.063\ \delta 45 - 0.034\ \delta 46 - 4.50$$

These give the $\delta^{18}O$ and $\delta^{13}C$ values with respect to PDB (refer to Section 3.8). This is done by a series of comparisons: The sample is analysed in conjunction with a local standard gas (in this case WLS). WLS is analysed against an international standard (NBS-19), and NBS-19 has previously been run against PDB (Coplen et al., 1983). Thus the enrichment or depletion of the sample, relative to PDB, may be determined. (The standards WLS, NBS-19 and PDB mentioned here are all discussed in Section 3.8).

These equations are valid only when differences between the sample and standard are small ($<10^{o}/_{oo}$), as it is only in this range that correction factors for tail contribution, zero enrichment, memory effect, and valve mixing can be ignored (Grinstead, 1977).

3.8 Standards

The PDB standard (not now available) was the CO_2 obtained from the reaction of 100% H_3PO_4, at 25°C, with a belemnite guard from *Belemnitella americana*, a Cretaceous belemnite from the Pee Dee Formation in North Carolina, U.S.A. (Friedman and O'Neill, 1977). Various international standards have been run against PDB for comparative purposes. Following advice from Shackleton (Cambridge

University, U.K.) and Blattner (Institute of Nuclear Sciences, N.Z.), NBS-19 was adopted as a standard, which was obtained from the National Bureau of Standards (Washington, D.C.) in a coarsely ground form. Just before reaction with the H_3PO_4 it was ground up further to lower reaction times.

The NBS-19 (TS limestone) calibration values with respect to PDB, as quoted by the National Bureau of Standards, are presented in Table 3.4.

Table 3.4. Calibration of NBS-19 (Coplen et al., 1983).

cf. PDB	NBS-19	σ
$\delta^{13}C$	1.92	0.02
$\delta^{18}O$	-2.19	0.02

The δ45 and δ46 values obtained from running NBS-19 against the local standard, WLS, are given in Table 3.5.

Table 3.5. NBS-19 cf. WLS.

cf. WLS	NBS-19	σ
δ45	5.99	0.04 (over 100 values)
δ46	-1.45	0.10 (over 157 values)

WLS was the reference gas used as a running standard. It was prepared by Burns from the reaction of Waikato Limestone with 100% H_3PO_4. The bulk of this reference was contained in a 9l glass storage cylinder, and a small aliquot of gas was removed for use in the mass spectrometer. A new aliquot was used every three days, since the

reference gas slowly fractionates as it bleeds through a capillary tube in the mass spectrometer when it is running.

3.9 Experimental Problems

3.9.1 Acid Deterioration

During the course of the experimental work it became apparent that the H_3PO_4 used in CO_2 generation was not stable, in that over a period of several days the standard δ46 values would change. The average NBS-19 δ46 values for successive days are presented in Table 3.6.

Changing the method of production to that of Shackleton (pers. commun., 1987) did not result in any improvement. (Shackleton's method involved heating the acid in a water bath, so that the temperature did not rise above 100°C). However, as the values obtained for days 1 and 2 were always consistent these were used to determine the mean δ46 value for NBS-19 (given as $-1.45°/_{oo}$ in Table 3.5). A standard was run at the end of each day, and it was found that the acid did remain stable for the 8-10h that it was used in a days work. Hence on days 3 and 4 it was possible to adjust the δ46 values to correct them to the average for the standard. δ45 values were not found to alter with time (the standard deviation of 100 δ45 values, over all four days, was only $0.04°/_{oo}$).

Table 3.6. Variation of NBS-19 δ46 values with increasing age of H_3PO_4

Days after preparation.	NBS-19 δ46 (wrt WLS).	σ
1	-1.40	0.08 (over 82 values)
2	-1.51	0.12 (" 75 ")
3	-1.60	0.15 (" 46 ")
4	-1.72	0.23 (" 42 ")

Both Shackleton and Duplessy stated that their acid was usable for some months after production, but this was certainly not the case at Waikato where instability of the acid necessitated making up a new "batch" every week. It was thought that if the acid was made up in a large volume, and allowed a period of time for stabilisation, then the day to day stability could well be improved, but unfortunately this did not prove to be the case. Making up the acid on a weekly basis had to suffice, and did not in any way hinder the analytical process. It is possible that the inconstant behaviour observed with the H_3PO_4 arises as a result of the formation of a mixture of polyphosphoric acids, and that these continue to form through elimination of water and polymerisation. Long-term storage of the "100%" H_3PO_4 often resulted in the entire mass crystallising, even when stored at 50°C.

3.9.2 Instrumental Difficulties

For the benefit of future operators some of the problems encountered with the use of the 602e Micromass are mentioned here.

Apart from electronic faults (which should only be dealt with by the electronics technicians) the principal problem involves the integrity of the taps. Since the 602e at Waikato University is not devoted to only one mode of operation there is frequent changing of

the connections into the inlets. This unfortunately entails the ingress of a great deal of air and dust into the system which probably contributes to the problems of leaking taps (careless use will likewise contribute to this). Closure of the taps involves a knife edge pressing into a soft copper disk, and when the disk is less than clean a perfect seal is not achieved. Tightening of the taps to increase the pressure on the disks works for a while, but eventually the soft disk becomes impressed by the knife edge and so the seal slackens off again. Frequent tightening hence means frequent replacement of the copper disks, which is both time consuming and ultimately expensive. Care should be taken to treat the taps with respect.

In addition to leakage, some problems have been encountered with the incomplete opening of the taps: A spring washer is supposed to open the taps when the knife edge is lifted, but when these get older the "spring" of the metal is lost and the taps do not open sufficiently to allow the gas to flow through quickly. Fractionation then results, with the molecules containing the light isotopes moving more rapidly through the restricted tap opening than those containing the heavy isotopes. The translational velocities of the gas molecules are inversely proportional the square roots of the ratio of their molecular weights (Hoefs, 1973).

So for CO_2 $$\frac{\text{velocity } (^{12}C^{16}O^{16}O)}{\text{velocity } (^{13}C^{16}O^{16}O)} = \sqrt{\frac{45}{44}} = 1.011$$

and $$\frac{\text{velocity } (^{12}C^{16}O^{16}O)}{\text{velocity } (^{12}C^{18}O^{16}O)} = \sqrt{\frac{46}{44}} = 1.022 .$$

The delta values are obtained from the equation

$$\delta = 1000 \left(\frac{R_{sample}}{R_{standard}} - 1 \right).$$

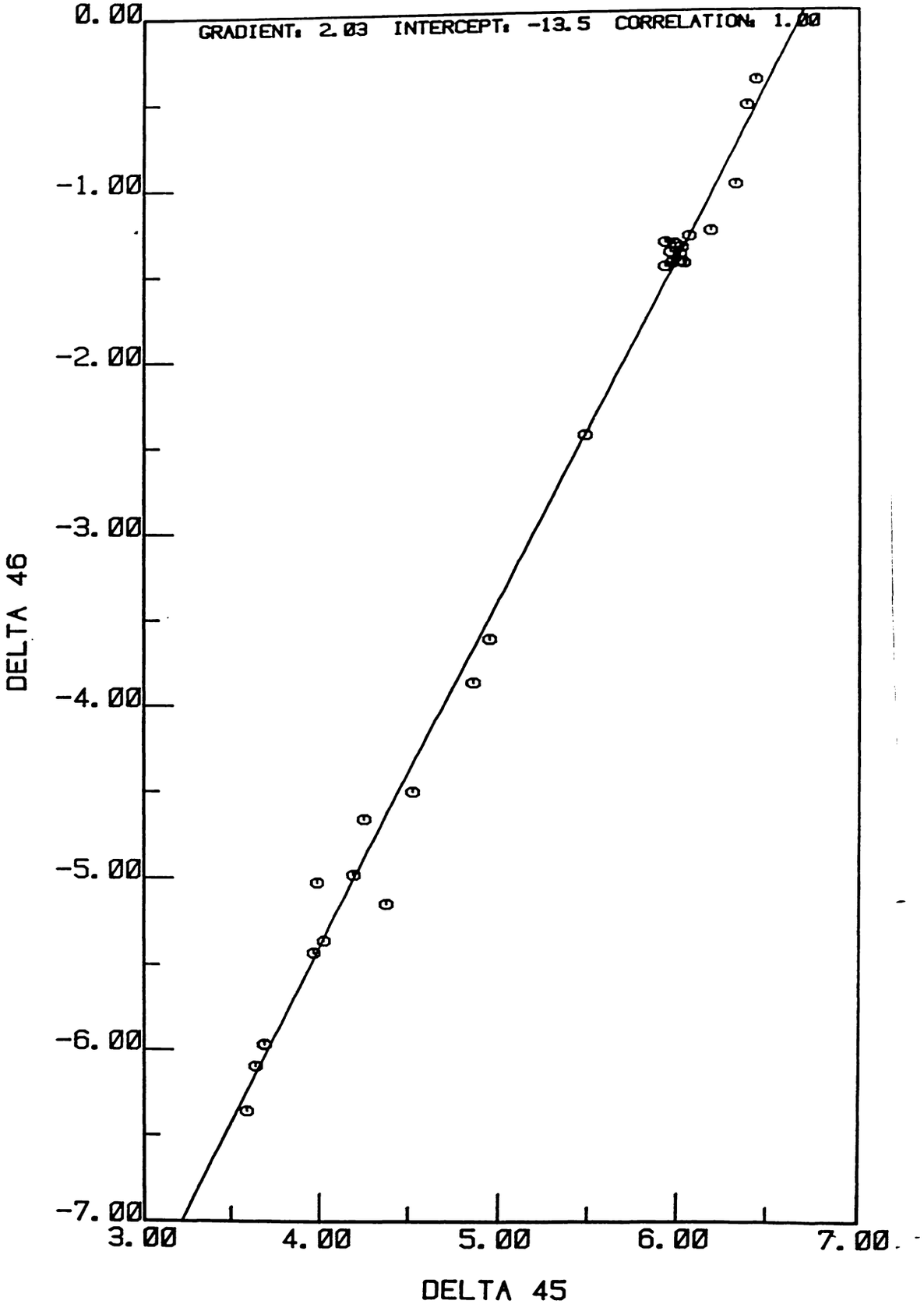

Figure 3.12. Plot of the δ45 and δ46 mass ratios of CO_2 generated from NBS-19. The gradient reflects the fractionation difference due to mass between δ45 and δ46.

The standard is the unfractionated gas volume in this case, so

$$R_{sample} = 1.011\ R_{standard} \qquad \text{for mass 45,}$$

and $$R_{sample} = 1.022\ R_{standard} \qquad \text{for mass 46.}$$

Thus for mass 46:

$$\delta 46 = 1000\ (1.022 - 1) = 22$$

and for mass 45:

$$\delta 45 = 1000\ (1.011 - 1) = 11\ .$$

Hence it may be seen that there is a 2:1 fractionation factor for δ46 cf. δ45, which is represented by the slope of the graph in Figure 3.12. The figure shows the spread of δ45 and δ46 values obtained from NBS-19 (against WLS) when the inlet tap on the sample was not opening sufficiently, and well illustrates the fractionation that occurs. The cluster of results around -1.40 to -1.50 (δ46) and 6.00 (δ45) are the unfractionated "correct" values.

Another problem which occurs is the "sticking" of the changeover valve, as it fails to shift completely between sample and reference. This is clearly seen by an unexpected drop in the ratio reading (usually only for one value) which affects three of the computed δ values. Clearly if this occurs too frequently it is a major problem. This usually means that the sapphire bearings on which it operates have become chipped and servicing is required.

3.9.3 Calculation Problems

Comparison of the results presented in Chapter 4 for Cores 593 and 594 with previously published data (Nelson et al., 1986, 1986a) reveal considerable differences in $\delta^{18}O$ and $\delta^{13}C$ values. This is partly due

to early problems with standards in the original work, and partly due to a subsequently detected error in the calculation of $\delta^{18}O$ and $\delta^{13}C$ values relative to PDB (see Section 3.7). This error has since been corrected, the previously published results being too light by $0.26^{o}/_{oo}$ for $\delta^{18}O$, and too heavy by $0.87^{o}/_{oo}$ for $\delta^{13}C$.

Chapter Four

PRESENTATION OF DATA

The $\delta^{18}O$, $\delta^{13}C$, and $\%CaCO_3$ values measured in this study are presented in this chapter. The stratigraphic logs for each of the DSDP cores (Kennett et al., 1986, (I)), and for the NZOI cores, where available, are in Appendix I.

Unless otherwise indicated the planktonic foraminiferal species analysed is *Globigerina bulloides*, and the benthic species is *Uvigerina* spp. In each of the tables '-' indicates that no data is available.

4.1 DSDP Cores

586 Site 586 is located near the equator at 0°29.84'S;158°29.89'E in a water depth of 2208m (see Figure 3.1). The sediments comprise a single lithologic unit of foraminifera-nannofossil ooze of which the top 4m were analysed in this study. No obvious reworking of the foraminifera could be detected by the shipboard scientists, and the biostratigraphy appeared undisturbed (Kennett et al., 1986, (I)).

As 586 yielded insufficient numbers of benthic foraminifera to make stable isotope analysis feasible it was decided to analyse two species of planktonic foraminifera. *G. bulloides* was absent, which was not unexpected as it is restricted to Subantarctic and temperate water masses and is rare in equatorial waters (Kennett and Srinivasan, 1983). Instead, *Globigerina ruber* and *Globigerina sacculifera* were picked from the top 4.2m of core. The results from these analyses are presented in Table 4.1.

Table 4.1. Results of the stable isotope analysis of *Globigerina ruber* and *Globigerina sacculifera* from DSDP Core 586.

Sub-bottom Depth (m)	*G. ruber* $\delta^{13}C$	$\delta^{18}O$	*G. sacculifera* $\delta^{13}C$	$\delta^{18}O$
0.01	1.24	-2.57	1.73	-2.40
0.11	1.13	-2.62	1.83	-1.67
0.21	1.25	-1.82	1.71	-1.06
0.31	1.02	-2.06	1.52	-1.19
0.40	1.14	-1.67	1.60	-1.52
0.51	1.29	-2.38	1.92	-1.57
0.61	0.96	-2.68	1.04	-2.42
0.71	0.88	-1.45	1.00	-1.01
0.81	0.67	-1.93	1.16	-1.23
0.91	0.64	-2.12	0.90	-1.72
0.99	0.98	-2.49	1.08	-1.99
1.01	0.52	-1.88	1.21	-1.36
1.09	0.93	-2.27	1.18	-1.78
1.20	0.81	-1.44	1.48	-0.81
1.31	1.14	-0.97	1.33	-0.51
1.41	-	-	1.62	-1.52
1.51	1.09	-1.75	1.45	-1.50
1.61	1.04	-0.91	1.54	-0.38
1.71	1.15	-0.82	1.58	-0.55
1.81	1.00	-1.11	1.63	-1.00
1.93	-	-	1.91	-0.03
2.01	1.32	-0.62	1.85	-0.47
2.12	1.71	0.02	1.89	-0.40
2.21	1.48	-0.72	1.48	-0.95
2.31	-	-	1.70	-1.39
2.41	1.54	-1.63	1.77	-1.37
2.51	1.56	-1.85	1.59	-1.46
2.61	1.72	-1.33	1.55	-1.41
2.71	1.80	-1.63	1.77	-1.33
2.81	2.06	-1.21	1.70	-1.92
2.91	1.73	-2.02	1.63	-1.76
3.01	2.00	-2.02	1.88	-1.98
3.11	1.65	-2.17	1.53	-1.92
3.21	1.77	-1.87	1.53	-2.06
3.31	1.93	-2.12	1.63	-1.78
3.41	1.42	-1.69	1.61	-2.04
3.51	1.17	-1.35	1.25	-1.42
3.61	0.74	-1.10	0.96	-1.57
3.71	-	-	1.53	-0.34
3.81	-	-	1.81	-0.24
3.91	-	-	2.16	-0.35
4.01	-	-	1.94	-0.29
4.11	-	-	1.80	-0.53
4.21	1.27	-0.74	1.83	-0.20

587 Site 587 is located at 21°11.08'S;161°19.99'E, in a water depth of 1101m (see Figure 3.1). After washing and sieving it was found that the coarse sand fraction (>125μm) consisted predominantly of coral and algal fragments, and that foraminifera were not present in sufficient

numbers to make analysis practicable. Consequently, no results are presented for 587.

588 Site 588 is located at 26°6.7'S;161°13.6'E, in a water depth of 1533m (see Figure 3.1). The top 6.5m of core consisted of an orange to brown (oxidised) foraminifer-bearing nannofossil ooze. Shipboard biostratigraphy indicated excellent preservation of the calcareous fossils in the upper part of the sequence (Kennett et al., 1986, (I)). Site 588 is in too northerly a position for *G. bulloides* to thrive, and once again an alternative species (*G. ruber*) was analysed. *Uvigerina* spp. were present and were picked as the benthic foraminifera. The results of these analyses from the top 3m of 588 are presented in Table 4.2.

Table 4.2. $\delta^{18}O$ and $\delta^{13}C$ values for *Globigerina ruber* and *Uvigerina* spp. from DSDP Core 588.

Sub-bottom	*G. ruber*		*Uvigerina*	
Depth (m)	$\delta^{13}C$	$\delta^{18}O$	$\delta^{13}C$	$\delta^{18}O$
0.02	0 .83	-0.74	-	-
0.11	0.60	-0.46	0.09	4.35
0.21	1.11	0.14	-0.06	4.42
0.31	0.78	-0.04	-0.13	4.69
0.41	0.58	-0.31	-0.02	3.82
0.51	0.74	-0.13	-	-
0.61	0.60	0.06	0.00	3.60
0.71	0.16	0.08	0.19	4.30
0.81	0.25	-0.01	-0.03	3.76
0.91	0.62	0.13	-0.22	4.96
1.00	0.51	0.19	-0.02	4.23
1.11	0.35	0.51	-0.16	4.15
1.21	0.54	0.51	-0.13	4.36
1.32	0.62	0.48	-0.24	4.48
1.41	0.56	-0.07	-0.05	3.63
1.49	0.77	-0.13	0.06	3.38
1.61	0.25	-0.10	-0.24	3.78
1.71	0.56	0.13	0.06	3.64
1.81	-0.02	-0.08	-0.03	4.58
1.91	0.02	0.04	-0.30	5.10
2.01	0.16	0.15	0.47	5.18
2.11	-	-	0.44	5.16
2.21	0.41	0.29	0.70	4.86
2.31	-0.83	-0.20	0.74	4.37

Table 4.2 cont.

Sub-bottom Depth (m)	*G. ruber* $\delta^{13}C$	$\delta^{18}O$	*Uvigerina* $\delta^{13}C$	$\delta^{18}O$
2.41	0.74	-0.34	0.81	4.44
2.51	0.38	-0.36	0.63	3.87
2.61	0.19	-0.49	0.44	4.07
2.71	0.41	0.06	0.23	5.64
2.81	0.66	0.18	0.43	4.12
2.91	0.50	0.02	0.12	5.24
2.99	0.86	0.32	0.61	5.15

589 Site 589 is located at 30°42.72'S;163°38.39'E, in a water depth of 1391m (see Figure 3.1). Failure of the shipboard positioning computer meant that only four Quaternary to latest Pliocene cores were taken at this site, to a sub-bottom depth of 36.1m (Kennett et al., 1986, (I)). Samples were taken from each of the alternating colour sequences seen in the core in an attempt to ensure an analytical point for each major Quaternary palaeo-event. The Brunhes/Matuyama boundary is located at ~11m (Barton and Bloemendal, 1986). The results of stable isotope measurements and $\%CaCO_3$ determinations are presented in Table 4.3.

Table 4.3. $\delta^{18}O$ and $\delta^{13}C$ values for *Globigerina bulloides* and *Uvigerina* spp, with $\%CaCO_3$ results from DSDP Core 589.

Sub-bottom Depth (m)	*G.bulloides* $\delta^{13}C$	$\delta^{18}O$	*Uvigerina* $\delta^{13}C$	$\delta^{18}O$	$(\%)CaCO_3$
0.16	-1.21	0.39	-0.29	3.11	87.60
0.60	-0.97	0.64	0.13	3.40	85.90
0.93	-1.52	0.31	-0.25	3.00	84.60
1.42	-0.72	0.57	-0.06	2.54	93.00
1.83	-1.51	0.08	-0.20	-	80.40
2.33	-0.89	-0.06	0.03	2.53	86.70
2.79	-0.71	1.02	0.28	3.14	86.30
3.34	-0.96	-0.02	0.41	2.44	88.20
3.94	-1.09	1.22	-0.12	2.77	73.00
4.42	-0.27	0.84	0.27	3.30	90.80
4.82	-0.16	0.09	-	-	89.90
5.16	-0.25	0.32	0.46	2.05	91.60
5.79	-0.95	1.30	-0.05	4.08	83.30
5.87	-0.96	1.22	-0.14	4.13	88.30
6.33	-0.43	0.51	-0.67	3.03	85.20
6.93	-	-	0.75	3.60	92.80
7.36	-	-	-0.20	3.77	87.10
7.95	-	0.54	0.27	3.21	86.70
8.42	-1.40	-0.29	-0.10	3.28	83.70

Table 4.3 cont.

Sub-bottom Depth (m)	*G.bulloides* $\delta^{13}C$	$\delta^{18}O$	*Uvigerina* $\delta^{13}C$	$\delta^{18}O$	(%)$CaCO_3$
8.57	-0.86	0.62	-0.16	2.86	85.10
9.10	-0.86	0.53	-	-	89.90
9.60	-1.13	1.14	-0.41	3.98	81.40
10.00	-1.01	0.73	-0.17	2.08	86.30
10.33	-1.22	0.86	-0.42	2.42	85.70
10.93	-0.47	0.47	0.15	3.06	89.90
11.46	-1.18	1.26	-0.71	3.50	86.00
11.83	-1.27	0.66	-0.21	3.52	84.00
12.41	-0.70	0.27	-0.21	2.28	91.30
12.93	-0.20	0.36	-0.11	2.47	83.70
13.21	-0.32	0.83	-0.12	2.12	86.40
13.69	-1.14	1.58	-0.23	3.78	80.50
14.19	-1.15	0.91	-0.37	3.31	80.90
14.48	-1.48	0.35	-0.39	3.57	79.70
14.73	-1.05	0.46	-0.41	2.51	81.00
15.11	-0.35	0.24	0.29	2.32	90.00
15.48	-0.91	0.24	-	-	91.30
15.97	-0.49	0.12	0.12	3.63	88.80
16.42	-0.16	0.46	0.46	3.85	86.70
16.64	-0.46	0.28	-0.36	3.28	86.30
17.26	-0.20	0.52	0.15	3.43	91.70
17.68	-0.88	0.15	0.41	4.06	89.00
17.79	-0.57	0.54	-0.30	3.11	82.60
18.07	0.02	0.59	0.01	3.02	89.20
18.24	-0.40	0.53	0.01	2.31	88.80
18.71	-0.36	0.52	-0.74	1.63	89.40
19.39	-0.62	0.82	0.03	3.01	81.60
19.81	-0.57	0.54	-0.32	3.51	78.40
20.15	-0.06	0.42	-0.10	1.66	88.30
20.66	-0.88	0.76	-0.30	3.32	90.10
21.03	-0.45	1.04	-0.13	2.81	83.30
21.65	-0.40	1.14	-0.23	2.63	87.40
22.10	-0.60	0.98	-0.39	3.29	79.80
22.29	-0.44	0.16	0.06	3.24	84.10
22.48	-0.02	0.64	-0.33	2.00	89.80
22.67	-0.56	0.68	-0.22	2.80	86.90
22.98	-0.76	0.56	0.01	3.99	85.50
23.21	-0.75	0.17	-	-	90.60
23.72	-0.57	0.52	-0.24	3.77	86.80
24.21	-0.68	-0.76	-0.26	2.40	87.70
24.32	-0.53	0.66	-0.19	2.71	83.60
24.70	-0.05	0.81	0.12	3.72	90.50
25.09	-0.42	0.48	-	-	87.80
25.40	-0.75	0.53	-0.49	3.11	85.40
25.71	-0.71	0.04	-	-	87.10
26.02	-0.55	0.07	-	-	87.30
26.30	-0.79	0.56	-0.12	3.43	87.60
26.88	0.26	0.24	-	-	88.90
27.35	-0.13	-0.49	0.11	4.82	84.00
27.69	0.33	-0.72	-0.10	2.35	86.40
28.03	-0.62	-0.11	0.36	4.00	84.70
28.21	-0.42	0.51	-0.12	2.96	84.00
28.42	-0.48	0.18	0.14	3.56	84.80
28.84	-	-	-	-	78.90

Table 4.3 cont.

Sub-bottom Depth (m)	*G.bulloides* $\delta^{13}C$	$\delta^{18}O$	*Uvigerina* $\delta^{13}C$	$\delta^{18}O$	(%)$CaCO_3$
29.31	-0.65	0.45	-	-	80.80
29.63	-0.74	0.39	-	-	87.70
30.04	-0.78	0.26	-0.59	3.01	89.50
30.15	-1.00	-0.08	-0.90	2.59	83.60
30.41	-0.90	0.62	-0.19	3.72	87.90
30.73	-0.59	0.53	-0.44	2.86	89.10
31.06	-0.79	0.61	-0.57	3.00	89.00
31.56	-0.85	0.19	-	-	89.20
31.97	-0.62	0.65	-0.60	2.90	87.80
32.32	-0.31	0.29	-	-	88.00
32.41	-0.57	0.11	0.04	3.29	86.00
32.53	-0.66	0.03	-0.47	3.13	87.30
32.68	-0.31	0.02	-0.43	3.18	88.90
32.89	-0.11	0.76	-0.52	2.89	85.20
33.06	-0.37	0.01	-0.10	3.82	88.70
33.26	-0.06	0.52	-0.17	2.51	88.10
33.45	-0.42	0.16	-0.68	3.74	81.40
33.92	-0.54	0.10	-0.08	1.68	86.20
34.21	-0.37	0.19	-0.56	2.64	80.50
34.43	-0.44	0.03	-0.15	2.60	87.70
34.89	-0.21	-0.02	0.00	3.72	91.40
35.83	0.01	0.70	-0.03	2.47	87.10

590 Site 590 is located at 31°10.02'S;163°21.51'E, in a water depth of 1299m (see Figure 3.1). Microfossil asemblages showed no evidence of reworking, and well preserved foraminifera were not unexpected as Site 590 is located in such shallow water that it was almost certainly above the lysocline during the entire Neogene (Kennett et al., 1986, (I)). Its position in waters transitional between warm subtropical and temperate meant that it was of particular interest to palaeoclimatologists. Carbon and oxygen isotope ratios for *G. bulloides* and *Uvigerina* spp. from the top 3m of 590 are presented in Table 4.4.

Table 4.4. $\delta^{18}O$ and $\delta^{13}C$ values for *Globigerina bulloides* and *Uvigerina* spp. from DSDP Core 590.

Sub-bottom Depth (m)	*G.bulloides* $\delta^{13}C$	*G.bulloides* $\delta^{18}O$	*Uvigerina* $\delta^{13}C$	*Uvigerina* $\delta^{18}O$
0.01	-0.99	-0.04	0.72	3.90
0.11	-1.48	0.17	0.79	4.17
0.21	-1.03	0.52	0.63	4.09
0.31	-2.14	0.99	0.21	4.89
0.40	-1.20	0.69	0.29	4.95
0.51	-1.52	1.18	0.50	5.35
0.61	-1.34	0.58	0.38	5.00
0.71	-1.27	0.62	0.40	4.51
0.80	-1.45	0.59	0.30	4.51
0.91	-1.53	0.68	0.27	4.37
1.01	-1.19	0.82	0.37	4.33
1.11	-1.30	0.83	0.29	4.61
1.21	-1.03	0.50	0.70	4.57
1.31	-0.87	0.63	0.53	3.95
1.41	-1.10	0.98	0.30	4.28
1.49	-0.70	0.74	0.89	4.10
1.61	-1.13	0.44	0.45	3.87
1.71	-	-	0.47	3.57
1.81	-1.37	1.27	0.35	5.05
1.91	-1.41	1.81	0.22	5.11
2.01	-1.29	1.30	0.30	5.18
2.11	-1.45	1.30	0.33	4.86
2.20	-1.51	1.47	0.57	5.49
2.31	-0.92	0.74	0.44	4.93
2.41	-1.27	0.78	0.31	5.01
2.51	-1.22	0.92	0.33	4.46
2.61	-0.84	1.08	0.14	4.50
2.71	-0.66	1.33	0.45	4.12
2.81	-0.81	0.63	0.72	4.34
2.91	-0.99	1.17	0.72	4.19
2.99	-1.06	0.89	0.66	4.08

591A Site 591A is located at 31°35.06'S;164°26.92'E in a water depth of 2131m (see Figure 3.1). Like 590 it is situated in transitional subtropical/temperate waters, and has a high productivity of calcareous biogenic material (Kennett et al., 1986, (I))- possibly related to the influence of the Subtropical Divergence that crosses both 590 and 591A (see Figure 3.1).

Results from the analysis of *G. bulloides* and *Uvigerina* spp. from this site are presented in Table 4.5.

Table 4.5. $\delta^{18}O$ and $\delta^{13}C$ values for *Globigerina bulloides* and *Uvigerina* spp. from DSDP Core 591A.

Sub-bottom	*G.bulloides*		*Uvigerina*	
Depth (m)	$\delta^{13}C$	$\delta^{18}O$	$\delta^{13}C$	$\delta^{18}O$
0.01	-1.41	-0.01	-0.55	3.61
0.11	-1.58	0.36	-0.62	4.30
0.21	-1.74	0.69	-0.42	4.54
0.31	-1.24	1.08	-0.32	4.92
0.41	-1.60	0.78	-0.60	4.61
0.51	-1.49	0.76	-0.17	4.88
0.61	-1.07	0.70	-0.23	4.57
0.71	-1.37	0.59	-0.20	4.38
0.81	-1.32	0.88	-0.22	4.60
0.91	-1.52	0.38	-0.13	4.59
1.01	-1.65	0.56	-0.41	4.38
1.11	-0.99	1.23	-0.28	4.49
1.21	-1.06	0.11	-	-
1.31	-	-	0.13	4.00
1.41	-0.97	-0.12	0.07	4.15
1.49	-0.89	0.04	-	-
1.61	-1.03	0.07	-	-
1.71	-1.15	0.23	0.08	4.05
1.81	-1.30	-0.09	0.02	4.51
1.91	-0.75	-0.06	0.01	3.74
2.01	-1.68	0.17	-0.54	5.01
2.11	-1.38	0.71	-0.36	5.13
2.21	-1.55	0.57	-0.70	5.17
2.31	-1.71	0.74	-0.55	4.84
2.41	-1.55	0.70	-0.73	5.30
2.51	-1.72	0.62	-0.62	5.48
2.61	-1.56	0.71	-0.53	4.68
2.71	-1.72	0.61	-0.76	4.81
2.81	-1.46	0.36	-0.79	4.29
2.91	-1.69	0.16	-0.41	4.89
2.99	-1.48	-0.01	-0.70	4.71
3.11	-1.00	-0.11	-0.22	4.42
3.21	-1.02	-0.22	-	-
3.31	-0.73	-0.04	0.14	4.58
3.41	-1.21	-0.33	0.03	4.33
3.51	-0.90	0.27	-0.10	3.71
3.61	-1.19	0.77	-0.30	4.13
3.71	-1.26	0.66	-0.28	4.73
3.81	-1.18	0.49	-0.30	4.33
3.91	-1.06	0.78	-0.31	3.87
4.01	-1.12	0.50	-0.33	4.00
4.11	-1.51	1.37	-0.36	4.74
4.21	-1.05	1.25	-0.61	5.17
4.31	-1.35	0.97	-0.61	4.89
4.41	-1.43	1.57	-0.51	4.89
4.49	-1.13	0.92	-0.67	5.10

592 Site 592 is located at 36°28.40'S;165°26.53'E, in a water depth of 1088m (see Figure 3.1). The core yielded well preserved planktonic and

benthic foraminifera (Kennett et al., 1986, (I)). The $\delta^{18}O$ and $\delta^{13}C$ values for *G. bulloides* and *Uvigerina* spp. from the top 3.6m of core are presented in Table 4.6a.

Table 4.6a. $\delta^{18}O$ and $\delta^{13}C$ values for *Globigerina bulloides* and *Uvigerina* spp. from DSDP Core 592.

Sub-bottom	*G.bulloides*		*Uvigerina*	
Depth (m)	$\delta^{13}C$	$\delta^{18}O$	$\delta^{13}C$	$\delta^{18}O$
0.01	-0.56	0.76	0.24	3.00
0.11	-1.01	0.68	0.37	3.38
0.20	-0.95	0.83	0.03	3.02
0.30	-0.35	2.08	0.03	4.15
0.41	-0.57	1.93	-0.06	4.20
0.51	-0.33	1.80	0.01	4.26
0.61	-0.45	1.76	0.08	3.80
0.71	-0.36	1.96	0.01	3.80
0.80	-0.39	1.84	0.14	3.65
0.89	-0.66	1.17	0.09	3.83
1.01	-0.75	0.73	0.14	3.00
1.11	-0.98	0.75	0.14	3.60
1.21	-0.93	0.81	0.36	3.57
1.31	-0.92	0.90	-	-
1.41	-0.79	0.99	-0.17	4.15
1.49	-0.82	1.46	-0.22	4.61
1.61	-1.27	1.04	-0.37	4.16
1.71	-1.63	0.46	-0.18	4.51
1.81	-1.35	0.82	-0.56	4.49
1.91	-1.00	0.66	-0.20	3.94
2.01	-1.19	0.42	-	-
2.11	-1.18	0.23	0.15	4.14
2.21	-1.04	0.17	-0.21	3.53
2.31	-1.27	0.20	0.09	3.86
2.41	-1.18	0.25	0.06	3.38
2.51	-1.20	0.04	0.06	3.06
2.61	-0.67	0.81	-0.27	4.11
2.71	-	-	-0.46	3.80
2.81	-1.06	0.72	-0.34	3.86
2.91	-1.05	0.33	-0.15	3.83
2.99	-0.61	0.37	0.02	3.43
3.11	-0.97	0.10	-0.19	3.42
3.21	-0.89	-0.48	0.01	3.24
3.31	-0.66	0.51	-0.18	3.61
3.41	-0.36	0.93	-0.19	3.87
3.51	-0.56	0.91	-0.04	3.29
3.61	-0.50	0.76	0.18	2.87

In addition, lower resolution (30-50cm sample intervals) analysis was carried out on planktonic and benthic foraminifera from the first 23m of the core. Shipboard palaeomagnetic appraisal locates the

Brunhes/Matuyama boundary at ~11m (Barton and Bloemendal, 1986). The results for the longer section of 592 are presented in Table 4.6b.

Table 4.6b. $\delta^{18}O$ and $\delta^{13}C$ values for *Globigerina bulloides* and *Uvigerina* spp. from DSDP Core 592.

Sub-bottom	*G.bulloides*		*Uvigerina*	
Depth (m)	$\delta^{13}C$	$\delta^{18}O$	$\delta^{13}C$	$\delta^{18}O$
0.30	-0.12	2.28	-0.13	3.30
0.80	-0.65	1.45	-0.05	3.31
1.28	-1.02	1.42	0.02	3.10
1.80	-0.71	1.53	-0.61	3.02
2.30	-0.93	1.13	-0.16	3.06
2.78	-0.43	1.96	-0.17	3.48
3.30	-0.15	1.29	0.01	2.60
3.80	-1.33	0.60	0.02	2.65
4.80	0.30	2.51	-0.10	3.24
5.30	0.19	1.64	-0.19	3.24
5.78	-0.94	0.67	0.35	2.76
6.30	-0.20	1.13	-0.35	1.70
6.80	-1.19	0.45	0.71	1.84
7.28	-0.94	0.32	0.24	2.92
7.80	-0.69	1.96	0.06	3.51
8.30	-0.61	1.86	-0.29	3.75
8.78	-0.62	1.51	-	-
9.30	-0.82	0.94	-0.95	3.17
9.80	-0.80	1.09	0.14	3.17
10.28	-1.12	0.48	-0.61	2.65
10.80	-0.74	1.86	0.35	3.23
11.30	-0.71	1.75	0.02	3.31
11.78	-0.32	1.47	0.31	2.80
12.30	-0.15	1.94	0.38	3.02
12.80	-0.46	1.53	-	-
13.28	-1.31	0.88	-0.20	2.82
13.80	-0.28	1.52	-0.34	3.18
14.40	-0.65	1.22	-0.13	3.28
14.90	-0.23	1.78	-0.12	2.74
15.38	-0.19	1.23	0.20	3.19
15.90	-0.37	1.14	0.03	3.36
16.40	-0.08	1.46	-0.11	3.05
16.88	-0.19	0.92	-0.24	2.93
17.40	0.05	1.25	0.12	2.50
17.90	-0.39	1.29	-0.35	3.56
18.38	-0.09	1.41	0.10	3.06
18.90	-	1.15	0.14	2.73
19.40	-0.50	1.50	0.21	2.69
19.88	-0.46	1.20	-0.10	3.84
20.40	-0.24	1.33	-0.06	3.07
20.90	-0.20	1.06	-	-
21.38	-0.04	1.34	-	-
21.90	0.06	1.12	-0.20	2.93
22.40	-	0.78	-0.25	2.21
22.88	-0.12	1.49	-	-

593 Site 593 is located at 40°30.47'S;167°40.47E, in a water depth of 1068m, 270km west of the northern South Island of New Zealand (see Figure 3.1). It was previously analysed at 30-40cm intervals for 53m of the core (Nelson et al., 1986a). As it was felt that higher resolution sampling could result in a useful Quaternary isotope reference section for the southern temperate waters, the core was resampled at 10cm intervals. The results from this high resolution sampling are presented in Table 4.7. The Brunhes/Matuyama boundary is located at 16.1m (Barton and Bloemendal, 1986).

Table 4.7. $\delta^{18}O$ and $\delta^{13}C$ values for *Globigerina bulloides* and *Uvigerina* spp. from DSDP Core 593.

Sub-bottom	*G.bulloides*		*Uvigerina*	
Depth (m)	$\delta^{13}C$	$\delta^{18}O$	$\delta^{13}C$	$\delta^{18}O$
0.07	-0.50	0.84	0.20	3.19
0.17	-0.74	0.89	0.00	2.71
0.31	-0.26	1.83	-0.25	3.73
0.38	-0.36	1.74	-0.14	4.38
0.57	-0.15	1.97	-0.18	4.27
0.62	-0.05	2.19	0.23	3.56
0.81	-0.17	1.38	-0.03	4.03
0.86	-0.85	0.92	-0.17	3.58
1.03	0.22	1.86	0.03	3.74
1.13	0.07	1.87	-0.07	3.68
1.29	-0.36	1.33	0.06	3.34
1.40	0.24	1.94	0.11	4.35
1.55	-0.19	1.13	-0.13	3.55
1.67	0.06	1.51	0.17	3.02
1.81	-1.44	-0.62	0.12	3.13
1.89	-1.43	-0.32	0.08	2.76
2.07	-1.62	-0.51	0.46	2.89
2.14	-1.31	-0.04	-0.04	3.18
2.31	-0.76	1.66	-0.42	3.97
2.38	-0.45	1.84	-0.45	3.76
2.51	-0.88	1.62	-0.46	4.04
2.65	-1.09	0.96	-0.44	3.97
2.79	-1.18	1.26	-0.33	3.30
2.92	-0.79	1.79	-0.39	3.68
3.10	-0.57	2.13	-0.45	3.83
3.18	-0.23	2.25	-0.35	4.05
3.31	-0.43	2.26	-0.31	3.42
3.41	-0.34	1.80	-0.23	3.69
3.57	-1.70	0.36	-0.26	2.99
3.64	-1.96	-0.13	-0.58	3.30
3.81	-0.99	0.96	-0.62	3.23
3.86	-1.55	-0.37	-0.18	2.43
4.03	-1.50	-0.54	0.20	2.71
4.14	-1.17	-0.05	0.17	3.19

Table 4.7 cont.

Sub-bottom Depth (m)	*G.bulloides* $\delta^{13}C$	*G.bulloides* $\delta^{18}O$	*Uvigerina* $\delta^{13}C$	*Uvigerina* $\delta^{18}O$
4.29	-1.32	0.55	0.23	3.28
4.41	-0.87	0.16	-0.07	3.46
4.59	-0.54	1.29	0.08	3.21
4.68	-0.36	2.03	-0.55	3.50
4.81	-0.52	1.77	-0.50	3.86
4.89	-1.14	1.28	-0.27	3.98
5.07	-0.52	1.86	-0.11	3.75
5.20	0.66	2.18	-0.26	3.17
5.28	-1.06	0.43	0.03	3.81
5.50	-0.81	0.53	-0.49	3.34
5.60	-0.28	0.05	-0.08	2.52
5.70	-0.88	1.51	0.19	3.01
5.80	-0.14	2.68	-0.55	3.99
5.91	-0.20	2.16	-0.63	3.70
6.01	0.23	2.84	-0.26	3.93
6.11	-0.72	0.96	-0.25	3.82
6.27	-0.04	2.04	-0.34	3.76
6.39	-1.02	0.29	-	-
6.54	-0.53	0.86	-	-
6.71	0.15	1.77	-0.14	3.40
6.77	0.18	1.86	-0.10	3.53
6.91	-0.10	1.47	-	-
7.01	-0.75	-0.14	-0.46	3.47
7.11	-0.99	-0.89	0.27	3.22
7.21	-0.71	-0.21	-	-
7.28	-0.52	0.35	-0.03	3.44
7.41	-0.85	-1.48	-	-
7.51	-0.41	-0.89	-	-
7.61	0.58	-0.97	0.06	1.59
7.76	0.32	-0.25	0.60	2.05
7.89	-0.94	-0.07	-	-
8.04	-0.58	0.78	-	-
8.21	0.37	2.86	0.10	4.44
8.31	-0.02	3.12	-	-
8.41	0.23	2.44	-	-
8.51	0.19	2.85	-	-
8.61	-0.66	2.25	-	-
8.71	-0.50	2.32	-	-
8.81	-0.41	2.01	-	-
8.91	-1.00	1.10	-	-
9.02	-0.24	2.03	-	-
9.12	-0.04	2.40	-	-
9.26	-0.57	1.95	-0.76	2.95
9.39	-0.80	0.94	-	-
9.54	-0.62	0.74	-	-
9.68	0.09	2.38	-	-
9.81	-0.44	1.91	-2.26	2.30
9.91	-0.24	2.33	-	-
10.01	0.06	2.12	-0.05	3.94
10.11	-0.28	1.05	-0.81	3.50
10.21	-1.31	0.67	-0.41	3.66
10.31	-1.34	0.48	-2.30	1.95
10.41	0.25	2.28	-0.99	2.47
10.51	-2.35	-0.68	-0.83	3.32

Table 4.7 cont.

Sub-bottom Depth (m)	*G.bulloides* $\delta^{13}C$	$\delta^{18}O$	*Uvigerina* $\delta^{13}C$	$\delta^{18}O$
10.61	-0.79	0.93	-0.23	3.24
10.73	-1.20	0.32	-0.73	2.28
10.89	0.04	0.96	-	-
11.04	0.27	1.08	-	-
11.21	-1.24	-0.25	0.24	2.71
11.31	-1.28	-0.08	-0.25	2.10
11.41	-0.21	1.08	-	-
11.52	-0.84	0.36	-0.03	2.67
11.62	-1.26	0.26	-0.11	2.59
11.71	-0.94	0.37	-0.23	2.36
11.80	0.08	1.37	-1.04	1.86
11.91	-0.34	1.34	-	-
12.01	-0.49	0.67	-0.29	2.41
12.11	-0.83	0.61	-2.27	1.11
12.26	-1.20	0.48	-0.79	2.24
12.39	-0.15	0.68	-	-
12.54	-0.18	1.40	-	-
12.71	-0.16	1.92	-0.68	3.37
12.81	-0.15	1.92	-0.55	3.37
12.91	-0.01	2.04	-0.60	2.99
13.01	-1.92	0.30	-1.26	2.84
13.10	-2.38	-0.61	-0.80	2.75
13.21	-0.36	1.20	-0.56	2.88
13.31	-0.04	1.25	-0.98	2.86
13.41	-0.33	0.85	-	-
13.48	-0.27	1.41	-	-
13.59	-0.53	1.39	-0.45	2.87
13.73	-0.50	1.14	0.15	3.06
13.89	-0.35	1.52	-0.01	3.27
14.80	-1.70	0.36	-0.87	3.21
14.90	-0.57	1.24	-1.27	2.58
15.00	-0.64	1.78	-	-
15.10	-0.43	1.98	-0.94	3.70
15.26	-0.72	1.56	-	-
15.33	-1.04	1.39	-1.16	2.72
15.50	-0.63	1.55	-	-
15.57	-0.45	1.77	-0.74	3.10
15.68	-0.07	0.87	-0.90	2.45
15.88	-0.47	1.45	0.20	2.63
15.98	-1.00	0.95	-0.30	3.52
16.10	-0.91	1.76	0.03	2.77
16.30	-0.67	2.05	-0.13	4.27
16.40	-0.74	2.04	-0.51	4.09
16.50	-0.38	2.17	-0.22	4.09
16.60	-0.37	2.03	-0.24	4.32
16.76	-0.34	1.72	-	-
16.80	-0.31	1.69	-0.81	2.94
16.90	-0.25	1.40	-0.51	3.18
17.00	-0.55	1.56	0.00	3.16
17.09	-0.34	1.62	-0.37	3.10
17.26	-1.57	0.62	0.22	3.55
17.38	-2.30	-0.41	-	-
17.50	-0.58	0.78	-1.12	3.71
17.70	-0.24	0.15	0.19	2.80

Table 4.7 cont.

Sub-bottom Depth (m)	*G.bulloides* $\delta^{13}C$	$\delta^{18}O$	*Uvigerina* $\delta^{13}C$	$\delta^{18}O$
17.80	-1.05	1.24	0.25	2.84
17.90	-1.19	1.29	-0.76	3.51
18.00	-0.03	3.06	-0.48	3.62
18.10	-0.62	2.21	-0.78	3.97
18.16	-0.54	1.90	-	-
18.30	-0.21	2.24	-0.50	3.56
18.40	-0.22	1.93	-1.05	2.69
18.46	-0.43	1.96	-0.96	3.28
18.56	-1.21	0.70	-0.49	3.93
18.70	-1.09	1.39	-	-
18.80	-0.87	1.35	-	-
18.88	-0.69	1.96	-1.06	3.91
19.00	-0.78	1.04	-0.89	2.91
19.07	-0.77	0.80	-0.95	3.73
19.20	-0.90	0.09	-0.45	2.15
19.31	-0.51	0.15	-0.64	2.62
19.40	-0.41	0.47	-0.51	2.92
19.50	-1.01	-0.36	-0.44	2.60
19.60	-0.07	1.22	-0.16	2.48
19.66	-0.51	0.90	0.01	2.48
19.80	0.05	1.83	-0.22	2.50
19.90	0.40	2.26	-0.20	2.92
20.01	-0.18	1.85	0.15	3.02
20.10	-1.10	0.63	-0.38	3.40
20.20	-1.42	0.53	0.15	3.00
20.30	-0.75	0.70	-0.31	2.79
20.38	-0.60	0.81	-0.39	2.53
20.50	-0.73	0.78	0.10	3.36
20.57	-0.36	1.22	-0.06	2.90
20.70	-0.23	1.22	-0.54	2.75
20.81	-0.32	0.97	-0.58	2.05
20.90	-0.77	0.62	-0.52	2.28
21.00	-0.31	1.41	-	-
21.10	-0.22	1.29	-0.15	3.32
21.16	-0.11	1.59	-	-
21.34	-0.14	1.45	-0.08	3.42
21.54	-0.27	1.08	-0.77	2.36
21.60	-0.40	0.64	-0.37	3.08
21.70	-0.70	0.63	2.39	4.17
21.80	-0.33	0.82	-0.16	2.60
21.88	-0.06	1.21	-0.02	3.78
22.00	-0.52	0.72	-	-
22.07	-0.80	0.43	-0.26	3.12
22.19	-0.26	1.19	-	-
22.30	-0.31	1.70	-0.27	3.71
22.40	-0.20	1.81	-0.34	3.54
22.50	0.03	2.24	-0.47	3.74
22.60	-0.07	1.99	-0.34	3.73
22.66	-0.12	2.27	-0.37	4.18
22.80	-0.44	1.45	-0.69	3.45
22.90	-0.51	1.26	-	-
23.00	-0.32	1.12	-	-
23.10	-0.62	0.99	-	-
23.20	-0.43	0.99	-0.20	2.30

Table 4.7 cont.

Sub-bottom Depth (m)	*G.bulloides* $\delta^{13}C$	*G.bulloides* $\delta^{18}O$	*Uvigerina* $\delta^{13}C$	*Uvigerina* $\delta^{18}O$
23.30	-0.35	0.98	0.03	2.28
23.50	-0.57	0.90	0.35	2.74
23.57	-0.55	1.25	-0.04	2.44
24.40	-0.48	1.07	-0.10	2.12
24.50	-0.47	1.17	0.05	2.61
24.61	-0.33	1.29	-0.22	2.37
24.70	-0.32	1.21	-0.78	3.25
24.80	-0.20	1.78	0.10	3.63
24.87	-0.37	1.52	-0.40	3.07
25.00	-0.47	1.74	-0.04	3.56
25.22	-0.60	1.63	-0.24	3.67
25.32	-0.32	1.54	0.12	3.67
25.40	-0.21	1.64	-0.03	3.76
25.50	-0.31	1.21	-0.13	3.21
25.59	-0.17	1.37	-0.43	2.56
25.70	-0.12	0.96	0.26	2.85
25.78	-0.17	1.32	-0.48	2.64
25.90	-0.14	1.71	-0.22	2.81
26.01	-0.53	1.56	-0.51	3.33
26.11	-0.18	1.87	-0.18	3.36
26.21	0.27	1.81	-0.13	3.37
26.32	-0.29	1.35	0.18	3.02
26.37	-0.36	1.23	-	-
26.51	0.01	1.32	0.41	3.11
26.72	-0.48	1.09	0.11	2.99
26.81	-0.67	1.25	-0.07	2.93
26.90	-0.23	1.64	-0.16	2.86
27.00	-0.17	1.47	0.14	3.47
27.09	-0.29	1.14	0.02	3.14
27.21	-0.40	1.03	-0.52	2.52
27.28	-0.42	1.48	-0.01	3.09
27.41	-0.51	1.56	-0.40	3.25
27.51	-0.29	1.49	-0.24	3.21
27.61	-0.06	1.77	-0.28	2.93
27.71	-0.17	1.21	-	-
27.78	-0.50	1.19	-0.03	3.07
27.87	-0.28	1.31	-0.31	2.90
28.01	-0.24	1.62	2.42	3.39
28.11	-0.66	0.95	-0.19	3.24
28.21	-0.20	1.57	-0.09	3.48
28.30	-0.22	1.22	0.16	3.39
28.41	-0.49	1.21	0.14	2.91
28.51	-0.60	0.98	-0.31	2.71
28.59	-1.28	0.54	-	-
28.69	-0.29	1.84	-0.10	3.11
28.91	-0.06	1.60	0.16	2.70
29.00	-0.43	1.00	-	-
29.21	-0.35	1.41	-0.11	2.99
29.30	0.02	1.53	-0.16	3.12
29.37	-0.34	1.43	-0.09	3.34
29.51	-0.25	1.15	-0.04	2.57
29.71	0.31	1.20	0.01	2.42
29.81	-0.20	0.88	-	-

Table 4.7 cont.

Sub-bottom Depth (m)	*G.bulloides* $\delta^{13}C$	*G.bulloides* $\delta^{18}O$	*Uvigerina* $\delta^{13}C$	*Uvigerina* $\delta^{18}O$
29.90	-0.06	0.85	-0.26	2.67
30.00	-0.15	1.33	-0.22	3.15
30.09	-0.30	1.13	0.27	3.25
30.19	-0.03	1.03	0.07	2.88
30.28	0.09	1.06	0.19	2.90
30.40	-0.31	1.27	0.03	3.58
30.51	-0.88	0.76	-0.12	3.14
30.61	-0.37	1.50	-1.32	2.54
30.71	-0.23	1.00	-0.62	2.94
30.81	-0.74	0.75	-0.42	3.36
30.87	-0.32	0.80	-0.18	3.23
31.01	0.02	1.07	0.32	3.45
31.11	0.09	1.03	0.41	3.25
31.22	-0.11	1.12	-0.14	2.98
31.31	0.33	1.60	0.12	3.21
31.41	0.04	1.07	0.20	2.92
31.51	0.09	0.85	0.19	3.09
31.59	-0.24	0.67	-	-
31.69	-0.17	0.96	0.10	3.07
31.78	-0.64	0.61	-0.29	2.86
31.91	-0.38	0.88	-0.54	3.15
32.01	-0.57	1.09	-0.13	3.39
32.11	-0.97	0.94	-0.26	3.60
32.21	-0.55	0.98	-0.03	3.43
32.29	-2.83	-	-0.18	3.02
32.37	-0.56	0.95	-0.79	2.21
32.47	-0.45	1.08	0.18	2.90
32.61	-0.68	0.71	-	-
32.71	-0.59	0.86	-0.60	2.29
32.81	-0.37	0.81	-0.49	2.41
32.90	-0.23	1.39	-0.68	2.93
33.01	-0.01	1.42	0.11	2.84
34.01	-0.17	1.16	-0.26	3.10
34.13	-0.22	1.17	-0.48	2.36
34.21	0.05	1.16	-0.32	2.59
34.31	-0.37	0.97	-0.27	2.88
34.41	-0.17	1.43	-0.05	2.85
34.47	-0.32	1.38	-0.62	2.53
34.61	0.01	1.81	-0.54	2.90
34.71	-0.12	1.83	-0.29	3.54
34.79	-0.11	1.69	-	-
34.90	0.10	1.47	-0.21	3.37
35.01	-0.06	1.45	-0.32	2.97
35.11	0.02	1.42	0.12	2.96
35.19	-0.37	1.32	-	-
35.30	-0.42	1.55	-0.68	3.06
35.39	0.60	1.87	-0.34	2.89
35.51	-0.32	1.24	-	-
35.62	0.05	1.54	-	-
35.71	0.04	1.36	-	-
35.81	0.10	1.12	-	-
35.92	0.34	1.43	-	-
35.97	0.19	1.12	-	-
36.10	0.21	1.15	-	-

Table 4.7 cont.

Sub-bottom	*G.bulloides*		*Uvigerina*	
Depth (m)	$\delta^{13}C$	$\delta^{18}O$	$\delta^{13}C$	$\delta^{18}O$
36.21	0.29	1.18	-	-
36.29	0.41	1.54	-	-
36.41	0.26	1.34	-	-
36.51	0.33	1.20	-	-
36.61	0.19	1.42	-	-
36.69	0.37	1.34	-	-
36.80	0.31	0.94	-	-
36.89	-0.05	1.22	-	-
37.01	0.00	1.82	-	-
37.09	0.07	1.44	-	-
37.21	-0.11	1.42	-	-
37.31	0.21	2.01	-	-
37.41	-0.21	1.14	-	-
37.47	0.32	2.14	-0.38	2.86
37.63	-0.13	1.27	-0.50	2.97
37.71	-0.16	1.65	-	-
37.82	-0.19	1.48	-	-
37.91	-0.20	1.46	-	-
38.01	-0.29	1.30	-0.77	3.09
38.11	-0.01	1.73	-0.98	3.49
38.19	0.23	1.31	-0.63	3.30
38.29	0.09	1.14	-0.40	2.74
38.39	-0.08	1.45	-0.27	2.92
38.51	-0.03	1.27	-0.14	3.17
38.61	-0.01	1.39	-0.19	2.77
38.71	-0.19	1.41	-0.32	2.96
38.81	-0.10	1.35	-0.22	3.37
38.91	0.05	1.52	-0.44	2.84
38.97	-0.05	1.36	-0.21	3.34
39.10	-0.17	1.05	-0.45	3.23
39.21	0.06	1.22	-0.33	3.00
39.32	-0.03	1.18	-0.38	3.24
39.41	0.13	1.46	-0.66	3.29
39.51	-0.16	1.16	0.09	3.30
39.59	-0.43	0.99	-0.62	3.09
39.69	-0.18	1.14	-	-
39.80	-0.05	1.55	-	-
39.89	0.05	1.48	-0.47	2.91
40.01	0.11	1.87	-	-
40.11	0.19	1.77	-0.22	3.21
40.21	-0.02	0.86	-0.19	2.95

Table 4.7 cont.

Sub-bottom Depth (m)	*G.bulloides* $\delta^{13}C$	$\delta^{18}O$	*Uvigerina* $\delta^{13}C$	$\delta^{18}O$
40.31	0.16	1.27	-	-
40.43	0.12	1.09	-0.14	3.24
40.47	0.09	1.10	-0.09	3.40
40.60	-0.15	1.04	-	-
40.71	-0.35	1.38	-	-
40.82	-0.32	1.40	-	-
40.91	-0.09	1.27	-1.18	4.01
41.01	0.03	1.12	-	-
41.11	0.04	0.89	-	-
41.19	-0.19	0.90	-	-
41.30	0.07	0.72	-	-
41.39	0.12	1.54	-0.21	3.66
41.51	0.07	1.29	-0.32	3.58
41.61	0.25	1.26	-	-
41.71	-0.07	1.13	-	-
41.81	-0.12	0.98	-0.08	3.47
41.91	0.09	1.05	-0.08	3.65
41.97	0.11	0.86	0.43	3.09
42.10	0.14	0.90	-	-
42.21	-	-	-	-
42.31	-0.10	0.99	-	-
42.41	0.11	1.25	-	-
42.51	0.14	1.13	-	-
42.61	0.26	1.22	-	-
42.69	0.34	0.99	-	-
42.80	0.42	1.11	-	-

594 Site 594 is located at 45°31.41'S;174°56.88'E, in a water depth of 1204m (see Figure 3.1). Its position on the southern margin of the Chatham Rise east of the South Island of New Zealand has meant that it has been subjected to both oceanic and terrigenous influences. Core 594 was previously sampled at 30cm intervals, and results from analysis of these samples appear in Cuthbertson (1985) and Nelson et al. (1986). Because of the excellent detail of glacial to interglacial oscillations apparent in the results from 30cm sampling intervals, it was decided to request the resampling of 594 at 10cm intervals over the first 20m, to determine the finer structure of stages 1 to 6. The results from the analysis of these samples are presented in Table 4.8.

Table 4.8. $\delta^{18}O$ and $\delta^{13}C$ values for *Globigerina bulloides* and *Uvigerina* spp., with $\%CaCO_3$ values from DSDP Core 594.

Sub-bottom Depth (m)	*G.bulloides* $\delta^{13}C$	$\delta^{18}O$	*Uvigerina* $\delta^{13}C$	$\delta^{18}O$	$\%CaCO_3$
0.01	0.44	1.59	-0.02	3.35	35.57
0.10	0.16	1.50	0.05	3.41	42.56
0.21	-0.07	0.97	0.15	3.33	45.21
0.30	0.54	1.91	0.25	3.31	44.03
0.41	0.55	2.20	-0.09	3.44	44.05
0.50	-0.04	1.32	-	3.52	41.83
0.61	0.17	1.91	-0.17	3.50	44.55
0.71	0.00	1.80	-0.31	3.43	40.72
0.81	-0.16	1.40	-0.09	2.92	32.92
0.91	-0.24	1.66	0.06	3.31	45.02
1.00	0.04	2.09	-0.24	3.36	44.57
1.10	-0.22	2.19	-0.60	3.36	41.95
1.21	-0.39	2.23	-0.81	3.76	31.40
1.31	-0.18	2.98	-0.24	3.97	38.39
1.41	-0.62	2.20	-0.50	4.16	31.82
1.49	-0.36	3.06	-0.53	4.17	25.21
1.61	-0.04	3.46	-0.41	4.34	12.53
1.71	0.30	2.60	-	-	5.10
1.81	-	-	-0.35	5.11	4.92
1.91	-0.39	3.51	-0.19	5.39	6.01
2.01	0.13	2.55	-0.41	4.75	6.31
2.11	-	-	-0.37	5.29	3.33
2.21	-0.55	2.41	-0.65	4.67	3.66
2.31	-0.18	3.49	-0.34	5.02	5.23
2.41	-0.91	3.27	-0.58	5.06	8.27
2.51	-0.43	3.72	-0.55	4.87	11.12
2.61	-0.20	3.42	-0.69	4.99	8.93
2.71	-0.67	3.97	-0.46	4.89	7.99
2.81	-	-	-0.49	5.04	6.76
2.91	-	-	-0.25	4.90	6.38
2.99	-0.25	3.43	-0.35	5.30	8.56
3.11	-0.23	2.76	-0.34	4.79	13.15
3.21	0.04	3.28	-0.15	4.63	8.41
3.31	-0.48	2.66	-0.28	4.82	7.18
3.41	-0.39	2.54	-0.11	4.89	5.51
3.51	-	-	-	-	3.64
3.61	0.25	3.45	-0.33	5.21	3.04
3.71	0.07	2.96	-0.30	4.60	5.07
3.81	-0.52	3.09	-0.19	4.69	6.78
3.91	-0.08	2.81	-0.13	4.39	14.10
4.00	0.13	3.29	-0.03	5.23	10.08
4.11	0.20	3.25	-0.37	4.28	7.96
4.21	-0.02	3.26	-0.30	4.80	3.51
4.31	-	-	-0.13	4.47	5.17
4.41	-	-	-0.16	4.66	8.00
4.49	-	-	-0.04	4.54	4.85
4.60	-0.57	2.61	0.11	4.69	10.40
4.71	0.16	3.65	-0.19	4.08	6.81
4.81	-0.16	2.28	-0.16	4.75	8.80
4.91	0.17	3.18	0.29	4.00	8.20
5.00	-0.12	2.77	-0.32	4.83	6.93

Table 4.8 cont.

Sub-bottom Depth (m)	*G.bulloides* $\delta^{13}C$	*G.bulloides* $\delta^{18}O$	*Uvigerina* $\delta^{13}C$	*Uvigerina* $\delta^{18}O$	$\%CaCO_3$
5.11	0.27	3.33	0.02	4.05	14.79
5.20	0.05	3.09	0.02	4.45	10.36
5.31	0.39	3.63	-0.01	4.99	6.52
5.41	0.45	3.29	-0.01	4.87	16.68
5.50	0.23	3.01	-0.05	4.42	20.26
5.61	0.26	2.71	-0.17	4.56	23.41
5.77	-	-	-0.15	4.25	3.22
5.87	0.28	3.39	-0.10	4.56	20.16
5.99	0.40	3.17	-0.19	4.26	9.39
6.09	0.06	2.97	-0.31	4.39	12.51
6.20	0.50	3.15	-0.20	4.26	21.61
6.30	0.43	3.00	-	4.46	30.18
6.40	0.35	2.76	-0.24	4.46	18.66
6.49	0.57	3.17	-0.01	4.50	5.75
6.59	-0.26	3.12	-0.41	4.28	9.53
6.70	0.02	3.21	-0.21	4.74	12.43
6.80	-0.14	2.77	0.01	4.74	16.57
6.90	0.04	3.08	-	-	15.66
7.00	0.02	3.10	-0.17	4.33	26.91
7.09	0.38	2.70	-0.41	4.34	23.27
7.21	0.06	3.02	-0.50	4.02	29.83
7.31	-0.89	2.05	-	-	19.44
7.40	-0.03	3.20	-	-	15.32
7.50	-0.10	3.11	-0.36	4.28	17.58
7.60	-0.14	3.07	-0.55	4.35	29.00
7.70	-0.31	2.70	-	-	31.62
7.80	-0.55	2.47	-0.57	4.42	35.09
7.89	-0.29	2.68	-0.46	4.27	38.64
8.00	-0.05	2.95	-0.21	5.06	24.99
8.10	-0.53	2.49	-0.35	4.40	29.54
8.21	-0.21	3.32	-0.55	4.86	12.23
8.30	0.22	3.61	-0.48	4.41	14.10
8.40	0.09	3.17	-0.52	5.00	7.38
8.50	-0.23	3.17	-0.37	4.79	6.81
8.60	0.13	3.60	-	-	6.44
8.70	0.35	3.92	-0.38	4.80	8.63
8.80	0.17	3.21	-0.51	4.80	12.34
8.90	0.25	3.29	-0.41	4.72	6.32
9.00	-0.03	3.60	-0.48	4.55	6.06
9.10	0.07	3.12	-0.41	4.93	5.47
9.20	-0.17	3.07	-0.71	4.22	6.25
9.29	-0.08	3.46	-0.44	4.73	5.07
9.40	0.07	3.40	-	-	4.14
9.49	-0.67	3.27	-0.38	4.63	5.99
9.60	-0.55	2.83	-0.36	4.83	5.04
9.70	-0.25	2.69	-0.41	4.76	7.28
9.80	-0.27	3.16	-0.47	4.90	9.25
9.89	0.02	3.67	-0.29	4.69	6.56
10.00	0.13	3.09	-	-	7.53
10.10	-0.06	3.23	-0.03	4.69	14.26
10.19	0.00	3.04	-0.65	4.07	14.27
10.30	-0.09	3.22	-0.50	4.75	18.00
10.41	0.56	3.42	-0.66	3.91	31.49
10.50	0.65	3.97	-0.44	4.18	35.26

Table 4.8 cont.

Sub-bottom Depth (m)	*G.bulloides* $\delta^{13}C$	$\delta^{18}O$	*Uvigerina* $\delta^{13}C$	$\delta^{18}O$	$\%CaCO_3$
10.59	0.31	3.00	-0.30	4.09	35.73
10.68	0.41	3.46	-	-	30.80
10.80	0.77	2.91	-0.34	3.79	49.29
10.89	0.70	3.10	-0.23	4.15	45.25
10.99	0.58	3.23	-0.42	3.68	35.19
11.10	0.19	2.54	-0.22	4.12	35.96
11.18	0.34	2.59	-0.44	3.80	30.21
11.30	0.18	2.47	-0.33	3.94	40.34
11.39	0.19	2.47	-0.27	3.83	44.60
11.49	0.26	2.08	-0.19	3.81	38.34
11.59	0.28	2.55	-0.44	3.72	47.62
11.69	0.04	1.95	-0.31	3.59	43.16
11.79	0.02	2.32	-0.19	2.91	37.01
11.90	-0.08	2.40	-0.10	3.37	44.12
12.01	0.16	1.79	-0.24	3.79	48.84
12.11	0.21	2.09	-0.31	3.21	47.85
12.19	0.34	2.30	-0.34	3.67	52.51
12.28	-0.03	2.16	0.01	3.47	54.58
12.39	0.29	2.42	-0.15	3.70	50.61
12.49	0.17	2.10	-0.14	3.78	46.26
12.59	0.66	3.24	-0.33	4.02	29.76
12.69	0.01	2.61	0.01	4.59	23.84
12.79	0.10	2.49	-0.04	4.36	28.10
12.89	0.61	3.16	-0.27	3.88	29.88
12.99	0.52	2.90	-0.16	4.59	36.57
13.09	0.16	2.67	-0.46	3.84	35.72
13.18	0.18	2.29	-0.25	4.41	44.42
13.29	0.17	2.69	-1.17	3.19	49.00
13.40	0.21	2.34	-1.56	2.62	48.71
13.49	0.04	2.30	-1.01	3.75	47.35
13.59	0.27	1.92	-0.61	3.50	59.44
13.68	0.21	2.50	-0.66	3.95	55.42
13.78	-0.53	1.47	-0.45	3.59	53.45
13.88	0.05	2.71	-0.28	3.71	42.89
13.99	0.36	2.37	-1.48	2.84	48.16
14.09	0.31	2.70	-0.91	3.67	39.97
14.19	0.00	2.50	-0.64	3.47	43.55
14.29	0.27	2.73	-0.31	3.70	43.51
14.39	0.53	2.94	-0.09	3.73	47.80
14.49	0.51	3.03	-	-	39.90
14.52	0.70	2.97	-0.51	4.15	38.38
14.62	0.70	2.87	-0.34	3.93	38.83
14.72	0.69	3.12	-0.48	3.48	40.24
14.82	0.32	2.96	-	-	39.08
14.92	0.62	2.92	-	-	35.68
15.02	0.55	3.38	-0.36	4.07	40.30
15.12	0.66	3.27	-	-	30.57
15.22	0.69	2.81	-0.28	3.50	38.11
15.32	0.64	2.94	-0.29	3.57	47.27
15.39	0.60	2.83	-0.23	3.38	46.32
15.52	0.56	2.63	-0.32	3.58	41.21
15.53	0.19	1.96	-0.69	3.21	52.48

Table 4.8 cont.

Sub-bottom Depth (m)	*G.bulloides* $\delta^{13}C$	*G.bulloides* $\delta^{18}O$	*Uvigerina* $\delta^{13}C$	*Uvigerina* $\delta^{18}O$	$\%CaCO_3$
15.61	-0.04	1.64	-0.76	2.71	41.76
15.72	-0.29	1.04	-0.87	3.06	56.27
15.83	-0.07	1.51	-0.57	2.90	59.56
15.92	-0.55	1.01	-	-	55.38
16.02	-0.24	1.25	-	-	42.19
16.10	-0.10	1.96	-	-	55.46
16.20	-0.83	1.33	-	-	53.37
16.30	-1.21	0.94	-0.43	3.39	61.94
16.40	-1.00	1.18	-0.42	3.98	46.18
16.50	-	-	-0.31	3.86	49.22
16.60	-0.64	2.06	-0.45	4.01	46.47
16.71	-1.40	1.86	-1.01	3.97	34.58
16.80	-0.71	2.45	-0.36	4.25	36.83
16.90	-0.46	2.09	-	-	15.00
17.01	0.20	3.38	-	-	21.25
17.10	-0.30	3.92	-	-	14.84
17.21	0.24	3.10	-1.07	4.60	14.67
17.30	-0.37	2.36	-1.73	5.08	8.61
17.41	-0.55	2.72	-1.74	4.84	7.56
17.49	-1.37	1.66	-	-	8.05
17.60	-0.57	2.96	-1.87	4.72	9.76
17.71	-1.30	2.50	-	-	8.07
17.80	-0.14	3.05	-	-	9.86
17.91	-0.87	2.70	-	-	10.09
18.00	-0.41	3.11	-	-	12.83
18.11	-0.52	2.82	-	-	23.85
18.20	-0.25	3.08	-	-	21.15
18.30	-0.02	3.85	-0.92	4.45	20.55
18.40	-0.28	3.20	-1.19	4.17	14.44
18.51	-0.49	3.26	-1.16	4.01	16.22
18.61	-0.86	2.93	-0.75	4.51	17.39
18.71	-0.63	2.89	-0.79	4.34	21.58
18.80	-0.37	2.98	-0.90	4.48	22.88
18.90	-0.49	3.19	-0.77	4.63	32.64
19.00	-0.76	2.77	-0.94	4.73	23.52
19.10	-0.29	3.11	-0.91	4.50	19.72
19.20	-0.47	3.74	-	-	18.44
19.30	-0.60	2.91	-0.54	5.33	10.59
19.40	-0.45	3.35	-	-	12.35
19.50	-0.64	3.24	-	-	7.50
19.60	-0.63	3.34	-	-	21.54
19.70	-0.67	3.77	-1.23	5.40	4.07
19.80	-0.43	3.58	-0.79	5.04	4.01
19.90	-0.55	3.62	-0.95	4.63	4.44
20.01	-	-	-1.43	4.84	4.83
20.10	-	-	-	-	4.57
20.20	-	-	-1.11	4.67	2.86
20.30	-0.42	3.51	-0.81	4.87	4.04
20.40	-0.95	3.02	-1.11	4.45	5.90
20.50	-0.42	2.98	-0.69	4.14	11.88

*$\%CaCO_3$ results supplied by P.J.Cooke (MSc thesis, University of Waikato, 1988).

Since a "gap" of ~1m existed in Hole 594, additional samples were requested from Hole 594B. A rough initial alignment of the two cores was provided by colour stratigraphy, which was later refined by the good overlap of the carbonate and isotopic records. Results reported between 14.52m and 15.53m are derived from Hole 594B.

4.2 NZOI Cores

Q200, Q217, and Q219 (see Figure 3.1) were selected for sampling because colour and coarse fraction stratigraphy (Griggs et al., 1983) suggested that they contained a record of isotope stages 1 through 5. The results from the analysis of the top 2.8m of Q200, Q217, and Q219 are presented in Tables 4.9, 4.10, and 4.11 respectively.

Table 4.9. $\delta^{18}O$ and $\delta^{13}C$ values for *Globigerina bulloides* and *Uvigerina*, with $\%CaCO_3$ results for samples from NZOI Core Q200 (45°59.7'S;172°1.5'E, in a water depth of 1370m).

Sub-bottom	*G.bulloides*		*Uvigerina*		
Depth (m)	$\delta^{13}C$	$\delta^{18}O$	$\delta^{13}C$	$\delta^{18}O$	$\%CaCO_3$
0.03	0.51	1.88	0.05	3.23	-
0.10	0.10	1.64	-0.20	3.18	-
0.20	0.38	1.86	-0.22	2.89	-
0.28	-0.10	2.02	-0.21	3.17	-
0.40	-0.01	2.52	-0.50	3.87	-
0.50	0.09	3.20	-0.52	4.77	-
0.60	0.57	3.40	-0.12	4.95	6.90
0.69	0.25	3.30	-0.21	4.49	10.30
0.79	0.18	3.35	-0.20	4.20	14.70
0.90	0.22	3.24	-0.35	4.09	14.60
0.99	0.07	2.89	-0.06	4.43	13.20
1.08	0.46	3.35	-0.21	4.07	25.50
1.18	0.11	2.83	-0.18	4.29	25.80
1.28	0.38	3.30	-	-	35.60
1.38	0.14	3.28	-0.51	3.93	31.90
1.48	0.33	3.30	-0.40	4.26	17.90
1.58	-0.10	2.83	-0.77	4.41	9.60
1.68	0.21	3.23	-0.68	4.45	13.80
1.78	0.50	3.55	-0.71	4.48	16.20
1.88	0.62	2.98	-0.64	4.50	31.90
1.95	0.73	3.13	-0.53	3.89	59.70

Table 4.9 cont.

Sub-bottom	*G.bulloides*		*Uvigerina*		
Depth (m)	$\delta^{13}C$	$\delta^{18}O$	$\delta^{13}C$	$\delta^{18}O$	$\%CaCO_3$
2.04	0.77	2.93	-0.61	4.00	72.80
2.13	0.69	2.70	-0.43	3.76	81.10
2.23	0.69	2.60	-0.18	3.95	79.50
2.33	0.67	2.75	0.01	3.88	85.80
2.45	0.37	2.49	-0.28	3.42	83.30
2.53	0.73	2.77	0.23	4.12	78.90
2.62	0.73	3.05	-0.23	3.74	71.30
2.73	0.57	2.86	-0.14	3.94	79.60
2.78	0.71	2.58	-0.28	3.64	81.30

Table 4.10. $\delta^{13}C$ and $\delta^{18}O$ values for *Globigerina bulloides* and *Uvigerina*, with $\%CaCO_3$ results for samples from NZOI Core Q217 (46°27.9'S;175°4.0'E, in a water depth of 1936m).

Sub-bottom	*G.bulloides*		*Uvigerina*		
Depth (m)	$\delta^{13}C$	$\delta^{18}O$	$\delta^{13}C$	$\delta^{18}O$	$\%CaCO_3$
0.06	0.42	3.56	-0.29	4.35	16.00
0.17	0.68	1.93	-0.40	3.22	65.50
0.28	-	2.49	-0.13	3.51	49.00
0.38	0.24	2.10	-0.37	3.89	49.30
0.48	0.03	2.26	-	-	3.80
0.58	-	-	-	-	1.70
0.66	-	-	-	-	3.60
0.76	0.28	3.73	-0.33	5.15	5.30
0.86	0.50	3.67	-0.51	4.09	10.60
1.13	0.34	3.20	-	-	8.20
1.23	0.20	2.73	-	-	24.20
1.33	0.52	3.45	-	-	22.60
1.43	0.53	3.14	-	-	23.10
1.53	0.31	3.21	-0.62	4.54	13.50
1.63	0.04	3.87	-0.65	4.88	9.90
1.73	0.18	3.21	-0.72	4.04	4.60
1.83	-	-	-	-	5.90
1.93	0.32	3.94	-0.26	4.33	9.90
2.04	0.70	3.41	-	-	17.40
2.14	0.76	3.23	-	-	46.40
2.24	0.98	3.22	0.03	3.96	68.00
2.34	0.57	3.13	-0.05	3.92	75.20
2.44	0.12	2.81	-0.45	3.66	50.50
2.54	0.84	3.10	-0.77	3.73	71.10
2.64	0.78	3.01	-0.15	3.65	77.40
2.74	0.53	2.86	-0.22	4.16	48.80
2.84	-0.05	2.57	-0.64	3.11	43.40

Table 4.11. $\delta^{13}C$ and $\delta^{18}O$ values for *Globigerina bulloides* and *Uvigerina* with $\%CaCO_3$ results for samples from NZOI Core Q219 (45°0.9'S;174°59.2'E, in a water depth of 1122m).

Sub-bottom	*G.bulloides*		*Uvigerina*		
Depth (m)	$\delta^{13}C$	$\delta^{18}O$	$\delta^{13}C$	$\delta^{18}O$	$\%CaCO_3$
0.03	0.43	2.09	-0.43	3.18	22.60
0.10	0.12	2.17	-0.54	3.42	29.00
0.20	-0.03	1.88	-0.49	3.85	36.90
0.30	0.31	1.96	-0.30	3.32	42.20
0.40	0.32	2.25	-0.33	3.18	37.90
0.50	0.03	1.96	-0.41	3.08	28.90
0.60	-0.26	1.82	-0.40	3.52	27.10
0.70	0.12	3.10	-0.86	3.27	13.10
0.80	-0.05	2.46	-0.60	3.45	30.70
0.90	-0.36	2.21	-0.85	3.39	25.50
0.98	-0.02	2.11	-0.65	3.29	24.00
1.06	0.12	2.04	-0.46	2.84	23.30
1.16	0.63	2.56	-0.29	2.92	26.40
1.26	0.25	1.92	-0.26	3.12	40.40
1.36	0.39	2.21	-	-	0.90
1.46	0.09	1.96	-	-	4.40
1.56	0.17	2.83	-	-	27.00
1.66	0.21	2.74	-	-	42.70
1.76	0.24	2.25	1.02	3.21	52.40
1.86	0.28	2.37	1.18	3.01	50.40
1.94	0.00	2.21	-	-	52.10
2.02	0.13	2.25	-	-	57.60
2.12	0.06	3.00	-0.26	3.04	45.40
2.22	0.15	2.43	0.26	2.81	53.20
2.32	-0.14	1.83	-	-	54.40
2.42	-0.11	1.73	0.47	2.42	43.10
2.52	0.01	2.18	0.42	2.11	54.50
2.62	-0.65	2.02	0.43	2.34	42.00
2.70	0.02	2.11	0.13	2.84	-
2.75	-0.01	2.06	0.23	2.88	53.90

Cores Q580, Q585, and Q858 (see figure 3.1) were all chosen to provide a range of sites along the length of New Zealand off the east coast. The results from these cores are presented in Tables 4.12, 4.13, and 4.14 respectively.

Table 4.12. $\delta^{13}C$ and $\delta^{18}O$ values for *Globigerina bulloides* and *Uvigerina*, with $\%CaCO_3$ results for samples from NZOI Core Q580 (46°12.2'S;179°0.0'W, in a water depth of 3964m).

Sub-bottom	*G.bulloides*		*Uvigerina*		
Depth (m)	$\delta^{13}C$	$\delta^{18}O$	$\delta^{13}C$	$\delta^{18}O$	$\%CaCO_3$
0.08	0.57	2.13	-0.56	3.09	42.10
0.17	0.84	2.18	-	-	32.60
0.26	0.53	1.77	-0.59	3.22	38.90
0.36	0.23	2.01	-0.88	3.42	38.20
0.46	0.42	2.33	-0.84	3.61	41.30
0.52	-0.06	1.80	-0.89	3.39	19.30
0.60	0.12	2.37	-0.77	3.84	48.00
0.70	-0.32	2.42	-1.98	3.45	45.70
0.79	-1.15	2.46	-	-	37.40
0.86	-0.35	2.08	-2.09	3.51	24.70
0.97	-0.08	2.84	-3.40	3.16	20.30
1.07	-0.24	3.03	-1.69	4.28	13.40
1.17	-1.16	1.98	-1.34	4.54	7.70
1.27	-0.81	2.56	-1.45	4.75	4.00
1.37	-	-	-	-	1.60
1.47	-	-	-1.55	4.80	1.40
1.57	-0.91	2.86	-0.93	5.16	3.30
1.67	-	-	-1.32	4.75	2.10
1.77	-	-	-	-	0.70
1.87	-	-	-1.80	4.18	0.00
1.98	-0.91	2.67	-1.31	4.68	8.60
2.08	-	-	-1.66	4.54	0.30
2.18	-	-	-1.03	5.22	0.80
2.28	-1.27	2.06	-1.25	4.74	3.00
2.38	-0.34	2.76	-	-	3.00
2.48	-	-	-	-	2.50
2.58	-0.63	3.25	-1.27	4.12	1.30
2.68	-0.38	3.51	-1.05	5.37	2.40
2.79	-0.02	3.91	-1.46	4.71	2.40
2.90	-1.26	2.46	-1.29	4.51	0.70
3.00	-0.45	3.54	-1.53	4.36	7.40
3.10	-	-	-1.21	4.70	6.50
3.20	-0.53	3.12	-1.16	4.67	8.20
3.30	-	-	-1.07	4.82	8.20
3.40	-0.44	3.22	-1.15	4.72	8.30
3.50	-0.42	2.90	-1.42	4.39	9.10
3.60	-0.25	2.95	-1.10	4.70	7.70
3.70	0.35	3.38	-1.08	4.49	8.50
3.80	-	-	-1.07	4.47	6.20

Table 4.13. $\delta^{13}C$ and $\delta^{18}O$ values for *Globigerina bulloides* and *Uvigerina*, with $\%CaCO_3$ results for samples from NZOI Core Q585 (49°42.2'S;177°55.5'W, at a water depth of4354m).

Sub-bottom	*G.bulloides*		*Uvigerina*		
Depth (m)	$\delta^{13}C$	$\delta^{18}O$	$\delta^{13}C$	$\delta^{18}O$	$\%CaCO_3$
0.01	0.77	2.36	-	-	46.30
0.09	0.33	2.36	-0.03	4.26	64.10
0.19	0.40	3.29	-0.98	4.77	23.20
0.29	0.25	2.78	-1.10	4.57	13.40
0.39	-	-	-	-	7.00
0.51	-	-	-	-	11.50
0.63	-	-	-0.85	5.07	16.90
0.73	-	-	-0.86	4.16	19.30
0.83	0.37	3.32	-0.77	4.59	18.70
0.94	0.72	3.11	-0.77	4.50	17.30
1.04	1.09	3.85	-	-	28.40
1.14	0.91	3.48	-0.75	4.57	33.40
1.24	0.52	3.22	-0.81	4.58	41.20
1.35	0.70	3.22	-1.02	3.69	39.60
1.45	0.91	2.47	-0.65	3.92	37.30
1.55	0.73	2.82	-	-	53.80
1.65	0.52	2.40	-0.73	3.41	42.80
1.73	0.45	2.93	-	-	64.20
1.83	0.61	2.53	-0.43	4.42	45.60
1.93	-	-	-	-	46.80
2.04	0.68	2.83	-0.48	3.14	55.90

Table 4.14. $\delta^{13}C$ and $\delta^{18}O$ values for *Globigerina bulloides* and *Uvigerina*, with $\%CaCO_3$ results for samples from NZOI Core Q858 (39°49.6'S;178°3.5'W, at a water depth of 3735m).

Sub-bottom	*G.bulloides*		*Uvigerina*		
Depth (m)	δ^{13}	$\delta^{18}O$	$\delta^{13}C$	$\delta^{18}O$	$\%CaCO_3$
0.02	-	-	-	-	21.00
0.10	-	-	-	-	13.20
0.18	-	-	-0.52	3.41	14.40
0.28	-	-	-0.55	3.37	27.70
0.38	-	-	-1.17	3.42	27.50
0.48	-	-	-0.78	3.61	33.90
0.58	-	-	-	-	31.60
0.68	-0.77	1.70	-	-	22.80
0.78	-1.84	0.18	-0.95	4.02	23.20
0.88	-1.04	1.97	-	-	22.10
0.98	-0.49	2.23	-	-	13.40
1.06	-0.24	2.69	-	-	14.00

Table 4.14 cont.

Sub-bottom	*G.bulloides*		*Uvigerina*		
Depth (m)	δ^{13}	$\delta^{18}O$	$\delta^{13}C$	$\delta^{18}O$	$\%CaCO_3$
1.16	-0.50	2.50	-0.99	5.36	14.30
1.26	-0.60	2.44	-	-	9.30
1.38	-0.01	2.97	-	-	11.60
1.48	0.29	3.51	-	-	10.00
1.56	0.06	2.58	-1.42	3.39	7.30
1.66	-0.50	2.64	-	-	9.90
1.76	-0.16	2.67	-	-	12.20
1.86	-0.19	2.78	-0.93	5.15	13.10

The remaining site (Z2108) is to the west of New Zealand (33°22.59'S;161°36.75'E, in 1448m of water), and was chosen to provide a more complete transect of the Tasman Sea. The stable isotope ratios and $\%CaCO_3$ values from Z2108 are presented in Table 4.15.

Table 4.15. $\delta^{13}C$ and $\delta^{18}O$ values for *Globigerina bulloides* and *Uvigerina*, with $\%CaCO_3$ results for samples from Core Z2108.

Sub-bottom	*G.bulloides*		*Uvigerina*		
Depth (m)	$\delta^{13}C$	$\delta^{18}O$	$\delta^{13}C$	$\delta^{18}O$	$\%CaCO_3$
0.04	-0.98	-0.61	-0.44	2.64	84.50
0.14	-1.20	0.07	-1.18	3.02	84.30
0.24	-1.41	-0.11	-0.56	3.36	79.60
0.35	-2.65	0.00	-0.42	3.81	82.70
0.46	-1.77	0.40	-0.39	3.85	75.30
0.56	-1.53	0.01	-0.57	3.02	82.20
0.66	-1.30	0.42	-0.86	2.96	83.10
0.76	-1.74	-0.10	-0.84	2.98	76.10
0.86	-1.85	-0.11	-0.86	2.91	82.10
0.98	-1.72	-0.17	-0.48	3.09	77.10
1.06	-1.92	-0.21	-1.14	2.96	81.10
1.16	-2.24	-0.05	-0.54	3.46	81.90
1.27	-2.29	-0.16	-0.82	3.48	-9.90
1.36	-1.64	0.13	-0.67	3.12	78.40
1.46	-1.29	0.00	-0.75	3.26	84.20
1.56	-2.64	-0.69	-1.76	2.50	84.00
1.66	-2.53	-1.04	-0.92	2.54	85.80
1.75	-9.90	-9.90	-1.87	2.33	84.80
1.84	-2.25	-1.53	0.11	3.17	84.50
1.93	-9.90	-9.90	-0.51	2.75	84.70
2.07	-1.13	-0.08	-0.70	2.84	85.70

Table 4.15 cont.

Sub-bottom	*G.bulloides*		*Uvigerina*		
Depth (m)	$\delta^{13}C$	$\delta^{18}O$	$\delta^{13}C$	$\delta^{18}O$	$\%CaCO_3$
2.17	-2.29	-1.01	-0.72	2.76	86.00
2.27	-1.74	-0.71	-0.29	2.82	83.70
2.37	-1.95	-0.66	-0.58	1.84	83.10
2.47	-1.49	-0.16	-1.15	2.18	84.80
2.57	-1.56	0.57	-0.68	3.28	82.10
2.67	-1.95	0.37	-1.09	3.14	78.00
2.77	-1.68	1.03	-1.44	3.48	-9.90
2.87	-1.29	1.81	-1.01	3.47	77.30
2.97	-9.90	-9.90	-1.18	3.78	74.90
3.07	-2.09	0.34	-0.74	4.03	79.00
3.17	-2.01	0.15	-0.77	3.68	80.70
3.27	-9.90	-9.90	-1.12	3.35	75.90
3.37	-9.90	-9.90	-0.78	3.29	77.60
3.48	-2.43	-0.71	-0.93	2.87	80.70
3.58	-1.71	0.30	-0.62	3.88	80.80
3.68	-1.61	0.04	-0.43	3.99	76.00
3.78	-2.55	-0.64	-0.76	3.62	78.20
3.88	-1.56	0.20	-0.65	2.68	82.20
3.98	-2.34	-1.60	-0.22	2.80	80.60
4.05	-1.02	-0.02	-0.75	2.58	87.00

The results presented in this chapter will be discussed in Chapter 5.

Chapter Five

DISCUSSION OF RESULTS

The results obtained from the analysis of core samples in Chapter 4 will be discussed in this chapter. All of the carbonate, $\delta^{18}O$ and $\delta^{13}C$ data (where available) for each core are presented graphically (figures are referred to in the text).

The first step in the discussion of the $\delta^{18}O$ results involves the assignment of stage boundaries (Section 5.1.1). In most cases the records do not go back beyond stage 9, but longer sections of core were available from Sites 589, 592 and 593 (and also from previous analysis of Site 594; Cuthbertson, 1985). Following the assignment of stage boundaries, comparisons are made between the results obtained in this study and those previously derived for other $\delta^{18}O$ records (Section 5.1.2). Further discussion then focuses mainly on particular periods represented in the $\delta^{18}O$ record, including the Holocene (Section 5.1.3), the last glacial (Section 5.1.4), the nature of glacial to interglacial changes (Section 5.1.5), and the last interglacial (Section 5.1.6). In addition, the degree of synchroneity of cyclicity in the benthic and planktonic $\delta^{18}O$ record at Site 594 is considered (Section 5.1.7).

$\delta^{13}C$ results are then analysed (Section 5.2) using much the same format as for the $\delta^{18}O$ results. The chapter concludes with discussion of some aspects of the carbonate record (Section 5.3).

5.1 Discussion of $\delta^{18}O$ Results

5.1.1 Assignment of Stage Boundaries

The plots of data from Tables 4.1 to 4.15 show fluctuations between high and low $\delta^{18}O$ values, due to changes in ice volume and

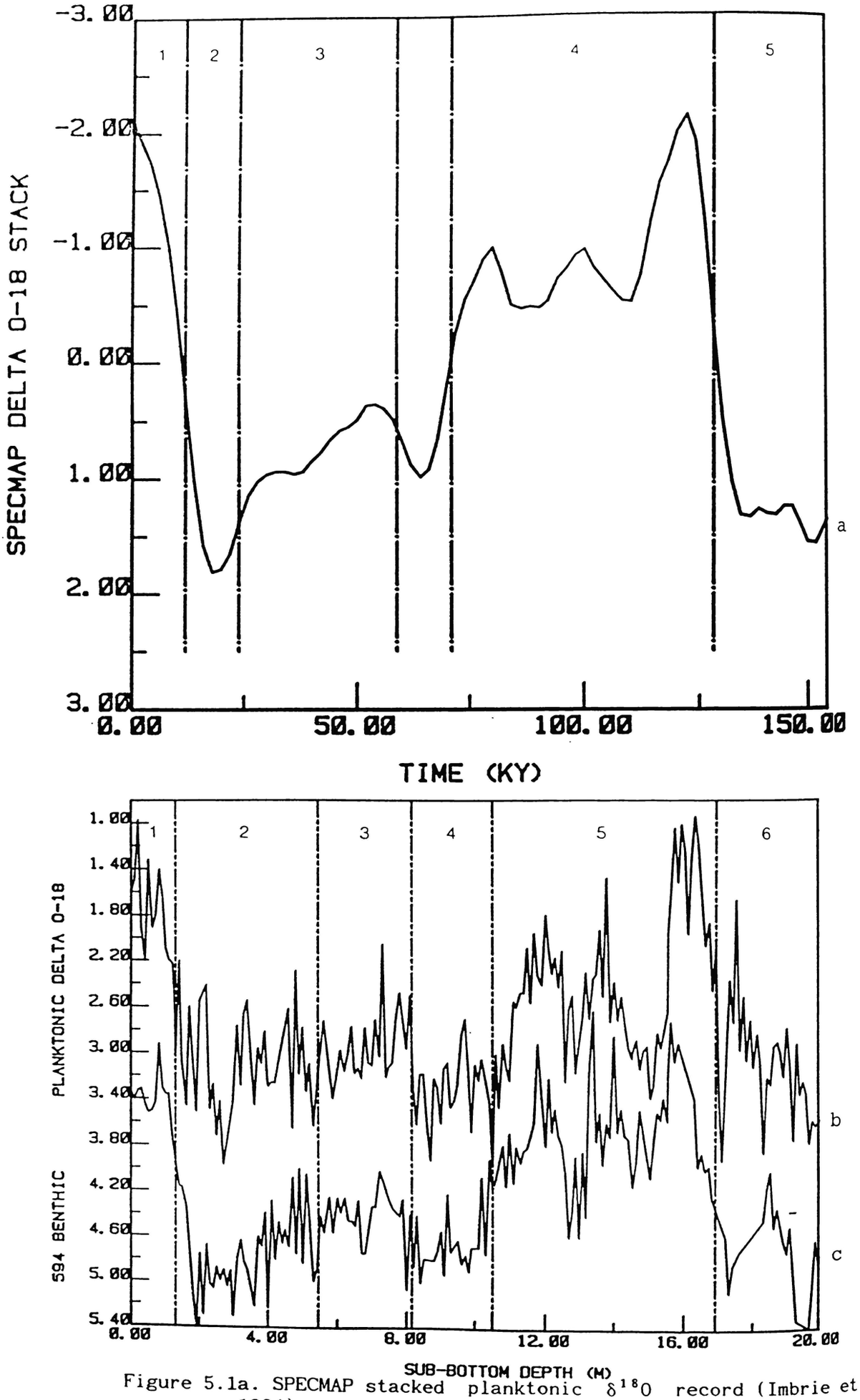

Figure 5.1a. SPECMAP stacked planktonic $\delta^{18}O$ record (Imbrie et al., 1984).
b. 594 planktonic $\delta^{18}O$ data.
c. 594 Benthic $\delta^{18}O$ data.
Dotted lines show isotope stage boundaries.

temperatures, from which the inferred placement of isotope stage boundaries can be made (Emiliani, 1955; Shackleton and Opdyke, 1976). Boundaries for the short (few metres long) cores from the east of New Zealand were selected following comparison with the detailed 594 record (Figure 5.1), while those from the west of New Zealand (Tasman Sea) were chosen by comparison with the long 593 record (Figure 5.10). The ages adopted for these boundaries are those derived by Imbrie et al. (1984). Justification of the stage boundaries chosen for each core is presented. Stage boundaries have been positioned roughly in the middle of the period of greatest change from glacial to interglacial (or vice versa) conditions indicated by the $\delta^{18}O$ record. The non-synchroneity of some of the benthic and planktonic records (see Section 5.1.7) created difficulties in the placement of stage boundaries, as the period of change was slightly offset in one record compared to the other. In addition, the marked sub-stage fluctuations in some records made it difficult to recognise where $\delta^{18}O$ values truly started to change from one extreme to another. Some attempt was made to put the assignment of stage boundaries on a statistical basis, but the mathematical modelling for such an exercise proved to be well beyond the scope of this thesis (Dr Ray Littler, School of Science statistical consultant, pers. commun., 1988).

East of New Zealand

594 The stage boundaries for 594 were largely determined on the basis of comparison to the spectral mapping group (SPECMAP) planktonic $\delta^{18}O$ stack (Imbrie et al., 1984) shown in Figure 5.1a, and to benthic data from cores V19-30 (Shackleton et al., 1983) and Meteor 12 392 (Figure 5.2a and c). Although the 594 record contains far greater detail than the SPECMAP plot, it is not difficult to see that, with smoothing, the

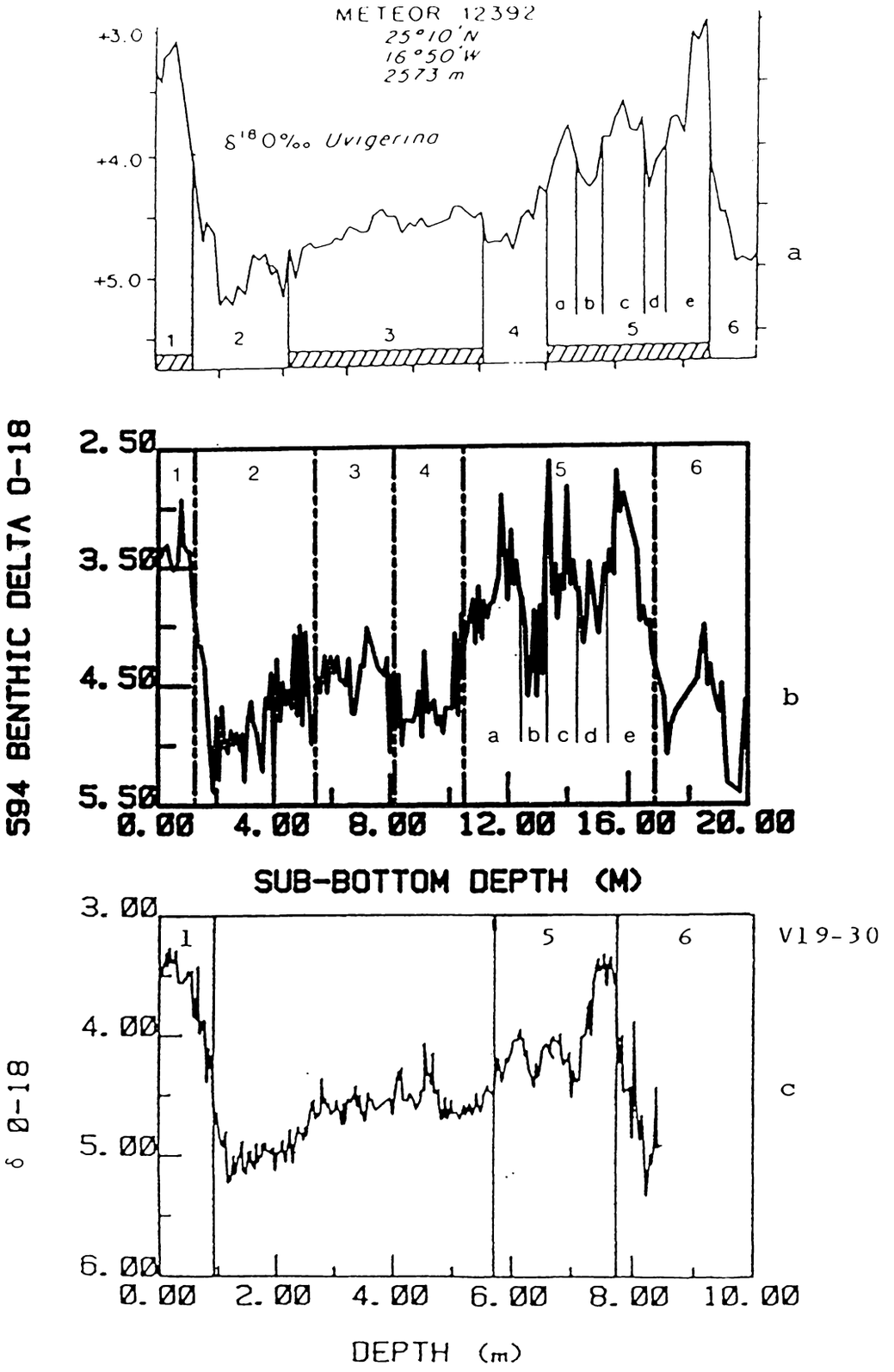

Figure 5.2a. *Meteor* 12 392 *Uvigerina* $\delta^{18}O$ record.
b. 594 benthic $\delta^{18}O$ data.
c. V19-30 benthic $\delta^{18}O$ data (Shackleton et al., 1983).

general shape of the 594 curve follows the major trends of the SPECMAP stack for stages 6 to 1. Radiocarbon dating of a sample from 0.3m sub-bottom depth in 594 yielded an age of 6.8ky, compatible with the stage 1 assignment.

594 shows far greater short term variability, and a slightly larger range from high to low values, than either of the V19-30 and M12 392 records. This is no doubt due to the preservation of short duration climatic fluctuations because of the very high sedimentation rates (~13cm/ky) and consequently extremely high resolution available in the 594 core. These fluctuations are not caused by analytical uncertainties as repetition of randomly chosen samples yielded results consistent within the standard deviation of the NBS-19 values.

Some difficulty arose over the assignment of the 2/3 stage boundary as it is not clearly defined in either the benthic or the planktonic $\delta^{18}O$ record. However, the $\%CaCO_3$ record (Figure 5.3e) displays peaks and troughs that are more or less synchronous (within a few cm sub-bottom depth) with the $\delta^{18}O$ record (Cuthbertson, 1985; Nelson et al., 1985). Because of this near-synchroneity, it was felt justified - in the case of 594 - to assume that changes from high to low carbonate content correspond to stage boundary transitions occurring in the $\delta^{18}O$ record. This approach is not without precedent (e.g., Williams et al., 1988). Hence, as the 2/3 transition is clearest in the carbonate record, it was decided that this be used to define the 2/3 stage boundary. The $\delta^{18}O$, $\delta^{13}C$ and $\%CaCO_3$ records of Core 594 are shown in Figure 5.3, with the proposed stage boundaries marked.

The sub-bottom depths and ages of the stage boundaries are presented in Table 5.1, together with the sedimentation rate for each stage. The sedimentation rates for each stage have been derived from

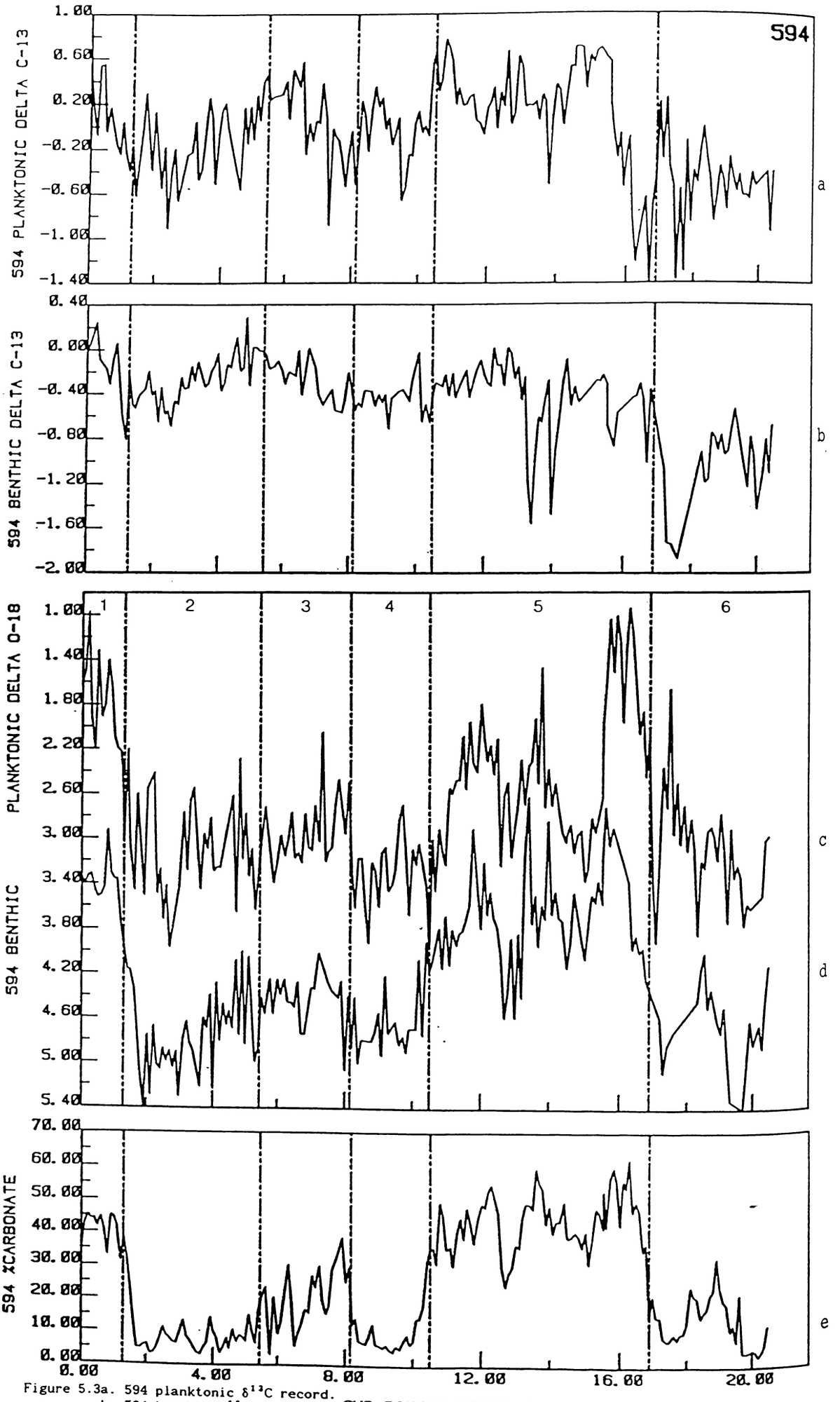

Figure 5.3a. 594 planktonic $\delta^{13}C$ record.
b. 594 benthic $\delta^{13}C$ record.
c. 594 planktonic $\delta^{18}O$ record.
d. 594 benthic $\delta^{18}O$ record.
e. 594 $\%CaCO_3$ record (Cooke, 1988).

the core length representing each stage, and the length of time for which the stage lasted. A constant sedimentation rate is assumed within each stage. These sedimentation rates can only be approximate since no compensation has been made for the increasing compaction of the sediment with burial depth, compression of the core during drilling, and subsequent dessication during storage (particularly for the older NZOI cores that are discussed later), but are a useful guide to general trends in glacial and interglacial sedimentation rates.

Table 5.1. Depths and ages of stage boundaries in Core 594, with sedimentation rates for each stage (see Figure 5.3).

Stage Boundary	Sub-bottom Depth(m)	Age (ky)
1/2	1.3	12
2/3	5.45	24
3/4	8.15	59
4/5a	10.5	71
5a/5b	12.4	
5b/5c	13.1	
5c/5d	14.5	
5d/5e	15.6	
5e/6	16.9	128

Stage	Sedimentation Rate (cm/ky)
1	10.8
2	34.6
3	9.1
4	18.3
5	11.2

Q200 (Figure 5.4). The values for planktonic and benthic $\delta^{18}\bar{O}$ are consistent with those obtained at Site 594 for stages 1, 2 and 3, with no isotopic evidence of stage 5. The proposed stage boundaries are

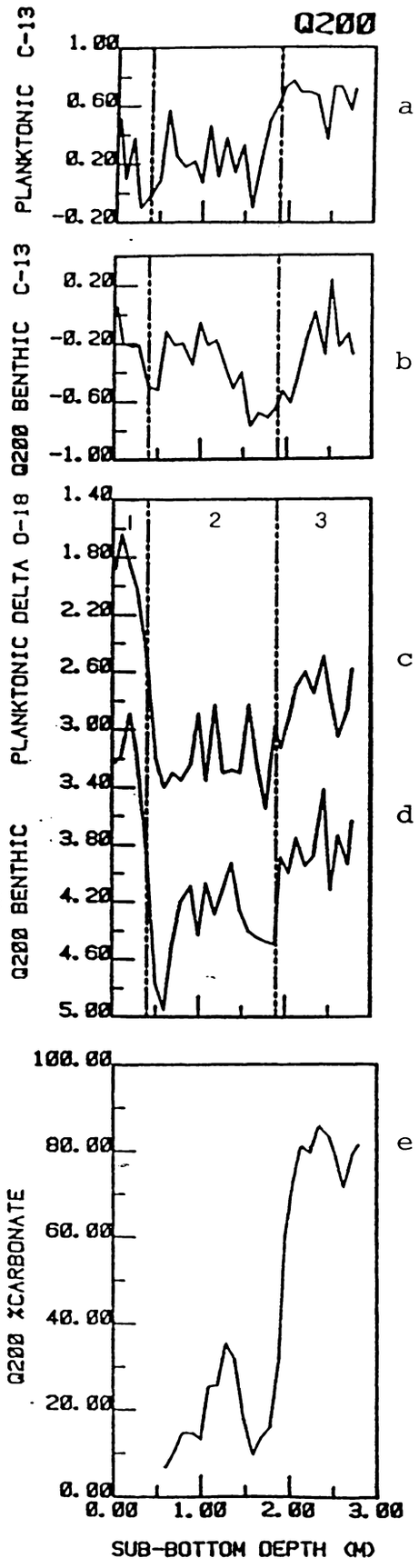

Figure 5.4a. Q200 planktonic $\delta^{13}C$ record.
b. Q200 benthic $\delta^{13}C$ record.
c. Q200 planktonic $\delta^{18}O$ record.
d. Q200 benthic $\delta^{18}O$ record.
e. Q200 $\%CaCO_3$ record.

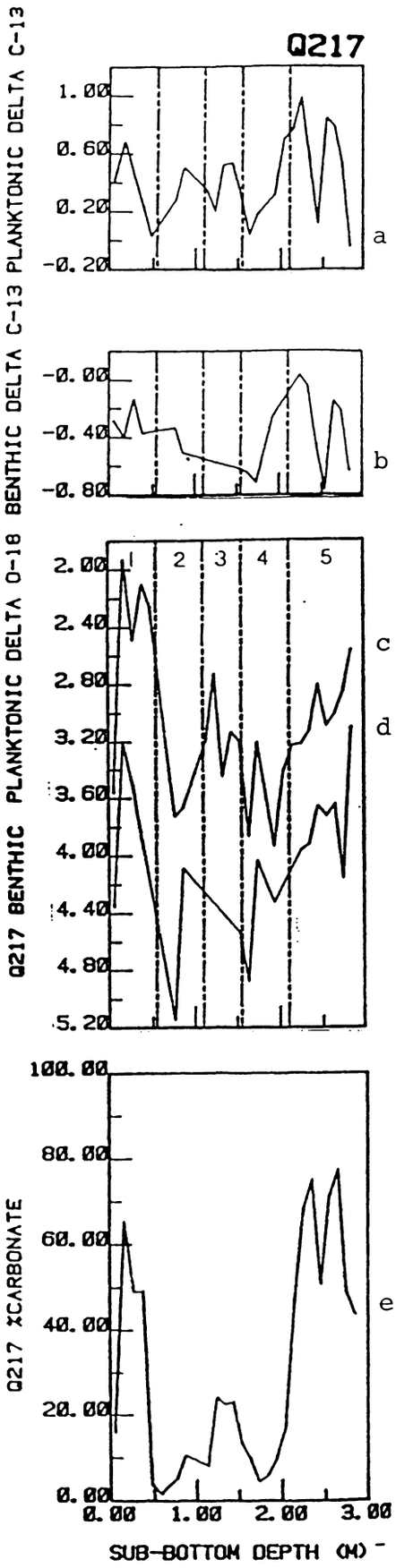

Figure 5.5a. Q217 planktonic $\delta^{13}C$ record.
b. Q217 benthic $\delta^{13}C$ record.
c. Q217 planktonic $\delta^{18}O$ record.
d. Q217 benthic $\delta^{18}O$ record.
e. Q217 $\%CaCO_3$ record.

presented in Table 5.2. Some doubt must exist as to whether the second interglacial labelled in the record represents stage 3 (as suggested by the isotopic analysis) or stage 5, since Griggs et al. (1983) report pelagic-hemipelagic changes in Q200 which suggest a record of stages 5 to 1. However, this is not supported by the isotopic ratios, as the $\delta^{18}O$ values between 2 to 3m sub-bottom depth (the section in question) do not approach the extremes of the low values for stage 1, which would be expected if it was stage 5. They are, however, compatible with a stage 3 interpretation.

Table 5.2. Proposed stage boundaries, depths and sedimentation rates for Q200 (see Figure 5.4).

Stage Boundary	Sub-bottom Depth(m)	Age (ky)	Stage	Sedimentation Rate (cm/ky)
1/2	0.4	12	1	3.0
2/3	1.9	24	2	12.5

Q217 (Figure 5.5). The planktonic foraminiferal $\delta^{18}O$ values do not clearly establish whether or not the core records stages 3 to 1, or 5 to 1. However, benthic foraminiferal values indicate a record of stages 5 to 1, as the extreme low value of $3.2^{o}/_{oo}$ recorded during stage 1 was previously reached at 2.8m sub-bottom depth. This supports published data on stage boundaries based on colour and grain size (Griggs et al., 1983), and correlates with an apparently clearer definition of stages 5 to 1 represented by the carbonate data. The

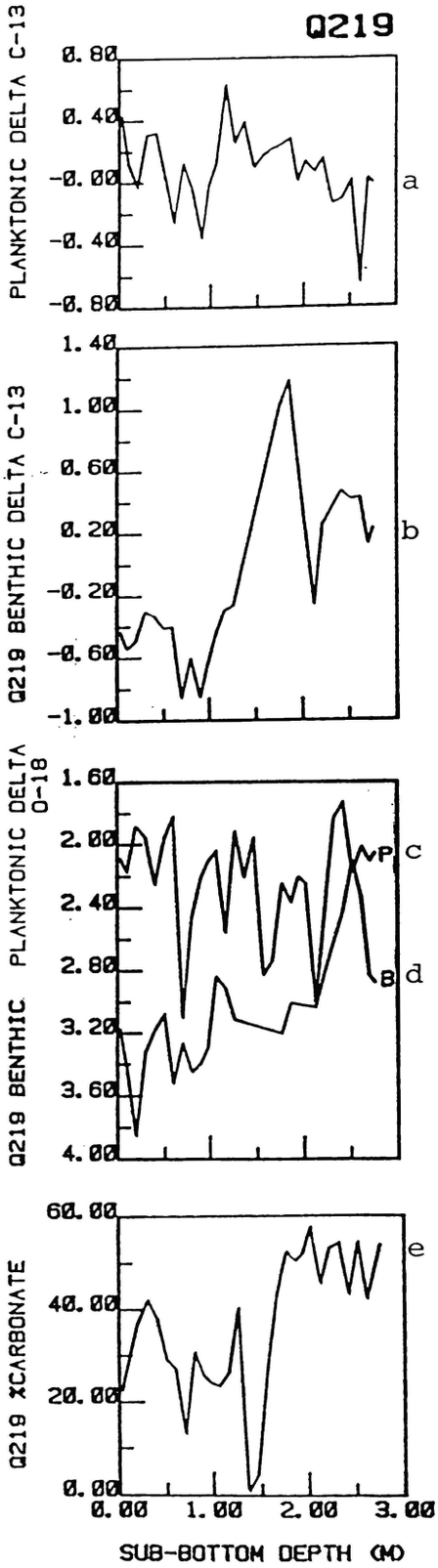

Figure 5.6a. Q219 planktonic $\delta^{13}C$ record.
b. Q219 benthic $\delta^{13}C$ record.
c. Q219 planktonic $\delta^{18}O$ record.
d. Q219 benthic δ^{18} record.
e. Q219 $\%CaCO_3$ record.

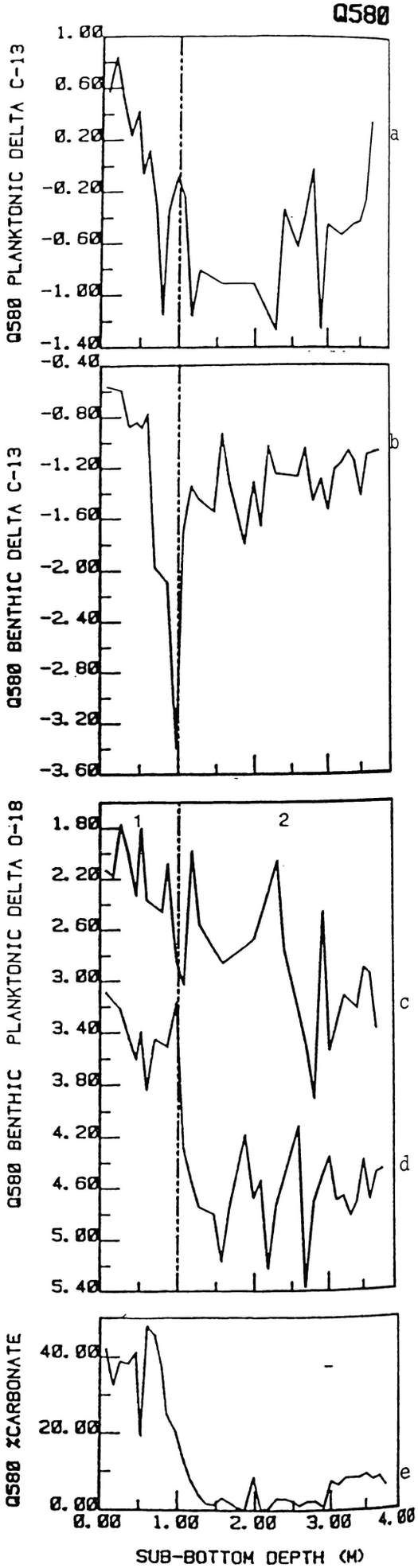

Figure 5.7a. Q580 planktonic $\delta^{13}C$ record.
b. Q580 benthic $\delta^{13}C$ record.
c. Q580 planktonic $\delta^{18}O$ record.
d. Q580 benthic $\delta^{18}O$ record.
e. Q580 $\%CaCO_3$ record.

proposed boundaries are presented in Table 5.3, along with sedimentation rates.

Table 5.3. Proposed stage boundaries and sedimentation rates for Q217 (see Figure 5.5)

Stage Boundary	Sub-bottom Depth(m)	Age (ky)	Stage	Sedimentation Rate (cm/ky)
1/2	0.55	12	1	4.6
2/3	1.1	24	2	5.4
3/4	1.55	59	3	1.3
4/5	2.1	71	4	4.6

Q219 (Figure 5.6). Fluctuations in the planktonic $\delta^{18}O$ record are insufficiently extreme to denote full glacial to interglacial variations. The low values (averaging $2.2^{o}/_{oo}$ in the planktonic record) would seem to indicate that the record is either all stage 1 or all stage 5, but the evidence is inconclusive. The sand mineralogy determined by Griggs et al. (1983) likewise does not allow stage definition. For this reason, no stage boundaries are defined for Q219.

Q580 (Figure 5.7). The benthic foraminiferal plot suggests a 1/2 boundary at ~1m sub-bottom depth that is not apparent in the planktonic record. Incursions of the cold-water Western Boundary Current (WBC) could have resulted in the confused planktonic signal. However, since the $\%CaCO_3$ curve appears to support a transition at 1m

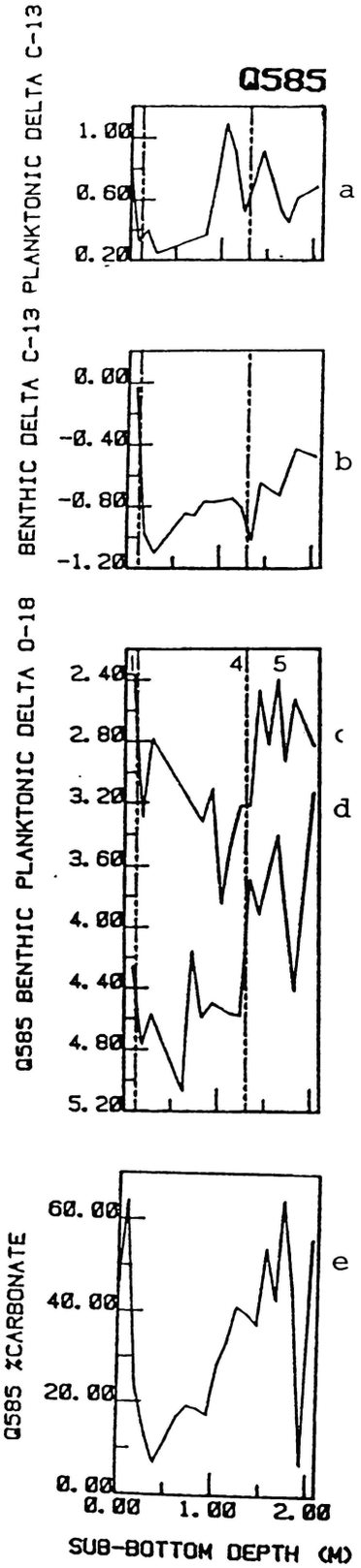

Figure 5.8a. Q585 planktonic $\delta^{13}C$ record.
b. Q585 benthic $\delta^{13}C$ record.
c. Q585 planktonic $\delta^{13}C$ record.
d. Q585 benthic $\delta^{18}O$ record.
e. Q585 $\%CaCO_3$ record.

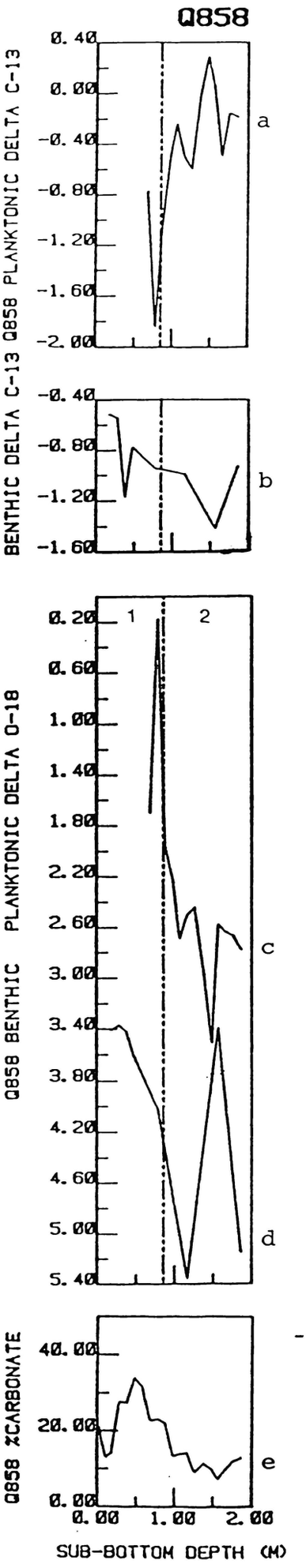

Figure 5.9a. Q858 planktonic $\delta^{13}C$ record.
b. Q858 benthic $\delta^{13}C$ record.
c. Q858 planktonic $\delta^{18}O$ record.
d. Q858 benthic $\delta^{18}O$ record.
e. Q858 $\%CaCO_3$ record.

this has been taken as the position of the 1/2 boundary, yielding a sedimentation rate of 8.3cm/ky for stage 1.

Q585 (Figure 5.8). Based on the $\delta^{18}O$ values, much of the Holocene appears to be missing, with the proposed 1/2 boundary very close to the sea floor at 0.13m, and the 4/5 boundary at ~1.3m. The thinness of the Holocene may reflect the proximity of the site to the WBC, as it flows between the Campbell Plateau and the Bollans Sea Mount, with consequent erosion (L.Carter, pers. commun., 1987).

Q858 (Figure 5.9). The isotope data from this site are inconsistent and confusing. Peculiarities in the benthic record have been suggested by Carter (NZOI, pers. commun., 1987) to be due to upslope incursions of the WBC. If this was the case, changes in water temperature brought about by the flow may have induced dissolution of the calcite, as Q858 is in deep water (3735m), close to the CCD. The planktonic data do, however, suggest a 1/2 boundary at 0.85m. This is supported by Carter's interpretation of a lithologic change, dated at about 13ky, corresponding closely to the Pleistocene/Holocene boundary (L.Carter, pers. commun., 1987).

West of New Zealand

593 The stage boundaries for this long core were determined by comparison with the SPECMAP $\delta^{18}O$ stack (Figure 5.10) and the records of cores V28-239 and DSDP 502 (Figure 5.11). The Brunhes/Matuyama boundary is given as 16.1m (Kennett et al., 1986). The proposed isotope stage boundaries for Core 593 back to the Brunhes/Matuyama boundary are marked in Figure 5.12 and presented in Table 5.4.

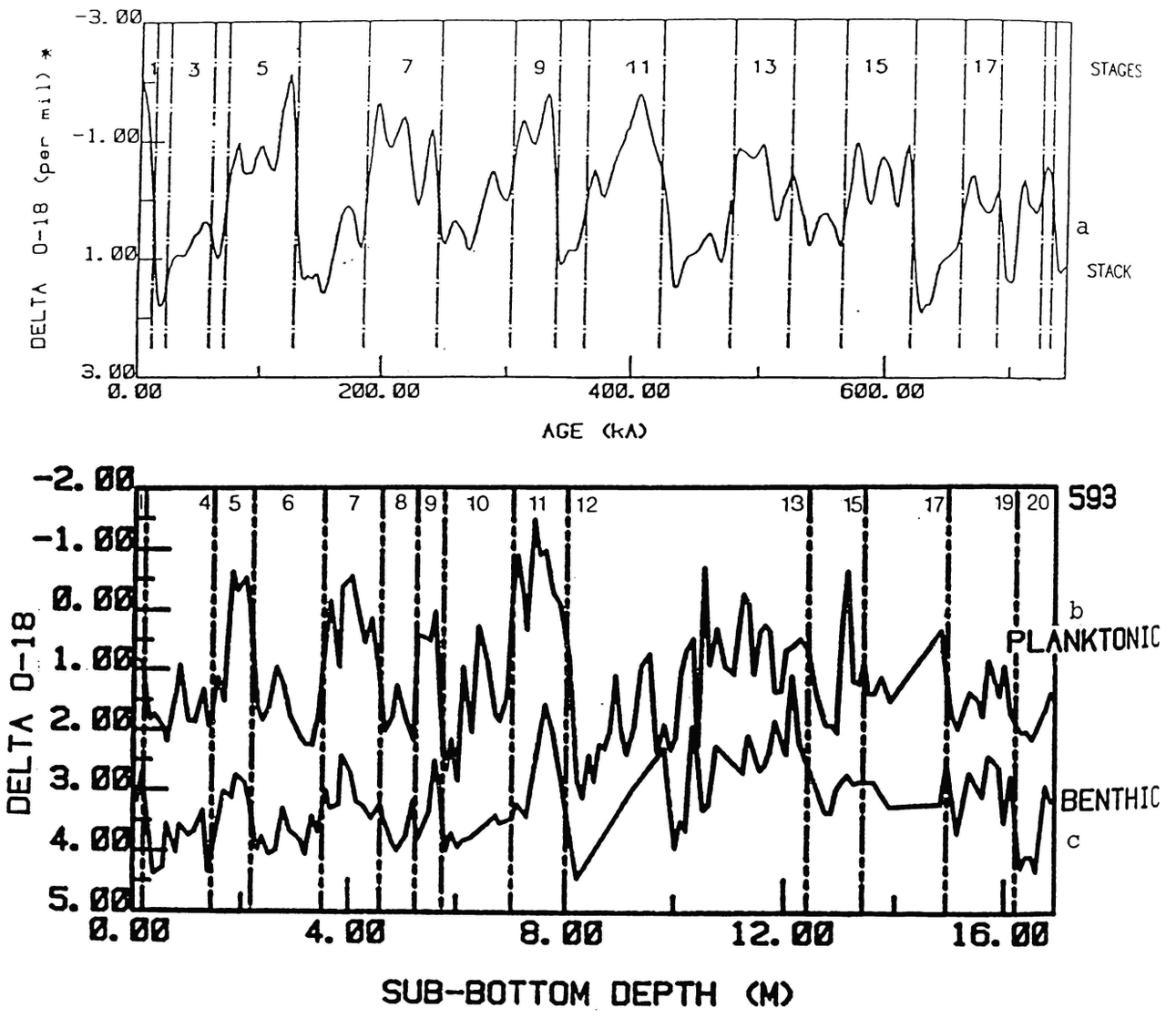

Figure 5.10a. SPECMAP stacked planktonic $\delta^{18}O$ record (Imbrie et al., 1984).
b. 593 planktonic $\delta^{18}O$ record.
c. 593 benthic $\delta^{18}O$ record.

(Figures 5.13 and 5.14 of the $\delta^{18}O$ and $\delta^{13}C$ records, respectively, for the top 43m of core analysed are included here for completeness).

Table 5.4. Proposed stage boundaries for 593, with sedimentation rates (see Figure 5.12).

Stage Boundary	Sub-bottom Depth(m)	Age (ky)
1/2	0.2	12
4/5	1.45	71
5/6	2.2	128
6/7	3.5	186
7/8	4.6	245
8/9	5.25	303
9/10	5.75	339
10/11	7.0	362
11/12	8.0	423
13/14	12.4	524
15/16	13.4	620
17/18	14.9	689
19/20	16.2	736

Stage	Sedimentation Rate (cm/ky)
1	1.6
5	1.3
6	2.2
7	1.9
8	1.1
9	1.4
10	5.4
11	1.6

Reinforcement of the stage assignments is provided by the first appearance of *Emiliania huxleyi* at 5.07m (Kennett et al., 1986; Lohman, 1986, pers. data), which is assigned as stage 8 and is consistent with Thierstein et al. (1977) who proposed that it evolved approximately 270ky BP. In addition the last appearance of *Pseudoemiliania lacunosa* at 9.9m (Kennett et al., 1986; Lohman, 1986,

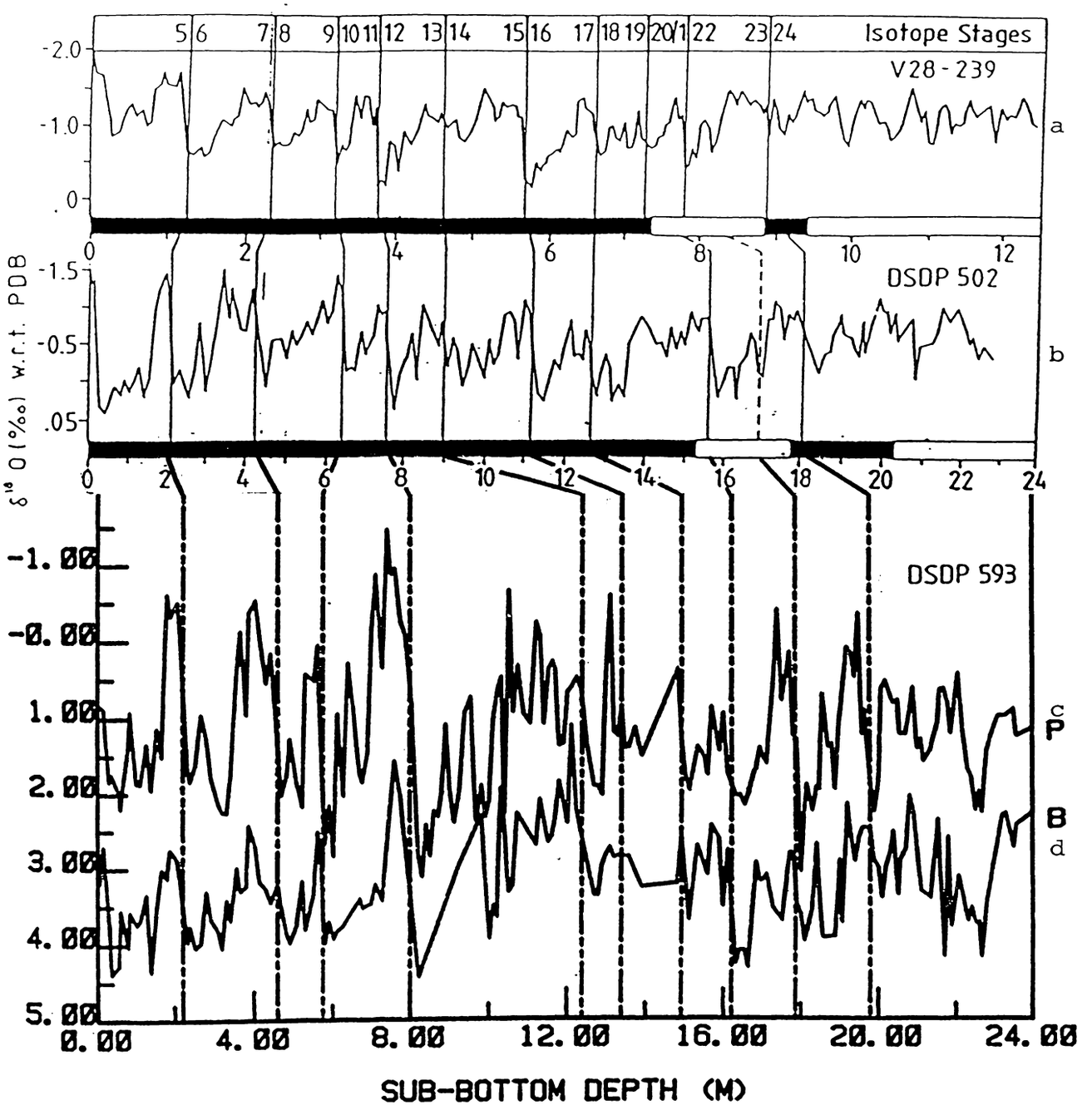

Figure 5.11a. V28-239 planktonic $\delta^{18}O$ record.
b. DSDP502 planktonic $\delta^{18}O$ record.
c. 593 planktonic $\delta^{18}O$ record.
d. 593 benthic $\delta^{18}O$ record.

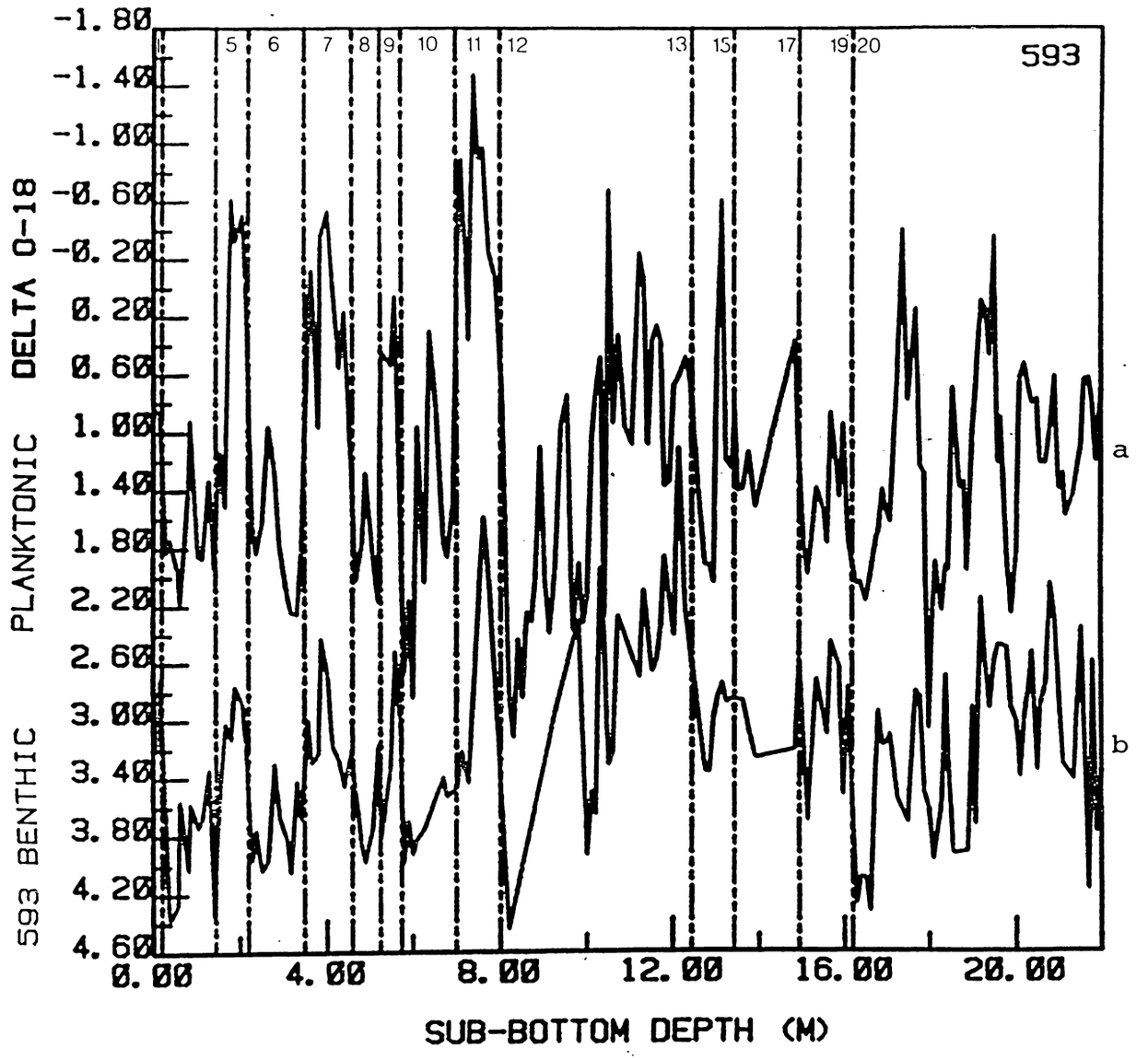

Figure 5.12a. 593 planktonic $\delta^{18}O$ data and
b. benthic $\delta^{18}O$ data, with isotope stages numbered back to the Brunhes/Matuyama boundary.

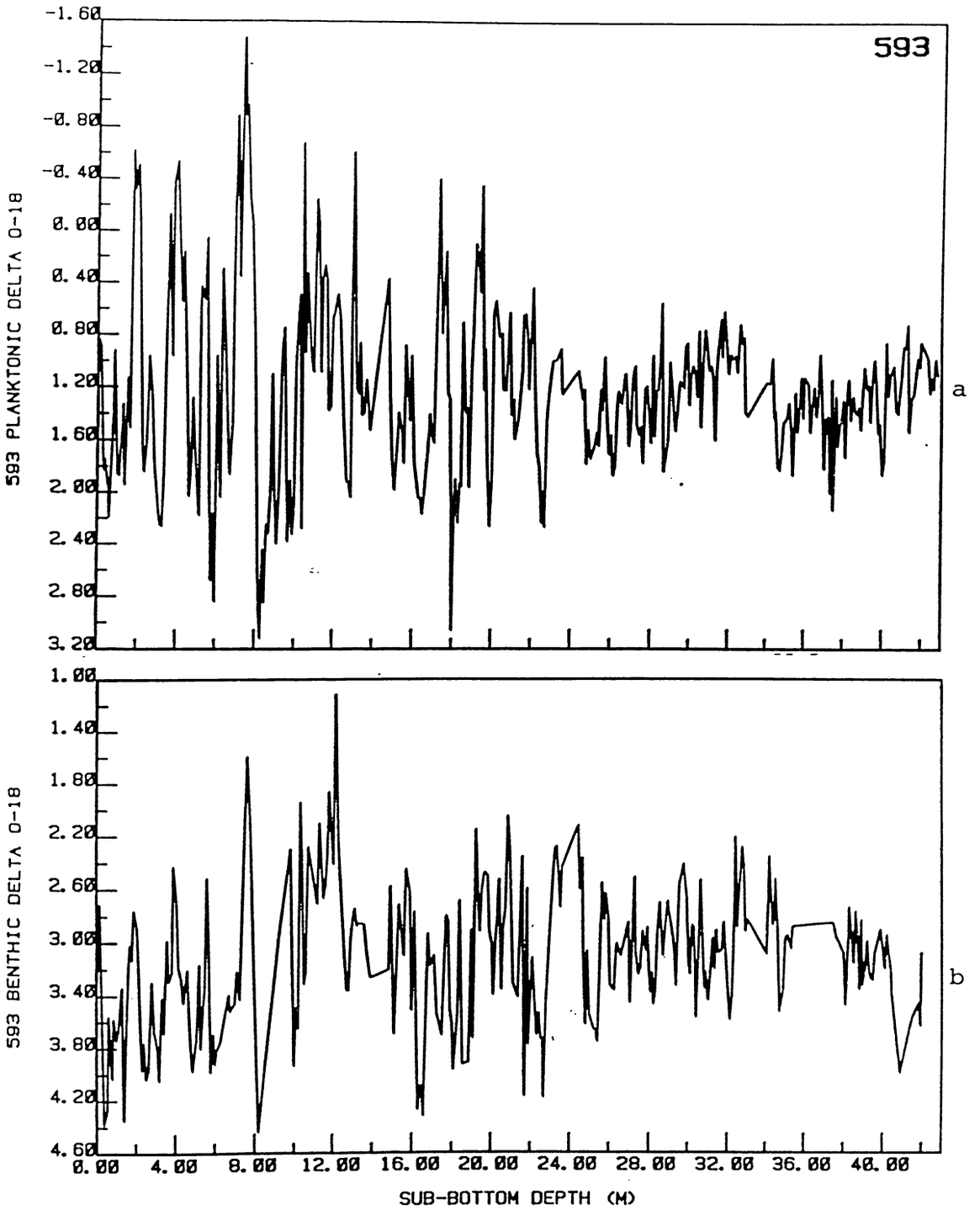

Figure 5.13. Complete record of planktonic (a) and benthic (b) $\bar{\delta}^{18}O$ data obtained from the analysis of 593 in this study.

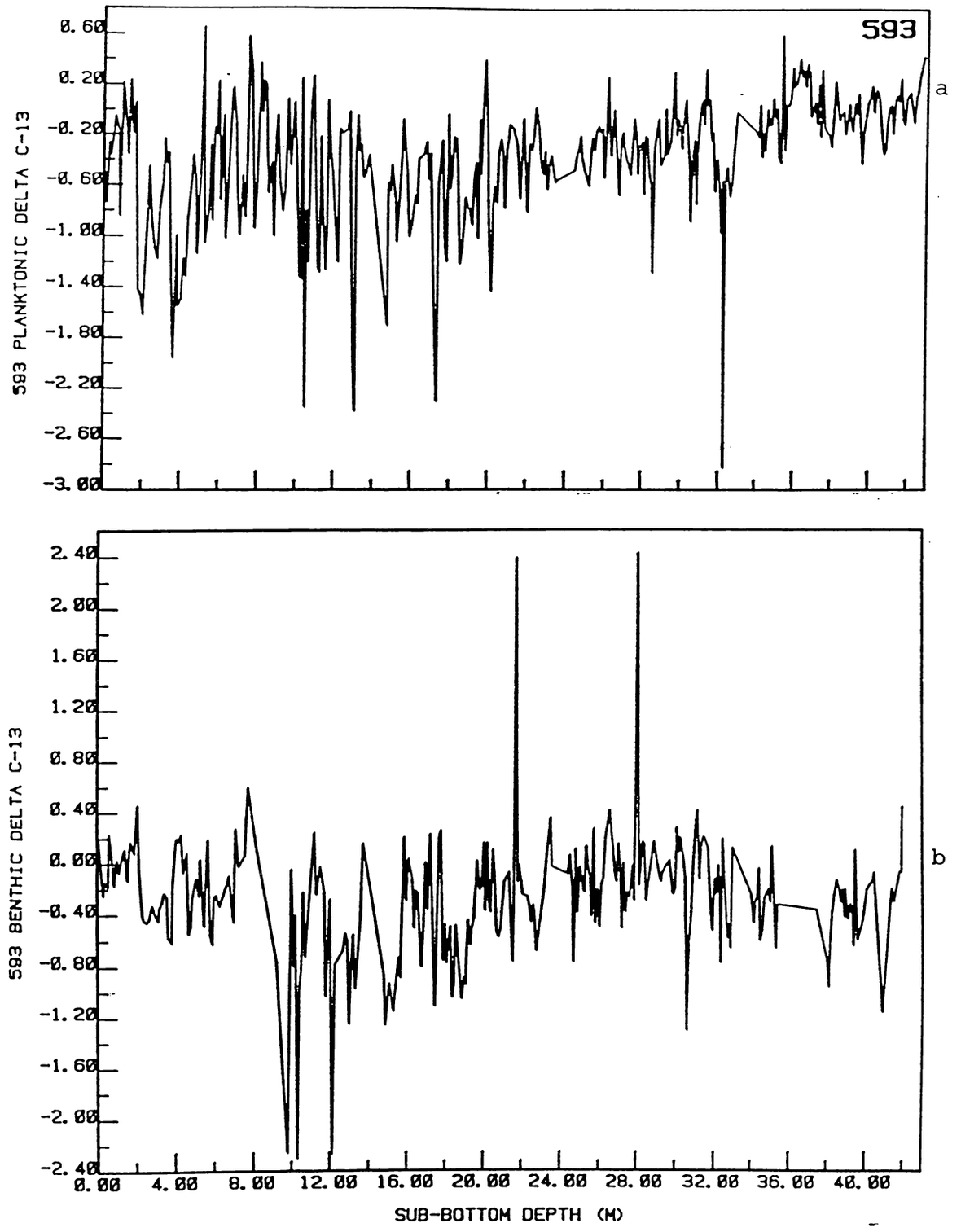

Figure 5.14. Complete record of planktonic (a) and benthic (b) $\delta^{13}C$ data obtained from the analysis of 593 in this study.

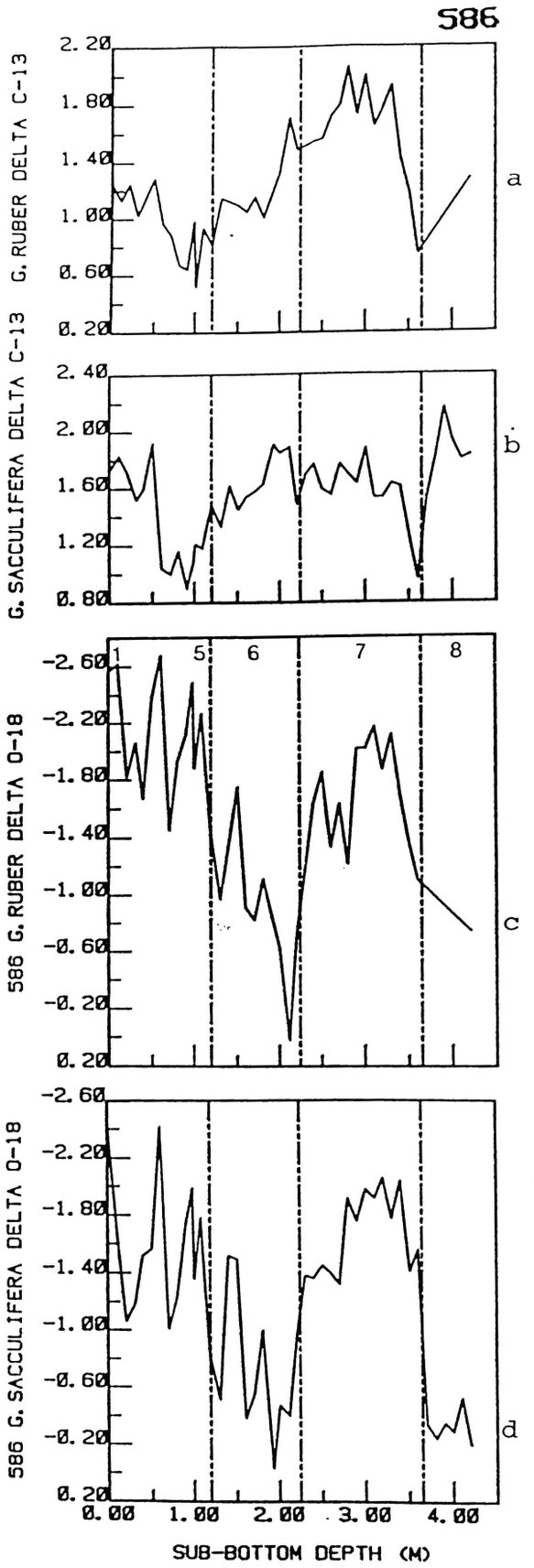

Figure 5.15a. 586 *Globigerina ruber* $\delta^{13}C$ record.
b. 586 *Globigerina sacculifera* $\delta^{13}C$ record.
c. 586 *Globigerina ruber* $\delta^{18}O$ record.
d. 586 *Globigerina sacculifera* $\delta^{18}O$ record.

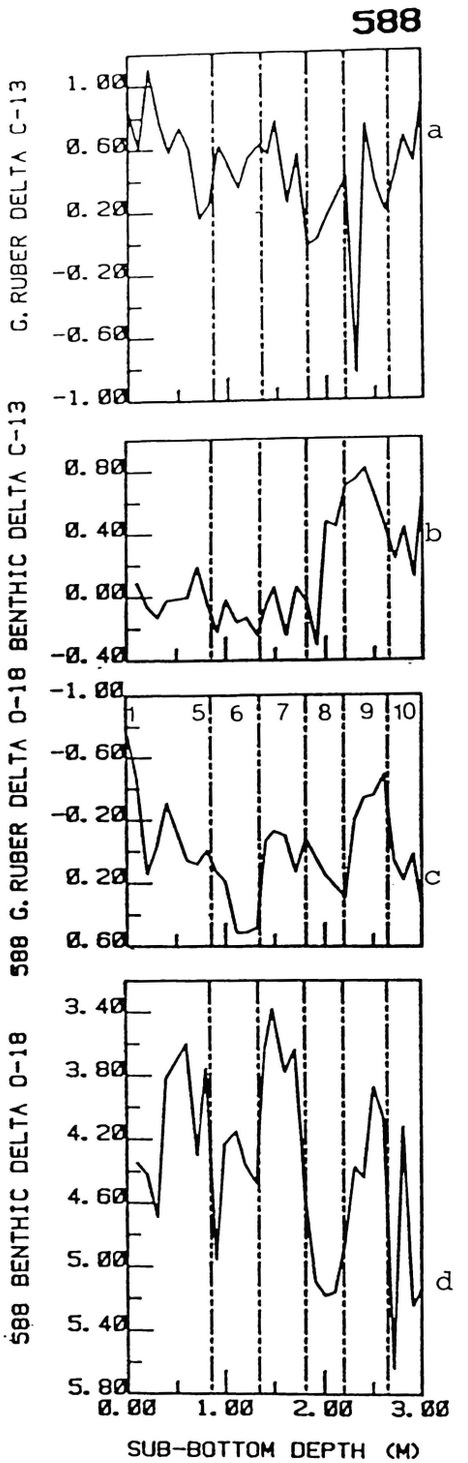

Figure 5.16a. 588 *Globigerina ruber* $\delta^{13}C$ record
b. 588 benthic $\delta^{13}C$ record.
c. 588 *Globigerina ruber* $\delta^{18}O$ record.
d. 588 benthic $\delta^{18}O$ record.

pers. data), which would place it in stage 12 (one of the most extreme glacials), is in good agreement with comparable bioevents between 410 and 460ky BP (Hays and Shackleton, 1976; Gartner, 1977; Shackleton, 1977; Thierstein et al., 1977) occurring in a period of extreme ^{18}O enrichment (Prell, 1982; Imbrie et al., 1984).

586 (Figure 5.15). The two planktonic species analysed from Site 586 were *Globigerina ruber* and *Globigerina sacculiferra*, and so direct comparison with the isotopic ratios of *Globigerina bulloides* is difficult. Moreover, there were insufficient benthics to analyse. However, the range of values between fluctuations, and in particular the shape of the high $\delta^{18}O$ region (which is typical of stage 6 - cf. 594), are compatible with the boundaries presented in Table 5.5.

Table 5.5. Proposed stage boundaries for 586, with sedimentation rates (see Figure 5.15).

Stage Boundary	Sub-bottom Depth(m)	Age (ky)
5/6	1.2	128
6/7	2.25	186
7/8	3.65	245

Stage	Sedimentation Rate (cm/ky)
6	1.8
7	2.4

The differences in isotopic composition between the two planktonic species remained more or less constant, with *G.sacculifera* generally ~0.1°/$_{oo}$ heavier in ^{18}O and ~0.6°/$_{oo}$ lighter in ^{13}C than *G.ruber*. That *G.sacculifera* should be heavier in ^{18}O is not unexpected as on average

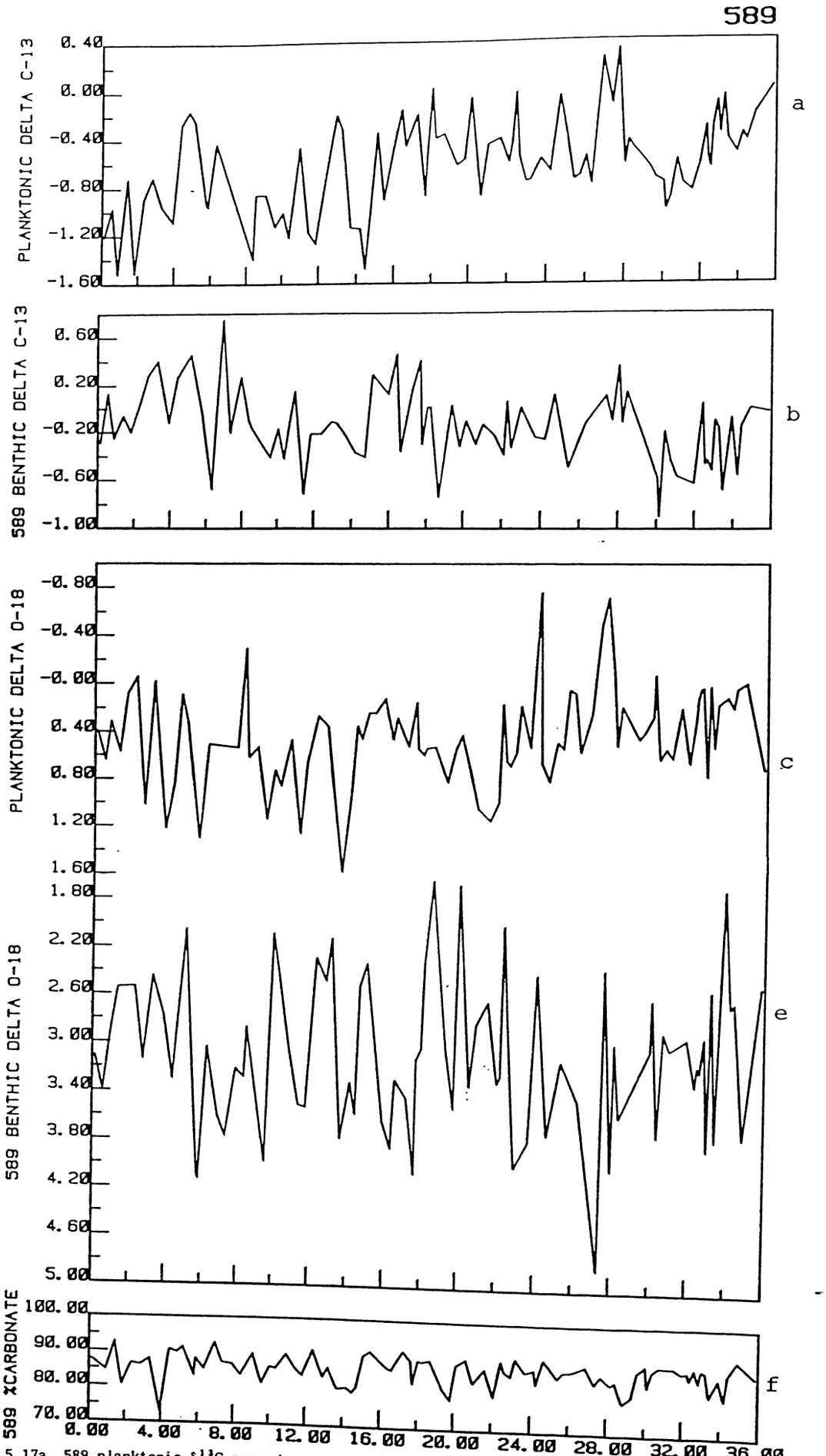

Figure 5.17a. 589 planktonic $\delta^{13}C$ record.
b. 589 benthic $\delta^{13}C$ record.
c. 589 planktonic $\delta^{18}O$ record.
d. 589 benthic $\delta^{18}O$ record.
e. 589 $\%CaCO_3$ record.

it lives at a slightly greater depth (~50m deeper), and hence in slightly cooler water, than *G.ruber* (Bé, 1977).

588 (Figure 5.16). The proposed stage boundaries for 588 are presented in Table 5.6. These were largely chosen on the basis of the clear fluctuations in the benthic record. Boundaries above the 5/6 transition (i.e. stages 5 to 1) are not clearly identifiable.

Table 5.6. Proposed stage boundaries for 588, with sedimentation rates (see Figure 5.16).

Stage Boundary	Sub-bottom Depth(m)	Age (ky)
5/6	0.85	128
6/7	1.35	186
7/8	1.81	245
8/9	2.2	303
9/10	2.65	339

Stage	Sedimentation Rate (cm/ky)
6	0.9
7	0.8
8	0.7
9	1.3

589 (Figure 5.17). The 589 record is of low resolution, from 40cm sampling intervals, and since there are only ~5 major peaks before the Brunhes/Matuyama boundary at 11m realistic assignment of stage boundaries is not possible. Comparison of the relative heights of the peaks suggests that the 11/12 stage boundary is at ~5.3m, as stage 12 is generally the most positive stage in the isotopic record back to the Brunhes/Matuyama boundary. It is impossible to determine if the two peaks evident between the top of the core and 5.3m represent 5, 7

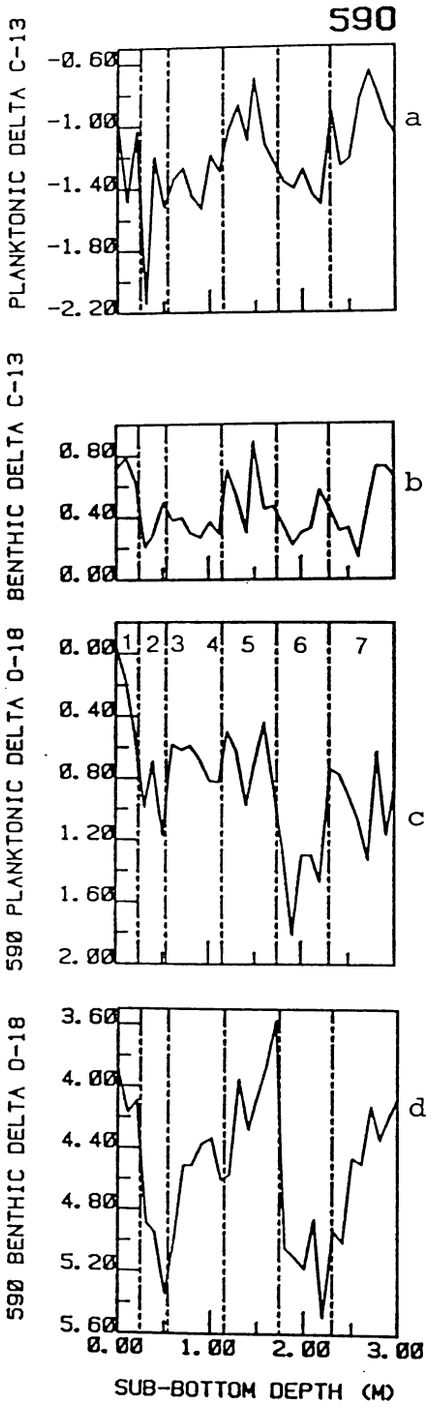

Figure 5.18a. 590 planktonic $\delta^{13}C$ record.
b. 590 benthic $\delta^{13}C$ record.
c. 590 planktonic $\delta^{18}O$ record.
d. 590 benthic $\delta^{18}O$ record.

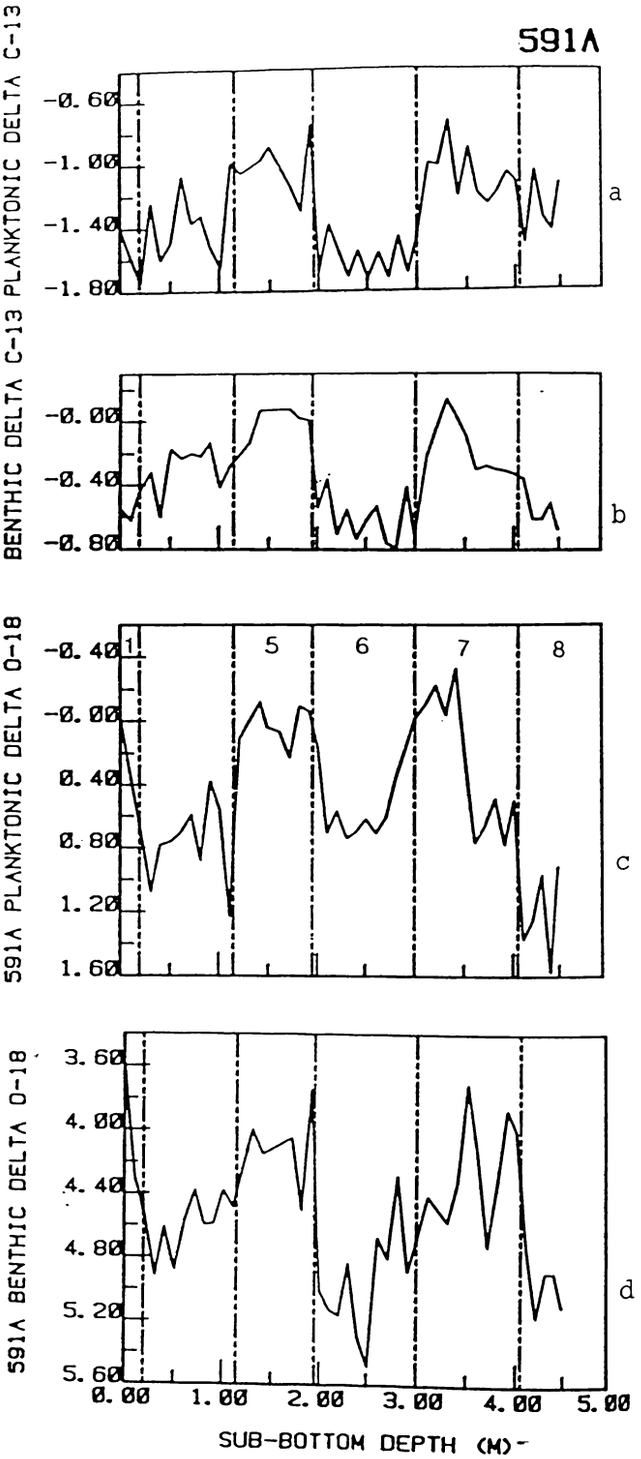

Figure 5.19a. 591A planktonic $\delta^{13}C$ record.
b. 591A benthic $\delta^{13}C$ record.
c. 591A planktonic $\delta^{18}O$ record.
d. 591A benthic $\delta^{18}O$ record.

or 9, although stage 1 is almost certainly missing. When 589 was sampled on board *Glomar Challenger* a plug was taken from each of the alternating colour sequences (Section 4.1) to ensure an analytical point for each palaeo-event. The absence of sufficient major peaks before the Brunhes/Matuyama boundary would indicate that colour sequences alone are not reliable indicators of glacial/interglacial changes.

590 (Figure 5.18). Both planktonic and benthic $\delta^{18}O$ values suggest a record of stages 7 to 1, with the boundaries defined in Table 5.7.

Table 5.7. Proposed stage boundaries for 590, with sedimentation rates (see Figure 5.18).

Stage Boundary	Sub-bottom Depth(m)	Age (ky)
1/2	0.25	12
2/3	0.55	24
4/5	1.15	71
5/6	1.75	128
6/7	2.3	186

Stage	Sedimentation Rate (cm/ky)
1	2.1
2	2.5
5	1.0
6	0.9

591A (Figure 5.19). A record of isotope stages 8 to 1 was obtained, with the stage boundaries defined in Table 5.8.

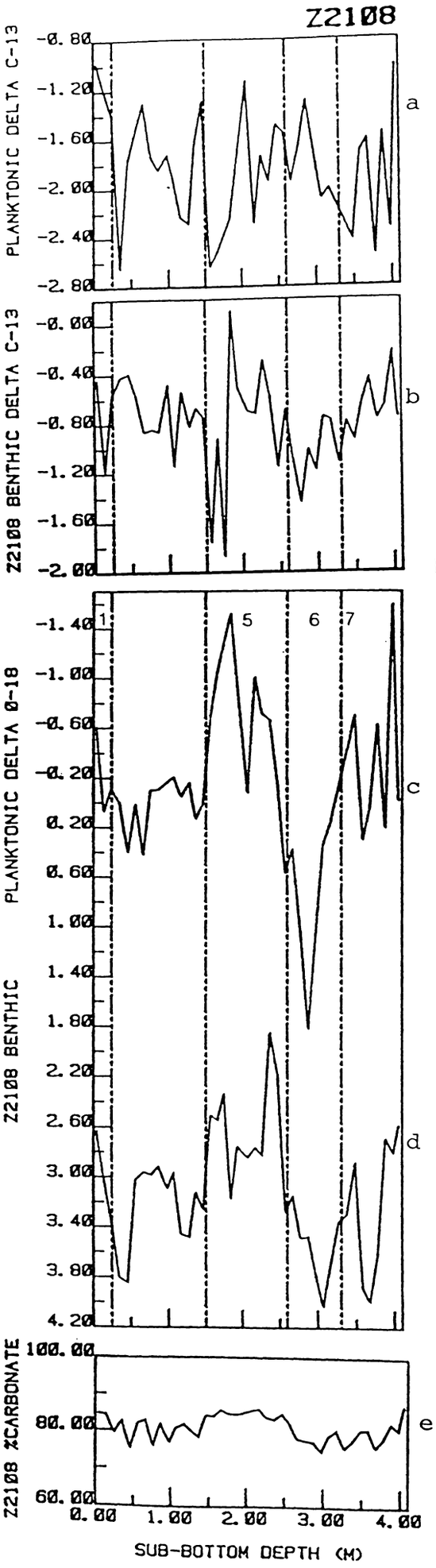

Figure 5.20a. Z2108 planktonic $\delta^{13}C$ record.
b. Z2108 benthic $\delta^{13}C$ record.
c. Z2108 planktonic $\delta^{18}O$ record.
d. Z2108 benthic $\delta^{18}O$ record.
e. Z2108 $\%CaCO_3$ record.

Table 5.8. Proposed stage boundaries for 591A, with sedimentation rates (see Figure 5.19).

Stage Boundary	Sub-bottom Depth(m)	Age (ky)
1/2	0.15	12
4/5	1.5	71
5/6	2.0	128
6/7	3.0	186
7/8	4.1	245

Stage	Sedimentation Rate (cm/ky)
1	1.3
5	0.9
6	1.7
7	1.9

Z2108 (Figure 5.20). The benthic $\delta^{18}O$ record of Z2108 is consistent with that of 593, and provides an interpretable curve from the base of the Holocene back to stage 7, with a similar sedimentation rate to 592. The boundaries are defined in Table 5.9.

Table 5.9. Proposed stage boundaries for Z2108, with sedimentation rates (see Figure 5.20).

Stage Boundary	Sub-bottom Depth(m)	Age (ky)
1/2	0.25	12
4/5	1.5	71
5/6	2.6	128
6/7	3.3	186

Stage	Sedimentation Rate (cm/ky)
1	2.1
5	1.9
6	1.2

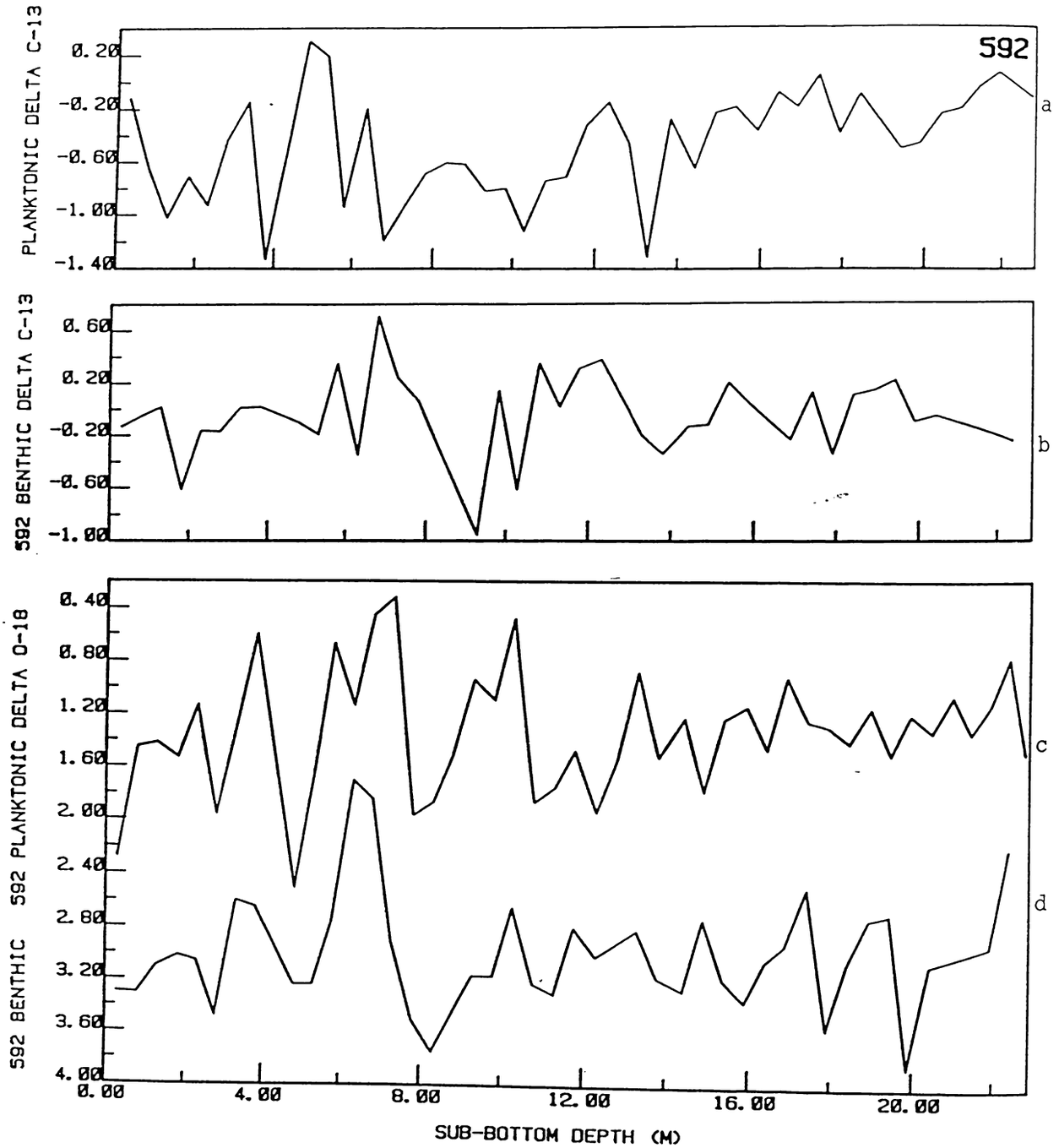

Figure 5.21. Low resolution
a. 592 planktonic $\delta^{13}C$ record.
b. 592 benthic $\delta^{13}C$ record.
c. 592 planktonic $\delta^{18}O$ record.
d. 592 benthic $\delta^{18}O$ record.

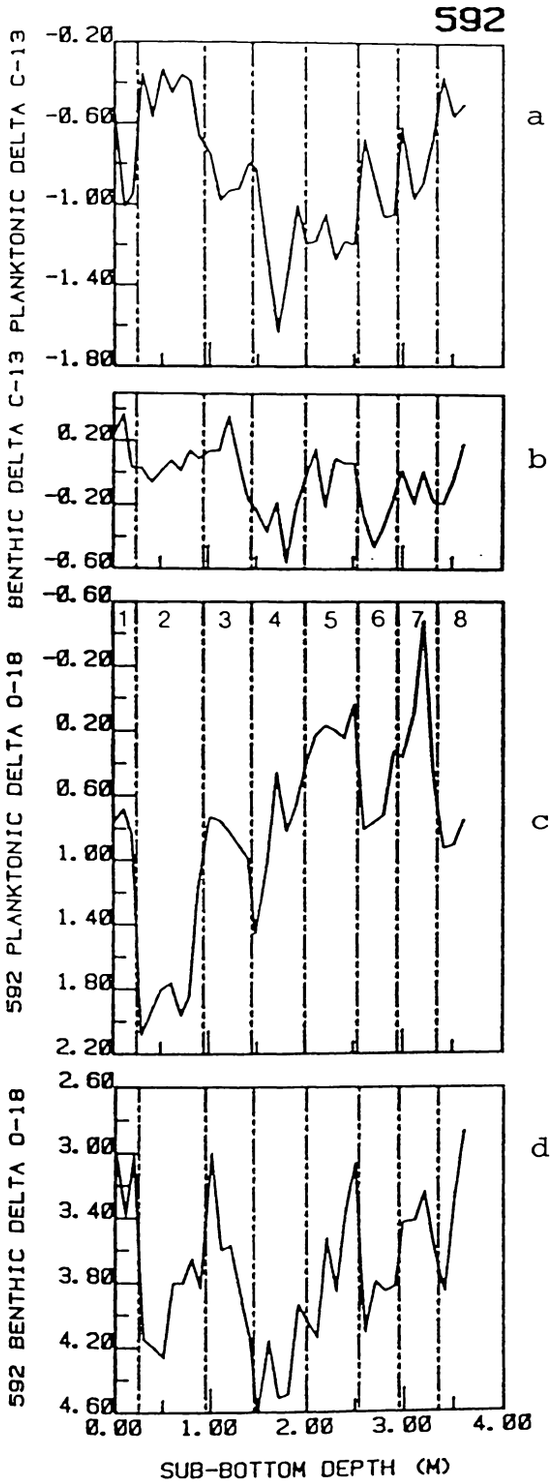

Figure 5.22. High resolution
a. 592 planktonic $\delta^{13}C$ record.
b. 592 benthic $\delta^{13}C$ record.
c. 592 planktonic $\delta^{18}O$ record.
d. 592 benthic $\delta^{18}O$ record.

592 The long, low resolution record of Site 592 (Figure 5.21) was of little help in assigning stage boundaries, and attention was focused on the short, high resolution, record (Figure 5.22). The positions of the boundaries are shown in Table 5.10.

Table 5.10. Positions of the stage boundaries in 592, with sedimentation rates (see Figure 5.22).

Stage Boundary	Sub-bottom Depth(m)	Age (ky)	Stage	Sedimentation Rate (cm/ky)
1/2	0.25	12	1	1.2
4/5	0.8	71	5	1.1
5/6	1.4	128	6	1.0
6/7	2.0	186	7	0.8
7/8	2.5	245	8	0.7
8/9	2.9	303	9	1.4
9/10	3.4	339		

(Note: As the results plotted in Figures 5.3 to 5.9 and Figures 5.12 to 5.22 feature repeatedly in later discussions, additional unbound copies of these graphs are provided for convenience in the envelope inside the back cover).

Summary

Some of the cores (e.g., 588) have very low sedimentation rates (<1cm/ky) over some, or all, stages and it is not surprising that

Table 5.11. Summary of the sub-bottom depths of the stage boundaries in each core, and the derived sedimentation rates for each stage.

Stage boundary depth (sub-bottom, m). (Sedimentation rate for stage, cm/ky).	West of New Zealand							East of New Zealand					
	586	588	590	591A	Z2108	592	593	Q858	594	Q200	Q580	Q217	Q585
1/2	-	-	0.3	0.2	0.3	0.3	0.2	0.8	1.3	0.4	1.0	0.6	0.1
(1)			(2.1)	(1.3)	(2.5)	(1.2)	(1.6)	(6.7)	(10.0)	(3.0)	(8.3)	(4.6)	-
2/3	-	-	0.6	-	-	-	-	-	5.5	1.9	-	1.1	-
(2)			(2.5)						(34.6)	(12.5)		(5.4)	
3/4	-	-	-	-	-	-	-	-	8.2	-	-	1.6	-
(3)									(9.1)			(1.3)	
4/5	-	-	1.2	1.5	1.5	0.8	1.5	-	10.5	-	-	2.1	1.3
(4)									(18.3)			(4.6)	
5/6	1.2	0.8	1.8	2.0	2.6	1.4	2.2	-	16.9	-	-	-	-
(5)			(1.0)	(0.9)	(1.9)	(1.1)	(1.3)		(11.2)				
6/7	2.8	1.3	2.3	3.0	3.3	2.0	3.5						
(6)	(2.7)	(0.9)	(1.7)	(1.2)	(1.2)	(1.0)	(2.2)						
7/8	3.7	1.8	-	4.1	-	2.5	4.6						
(7)	(1.5)	(0.8)		(1.9)		(0.8)	(1.9)						
8/9	-	2.2	-	-	-	2.9	5.3						
(8)		(0.7)				(0.7)	(1.3)						
9/10	-	2.7	-	-	-	3.4	5.8						
(10)		(1.3)				(1.4)	(1.1)						

their palaeo-isotopic record is lacking in detail. Ruddiman (1977) suggested that 5-10ky duration episodes may only be resolved where sedimentation rates are >3cm/ky, and that 1cm/ky is the lowest possible sedimentation rate to pick up 10ky episodes.

The depths of stage boundaries within all cores and, where possible, the derived sedimentation rates for each stage are presented in Table 5.11. The cores are listed in latitudinal sequence, from north to south, for cores to the west and to the east of New Zealand. Figure 5.23 summarises the sub-bottom depths of the stage boundaries for each core, where they can be determined.

West of New Zealand the sedimentation rates for each stage do not vary greatly from core to core, and do not show consistent variations between glacial and interglacial stages.

East of New Zealand, however, the influence of terrigenous sediment input from the Southern Alps of the South Island has resulted in a noticeable difference between glacial and interglacial sedimentation rates. During cooler periods increased erosion of the Southern Alps due to glacial action results in an increased volume of terrigenous sediment transported by rivers to the east coast shelf (Griggs et al., 1983; Nelson et al., 1986). In some cases these rivers extended across the continental shelf and discharged directly into the Bounty Trough from the Otago Canyons (Carter and Carter, in press). During interglacial periods alpine erosion was less severe, and the resultant sediment was generally trapped in glacial lakes and piedmont plains. In addition, during interglacial periods a northeasterly transport regime evolved which resulted in river sediments being diverted from the Bounty Trough, and carried instead along the shelf (Carter and Herzer, 1979; Carter et al., 1985). Consequently, higher sedimentation rates are evident during glacial (compared to

Figure 5.23. A summary of the sub-bottom depths of the stage boundaries within each core.

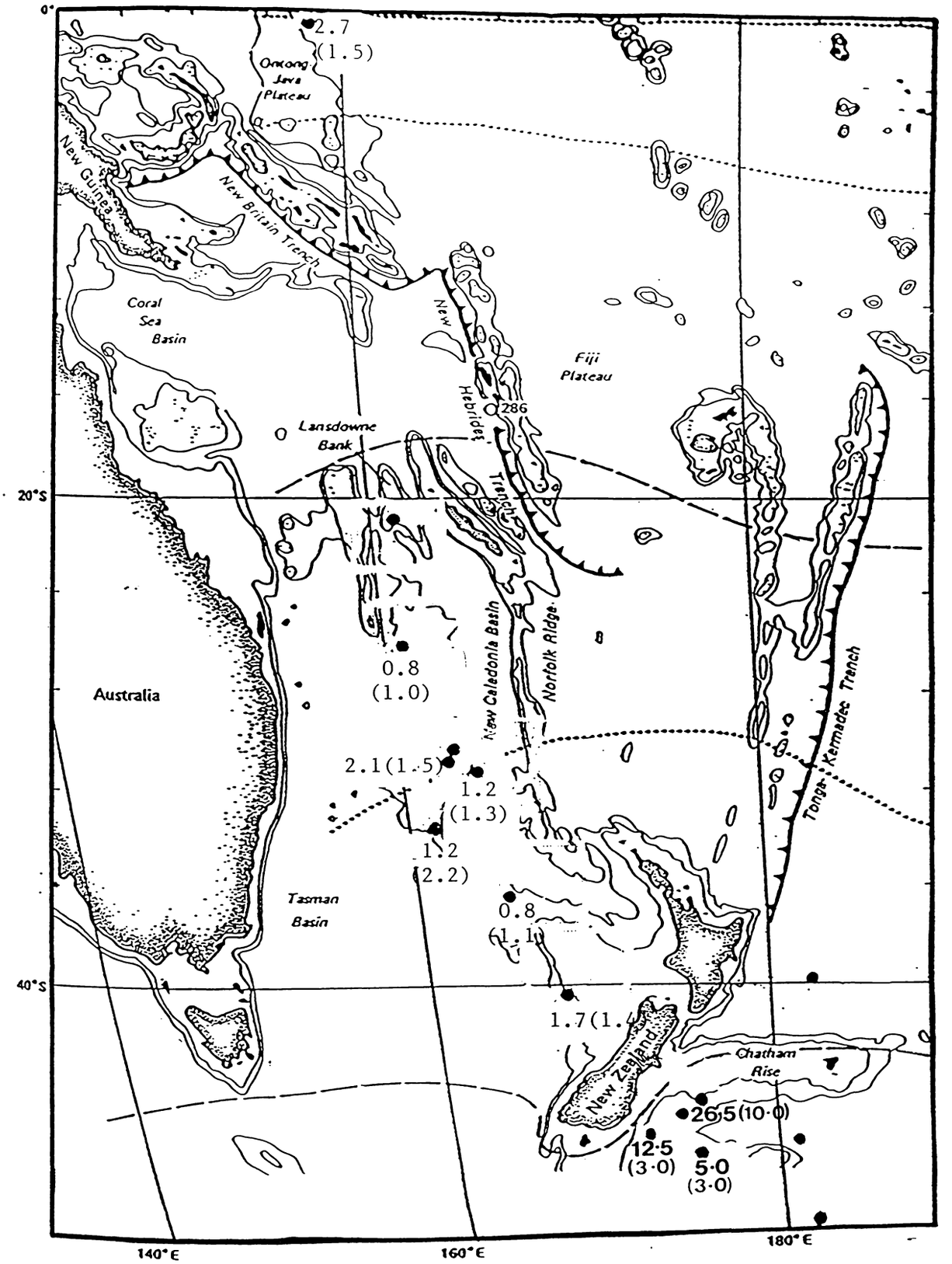

Figure 5.24. Mean glacial and interglacial (in brackets) sedimentation for the sites studied (where determinable) in cm/ky.

interglacial) periods at Sites 594, Q200 and Q217 (the only sites for which a sufficient number of sedimentation rates can be determined). The mean glacial and interglacial sedimentation rates for the sites studied are shown in Figure 5.24.

Less easily explained, however, is the reason for the vast difference in sedimentation rates (during both glacial and interglacial periods) seen at Site 594, compared to those of Q200 and Q217. Bearing in mind their close proximity, these sites should all have been exposed to similar amounts of glacial outwash from the South Island. Seismic profiles (L. Carter, pers. commun., 1987) confirm the exceptional sediment thickness at Site 594. In the case of Q217 its position close to the Bounty Channel makes it likely that sediment transport, as opposed to levee deposition, prevailed. In addition, wave current erosion of the Chatham Rise during periods of lower sea levels may have contributed to the sediment budget at Site 594, resulting in disparate sedimentation rates between the sites (L. Carter, pers. commun., 1987).

5.1.2 Stratigraphic Comparisons

In order to show the world-wide nature of climatic changes reflected in the $\delta^{18}O$ record of the region of study, and to identify events unique to this region, it is necessary to correlate the $\delta^{18}O$ record of sites analysed in this thesis with records obtained from elsewhere in the world. Attention is focused in this section on the planktonic $\delta^{18}O$ records of Cores 594 and 593, in order to obtain a detailed $\delta^{18}O$ stratigraphy of climatic changes determined from sediments to the east (Southwest Pacific Ocean) and to the west (Tasman Sea) of New Zealand.

594 Particular attention is paid to the record of Site 594 because of its exceptionally high resolution nature. Compared to other cores in this study it is obvious that 594 contains the most detailed record of stages 6 to 1. This is largely due to the high sedimentation rate at Site 594, which has minimised intersample mixing and permitted a sampling interval of only 10cm. This has resulted in a reduction of both the smoothing of the isotopic signature caused by bioturbation (Shackleton and Opdyke, 1976) and the missing of short-term events as is commonly the case for low sedimentation rate sites.

The short-term fluctuations (of ~0.7°/$_{oo}$) in the 594 curve are thus not unexpected, even though they are not seen in the 502 (Prell, 1982) or V28-238 (Shackleton and Opdyke, 1973) records. A comparison of 594 to V19-30 (Shackleton et al., 1983) is presented in Figures 5.2b and c, since the latter shows similar short-term fluctuations. V19-30 has a lower sedimentation rate than 594 (stages 6 to 1 being represented by ~9m of core, compared to ~20m at 594), but was sampled at closer intervals (~3cm), thereby retaining some of the fine detail, although the highs and lows are not nearly as evident in V19-30 as they are in 594. A marked similarity in the range of glacial to interglacial benthic $\delta^{18}O$ values may be seen between M12 392, V19-30 and 594 (Figure 5.2).

The general shape of the 594 planktonic $\delta^{18}O$ record for stage 5 is very similar to that seen in the SPECMAP stacked record, with the peaks of 5a and 5c being less intense than 5e (Figure 5.19). It is noticeable, however, that the benthic 5a,c and e peaks in 594 are all of comparable size, and an explanation for this is offered in Section 5.1.6.

Compared to 594, the other sites analysed off the east coast of New Zealand contain a far less detailed isotopic record. The details

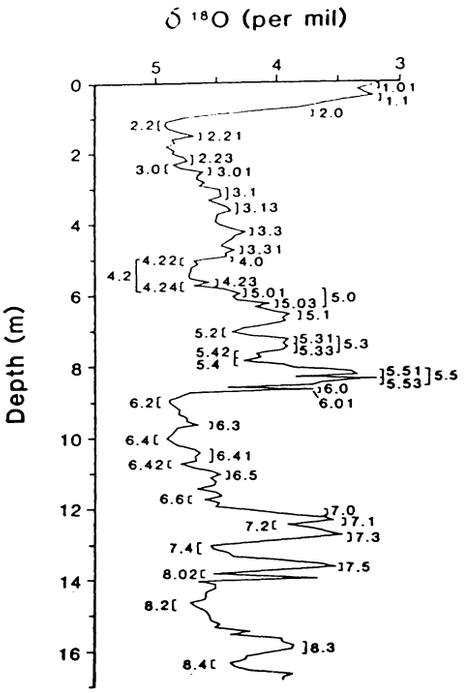

Figure 5.25. The benthic $\delta^{18}O$ record of V19-29 with isotopic events identified by Pisias et al. (1984, figure 2).

of the fine structure preserved in 594 are thus of great interest. For this reason an attempt has been made to label substage isotopic events using the method of Prell (1983) as outlined in Pisias et al. (1984). The numerical isotopic taxonomy follows that of Prell: The integer part of the number represents the isotopic stage in which the event occurred; the first digit to the right gives the substage event number identified in Prell's study of low sedimentation rate cores; and the second digit to the right marks substage events identified in the later study of high sedimentation rate cores (Pisias et al., 1984). Even numbers represent relatively enriched periods, and odd numbers relatively depleted periods. Pisias et al. (1984) used benthic $\delta^{18}O$ results from V19-29 (Figure 5.25) as their standard, because of the core's length and detail. 594 contains greater detail than V19-29 and thus lends itself well to this technique. The benthic $\delta^{18}O$ plot for 594 is presented in Figure 5.26, with the isotopic events numbered.

A "taxonomy" of the substage boundaries identified in 594, using the nomenclature developed by Pisias et al. (1984), follows. Events marked with an (a) are those originally identified by Prell (1983), those with (b) were subsequently identified by Pisias et al. (1984) in V19-29, while events marked (c) are those identified in the high resolution record of 594. In some cases these were events which were identified by Pisias et al., but for which a different position within the stage is suggested, due to the greater number of peaks in the 594 isotopic stratigraphy, or for which a renumbering is suggested consistent with the 594 record. In other cases they are additional events not seen in the V19-29 record. For reasons which will become apparent, and discussed later in this section, two versions of an isotopic taxonomy for 594 are suggested.

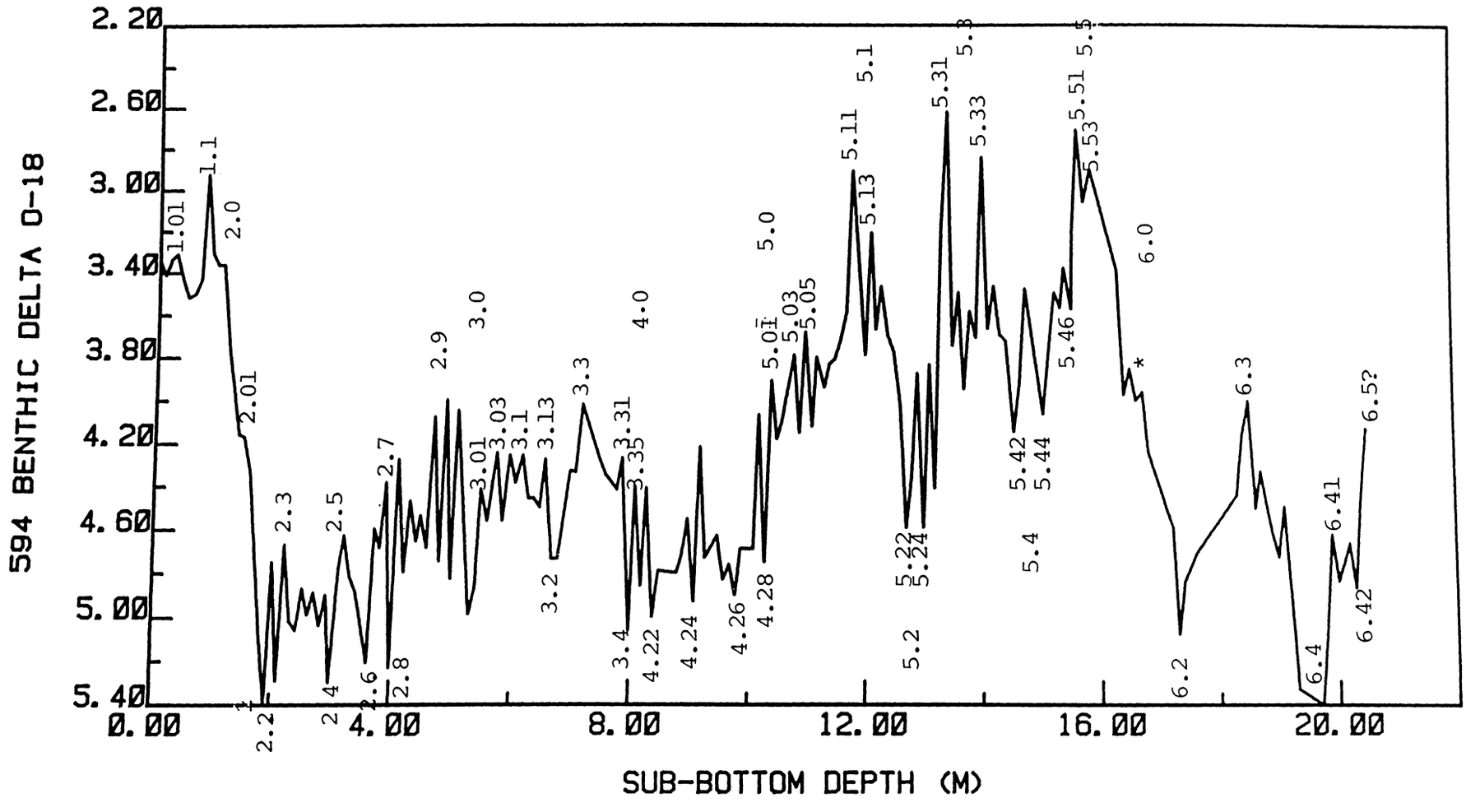

Figure 5.26. A proposed isotopic taxonomy for the 594 benthic $\delta^{18}O$ record (version #1).

Isotopic Taxonomy of 594 (#1)

1.01(b)	0.00-0.40m	Youngest negative peak.
1.1(a)	0.75-0.85m	Most negative peak in stage 1.
2.0(a)	1.20-1.30m	1/2 stage boundary.
2.01(b)	1.41-1.49m	Minor peak mid-way up termination I.
2.2(a)	1.85-1.95m	Most positive valley in stage 2, close to base of termination I.
2.3(b,c)	2.15-2.25m	Youngest of four peaks in 594 stage 2, this was identified by Prell et al. (1983) as 2.21, however the stage 2 record of 594 has far more marked peaks and valleys than V19-29, and the classification of all of stage 2 as part of the 2.2 valley does not seem justified for the 594 record.
2.5(b,c)	3.05-3.50m	Described by Pisias et al. (1984) as lying near the 2/3 boundary (and identified as 2.23), but because of the increased number of peaks in 594 stage 2 this is here described as the second youngest peak, about mid-way through the stage, and of a comparable magnitude to 2.3.
2.7(c)	3.65-3.95m	The second oldest of the four peaks in the 594 stage 2 record.
2.9(c)	4.15-5.15m	A broad peak that could possibly be further subdivided. The oldest and most negative of those in stage 2.
3.0(a)	5.40-5.50m	2/3 stage boundary.
3.01(b)	5.45-5.55m	A minor peak very close to event 3.0.
3.03(c)	5.65-5.80m	A second minor peak identified in 594. A very small peak lying between 3.01 and 3.1 was evident

		in V19-29, but Pisias et al. did not label it. However, in 594 it is of greater magnitude and is identified.
3.1(b)	5.90-6.25m	The third minor peak in stage 3, of comparable magnitude to 3.03, but more negative than 3.01.
3.13(b)	6.52-6.65m	The fourth minor peak of stage 3, little different in magnitude to 3.1 and 3.03.
3.3(b)	7.00-7.40m	The most negative and most clearly defined of all the stage 3 peaks.
3.31(b,c)	7.85-7.95m	Suggested in 594 to be the second oldest of the stage 3 peaks.
3.5(b,c)	8.05-8.15m	Identified as 3.31 by Pisias et al., the oldest of the stage 3 peaks, lying on the 3/4 transition.
4.0(a)	8.10-8.20m	3/4 stage boundary.
4.2(a)	8.35-10.35m	Described by Prell (1983) as the complete stage 4 in low resolution cores. Hence, all valleys identifiable within stage 4 are subdivisions of 4.2. The 594 record has more valleys in stage 4 than V19-29, and so the descriptions of 4.22 and 4.24 by Pisias et al. are not appropriate for 594.
4.22(b)	8.35-8.45m	Youngest of the four valleys located within stage 4, occurring at the base of the 3/4 stage boundary.
4.24(b,c)	9.05-9.15m	Slightly more negative than 4.22, located in 594 mid-way through the stage.
4.26(c)	9.55-9.85m	Of equal magnitude to 4.24, the second oldest of the valleys in stage 4.

4.28(c) 10.25-10.35m The oldest and most negative of the valleys, lying close to event 5.0.

5.0(a) 10.35-10.80m 4/5 stage boundary.

5.01(b) 10.35-10.45m The youngest of three minor peaks on the transition between stages 4 and 5.

5.03(c) 10.55-10.85m The middle of the transition peaks.

5.05(c) 10.95-11.05m The most negative, and oldest, of the peaks on the 4/5 transition.

5.1(a) 11.75-12.35m Youngest major peak in stage 5 (equivalent to substage 5a).

5.11(c) 11.75-11.95m Younger and most negative peak of the two which comprise 5.1.

5.13(c) 12.05-12.35m Older peak of 5.1.

5.2(a) 12.65-13.25m Valley separating 5.1 and 5.3.

5.22(c) 12.65-12.85m Younger of the two valleys comprising 5.2, of equal magnitude to 5.24.

5.24(c) 12.95-13.05m Second of the valleys comprising 5.2, which is the most positive substage of stage 5.

5.3(a) 13.30-14.25m Central major peak in stage 5. In 594 it is the most negative, comparable to substage 5c, and may clearly be divided into two peaks.

5.31(b) 13.30-13.45m Younger peak of two in 5.3, more negative than the older peak.

5.33(b) 13.95-14.25m Older minor peak of 5.3, separated from 5.31 by a valley of ~1°/$_{oo}$ magnitude.

5.4(a) 14.45-15.55m Major valley between 5.3 and 5.5.

5.42(b) 14.45-14.65m Younger of the two major valleys of 5.4.

5.44(b) 14.83-15.10m Older valley slightly more negative than 5.42 in 594.

5.46(b) 15.45-15.55m Minor valley of short duration, midway between events 5.4 and 5.5.

5.5(a) 15.55-16.35m The oldest major peak of stage 5 (equivalent to substage 5e). Composed of two minor peaks in high resolution cores.

5.51(b) 15.55-15.65m Younger minor peak of 5.5, more negative of the two present.

5.53(b) 15.75-16.00m Possibly not the same 5.53 as that identified by Pisias et al. as it is less negative than 5.51. It is possible that a third peak, 5.55 (equivalent to Pisias et al.'s description of 5.53), has been lost due to the lack of benthics over this section.

* 16.45-16.75m Probably represented by Pisias et al. as event 6.01, but since stage boundaries here were drawn in conjunction with the planktonic $\delta^{18}O$ results it is assigned to stage 5 in 594.

6.0(a) 16.85-17.15m 5/6 stage boundary.

6.2(a) 17.25-17.50m Youngest of the valleys in stage 6, located at the start of the 5/6 transition.

6.3(a) 18.35-18.55m Considerable peak in 594, approximately 1% lighter than the surrounding valleys (6.2 and 6.4).

6.4(a) 19.20-19.75m Most positive valley in stage 6.

6.41(b) 19.85-19.95m Middle peak located on the transition between 6.4 and 6.5.

6.42(b) 20.25-20.35m Minor valley separating 6.41 and 6.5, ~1‰ deep.

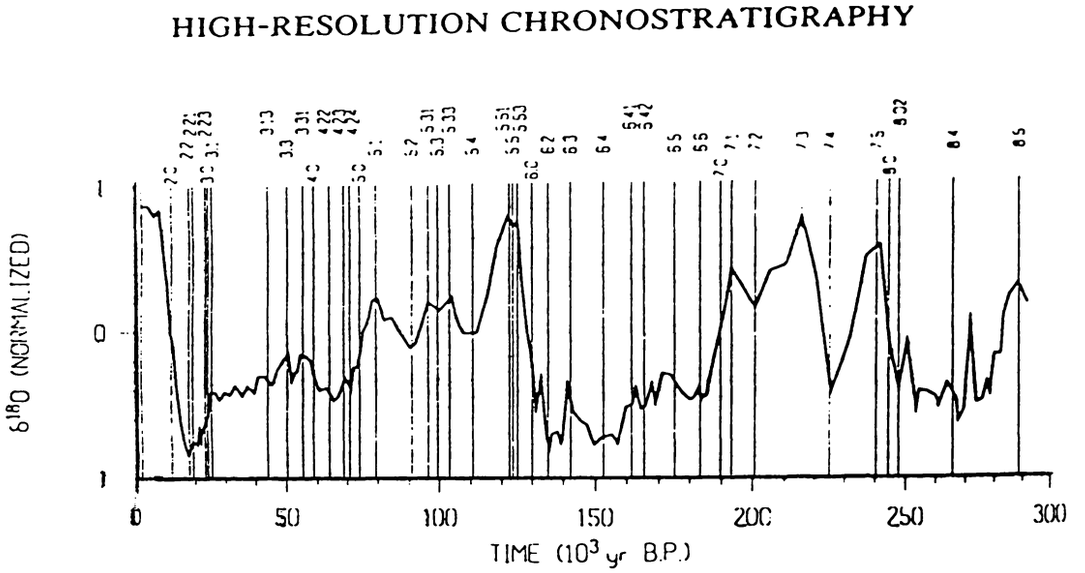

Figure 5.27. Orbitally based chronostratigraphy of a stacked $\delta^{18}O$ record, for features identified by Pisias et al. (1984) (from Martinson et al., 1987, figure 5.18).

6.5(a) 20.45m-? Probably the end of the oldest major peak in stage 6. Although no samples were analysed beyond this depth, the longer, lower resolution 594 record (Cuthbertson, 1985) supports this interpretation.

Following Pisias et al.'s (1984) precise description of V19-29, and a similar description of stacked records, Martinson et al. (1987) used the concept of "orbital tuning" to derive a high resolution chronostratigraphy for the numbered events. The age plot produced by Martinson et al. (1987), for the stacked $\delta^{18}O$ records of Pisias et al. (1984) is shown in Figure 5.27.

This has been used to plot the 594 results on an appropriate time scale (Figure 5.28). Age estimates are those given by Martinson et al. (1987) for features described by Pisias et al. (1984), where their description is appropriate to the 594 record. For events whose position in 594 differs from the description of Pisias et al. no age constraint is given. Age estimates used to produce Figure 5.28 are shown in Table 5.12.

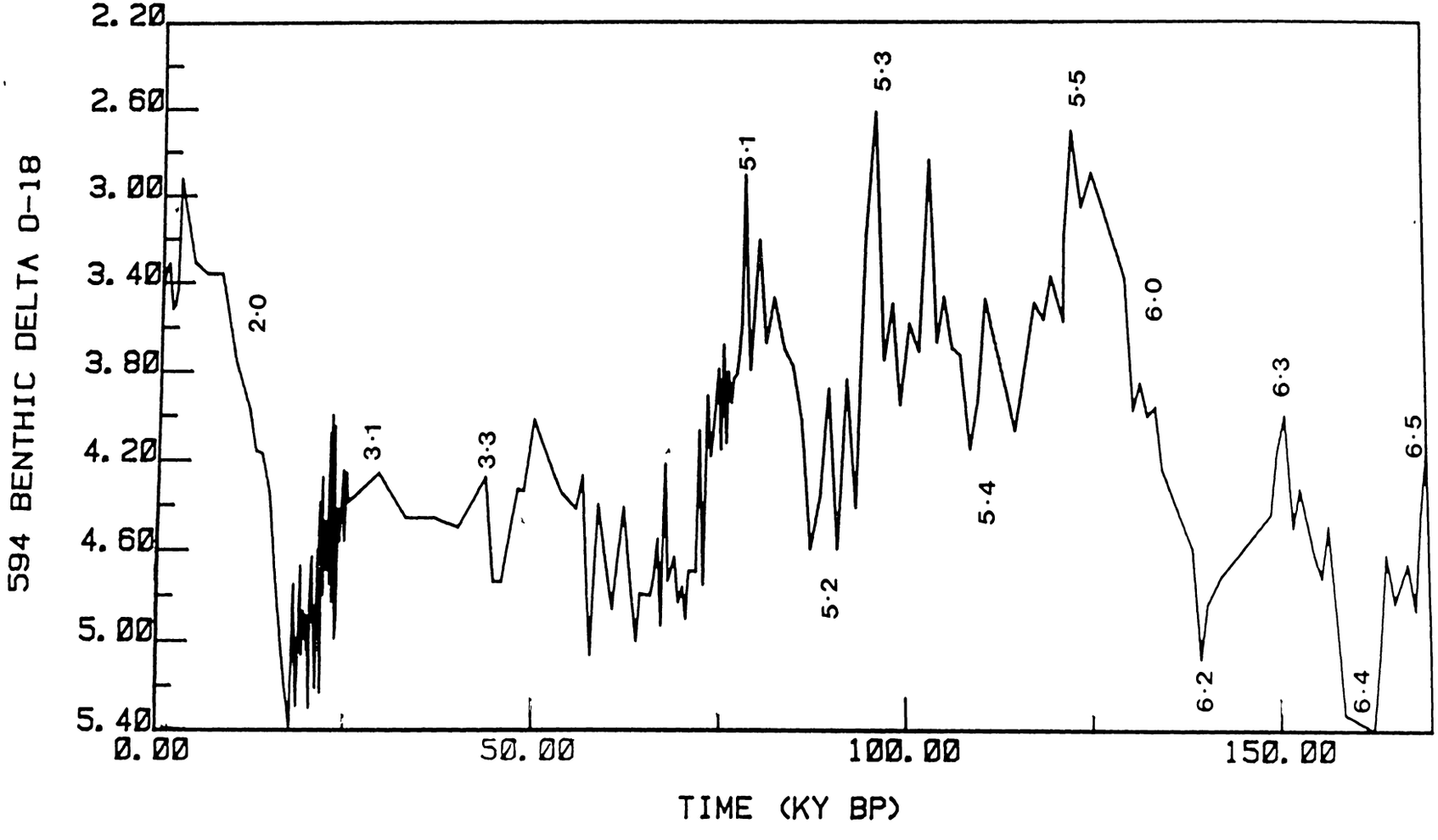

Figure 5.28. 594 benthic $\delta^{18}O$ data plotted on a timescale derived from Martinson et al. (1984). (Based on isotopic taxonomy version #1).

Table 5.12. Dates and depths of events numbered in Figure 5.26.

Event	Sub-bottom Depth(m)	Age(ky)
1.1	0.81	2.32
2.0	1.31	12.05
2.2	1.91	17.85
2.3	2.21	19.22
3.0	5.45	24.11
3.1	6.09	25.42
3.13	6.59	43.88
3.3	7.21	50.21
3.5	8.10	55.45
4.0	8.15	58.96
4.22	8.40	64.09
5.0	10.50	73.91
5.12[a]	12.01	79.25
5.24[b]	12.99	90.95
5.31	13.40	96.21
5.3	13.68	99.38
5.33	13.99	103.29
5.43[c]	14.72	110.79
5.51	15.61	122.56
5.52[d]	15.72	123.82
5.53	15.83	125.19
6.0	16.90	129.84
6.2	17.30	135.10
6.3	18.51	142.28
6.4	19.50	152.58
6.41	19.90	161.34
6.42	20.30	165.35

[a]Centre of 5.1 [c]Centre of 5.4

[b]Centre of 5.2 [d]Centre of 5.5

The assignment of the 1.1 peak at 0.81m does present difficulties as the age of 2.32ky is incompatible with the radiocarbon date of 6.8ky for 0.3m sub-bottom depth in 594. The error of the date in Table

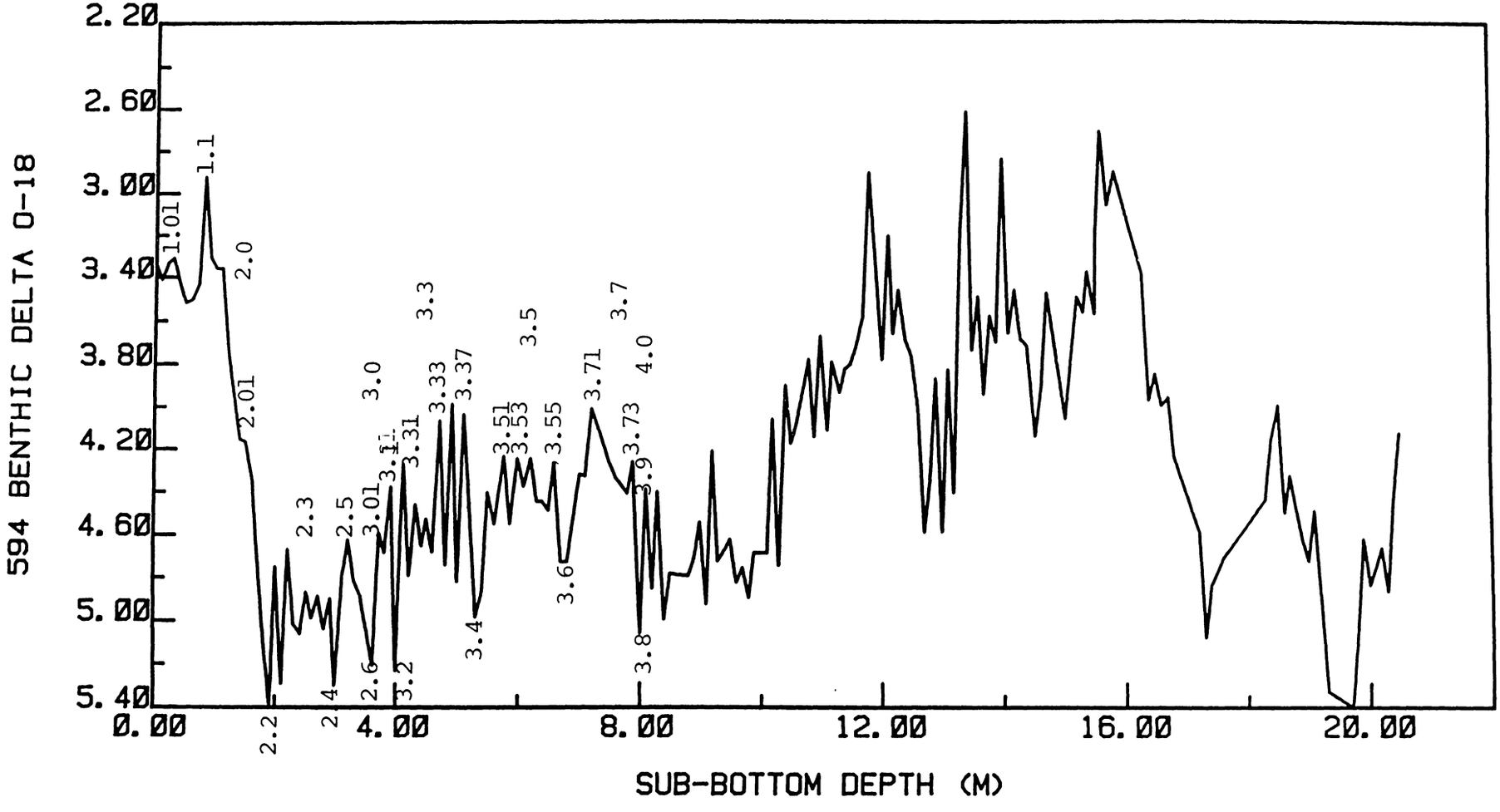

Figure 5.29. A second proposed isotopic taxonomy for the 594 benthic $\delta^{18}O$ record.

5.12 (of ±2.1ky) cannot alone account for this. If the radiocarbon date of 6.8ky is correct, then there must be missing peaks at the top of 594, and more peaks earlier in stage 1 than are seen elsewhere.

In addition to this problem, it is evident in Figure 5.28 that the assigned position of the 2/3 stage boundary therein results in significant compression of stage 2. The uncertainty of the position of the 2/3 stage boundary (see Section 5.1.1) makes it advisable to present a second possible isotopic "taxonomy". In version #1 the 2/3 stage boundary was assumed to be at 5.45m, which is compatible with the carbonate data, but which is by no means definite. An alternative position for the 2/3 stage boundary at 3.65m (which is a more reasonable position for it in terms of the $\delta^{18}O$ record) results in a somewhat different description of the peaks in stages 2 and 3. For this reason a second isotopic taxonomy follows. The peaks numbered in version #2 are shown in Figure 5.29.

Isotopic Taxonomy of 594 (#2)

1.01(b)	0.00-0.40m	Youngest negative peak.
1.1(a)	0.75-0.85m	Most negative peak in stage 1.
2.0(a)	1.20-1.30m	1/2 stage boundary.
2.01(b)	1.41-1.49m	Minor peak mid-way up termination I.
2.2(a)	1.85-1.95m	Most positive and youngest of the stage 2 valleys.
2.3(b,c)	2.15-2.25m	Younger of two peaks in stage 2, identified by Pisias et al. (1984) as 2.21.
2.4(c)	2.95-3.15m	Middle one of three valleys n stage 2.
2.5(b,c)	3.05-3.50m	Older peak of stage 2 (identified by Pisias et al. (1984) as 2.23).
2.6(c)	3.55-3.65m	Oldest valley of stage 2.
3.0(a)	3.65-3.70m	2/3 stage boundary.

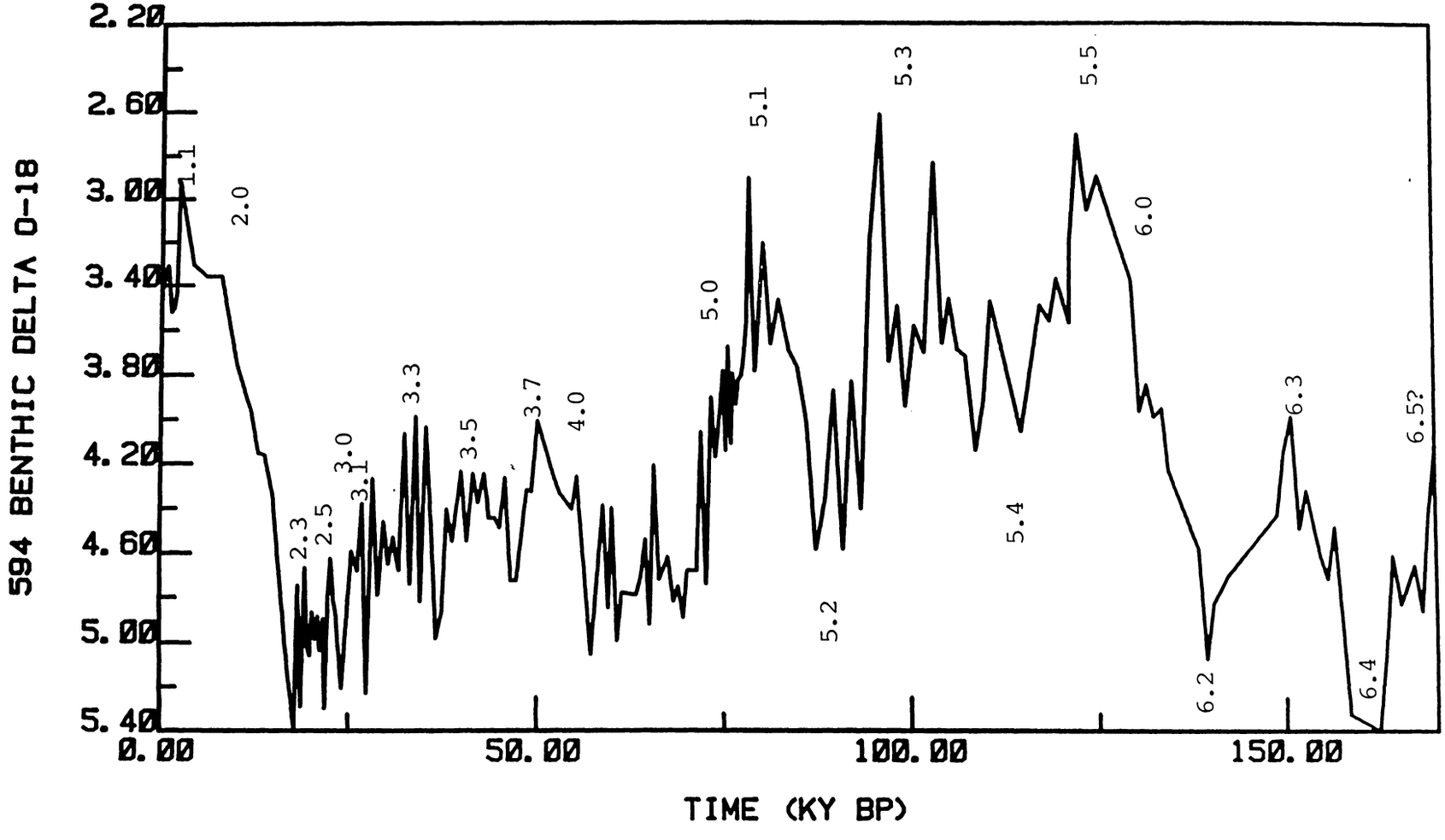

Figure 5.30. 594 benthic $\delta^{18}O$ data plotted on a timescale derived from Martinson et al. (1984). (Based on isotopic taxomomy #2).

3.01(b) 3.65-3.75m Minor peak of ~0.15°/$_{oo}$ magnitude, located right on the 2/3 transition.

3.1(b) 3.85-3.95m Youngest and least negative of the stage 3 peaks.

3.2(c) 3.95-4.05m Most positive valley in stage 3.

3.3(c) 4.05-5.25m A very broad peak, incorporating the most negative values of stage, that could probably be sub-divided into 3.31, 3.33, 3.35, and 3.37 (as shown in Figure 5.29).

3.5(c) 5.45-6.65m The first of the broad peaks in stage 3, sub-divided(in Figure 5.29) into 3.51, 3.53, and 3.55.

3.7(b,c) 7.00-7.95m The oldest and most negative of the stage 3 peaks (identified by Pisias et al. (1984) as 3.3(?)).

3.71(c) 7.15-7.35m The more negative and younger of the two peaks comprising 3.7.

3.73(c) 7.85-7.95m First minor peak of 3.7.

3.9(b,c) 8.05-8.15m A minor peak located right on the 3/4 stage boundary (identified by Pisias et al. (1984) as 3.31).

4.0(a) 8.10-8.20m 3/4 stage boundary.

4.0->6.5 The isotopic taxonomy for the rest of 594 (over stages 4, 5 and 6), with the 2/3 stage boundary located at 3.65m, is identical to that proposed in version #1, with a 2/3 stage boundary at 5.45m.

A second plot of 594 benthic $\delta^{18}O$ results, versus time, was drawn for version #2 of the isotopic taxonomy (Figure 5.30). Age estimates (from Martinson et al., 1987) used to compose Figure 5.30 are listed

in Table 5.13. An identical approach to that used in estimation of ages for Table 5.12 was used (i.e., the ages are those given by Martinson et al. (1987) for features described by Pisias et al.(1984) where they are identifiable in the 594 record - even though they may have been renumbered).

Table 5.13. Dates and depths of events numbered in Figure 5.29.

Event	Sub-bottom Depth(m)	Age(ky)
1.1	0.81	2.32
2.0	1.31	12.05
2.2	1.91	17.85
2.3	2.21	19.22
3.0	3.65	24.11
3.1	3.71	25.42
3.7	7.21	50.21
3.9	7.89	55.45
4.0	8.15	58.96
4.22	8.40	64.09
5.0	10.50	73.91
5.12[a]	12.01	79.25
5.24[b]	12.99	90.95
5.31	13.40	96.21
5.3	13.68	99.38
5.33	13.99	103.29
5.43[c]	14.72	110.79
5.51	15.61	122.56
5.52[d]	15.72	123.82
5.53	15.83	125.19
6.0	16.90	129.84
6.1	17.30	135.10
6.3	18.51	142.28
6.4	19.50	152.58
6.41	19.90	161.34
6.42	20.30	165.35

[a]Centre of 5.1
[b]Centre of 5.2
[c]Centre of 5.4
[d]Centre of 5.5

This second isotopic taxonomy appears to give a much more convincing plot of $\delta^{18}O$ versus time, without the extreme compression of stage 2, and the spreading out of stage 3. The problem of the

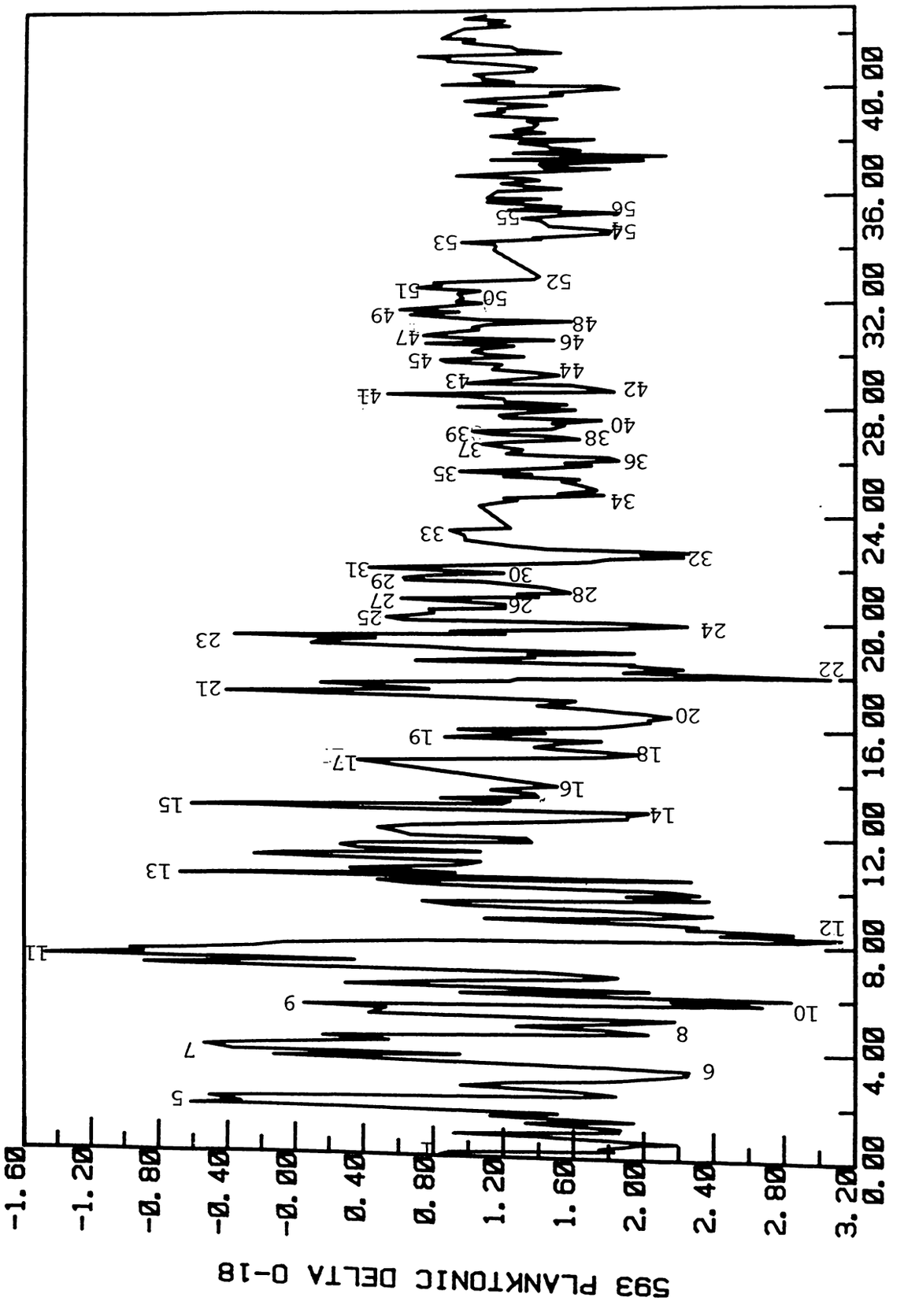

Figure 5.31. Numbering of 593 planktonic $\delta^{18}O$ isotope stages back to the 55/56 stage boundary.

anomalous radiocarbon date in stage 1 still remains however, and needs verification.

The sedimentation rates of stages 2 and 3 for Core 594 (for version #2) are 20.0 and 12.9cm/ky respectively.

593 A detailed isotope taxonomy did not seem to be a suitable approach to 593, as it lacks the fine structure of the 594 record. However, a considerably greater length of core material has been studied at this site. 43m of core were sampled from Site 593, well before the Brunhes/Matuyama boundary at 16m, and stages 24 to 1 are resolvable (Figure 5.12). Below stage 24 (at about 20m) the record shows low variability, also noted in the lower resolution analysis of 593 by Nelson et al. (1986). This is consistent with Prell (1982) who noted two modes of Quaternary $\delta^{18}O$ variations, with the increased intensity occurring since the beginning of the Jaramillo Subchron and related to the growth of significant amounts of sea ice in the Arctic Ocean (Williams et al., 1981). (Similarly, two modes of variation may be observed in the low resolution Site 592 record in which there is considerably less variation below 11m sub-bottom depth (Figure 5.21).

The decreased intensity of the peaks beyond stage 24 makes further assignment of the stages more difficult. However, the magnetic polarity stratigraphy (Kennett et al., 1986) indicates that the top 43m of Core 593 should represent ~2my, and Williams et al. (1988) have succeeded in assigning stage numbers back to stage 63 at ~1.8my (discussed in Section 1.5, see Figure 1.4). An attempt has been made to number the lower variability planktonic $\delta^{18}O$ record of 593 beyond stage 24 in a similar fashion (Figure 5.31).

The shape of the peaks, and their relative intensities in the 593 record, are similar to those of the composite record presented by

Williams et al. (1988) (see Figure 1.4) back to stage 56. Beyond this point, however, differentiation of the peaks is virtually impossible. Gaps in the benthic record mean that it is of little assistance over this time period, and no further resolution of the peaks beyond stage 56 seems possible with the available data.

5.1.3 The Holocene

Before the isotope results may be used to make assumptions on the nature of past oceanographic events, it must be shown that the Holocene $\delta^{18}O$ values are a reasonable reflection of present day conditions. For this reason, a comparison is made in Table 5.14 of temperatures measured in bottom waters and at 200m below the sea surface (from Ridgway et al., 1979; see Figures 2.4 and 2.9) with isotope-derived temperatures from benthics and planktonics for all sites where data are available.

The isotopic temperatures have been calculated using the following equation (Murphy and Kennett, 1986):

$$T=16.9-4.38(\delta_c-\delta_w)+0.1(\delta_c-\delta_w)^2$$

where δ_c = isotopic composition of carbonate, taken from the mean of the identifiable Holocene values,

and δ_w = isotopic composition of water.

The isotopic composition of sea water is taken to be ~$0.0^{o}/_{oo(SMOW)}$. However, some consideration of differences in salinity must be taken into account. As sea water is evaporated it becomes enriched in ^{18}O and increases in salinity, with the relationship being

$$\delta^{18}O=0.5(\text{salinity}-35^{o}/_{oo})^{o}/_{oo}$$

Table 5.14. A comparison of modern measured temperatures with isotopically derived Holocene temperatures, taking into account differences in salinity between the sites.

West of New Zealand			Benthic					Planktonic				
Core	Depth (m)	Water body	Bottom T (°C)	Salinity (°/oo)	Est.$\delta^{18}O$ (sea)	Benthic $\delta^{18}O$	Derived T (°C)	200m T (°C)	Salinity (°/oo)	Est $\delta^{18}O$ (sea)	Planktonic $\delta^{18}O$	Derived T (°C)
588	1533	DW	2.3	34.7	-0.15	-	-	23.0*	35.4	0.20	-0.7	20.9
589	1391	DW	2.2	34.7	-0.15	-	-	16.5	35.4	0.20	0.1[a]	17.3
590	1299	DW	2.2	34.7	-0.15	4.0	0.5	16.5	35.4	0.20	0.0	17.7
591A	2131	DW	1.8	34.7	-0.15	3.9	0.8	16.5	35.4	0.20	0.0	17.7
Z2108	1448	DW	3.5	34.7	-0.15	2.7	5.2	14.0	35.2	0.10	-0.6	20.0
592	1098	AIW	2.4	34.45	-0.28	3.2	2.8	13.5	35.2	0.10	0.7	14.2
593	1068	AIW	3.5	34.6	-0.20	3.1	3.5	12.0	35.2	0.05	0.9	13.1
East of New Zealand												
594	1204	DW	3.5	34.7	-0.15	3.4	2.6	7.5	34.5	-0.25	1.7	8.7
Q200	1370	DW	3.0	34.7	-0.15	3.2	3.3	7.5	34.4	-0.30	1.7	8.5
Q580	3964	DW	1.5	34.7	-0.15	3.5	2.2	7.0	34.3	-0.35	2.0	7.2
Q217	1936	DW	2.5	34.7	-0.15	3.3	2.9	7.5	34.4	-0.20	2.2	7.0
Q585	4354	DW	1.0	34.7	-		-	6.0	34.3	-0.35	2.4	5.7

[a]Interglacial mean used (Holocene missing).

*Surface temperature at 588 = 25°C.

DW = Deep Water.

AIW = Antarctic Intermediate Water.

(discussed in 1.10) (Craig and Gordon, 1965). The same relationship holds where sea water is diluted by continental runoff. The salinity undergoes major changes between the Circumpolar waters (low salinity) and the North Tasman (high salinity) (Figures 2.7 and 2.8). Moreover, at higher latitudes the warm surface waters become increasingly thinner so that definition of the planktonic foraminiferal habitat becomes less precise. To further complicate the problem, seasonal temperature changes occur, and the planktonic foraminiferal depth range is uncertain. Estimates of the temperatures and salinities at 200m depth were derived from NZOI charts (Ridgway, 1979). 200m is slightly deeper than the expected depth habitat of ~100m for *G.bulloides* (Bé, 1977), but extensive information was available from the NZOI on 200m temperatures and isohalines, and where information was available for 100m there was very little difference. In any case, continued skeletal deposition below the photic zone (Erez and Honjo, 1981) means that the isotopic composition of planktonic foraminifera may most realistically be interpreted as representing an integrated isotopic ratio over a few hundred metres of the sea-water column. At Site 588 both surface and 200m temperatures are given as the planktonic species used was *G.ruber*, which lives in the top 50m of the sea water column (closer to the surface than *G.bulloides*).

The salinity of bottom waters also changes due to the composition of the surface waters at their source, having been subjected to differing compositions of continental run-off (dependent on the nature of the landmass from which they were derived) and different modes of deep water formation. Thus the Antarctic Intermediate Waters (AIW) have a salinity of ~34.45°/$_{oo}$ (Ridgway, 1979) and the Deep Waters ~34.7°/$_{oo}$ (Brodie, 1965).

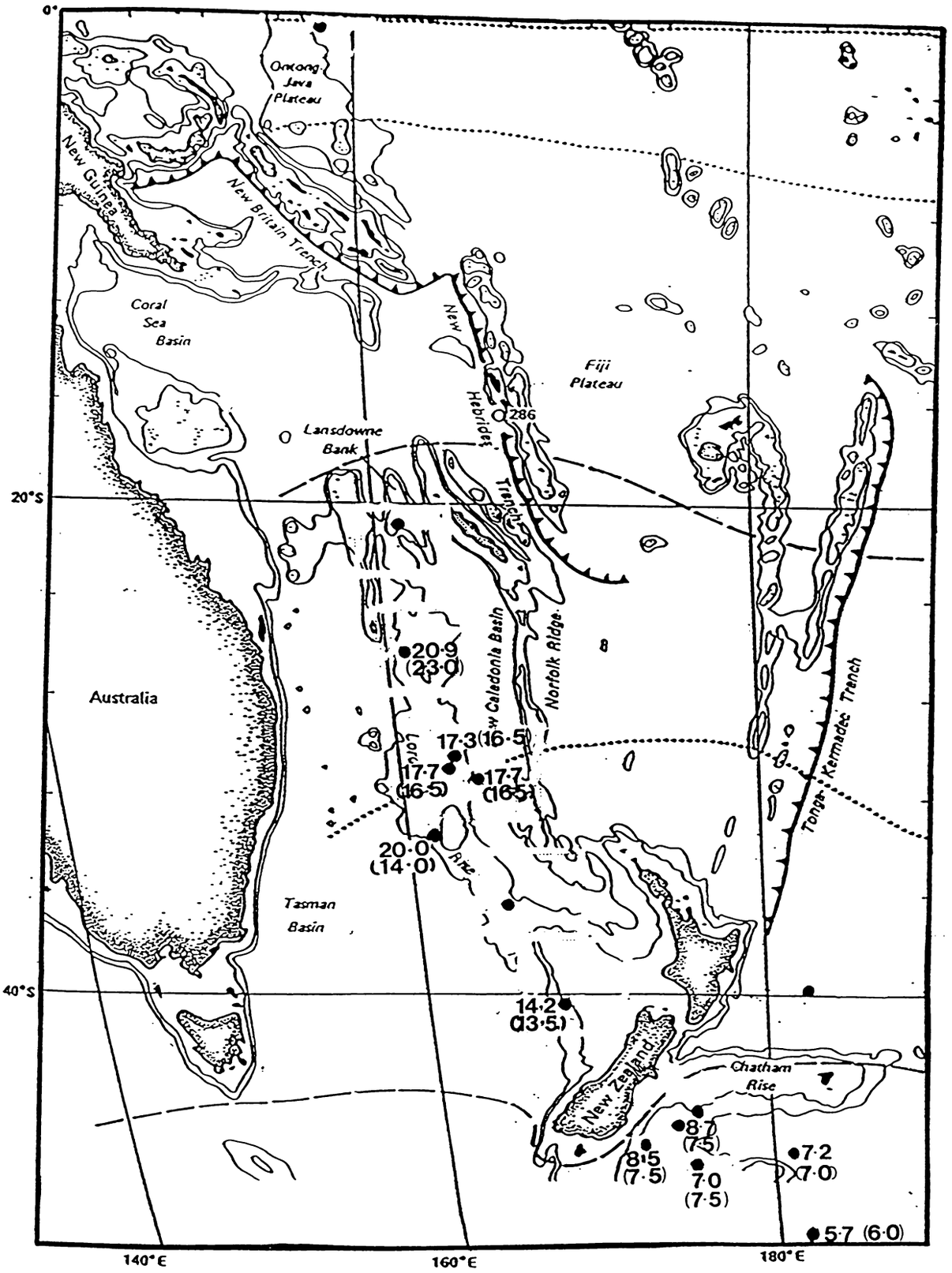

Figure 5.32. Map showing, where possible, isotopically derived Holocene surface water temperatures (^{o}C) at each of the sites studied. Modern measured temperatures are given in brackets.

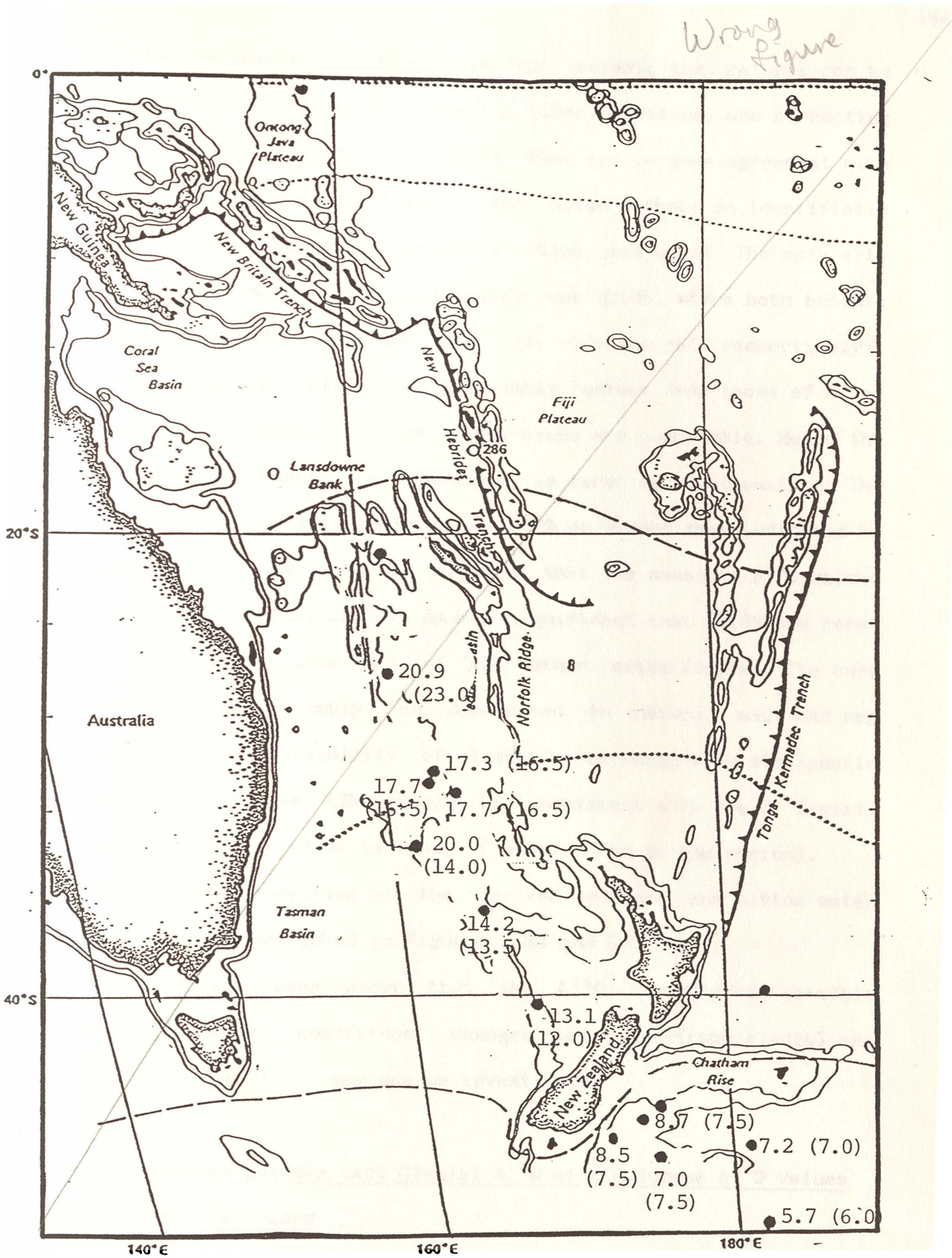

Figure 5.33. Map showing, where possible, isotopically derived Holocene bottom water temperatures (^{o}C) at each of the sites studied. Modern measured temperatures are given in brackets.

It may be seen from Table 5.14 that isotopic temperatures can be calculated (using Murphy and Kennett's (1986) equation, and correcting for salinity differences from 35°/$_{oo}$) that are in good agreement with the modern measured temperatures. (For sites without an identifiable Holocene a mean stage 5 interglacial value was used). The only site which yielded a significant discrepancy was Z2108, where both benthic and planktonic values are too warm (by ~2°C and ~6°C respectively). The $\delta^{18}O$ values for Z2108 are noticeably offset from those of other cores in the vicinity, yet the $\delta^{13}C$ values are comparable. Hence the offset in values cannot be explained in terms of fractionation. The presence of a water mass depleted in ^{18}O or warmer than indicated by Ridgway, would be required. It appears that the absolute $\delta^{18}O$ values for Z2108 are suspect, and it may be significant that Z2108 was cored 12-15 years earlier than all of the other sites studied. The core itself was very crumbly and dessicated in nature, and one may speculate on the possibility of isotopic exchange with atmospheric oxygen during storage. (This would be consistent with the $\delta^{13}C$ still being comparable in value to those of other cores in the region).

Diagrammatic summaries of the derived surface and bottom water temperatures are presented in Figures 5.32 and 5.33.

Since it has been shown that the $\delta^{18}O$ record gives sensible estimates of modern conditions, changes between extreme glacial and interglacial conditions may now be investigated.

5.1.4 Comparison Between Last Glacial $\delta^{18}O$ with Holocene $\delta^{18}O$ Values

The Benthic $\delta^{18}O$ Record

Changes in the benthic foraminiferal $\delta^{18}O$ values reflect the cyclically changing composition of ocean water in response to the removal and addition of ~130m of water from the ocean masses between

Table 5.15. A comparison of Holocene $\delta^{18}O$ values, with glacial $\delta^{18}O$ values for each of the sites studied.

Holocene and Glacial Extremes

West of New Zealand

Core	Holocene[a] Benthics	Glacial[a] Benthics	Difference
590	4.0	5.3	1.3
591A	3.9	4.8	0.9
Z2108	2.7	3.9	1.4
592	3.2	4.5	1.3
593	3.1	4.1	1.0

Core	Holocene[a] Planktonics	Glacial[a] Planktonics	Difference
588	-0.7	0.5	1.2
590	0.0	1.5	1.5
591A	0.0	1.4	1.4
Z2108	-0.6	0.6	1.2
592	0.7	1.9	1.2
593	0.9	2.1	1.2

East of New Zealand

Core	Holocene[a] Benthics	Glacial[a] Benthics	Difference
594	3.4	5.1	1.7
Q200	3.2	4.7	1.5
Q580	3.5	4.9	1.4
Q217	3.5	4.9	1.6

Core	Holocene[a] Planktonics	Glacial Planktonics	Difference
594	1.7	3.6	1.9
Q200	1.7	3.3	1.6
Q580	2.0	3.5	1.5
Q217	2.2	3.7	1.5
Q585	2.4	3.8	1.4

[a]Mean $\delta^{18}O$ (‰)

glacial and interglacial periods (Emiliani, 1970), as well as changes in the temperature of Deep Waters. The average change in $\delta^{18}O$ values between the Last Glacial and the Holocene is summarised for each of the cores studied in Table 5.15. The mean change is $1.4^{o}/_{oo}$, and ranges from $1.9^{o}/_{oo}$ at Site 594 to $1.0^{o}/_{oo}$ at Site 593.

The sites may be divided into two groups: Sites 590, 591A, Z2108, 592 and 593 to the west of New Zealand all show a $\delta^{18}O$ change of $\sim 1.3^{o}/_{oo}$. This is only slightly greater than the $1.1^{o}/_{oo}$ increase in the mean $\delta^{18}O$ of ocean water (Chappell and Shackleton, 1986; Labeyrie et al., 1987) and would indicate a cooling of ~0.8°C ($\Delta T \simeq 4.2°C/1^{o}/_{oo}$; Hecht, 1985) in the Deep Waters of the Tasman Sea. This is 1.2°C less than the average cooling by ~2°C of oceanic Deep Waters (Labeyrie et al., 1987). Because all of these cores are located in the Tasman Basin, or on its flanks, it is likely that this basin became more isolated during the last glacial from the northerly flow which currently takes Deep Waters from the Circumpolar Current into the Pacific, allowing a localised cell of bottom waters of higher temperatures to develop.

To the east of New Zealand, Sites 594, Q200, Q580 and Q217 display a mean glacial to Holocene change of $\sim 1.6^{o}/_{oo}$ (=> a temperature drop of ~1.7°C), with values very similar to those of Cores MD73-025 and MD84-527 (Labeyrie et al., 1987) from the south Indian Ocean. It appears that the waters to the east of New Zealand behaved in concert with other Southern Ocean sites.

The Planktonic $\delta^{18}O$ Record

The differences in planktonic Holocene and glacial values are very similar to the trends seen in the benthic signal, with Sites 588-593 to the west of New Zealand displaying a mean planktonic $\delta^{18}O$ change of

Table 5.16. A comparison of the glacial to interglacial extremes recorded at each of the sites.

West of New Zealand

Core	I.G.[a] Benthics	Glacial[a] Benthics	Difference
588	3.6	5.1	1.5
589	2.2	4.0	1.8
590	3.8	5.3	1.5
591A	3.9	5.2	1.3
Z2108	2.4	3.9	1.5
592	3.1	4.5	1.4
593	2.7	4.1	1.4

Core	I.G.[a] Planktonics	Glacial[a] Planktonics	Difference
586[b]	-2.1	-1.3	0.8
588[b]	-0.5	0.5	1.0
589	0.1	1.2	1.1
590	0.3	1.2	1.1
591A	-0.1	1.4	1.5
Z2108	-0.9	0.6	1.5
592	0.2	1.9	1.7
593	-0.5	2.1	2.6

East of New Zealand

Core	I.G.[a] Benthics	Glacial[a] Benthics	Difference
594	3.3	5.1	1.8
Q200	3.2*	4.7	1.5
Q580	3.5	4.9	1.4
Q217	3.3*	4.9	1.6
Q585	3.5	5.0	1.5

Core	I.G.[a] Planktonics	Glacial[a] Planktonics	Difference
594	1.3	3.6	2.3
Q200	1.7*	3.3	1.6
Q580	2.0*	3.5	1.5
Q217	2.2*	3.7	1.5
Q585	2.5	3.8	1.3

I.G. = Interglacial

[a] Mean $\delta^{18}O$ (‰)

[b] Globigerina ruber

* Holocene mean, not interglacial

~1.3°/$_{oo}$, compared to a 1.6°/$_{oo}$ difference to the east of New Zealand (Table 5.15). The southernmost of the western sites (593) has a mean glacial value of 2.1°/$_{oo}$, considerably lighter than the mean glacial value of ~3.6°/$_{oo}$ for sites to the east of New Zealand. This suggests that cool Subantarctic surface currents did not predominate as far north as Site 593, although it is the coolest of the western sites and must have been exposed to some Subantarctic influence. Warmer Subtropical Surface Waters appear to have been dominant to the west of New Zealand in the Tasman Sea, even during glacial periods, suggesting generally similar surface circulation patterns to the present day (Figure 2.11).

5.1.5 Glacial to Interglacial Extremes

Table 5.16 shows the mean glacial and interglacial extremes of the $\delta^{18}O$ record for each site. In most cases there is little difference from the Holocene to glacial comparison discussed previously, although four sites (589, 592, 593 and 594) stand out as anomalous.

Site 589 displays considerable non-synchronous fluctuations in the benthic and planktonic $\delta^{18}O$ records, well beyond the Brunhes/Matuyama boundary, which indicates a somewhat suspect palaeoclimatic record.

At Site 594, if the mean interglacial planktonic value is derived from stages 1 and 5e, then the difference of 2.3°/$_{oo}$ is more extreme than that occurring at other sites to the east of New Zealand. However, since 594 has the highest sedimentation rate of all the sites studied it is most likely that the true extreme values have been modified in the other eastern sites.

Site 593 has mean planktonic interglacial values of -0.5°/$_{oo}$. This is much lighter than the mean Holocene value of 0.9°/$_{oo}$. It does not seem likely that the Holocene is partially lost in 593, as the benthic

Table 5.17. Benthic $\delta^{18}O$ values for stages 1 to 6 at each of the sites studied, with isotopically derived bottom water temperatures for stage 1 and 5 (in brackets).

	West of New Zealand						East of New Zealand					
Stage Number	588	590	591A	Z2108	592	593	Q858	594	Q200	Q580	Q217	Q585
1	-	4.0 (0.5)	3.9 (0.8)	2.7 (5.2)	3.2 (2.8)	3.1 (3.5)	3.4	3.4 (2.6)	3.0 (3.3)	3.4 (2.2)	3.4 (2.9)	-
2	4.7	5.2	4.8	3.8	4.2	4.3	5.0	5.0	4.4	4.9	5.0	-
3	-	4.4	-	3.0	3.1	3.6	-	4.3	3.7	-	4.4	-
4	-	4.6	-	3.4	4.4	4.3	-	4.7	-	-	-	-
5	3.7	3.7 (1.5)	3.8 (1.2)	1.9 (8.3)	3.1 (3.2)	2.8 (4.6)	-	3.0 (4.1)	-	-	3.1 (3.7)	3.2 (3.3)
6	-	5.3	5.2	3.8	4.0	4.0	-	4.7	-	-	-	-

Table 5.18. Planktonic $\delta^{18}O$ values for stages 1 to 6 at each of the sites studies, with isotopically derived surface water temperatures for stage 1 and stage 5 (in brackets).

	West of New Zealand							East of New Zealand				
Stage Number	586	588	590	591A	Z2108	592	593	594	Q200	Q580	Q217	Q585
1	-2.6	-0.7 (20.9)	0.0 (17.7)	0.0 (17.7)	-0.6 (20.0)	0.7 (14.2)	0.9 (13.1)	1.6 (8.7)	1.7 (8.5)	2.0 (7.2)	2.2 (7.0)	2.4 (5.7)
2	-	-	1.0	1.0	-	1.9	2.2	3.3	3.3	3.5	3.6	-
3	-	-	0.6	0.4	-	0.7	1.0	2.8	2.6	-	3.0	-
4	-	-	0.8	1.2	-	0.1	1.8	3.4	-	-	3.8	-
5	-2.5	-	0.5 (15.8)	-0.1 (18.2)	-1.2 (22.7)	0.1 (16.9)	-0.5 (19.3)	1.2 (10.8)	-	-	2.6 (5.6)	2.5 (5.2)
6	-0.8	0.5	1.6	0.7	1.4	0.7	2.2	3.4	-	-	-	-

foraminiferal value is comparable to the other interglacial extremes in the core. In addition, the modern planktonic value of $0.9^{o}/_{oo}$ gives a reasonable estimation of modern water temperature (Section 5.1.3). It is possible therefore that during past interglacial periods Site 593 has been exposed to far warmer surface currents than it is experiencing at present. An interglacial strengthening of the part of the East Australian Current that flows south to Tasmania before flowing east across the Tasman Sea could expose Site 593 to warmer surface currents and could account for the warmer temperatures.

Site 592 likewise displays heavier Holocene values (by $0.5^{o}/_{oo}$) compared to other interglacials. As reasonable modern isotopic temperatures can be derived from the planktonic Holocene $\delta^{18}O$ values, and the benthic Holocene $\delta^{18}O$ values are comparable to other interglacial extremes, it would appear that the Holocene record is complete and has not been lost. Consequently it may be concluded that Site 592 is also presently exposed to cooler currents than has been the case during the previous interglacial. Thus it appears that the East Australian Current has taken a more northerly route during the Holocene than in most previous interglacials. This is likely to have had a significant effect on the Holocene climate of New Zealand, with cooler current influences in the Tasman Sea resulting in lower on-land temperatures, compared to previous interglacials.

5.1.6 The Last Interglacial (Stage 5e)

In the SPECMAP stack record (Figure 5.1a) isotope stage 5 has two lesser peaks (5a and 5c) that are heavier than the Holocene peak, and one peak (5e) that is of comparable magnitude. This pattern is clearly seen in the planktonic record of 594 (Figuree 5.1b), where the high sedimentation rate has ensured a complete record. The cooler periods

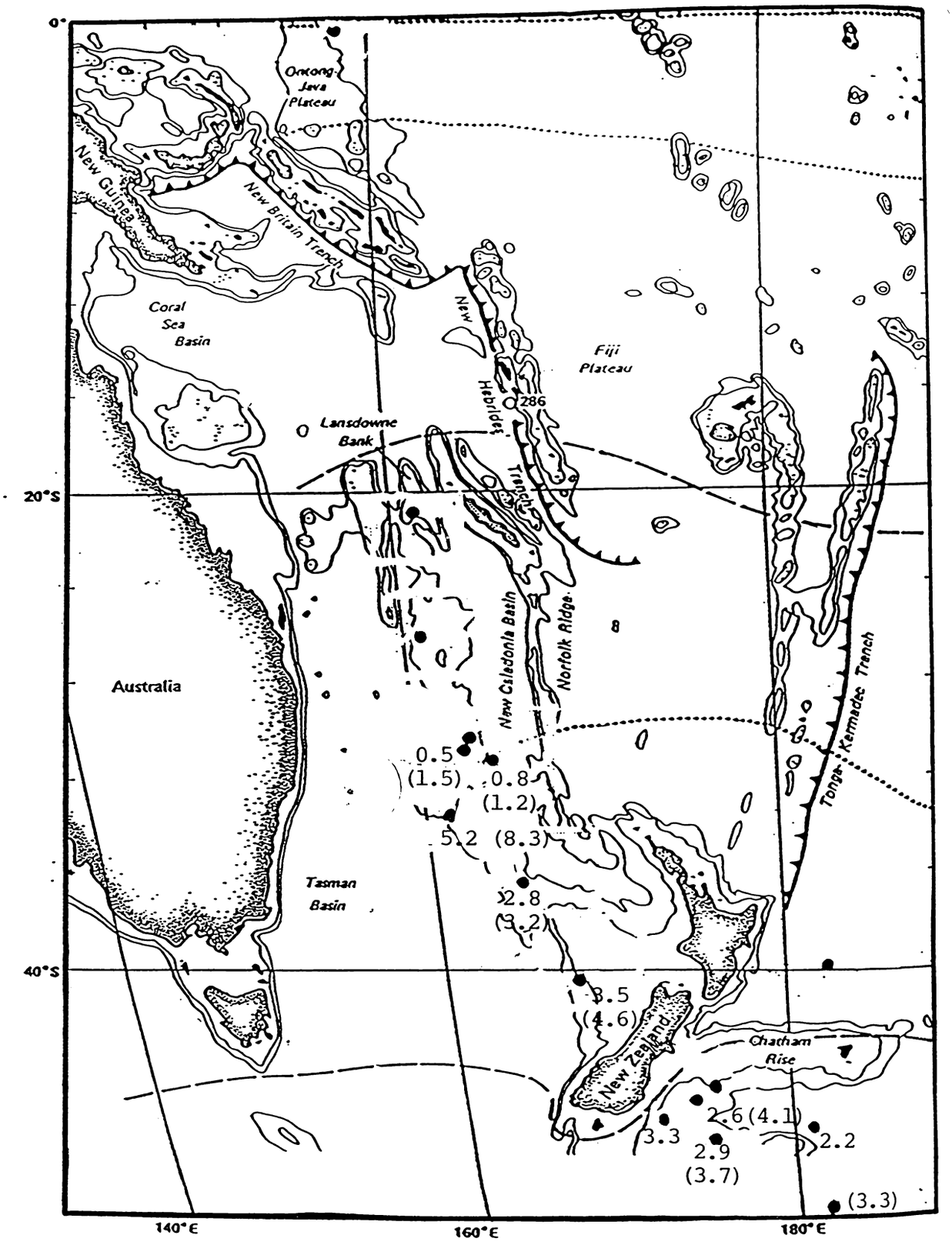

Figure 5.34. Stage 5 and stage 1 (in brackets) bottom water temperatures derived from the benthic $\delta^{18}O$ record.

of stage 5 (b and d) appear to be much more intense in the 594 record than in the SPECMAP stack. The position of 594 immediately south of the Subtropical Convergence could account for the greater sensitivity of the substage fluctuations.

In the benthic record of 594 (Figure 5.1c) 5a, c and e are all of approximately equal magnitude, whereas the SPECMAP stack (Figure 5.1a) shows 5e as the lightest. This may be indicative of incursions of Antarctic glacial meltwater during the substage warming of 5a,c and e, (as it is relatively small in volume,it is possible that it has sunk before reaching Site 594 (Section 5.1.7)) rather than Northern Hemisphere meltwater. The proximity of Site 594 to the Antarctic may result in meltwater spikes that are transferred more rapidly, and with less mixing of the isotopically light water, so that no differentiation is seen in the intensity of periods of warming.

The fine structure of the benthic record of 594 has been described in Section 5.1.2. The stage 5e benthic isotopic record is incomplete due to a lack of suitable foraminifera for analysis. Consequently some doubt exists as to the precise structure of 5e. The planktonic record (Figure 5.1b) reveals two major peaks, one of which (the younger) could be further sub-divided into two minor peaks. The shape of the younger peaks is similar in the benthic record, and it is likely that the older major peak has been missed. There is no suggestion of three peaks in other stage 5e records, but it is likely that the greater sub-stage sensitivity of 594, because of its location and high sedimentation rate, has allowed the fine detail of events within 5e to be determined, with two cooler episodes rather than only one, as is usually seen (e.g., compare to the record of V19-29, Figure 5.25).

Comparisons between the relative interglacial intensities of stage 5 and the Holocene are difficult at the other sites studied, as it is

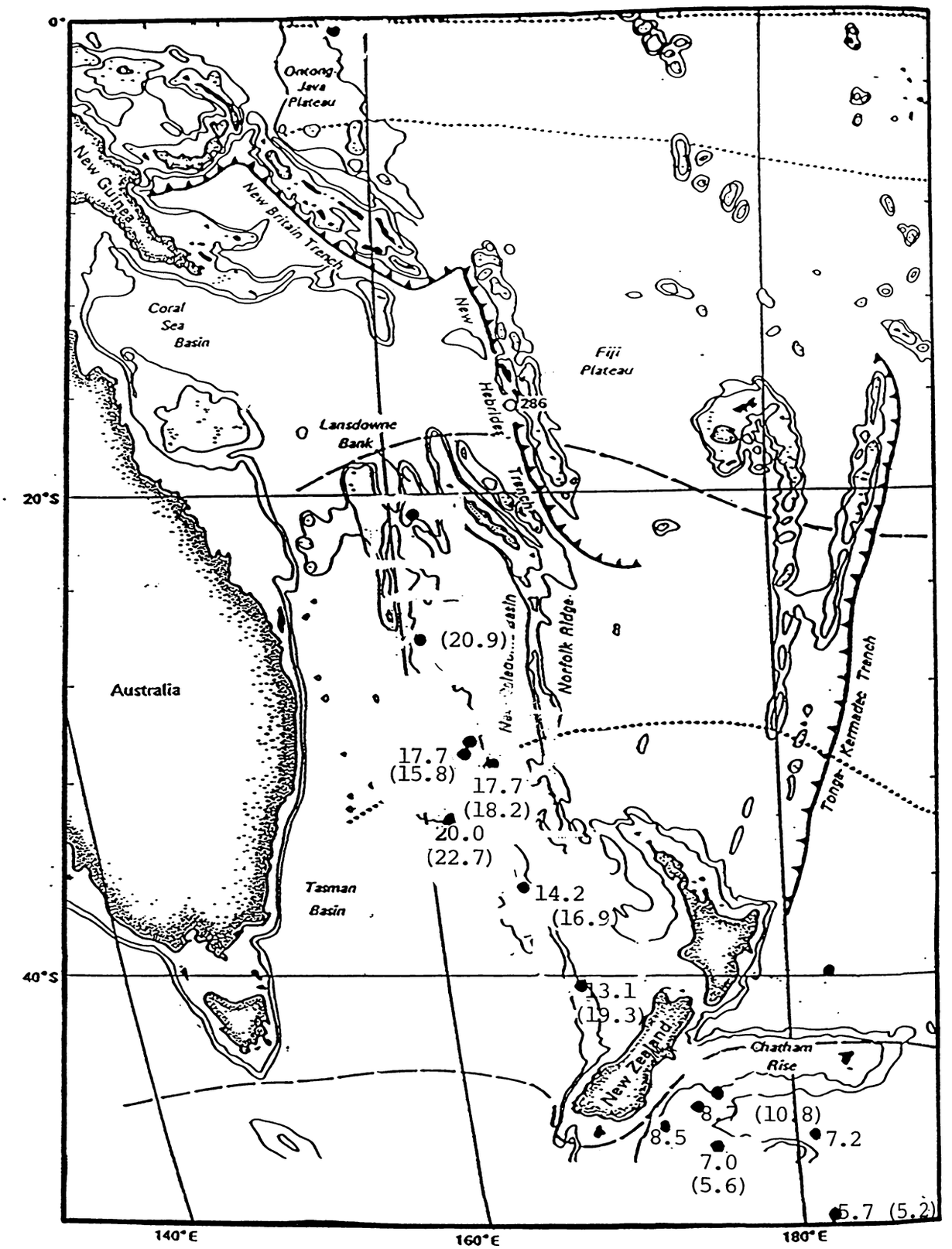

Figure 5.35. Stage 5 and stage 1 (in brackets) surface water temperatures derived from the planktonic $\delta^{18}O$ record.

uncertain whether or not all of the Holocene is present, and whether the extremes of stage 5 have been resolved.

A summary of the benthic and planktonic $\delta^{18}O$ values for stages 6 to 1 is presented in Tables 5.17 and 5.18 and Figures 5.34 and 5.35. The numbers in brackets are derived palaeotemperatures for stage 1 and 5(e, where identifiable), assuming the sea levels of 5e were comparable to those of today (Shackleton, 1987), and the composition of the sea water similar (see Figure 1.2b).

5.1.7 Synchroneity of the Benthic and Planktonic $\delta^{18}O$ Records of 594

The $\delta^{18}O$ record of the glacial/interglacial transitions of 5/6 and 1/2 are noticeably more saw-toothed in appearance in the planktonic, compared to the benthic, record of 594, as the planktonics appear to have more quickly reflected ice sheet fluctuations. The deglacial $\delta^{18}O$ signal is partly composed of ice sheet meltback and partly of a change in temperature. The meltwaters can only be transferred by NADW circulation, but the temperature change could be rapidly transferred via the atmosphere. If the change in temperature were a significant part of the signal, then we would see not only rapid fluctuations in the planktonic signal but also different shapes of signals in different parts of the world, which is not the case. It would thus appear that the circulation of NADW is of most importance in transferring the meltwater signal, and it is difficult to understand why it is observed first in the surface planktonics, rather than in the bottom dwelling benthics, as one might expect. However, our model of the circulation of meltwater is imprecise, and since most of the cores in this study are located at 1 000-2 000m it is possible that the deglacial signal may have been circulated above or below this depth, and so has not been recorded immediately by the benthic

foraminifera. Further study to determine the depth at which the meltwater signal is circulated, once the cool waters have sunk, would help to clarify this. The complexity of the mixing of NADW and AIW is not yet fully understood.

The saw-toothed nature of the planktonic signal is also partly due to the sensitivity of planktonic foraminifera to surface climatic conditions, and some fluctuations are the result of local phenomena. The $\delta^{18}O$ values of benthic foraminifera, however, are largely indicative of ice volume changes whose response is smoothed after ocean mixing.

Lack of synchroneity can provide information on patterns of circulation, and whether or not the glacial meltwaters were circulated first to surface or to bottom waters. The planktonic isotopic record for 594 is very noisy (Figure 5.3c), but it would appear that the planktonic stage I_A glacial termination signal leads that of the benthic record (Figure 5.3d). This is compared with I_A leads in other cores, presented in Table 5.19. (The graphs provided by C.H.Hendy, pers. commun., 1988, are in Appendix II). Locations of cores are shown in Figure 5.36.

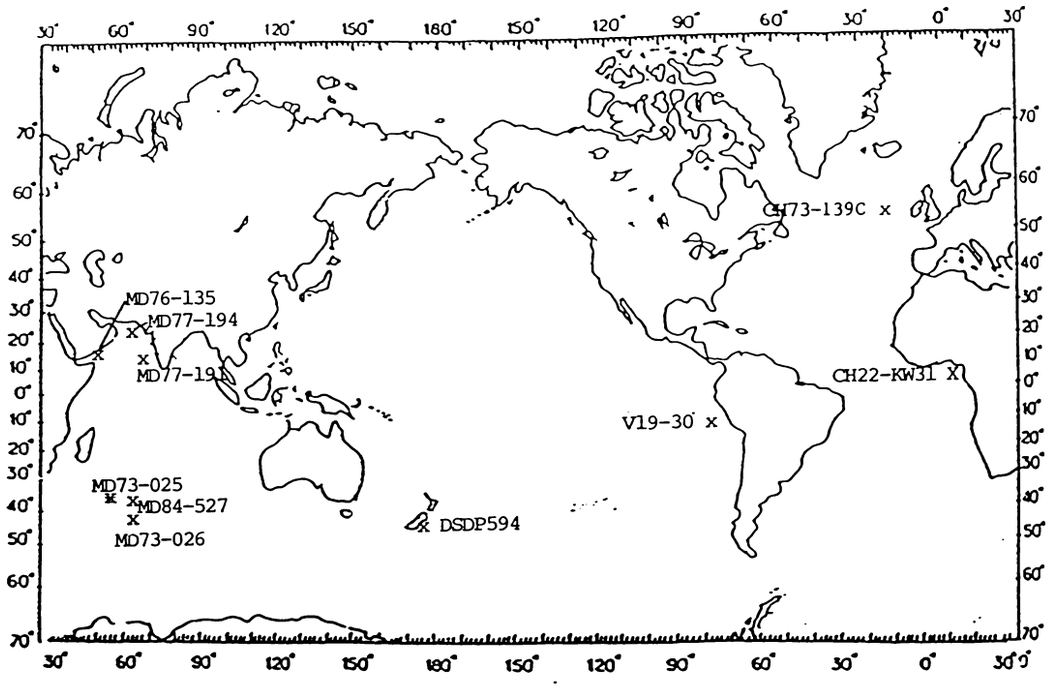

Figure 5.36. Locations of the cores for which lead/lag relationships have been determined.

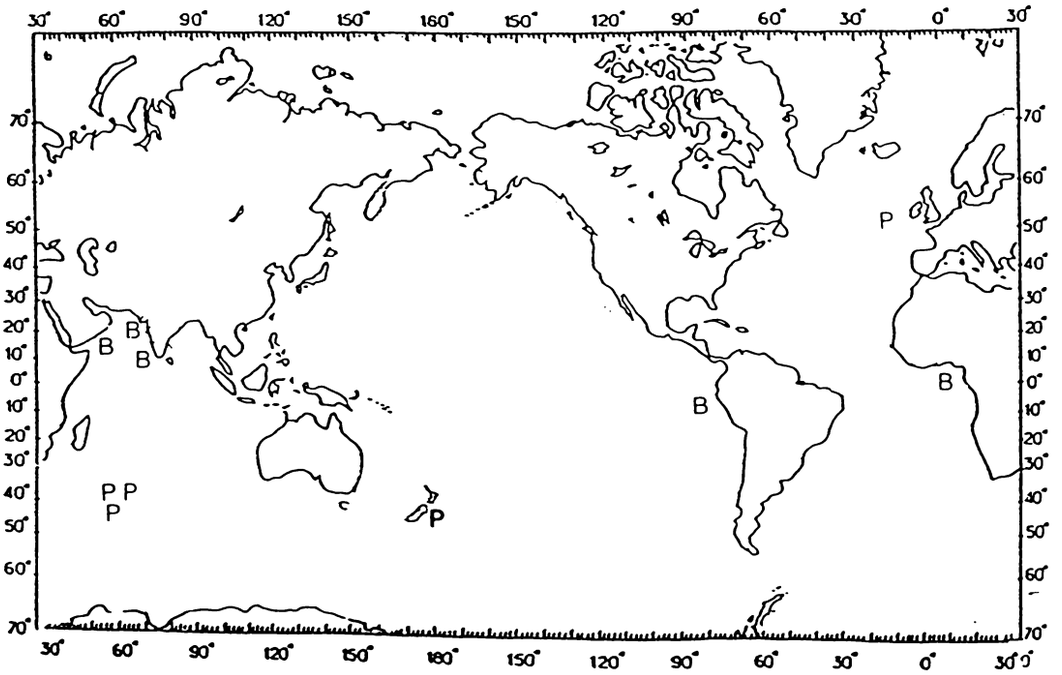

Figure 5.37. The leading $\delta^{18}O$ signal over Termination I_A at various locations world-wide (B = benthic, P = planktonic).

Table 5.19. Lead-lag relationships in $\delta^{18}O$ records of termination I_A, from a variety of deep-sea cores. (C.H.Hendy, pers. commun. 1988, unless marked otherwise).

Core[a]	Location	Ocean System	Lead Signal
CH73-139C	54°38'N; 16°21'W	Nth. Atlantic	Planktonics
CH22-KW31	03°31'N; 05°34'E	Sth. Atlantic	Benthics
MD73-025	43°49'S; 51°19'E	Sth. Indian	Planktonics
MD73-026[b]	44°59'S; 53°17'E	Sth. Indian	Planktonics
MD76-135	14°27'N; 50°31'E	Nth. Indian	Benthics
MD77-191	07°30'N; 76°43'E	Nth. Indian	Benthics
MD77-194	10°28'N; 75°14'E	Nth. Indian	Benthics
MD84-527[b]	43°49'S; 51°19'E	Sth. Indian	Planktonics
DSDP 594	45°31'S; 174°57'E	SW Pacific	Planktonics
V19-30[c]	03°23'S; 83°21'W	East Pacific	Benthics

[a]Core locations are shown in Table 5.19 and Figure 5.31.
[b]Labeyrie et al., 1986.
[c]Discussed with Shackleton *in* Ruddiman and Duplessy, 1985.

These lead-lag relationships for Termination I_A are also depicted in Figure 5.37 to show their geographic consistency. It is evident that at low latitudes in the Atlantic (CH22 KW31), Indian (MD76 135, MD77 191, MD77 194) and Pacific (V19-30) Oceans the I_A termination is first seen in the benthic record. However, at high latitudes in the Atlantic (CH73-139), Indian (MD73-025, MD73-026, MD84-527) and Pacific (DSDP594) Oceans the planktonic deglaciation signal leads the benthic record.

Berger and Killingly (1982) postulated that the meltwater signal would occur first, worldwide, in the planktonic foraminiferal isotopic record, as a global meltwater "lid" would isolate the deep ocean from the deglacial signal. The above results would suggest that while this

may be true in higher latitudes, the meltwater "lid" cannot extend worldwide as the meltwater signal is retarded in low latitude surface waters. This could be explained by the sinking of the cold meltwaters as they reach less dense tropical waters, thus affecting benthic foraminifera in low latitudes before finally upwelling and appearing in the planktonic signal.

During the 2 to 1 and 4 to 3 transitions (from relatively cold to warm conditions) the meltwater signal is first evident in the planktonic isotopic record. Through stage 5, however, cold to warm transitions are registered first in the benthic record. These lead/lags are summarised in Table 5.20.

Table 5.20. Lead-lag relationships in the $\delta^{18}O$ record of 594 (see Figure 5.3c and d).

Stage	Lead Signal	Relative ΔT
6 -> 5e	?	cold -> warm
5e -> 5d	Planktonic	warm -> cold
5d -> 5c	Benthic	cold -> warm
5c -> 5b	Planktonic	warm -> cold
5b -> 5a	Benthic	cold -> warm
5a -> 4	?	warm -> cold
4 -> 3	Planktonic	cold -> warm
3 -> 2	?	warm -> cold
2 -> 1	Planktonic	cold -> warm

? Indicates that the lead signal cannot be determined from the available data.

Since stage 5 is interglacial, with warmer temperatures prevailing, the volume of meltwaters from the glaciers in cold to warm substage transitions was considerably less than the volume involved in full glacial to interglacial transitions, resulting in a relative lessening of the extent of the meltwater surface "lid". Thus it is not unreasonable that the benthics should lead the planktonics from 5d to 5c and 5b to 5a.

Analysis of the lead-lag relationships in the lower resolution sampling of 594 (Cuthbertson, 1985) is difficult as the distance between samples is greater, but it would appear that for transitions from 18 to 17, 16 to 15, 12 to 11 and 10 to 9 (i.e. cold to warm) the

planktonic $\delta^{18}O$ signal leads the benthic signal, compatible with the arrival of cold glacial Antarctic meltwater at the surface in higher latitudes, before its presence is recorded in deeper waters. (The lead signal in the transitions from 14 to 13 and 8 to 7 is impossible to determine).

5.2 Discussion of Aspects of the $\delta^{13}C$ Results

The $\delta^{13}C$ results appear with the $\delta^{18}O$ results presented in Section 5.1 (Figures 5.3 to 5.10 and 5.12 to 5.22). Since additional unbound copies of these figures have been provided in the envelope at the back of this thesis, for ease of comparison and discussion, the figures have not been repeated here.

5.2.1 Changes from the Last Glacial to Present Day

In all of the cores studied a marked difference between mean glacial and interglacial $\delta^{13}C$ values occurs in the benthic foraminiferal record. From glacial to interglacial periods the mean benthic $\delta^{13}C$ increase is $\sim 0.95^{o}/_{oo}$. This difference between benthic glacial and interglacial values has been previously observed (outlined in Section 1.7), and the more negative values during glacial periods could support the case for decreased production of NADW during the last glacial (suggested by many authors, e.g., Duplessy et al.,1975; Schnitker, 1979; Streeter and Shackleton, 1979). Considerably decreased flow rates of NADW result in a slower turnover and hence greater assimilation of isotopically light organic material. In addition, a decrease in the volume of NADW during glacial periods (supported by $\delta^{13}C$ values presented by Curry and Lohmann, 1982) results in a vertical migration of the NADW/AABW boundary, which would influence the benthic $\delta^{13}C$ values from the core sites (AABW is reported by Kroopnick (1980) to be $0.5^{o}/_{oo}$ lighter than the overlying

deep NADW). A summary of the mean Holocene and last glacial maximum $\delta^{13}C$ values of benthic and, where determinable, planktonic foraminifera is presented in Tables 5.21 and 5.22.

Table 5.21. A summary of mean Holocene and last glacial maximum $\delta^{13}C$ values of benthic and planktonic foraminifera from the cores studied.

West of N.Z.				N	East of N.Z.			
Core No.	Mean interglacial $\delta^{13}C$ PF[1]	BF[2]	Δ[3]		Core No.	Mean interglacial $\delta^{13}C$ PF	BF	Δ
586	-	-	-		Q858	-	-0.3	-
588	0.7*	0.7	0.0		Q219	-	-	-
589	-0.2	0.4	0.6		594	0.5	0.0	-0.5
590	-0.9	0.8	1.7		Q200	0.6	0.0	-0.6
591A	-0.9	0.1	1.0		Q580	0.4	-0.8	-1.2
Z2108	-1.3	-0.4	0.9		Q217	0.7	-0.2	-0.9
592	-	0.3	-	↓	Q585	-	-0.3	-
593	-	0.2	-	S				

				N				
Core No.	Mean glacial $\delta^{13}C$ PF	BF	Δ		Core No.	Mean glacial $\delta^{13}C$ PF	BF	Δ
586	-	-	-		Q858	-	-1.4	-
588	0.0*	-0.2	-0.2		Q219	-	-	-
589	-1.4	-0.6	0.8		594	-0.9	-1.4	-0.5
590	-1.6	0.2	1.4		Q200	0.0	-0.8	-0.8
591A	-1.7	-0.7	1.0		Q580	-1.0	-2.0	-1.0
Z2108	-2.4	-1.5	0.9		Q217	0.0	-0.7	-0.7
592	-	-0.4	-	↓	Q585	-	-0.7	-
593	-	-1.7	-	S				

[1] *G. bulloides* unless otherwise indicated.

[2] *Uvigerina* spp.

[3] Δ = BF-PF

* *G. ruber*

Table 5.22. A summary of the glacial/interglacial differences ($\Delta\delta^{13}C$ = G - IG) for planktonic and benthic foraminifera.

West of N.Z.					East of N.Z.			
Core No.	Planktonic[1] G	IG	$\Delta\delta^{13}C$		Core No.	Planktonic[1] G	IG	$\Delta\delta^{13}C$
				N				
588[2]	0.0	0.7	-0.7	|	594	-0.9	0.5	-1.4
589	-1.4	-0.2	-1.2	|	Q200	0.0	0.6	-0.6
690	-1.6	-0.9	-0.5	|	Q580	-1.0	0.4	-1.4
591A	-1.7	-0.9	-0.8	↓	Q217	0.0	0.7	-0.7
Z2108	-2.4	-1.3	-1.1	S				
Core No.	Benthic[3] G	IG	$\Delta\delta^{13}C$		Core No.	Benthic[3] G	IG	$\Delta\delta^{13}C$
				N				
588	-0.2	0.7	-0.9	|	Q858	-1.4	-0.3	-1.1
589	-0.6	0.4	-1.0	|	594	-1.4	0.0	-1.4
590	0.2	0.8	-0.6	|	Q200	-0.8	0.0	-0.8
591A	-0.7	0.1	-0.8	|	Q580	-2.0	-0.8	-1.2
Z2108	-1.5	-0.4	-1.9	|	Q217	-0.7	-0.2	-0.5
592	-0.4	0.3	-0.7	|	Q585	-0.7	-0.3	-0.4
593	-1.7	0.2	-1/9	↓				
				S				

[1]*Globigerina bulloides*

[2]*Globigerina ruber*

[3]*Uvigerina* spp.

IG = Interglacial G = Glacial

Previous workers in the Caribbean, the Atlantic and the Pacific have not found any significant glacial to interglacial difference in the planktonic foraminiferal $\delta^{13}C$ record. In this study, however, $\delta^{18}O$ and $\delta^{13}C$ variations are synchronous at sites 588, 589, 590, 591A, and Z2108 to the west of New Zealand, and at sites 594, Q200, Q217, and Q580 to the east of New Zealand. If periods of higher carbonate productivity in the Tasman Sea in the vicinity of the Subtropical

Divergence (marked in Figure 3.1), and in the Southwest Pacific in the vicinity of the Subtropical Convergence close to the South Island, coincided with warm interglacial periods, this could account for the consistency of the planktonic $\delta^{13}C$ values at these core sites with the $\delta^{18}O$ climatic record, as a higher productivity results in an increase in organic chemical reactions, and thus an increase in the fractionation of the carbon isotopes.

A comparison of modern reactive phosphorous levels and primary productivity with Holocene planktonic $\delta^{13}C$ values shows a rough correlation between modern $\delta^{13}C$ and modern productivity. Heavier $\delta^{13}C$ values from the east of New Zealand are associated with higher reactive phosophorus and primary productivity levels. Whilst to the west, lighter $\delta^{13}C$ values are associated with relatively lower levels of reactive phosphorus and productivity (Table 5.23).

Table 5.23. Holocene planktonic $\delta^{13}C$ values, reactive phosphorous levels[1] and primary productivity[2] at each of the core sites.

	Core No.	Reactive Phosphorus ($\mu g/l$)	Primary Productivity (^{14}C uptake $mgC/m^3/hr$)	Planktonic $\delta^{13}C$
East	590	0.1-0.2	0.15	-1.2
	591A	0.1-0.2	0.15	-1.4
	592	0.1	0.06	-0.6
	593	0.0-0.1	0.5	-0.6
West	Q219	0.5	0.6	0.4
	594	0.8-0.9	0.6	0.4
	Q200	0.6	0.6	0.35
	Q217	0.7	0.6	0.5
	Q580	0.8	1.0	0.7
	Q585	0.9	0.6	0.5

[1]Approximated from Bradley and Taylor, 1980.

[2]Approximated from Bradley, 1980.

In all of the cores studied for which the Stage 1/2 transition is identified (i.e., Sites Q200, Q217, Q580, Q585, Q858, Z2108, 590, 591A, 592, 593, and 594) lighter $\delta^{13}C$ values (by 0.4 to 0.8°/$_{oo}$) occurred at, or very close to, the stage boundary. This minimum is seen in both the planktonic and benthic record, indicating an ocean-wide phenomenon affecting both top and bottom waters. The most likely cause is the re-establishment of greater volumes of NADW flowing into the Southern Ocean and hence into the Pacific, displacing the relatively stagnant, isotopically light, glacial deep water and resulting in a transient drop in $\delta^{13}C$ values as the ^{12}C-rich waters are remobilised and "flushed" out of the deep water flow paths. An

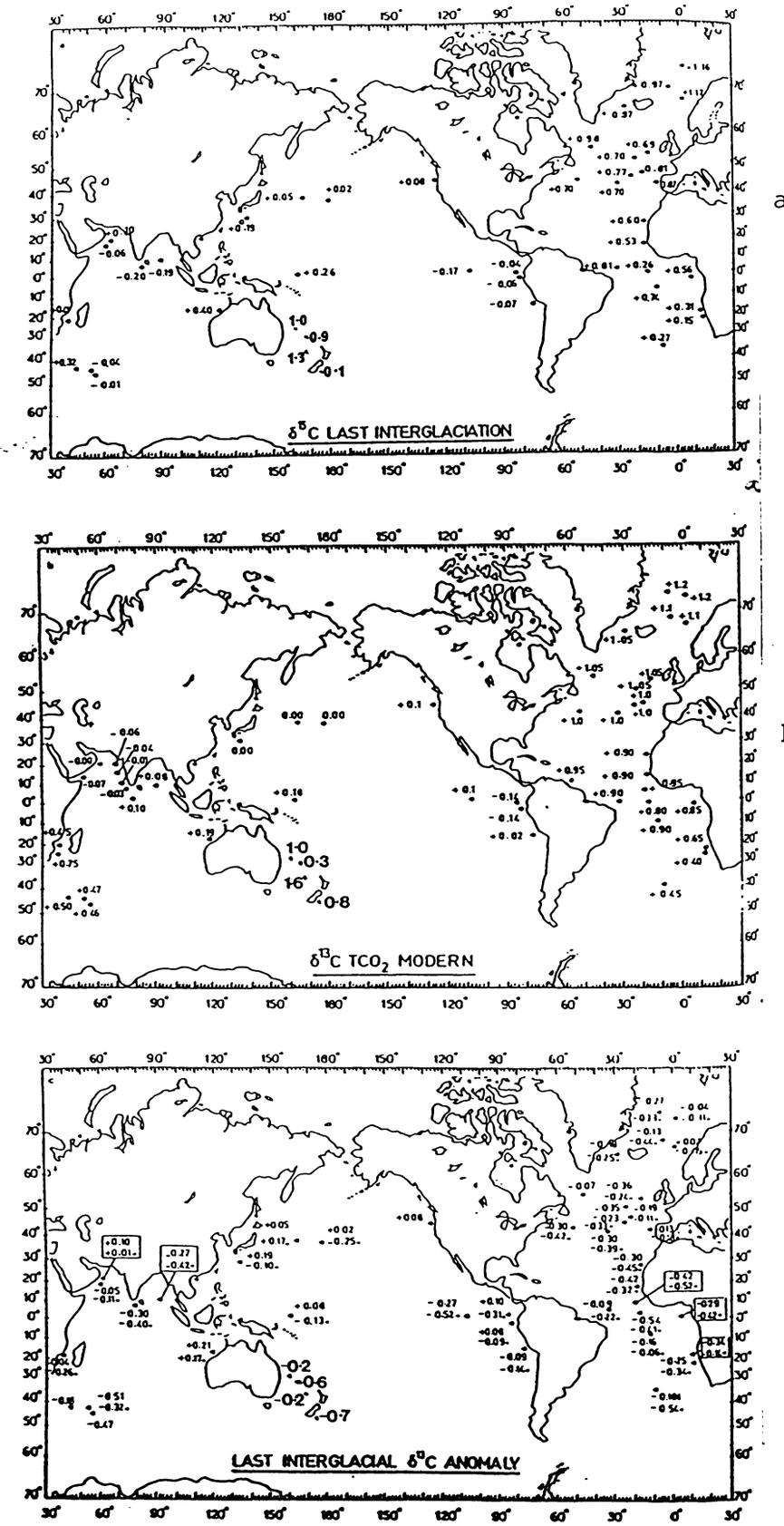

a

b

c

Figure 5.38a. Mean $\delta^{13}C$ values for the last interglacial.

b. Mean Holocene $\delta^{13}C$ values.

c. Last interglacial $\delta^{13}C$ anomaly.

examination of the long, lower resolution, record of DSDP Site 594 (presented in Cuthbertson, 1985) shows that this phenomenon probably occurred regularly throughout the Brunhes Epoch at glacial/interglacial transitions.

5.2.2 The Last Interglacial

A comparison of the mean $\delta^{13}C$ values of benthic foraminiferal tests from the last interglacial stage 5e with modern total CO_2 (TCO_2) or Holocene benthic $\delta^{13}C$ values was made by Duplessy et al. (1984) in order to deduce differing patterns of circulation in deep waters. Results from cores studied in this thesis, where 5e is identifiable, are added to their data in order to help fill the considerable data "gap" in the Southwest Pacific region (Table 5.24, Figure 5.38).

Table 5.24. A comparison of Holocene and 5e benthic $\delta^{13}C$ values (after Duplessy et al., 1984).

Core No.	Water Depth(m)	Water Body	Holocene $\delta^{13}C$	5e $\delta^{13}C$	Last interglacial anomaly*
594	1204	DW	0.8	0.1	-0.7
592	1098	AIW	1.2	1.0	-0.2
591A	2131	DW	(0.3)	0.9	(0.6)
590	1299	DW	1.6	1.3	-0.3

[a] Corrected to *Cibicides* by $\delta^{13}C_{Uvi.} + 0.90^{o}/_{oo}$ (after Duplessy et al., 1984).

* From 5e $\delta^{13}C$ - Holocene $\delta^{13}C$.

The anomalies presented support the observation of low TCO_2 $\delta^{13}C$ in the Circumpolar Deep Water (CDW) during 5e, relative to the modern situation. Significant departures from modern $\delta^{13}C$ values are also seen in the Tasman Sea (Sites 590, 591A and 592). This depletion

compared to the present day is explained by Duplessy et al. (1984) in terms of a decreased global organic carbon reservoir - from a reduction in continental biomass, or from decreased amounts of deposition of organic-rich sediment on the continental shelves.

A mean difference of $-0.35°/_{oo}$ between the last interglacial and today in the CPDW of the Southern Ocean may be calculated from the data presented by Duplessy et al. (1984). Inclusion of the Site 594 anomaly value gives a slightly greater mean difference of $-0.43°/_{oo}$.

A systematic appraisal of the isotope Stage 5e record at Site 594 shows consistently more negative planktonic and benthic $\delta^{13}C$ values during the warmer periods of stage 5 (i.e. a,c and e, indicated by lower $\delta^{18}O$ values). These are summarised in Table 5.25.

Table 5.25. Summary of mean $\delta^{18}O$ and $\delta^{13}C$ values for benthic and planktonic foraminifera at Site 594 over stage 5.

Stage	Relative Temp.	Planktonic Mean $\delta^{18}O$	Planktonic Mean $\delta^{13}C$	Benthic Mean $\delta^{18}O$	Benthic Mean $\delta^{13}C$
5a	Warm	2.0	0.0	3.2	-0.3
5b	Cold	3.1	0.6	4.3	0.0
5c	Warm	1.9	-0.4	2.9	-1.1
5d	Cold	3.2	0.6	4.0	-0.4
5e	Warm	1.1	-0.5	3.0	-0.8

It is likely that the synchronous appearance of isotopically light CO_2 in both top and bottom waters at 594 during substages 5a, 5c, and 5e, may be caused by an increased AABW flux into the Southwest Pacific during interglacial stages coupled with upwelling, interrupted

by periods of reduced flow during the colder substages of 5b and 5d when contrasting high $\delta^{13}C$ values occurred. Duplessy et al. (1984) proposed enhanced production of AABW during substage 5e, and this study suggests that it was a feature of all of the warm substages of 5 (i.e., 5a, 5c, and 5e).

5.2.3 $\delta^{13}C$ Differences between Sites to the West and East of New Zealand

Kroopnick (1974) noted that generally higher $\delta^{13}C$ values are obtained from surface-dwelling planktonics compared to those of benthics that have grown in deeper, cooler, conditions. In addition, sediment-burrowing benthic foraminiferal tests have probably been exposed to pore waters that are ^{12}C-enriched from the rain of organic material from the surface. However, absolute comparisons of planktonic and benthic results would have to take into consideration the degree of disequilibrium in the species used. (Duplessy et al.(1984) indicate that *Uvigerina* spp. $^{13}C/^{12}C$ ratios do not reflect an equilibrium situation, and apply a correction factor of $+0.9^{o}/_{oo}$ to normalise them to *Cibicides*, which are considered to be at equilibrium). Since the degree of disequilibrium of *G. bulloides* is in dispute (Section 1.9), comparisons of absolute $\delta^{13}C$ values are difficult. However, some general trends may be noted.

The $\delta^{13}C$ values of benthics to the east of New Zealand during glacial periods have a mean value of $-1.2^{o}/_{oo}$, and during interglacials a mean of $-0.3^{o}/_{oo}$. Values to the west of New Zealand, however, are consistently heavier, on average by $0.5^{o}/_{oo}$ (mean glacial $\delta^{13}C$ is $-0.7^{o}/_{oo}$, mean interglacial $\delta^{13}C$ is $0.2^{o}/_{oo}$) (Table 5.21). Since Kroopnick (1980) showed that the dominant effect on bottom water ^{13}C distribution is circulation, the water to the east of New Zealand

must be considerably different in structure compared to the water mass to the west of New Zealand. This would be consistent with a greater dominance of isotopically light AABW to the east, with NADW predominating to the west. (See Figure 2.2 for oceanographic structure).

5.3 Carbonate Results

Carbonate analyses for all of the NZOI cores were carried out. Raw data from these are presented in Tables 4.9 to 4.15, and graphically in Figures 5.4 to 5.9 and 5.20 (refer to unbound copies inside the back cover). The high resolution carbonate stratigraphy of Site 594 has been documented by Cooke (1988). Previous moderately high resolution carbonate analysis for the entire Brunhes for Site 594 has been discussed by Nelson et al. (1986).

A marked cyclicity is evident in the carbonate record of 594. The 5/6 stage boundary is clearly seen with an increase in $\%CaCO_3$ from 7% to 61% marking 5e. The cooler substage 5d is then recognisable with a drop to values of 35-40%. A further rise (up to ~60%) and fall (to ~30%) mark 5c and 5b respectively. The 5/4 transition is obvious, with a drop from ~50% to 4%. Stage 3 is seen to be a period of moderate $CaCO_3$ content of 20-40%, with a clearer division between stages 2 and 3 (assuming version #1 of the isotopic taxonomy, Section 5.1.2) than is seen in the isotopic record. The transition from 2 to 1 is similarly well marked, with an increase in $CaCO_3$ from ~10% to 45%.

Down-core correlation between low $\%CaCO_3$ and high $\delta^{18}O$ values has been explained in terms of the terrigenous material deposited at Site 594 from the South Island during periods of accelerated erosion (Cuthbertson, 1985; Nelson et al., 1986). NZOI Cores Q200, Q217, Q580

and Q585, in the vicinity of 594, also display high $CaCO_3$ values during interglacial periods, and low $CaCO_3$ contents during glacial periods. This down-core correlation between high carbonates and high temperatures is not found world-wide (for example, in eastern equatorial Pacific cores high carbonate is associated with glacial periods because of increased dissolution during interglacials (Valencia, 1977), but is known in the Atlantic. This apparent anomaly can be explained by considering the oceanic conditions which are thought to have been prevalent, with increased upwelling intensity in the eastern equatorial Pacific occurring below the lysocline.

A summary of the $CaCO_3$ content for stages 6 to 1 in 594 is presented in Table 5.26. Using sedimentation rates derived in Section 5.1.1, these percentage values have been used to approximate the carbonate sedimentation rate:

$$\%CaCO_3 \text{ X Sed. rate} \Rightarrow CaCO_3 \text{ Sed. rate.}$$

Table 5.26. Total sedimentation rate, $CaCO_3$ content and carbonate sedimentation rate at Site 594, for stages 1 to 6.

Stage	Sed.Rate (cm/ky)	~%$CaCO_3$	$CaCO_3$ Sed.Rate (cm/ky)
1	10.8	60	6.5
2	34.6	7	2.4
3	9.1	25	2.3
4	18.3	7	1.3
5	11.2	50	5.6
6	-	20	-

The higher accumulation rate of carbonate during interglacial stages 1 and 5 at Site 594 is obvious. It is not unreasonable that this should be so, as Griggs et al. (1983) note the temperature dependence of calcareous foraminifera, only one species of which (*Neogloboquadrina pachyderma*) is found south of the subpolar front. Thus the northward migration of calcareous species during colder glacial periods, and the increased terrigenous dilution during glacials, lead to a lower $CaCO_3$ content in the sediments during glacial periods. During interglacial periods of lower terrigenous dilution, where $CaCO_3$ values are higher, Griggs et al. (1983) report an increase in carbonate species diversity with increasing warmth of surface waters. Recent micropalaeontological studies suggest that dissolution does not play a great part in variations in $\%CaCO_3$ at Site 594 (Cooke, 1988). Thus for Site 594 increased carbonate productivity may be inferred during interglacial periods (which broadly coincides with periods of increased carbonate productivity determined by the $\delta^{13}C$ results (Section 5.2). It may be that this situation is unique to 594 because of its location. Certainly it is opposite to the periods of higher productivity determined during the glacial periods at Site 593 by Dudley and Nelson (1988). Siliceous productivity during glacials may well be increased at Site 594, as the nature of the terrigenous sediments being deposited, in conjunction with the northwards migration of siliceous organisms with the colder southern waters, would both make this likely.

Low $CaCO_3$ values in 594 stage 3 (Figure 5.3e) (compared to stages 1 and 5), synchronous with the lack of extreme interglacial benthic and planktonic $\delta^{18}O$ values, supports the classification by M^{c}Glone (1985) of stage 3 as an interstadial (see Figure 2.15), rather than a

full interglacial. Stage 3 is similarly not represented by high carbonate percentages in Q200 (Figure 5.4e), Q217 (Figure 5.5e) and Q585 (Figure 5.8e) (the only other cores for which stage 3 is identifiable), further supporting an interstadial nomenclature.

Conclusions

SUMMARY AND SYNTHESIS

Summary

This thesis has concentrated on the palaeoceanographic implications of glacial-interglacial oscillations in the $^{18}O/^{16}O$ and $^{13}C/^{12}C$ ratios of calcareous foraminifera in (late) Quaternary deep-sea sediment cores from the Tasman Sea and Southwest Pacific Ocean. The sites cover a latitudinal range from the equator to 49°S. Particular attention has been paid to the isotopic records of DSDP Sites 593 and 594, to obtain reference curves for the Tasman Sea to the west of New Zealand (593), and the Southwest Pacific Ocean to the east of New Zealand (594).

The Site 593 record in the southern Tasman Sea extends to 44m sub-bottom depth, and reveals isotopic events back to the 55/56 stage boundary. The two modes of Quaternary isotopic variation (Prell, 1982) are evident, with low glacial to interglacial variability (of ~0.7°/$_{oo}$) from 1.9-0.9my, and greatly increased variability (of ~2.8°/$_{oo}$) from the 23/24 stage boundary (end of the Jarimillo Subchron) due to a change in global ice budget. Of the other sites to the west of New Zealand, only Sites 589 and 592 were analysed beyond the beginning of the Jarimillo Subchron, of which Site 592 also displayed the expected two modes of variation.

Attention to the east of New Zealand was focused on the fine detail obtainable from Site 594, already known to have a high sedimentation rate and an exceptionally well preserved isotopic record (Cuthbertson, 1985). One of the most highly detailed isotopic records available for stages 1 to 6 has been produced and interpreted in this study. The near synchroneity of the $CaCO_3$ content and the $\delta^{18}O$ record has been previously noted (Cuthbertson, 1985; Nelson et al.,

1986), but uncertainty over the depth of the 2/3 stage boundary, whose position in the $CaCO_3$ curve is not matched in the isotope record, indicates a need for caution in using the $CaCO_3$ record to locate stage boundaries.

Other sites to the east of New Zealand, and most notably those in the vicinity of Site 594, do not possess similarly high sedimentation rates, and their records have not been as useful as those of Site 594. Differences in the accumulation rates may reflect variations in the depositional environment, and changes in the transport regime of currents in the Bounty Trough region.

The benthic $\delta^{13}C$ records of all the cores oscillated in concert with the $\delta^{18}O$ glacial-interglacial cycles, with low $\delta^{13}C$ values during glacial periods, as is the case universally. In addition, some of the planktonic $\delta^{13}C$ records show glacial to interglacial fluctuations, not commonly the case elsewhere, and may reflect consistent variations in carbonate productivity linked to cyclical glacial-interglacial conditions.

The influence of latitudinal position on isotopic lead/lag relationships over Termination I_A has been studied, and results suggest that glacial meltwaters in high-latitude sites are recorded first in the planktonic $\delta^{18}O$ record, while at low-latitude sites the meltwaters are recorded first in the benthic $\delta^{18}O$ values. A modification of the meltwater "lid" theory is proposed, with the lid extending only as far as the lower latitude waters, and not worldwide. The precise extension of the lid cannot be better defined at present as the higher latitude cores of this study (586 and 587) did not contain sufficient benthic foraminifera for analysis, and so the north to south transect is incomplete.

Late Quaternary Palaeoceanography of the Tasman Sea and Southwest Pacific Ocean: A Synthesis (Figure 6.1)

Glacial Surface Waters

Planktonic $\delta^{18}O$ results suggest that warmer subtropical surface waters (rather than cooler subantarctic surface waters) were dominant in the Tasman Sea, even during glacial periods, with similar surface circulation patterns to the present day, as even the southernmost of the sites (593) does not record the extremely heavy glacial planktonic $\delta^{18}O$ values (of ~3.5°/$_{oo}$) observed to the east of New Zealand.

In the Southwest Pacific a more northerly position of the Subtropical Convergence is suggested during glacials by the considerably heavier $\delta^{18}O$ values. Moreover, radiolarian microfossil-dominated assemblages, characteristic of the Antarctic water mass, are found only in glacial samples from Site 594 (Cooke, 1988). The extent of this shift in the Tasman Sea cannot be as far north as Site 593, as it does not have extremely heavy values comparable to those of sites off the east coast. In the Southwest Pacific a lack of cores to the north of the Chatham Rise makes determination of possible palaeopositions of the convergence difficult.

Glacial Deep Waters

Lighter benthic $\delta^{13}C$ results (by ~1°/$_{oo}$) during cool periods support decreased NADW production during glacial periods, with vertical migration of the NADW/AABW boundary. Renewed production of NADW on warming results in a sudden and transient decrease in the $\delta^{13}C$ values as the relatively stagnant, isotopically lighter waters, are "flushed" out of deep water flow paths, before the $\delta^{13}C$ values to heavier interglacial levels.

Cooling of the Deep Waters (~1200-1500m) in the Tasman Sea during the last glacial appears to have been less extreme than the cooling apparent at sites at comparable depths in the Southwest Pacific Ocean. To the east of New Zealand the temperature drop (of ~1.7°C) is comparable to that seen in other Southern Ocean sites. To the west, however, some isolation of the Tasman Sea from the northerly flow which takes Deep Water from the Circumpolar Current must have occurred, allowing a cell of higher temperature water (warmer by ~1°C) to develop in the Tasman Sea.

Interglacial Surface Waters

Planktonic $\delta^{18}O$ results from the Tasman Sea suggest a more southerly position of the eastward movement of the East Australian Current during the last interglacial (stage 5), as the $\delta^{18}O$ records of Sites 592 and 593 both indicate cooler Holocene temperatures than those prevalent during stage 5e. A more southerly position of the Subtropical Divergence (Tasman Front) during stage 5e is thus proposed.

Interglacial Deep Waters

Significant departures from modern benthic $\delta^{13}C$ values occur in the Tasman Sea, and at Site 594 in the Southwest Pacific, with TCO_2 ($\simeq \delta^{13}C$) generally lower by ~0.5°/$_{oo}$ in the last interglacial ocean compared to the present day.

Consistently lighter benthic $\delta^{13}C$ values to the east of New Zealand (during both glacial and interglacial periods) compared to the west point to a dominance of the isotopically lighter AABW in the Southwest Pacific Ocean, and of NADW in the Tasman Sea.

Heavier planktonic $\delta^{13}C$ values to the east (compared to the west) suggest greater upwelling and higher productivity in the Southwest Pacific compared to the Tasman Sea during glacials and interglacials.

Determination of the periods of enhanced $CaCO_3$ productivity in the Southwest Pacific are largely dependent on the observation by Cooke (1988) that there is little micropalaeontological evidence from calcareous foraminifera to suggest increased dissolution of $CaCO_3$ during glacial periods, as might otherwise have been predicted, as an increase in the strength of the more carbonate-aggressive AABW flow is suggested over glacial times. If this was the case, then $CaCO_3$ productivity must have been highest during the times of maximum accumulation of $CaCO_3$ (i.e., during interglacial periods). This is supported by heavier planktonic $\delta^{13}C$ values during interglacials ($\sim 0.5^{o}/_{oo}$) compared to glacials values (of -1.0 to $0.0^{o}/_{oo}$).

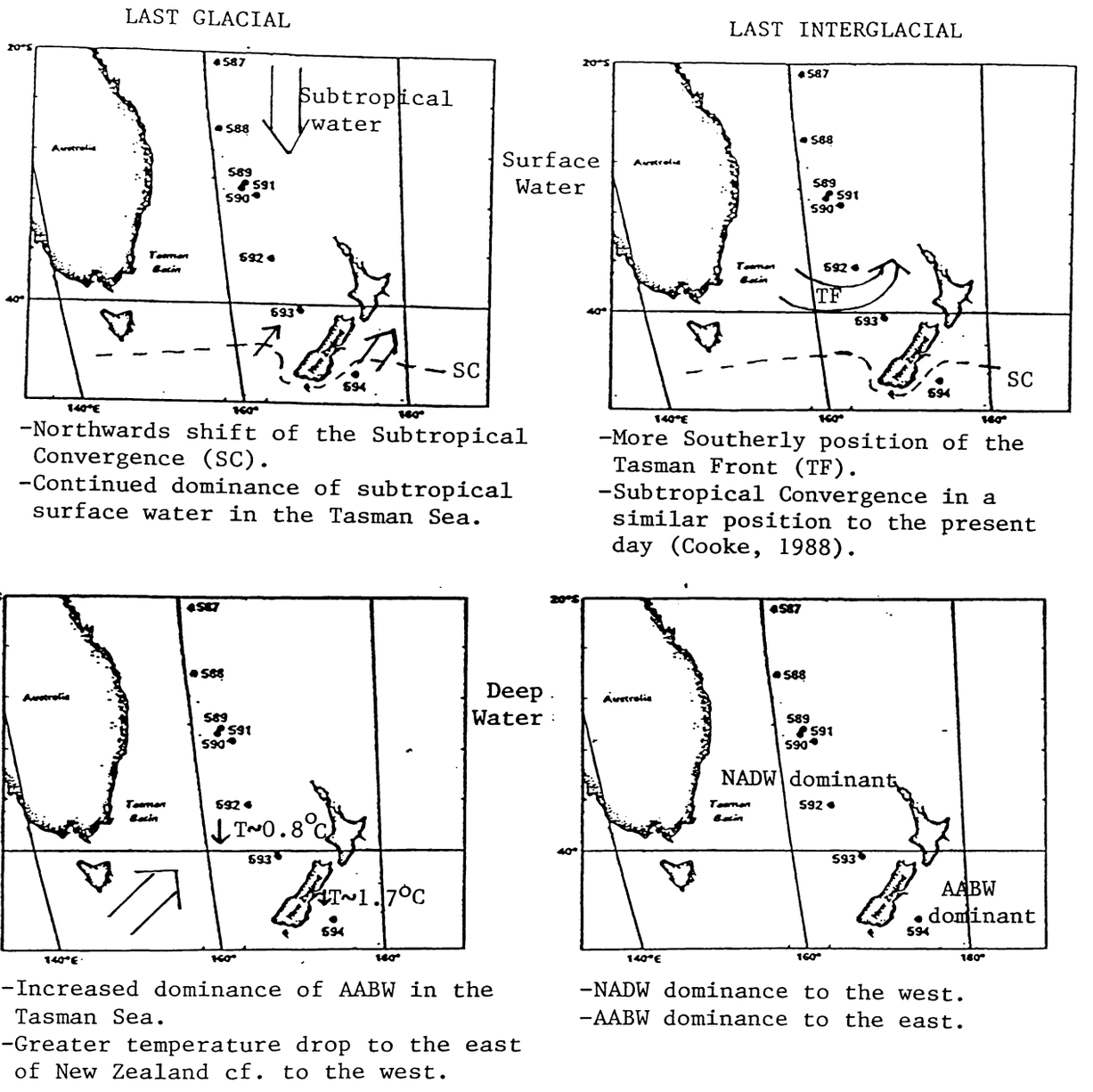

-Northwards shift of the Subtropical Convergence (SC).
-Continued dominance of subtropical surface water in the Tasman Sea.

-More Southerly position of the Tasman Front (TF).
-Subtropical Convergence in a similar position to the present day (Cooke, 1988).

-Increased dominance of AABW in the Tasman Sea.
-Greater temperature drop to the east of New Zealand cf. to the west.

-NADW dominance to the west.
-AABW dominance to the east.

Figure 6.1.Diagrammatic summary of aspects of the palaeoceanography of the latest Quaternary in the New Zealand region, compared to present day conditions.

Appendix One

HOLE 586

Date occupied: 19 November 1982

Date departed: 19 November 1982

Time on hole: 15 hr., 52 min.

Position: 00°29.84′S; 158°29.89′E

Water depth (sea level; corrected m, echo-sounding): 2208

Water depth (rig floor; corrected m, echo-sounding): 2218

Bottom felt (m, drill pipe): 2223.1. Note: water depth of 2218 m from rig floor from 586C logs used as site datum.

Penetration (m): 39.3

Number of cores: 5

Total length of cored section (m): 39.3

Total core recovered (m): 38.98

Core recovery (%): 99.2

Oldest sediment cored:
Depth sub-bottom (m): 39.3
Nature: Foraminifer-bearing nannofossil ooze
Age: Latest Pliocene
Measured velocity (km/s): Not measured

Basement: Not encountered

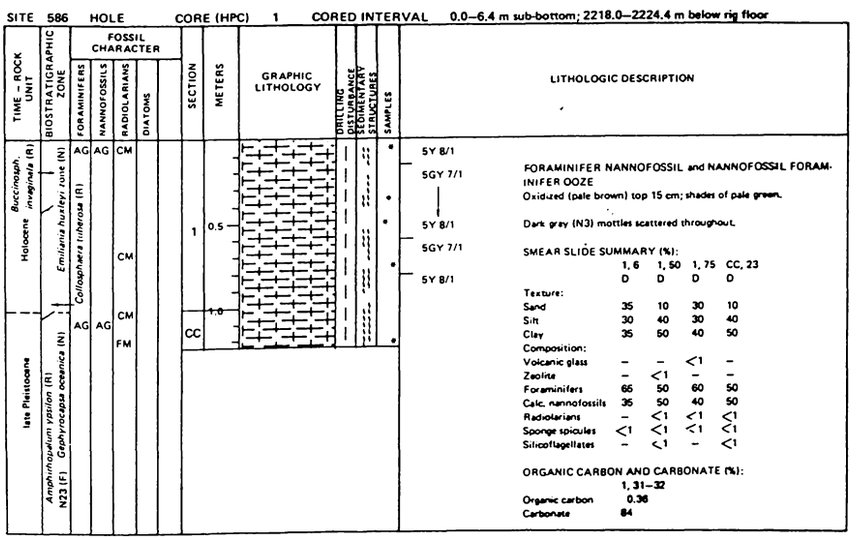

HOLE 587

Date occupied: 3 December 1982
Date departed: 5 December 1982
Time on hole: 40 hr.
Position: 21°11.087′S; 161°19.99′E
Water depth (sea level; corrected m, echo-sounding): 1101
Water depth (rig floor; corrected m, echo-sounding): 1111
Bottom felt (m, drill pipe): 1115
Penetration (m): 147
Numbers of cores: 17
Total length of cored section (m): 147 (89.5 in Pliocene)
Total core recovered (m): 88.81 (80.95 in Pliocene)
Core recovery (%): 60.4 (90% in Pliocene)
Oldest sediment cored:
Depth sub-bottom (m): 147
Nature: Calcareous sandstone
Age: Probably late Miocene
Basement: Not reached

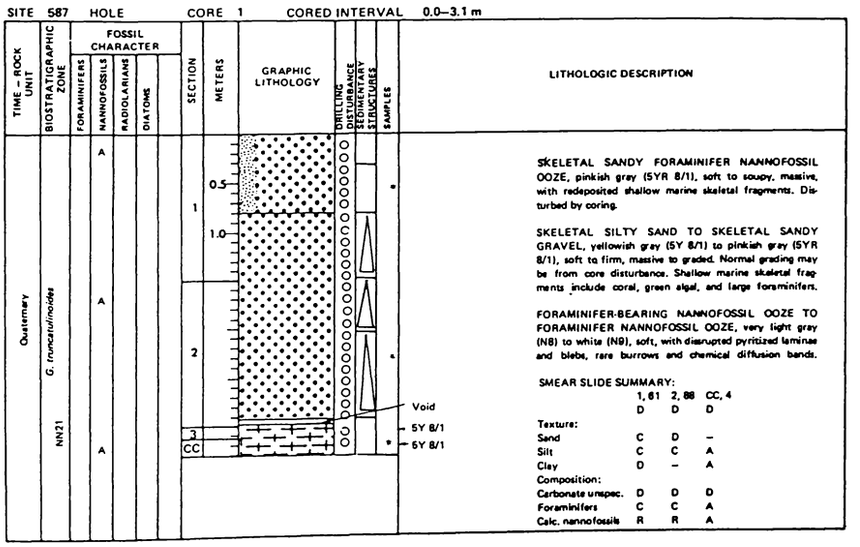

HOLE 588

Date occupied: 6 December 1982

Date departed: 8 December 1982

Time on hole: 30 hr.

Position: 26°06.7′S; 161°13.6′E

Water depth (sea level; corrected m, echo-sounding): 1533

Water depth (rig floor; corrected m, echo-sounding): 1543

Bottom felt (m, drill pipe): 1548

Penetration (m): 236.00

Number of cores: 26

Total length of cored section (m): 236.00

Total core recovered (m): 220.76

Core recovery (%): 93.5

Oldest sediment cored:
Depth sub-bottom (m): 236.00
Nature: Foraminifer–nannofossil ooze
Age: middle Miocene
Measured velocity (km/s): 1.617 km/s at 233 m

Basement: Not reached

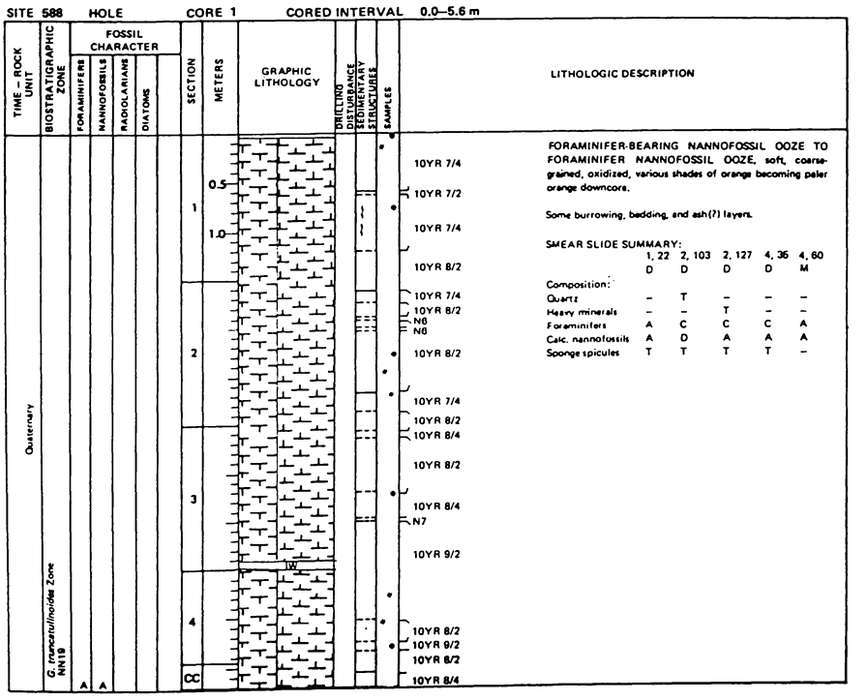

HOLE 589

Date Occupied: 12 December 1982
Date departed: 13 December 1982
Time on hole: 15.5 hr.
Position: 30°42.72′S; 163°38.39′E
Water depth (sea level; corrected m, echo-sounding): 1391
Water depth (rig floor; corrected m, echo sounding): 1401
Bottom felt (m, drill pipe): 1398.3
Penetration (m): 36.1
Number of cores: 4
Total length of cored section (m): 36.1
Total core recovered (m): 35.08
Core recovery (%): 97.2
Oldest sediment cored:
Depth sub-bottom (m): 36.1
Nature: Foraminifer–nannofossil ooze
Age: Quaternary
Basement: Not reached

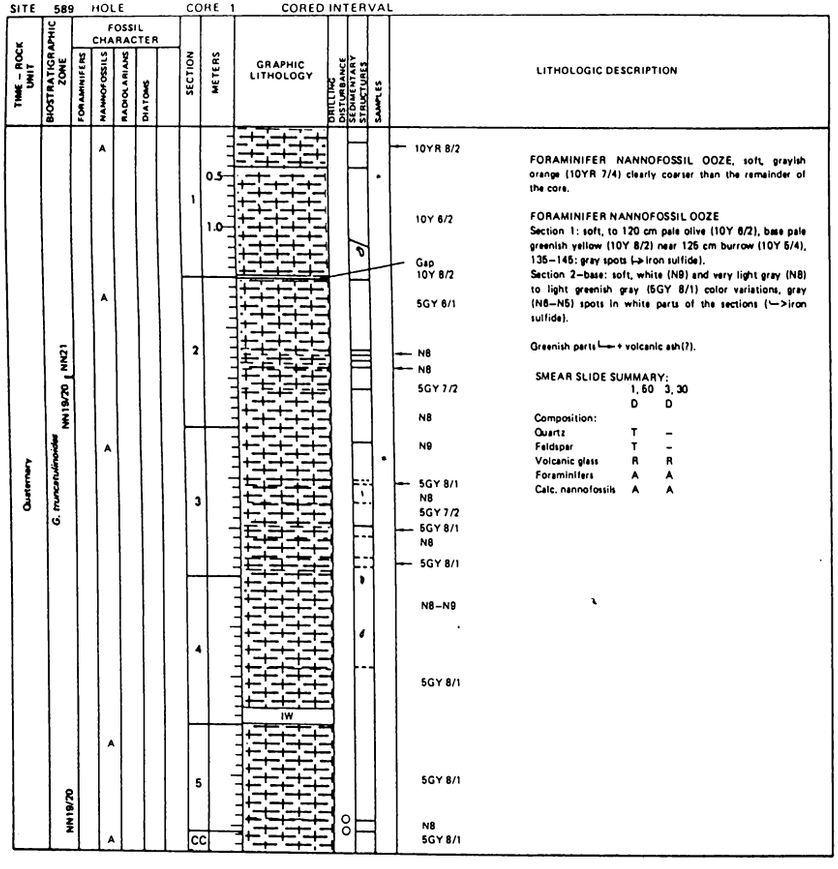
SITE 589 HOLE CORE 1 CORED INTERVAL
TIME – ROCK UNIT
BIOSTRATIGRAPHIC ZONE
FOSSIL CHARACTER
FORAMINIFERS
NANNOFOSSILS
RADIOLARIANS
DIATOMS
SECTION
METERS
GRAPHIC LITHOLOGY
DRILLING DISTURBANCE
SEDIMENTARY STRUCTURES
SAMPLES
LITHOLOGIC DESCRIPTION
Quaternary
G. truncatulinoides
NN19/20 , NN21
NN19/20
10YR 8/2
10Y 6/2
Gap
10Y 8/2
5GY 8/1
N8
N8
5GY 7/2
N8
N9
5GY 8/1
N8
5GY 7/2
5GY 8/1
N8
5GY 8/1
N8–N9
5GY 8/1
IW
5GY 8/1
N8
5GY 8/1
FORAMINIFER NANNOFOSSIL OOZE, soft, grayish orange (10YR 7/4) clearly coarser than the remainder of the core.
FORAMINIFER NANNOFOSSIL OOZE
Section 1: soft, to 120 cm pale olive (10Y 6/2), base pale greenish yellow (10Y 8/2) near 125 cm burrow (10Y 6/4), 135–145: gray spots (→ iron sulfide).
Section 2–base: soft, white (N9) and very light gray (N8) to light greenish gray (5GY 8/1) color variations, gray (N8–N5) spots in white parts of the sections (←→iron sulfide).
Greenish parts ←→ volcanic ash(?).
SMEAR SLIDE SUMMARY:
1, 60 D
3, 30 D
Composition:
Quartz T –
Feldspar T –
Volcanic glass R R
Foraminifers A A
Calc. nannofossils A A

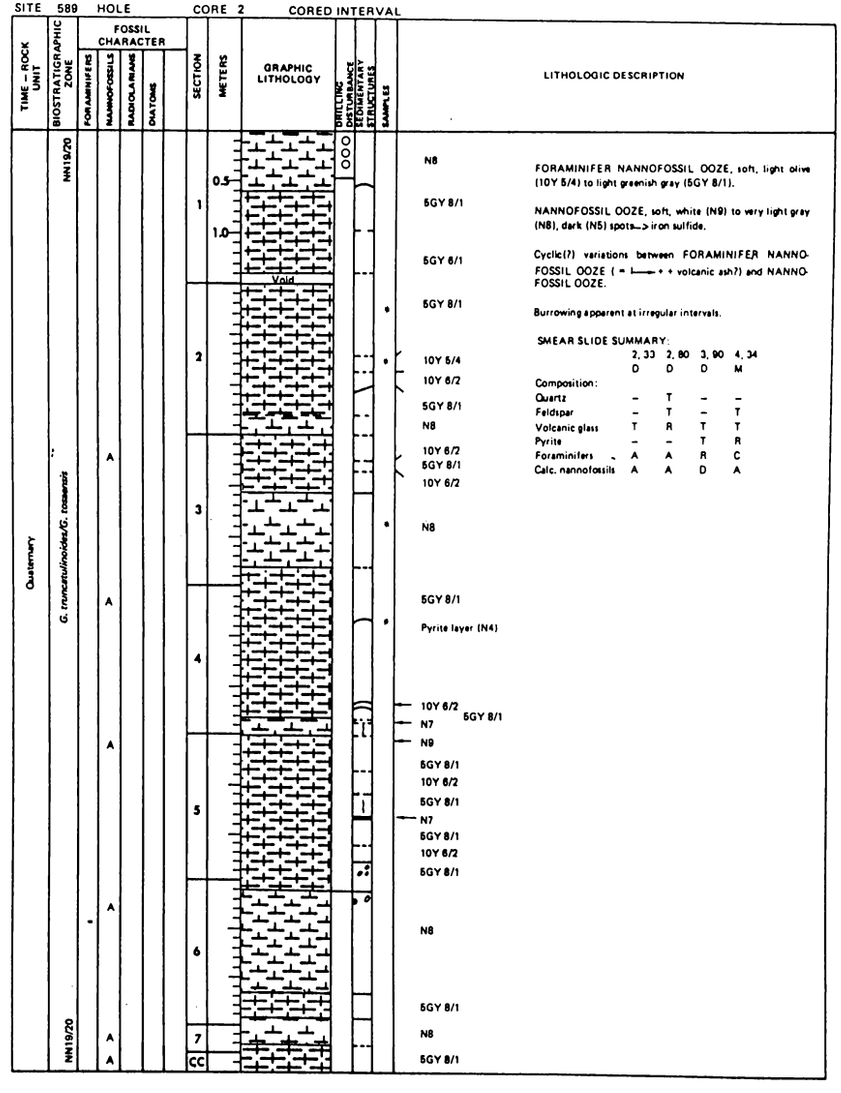
SITE 589 HOLE CORE 2 CORED INTERVAL
TIME – ROCK UNIT
BIOSTRATIGRAPHIC ZONE
FOSSIL CHARACTER
FORAMINIFERS
NANNOFOSSILS
RADIOLARIANS
DIATOMS
SECTION
METERS
GRAPHIC LITHOLOGY
DRILLING DISTURBANCE
SEDIMENTARY STRUCTURES
SAMPLES
LITHOLOGIC DESCRIPTION
Quaternary
G. truncatulinoides/G. tosaensis
NN19/20
Void
N8
5GY 8/1
5GY 8/1
5GY 8/1
10Y 5/4
10Y 6/2
5GY 8/1
N8
10Y 6/2
5GY 8/1
10Y 6/2
N8
5GY 8/1
Pyrite layer (N4)
10Y 6/2
5GY 8/1
N7
N9
5GY 8/1
10Y 6/2
5GY 8/1
N7
5GY 8/1
10Y 6/2
5GY 8/1
N8
5GY 8/1
N8
5GY 8/1
FORAMINIFER NANNOFOSSIL OOZE, soft, light olive (10Y 5/4) to light greenish gray (5GY 8/1).
NANNOFOSSIL OOZE, soft, white (N9) to very light gray (N8), dark (N5) spots → iron sulfide.
Cyclic(?) variations between FORAMINIFER NANNOFOSSIL OOZE (= ←→ + + volcanic ash?) and NANNOFOSSIL OOZE.
Burrowing apparent at irregular intervals.
SMEAR SLIDE SUMMARY:
2, 33 D
2, 80 D
3, 90 D
4, 34 M
Composition:
Quartz – T – –
Feldspar – T – T
Volcanic glass T R T T
Pyrite – – T R
Foraminifers A A R C
Calc. nannofossils A A D A

SITE 589 HOLE CORE 3 CORED INTERVAL

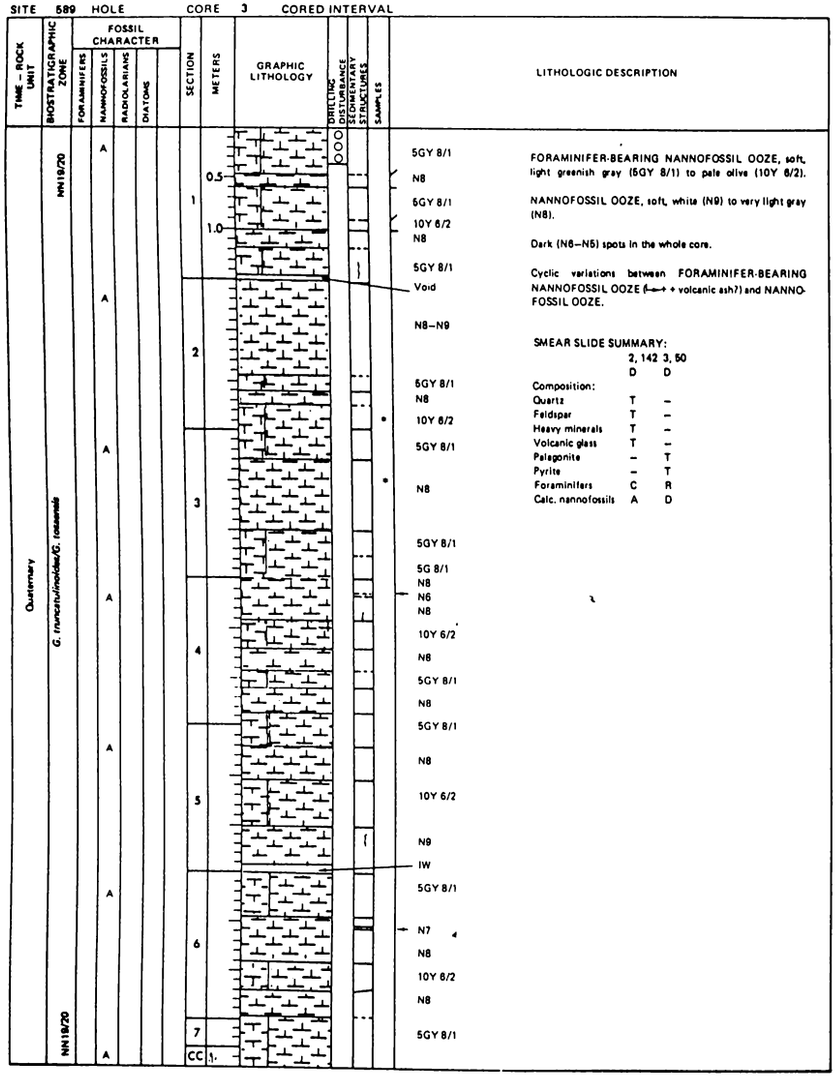

FORAMINIFER-BEARING NANNOFOSSIL OOZE, soft, light greenish gray (5GY 8/1) to pale olive (10Y 6/2).

NANNOFOSSIL OOZE, soft, white (N9) to very light gray (N8).

Dark (N8–N5) spots in the whole core.

Cyclic variations between FORAMINIFER-BEARING NANNOFOSSIL OOZE (⟷ + volcanic ash?) and NANNOFOSSIL OOZE.

SMEAR SLIDE SUMMARY:

	2, 142 D	3, 50 D
Composition:		
Quartz	T	–
Feldspar	T	–
Heavy minerals	T	–
Volcanic glass	T	–
Palagonite	–	T
Pyrite	–	T
Foraminifers	C	R
Calc. nannofossils	A	D

SITE 589 HOLE CORE 4 CORED INTERVAL

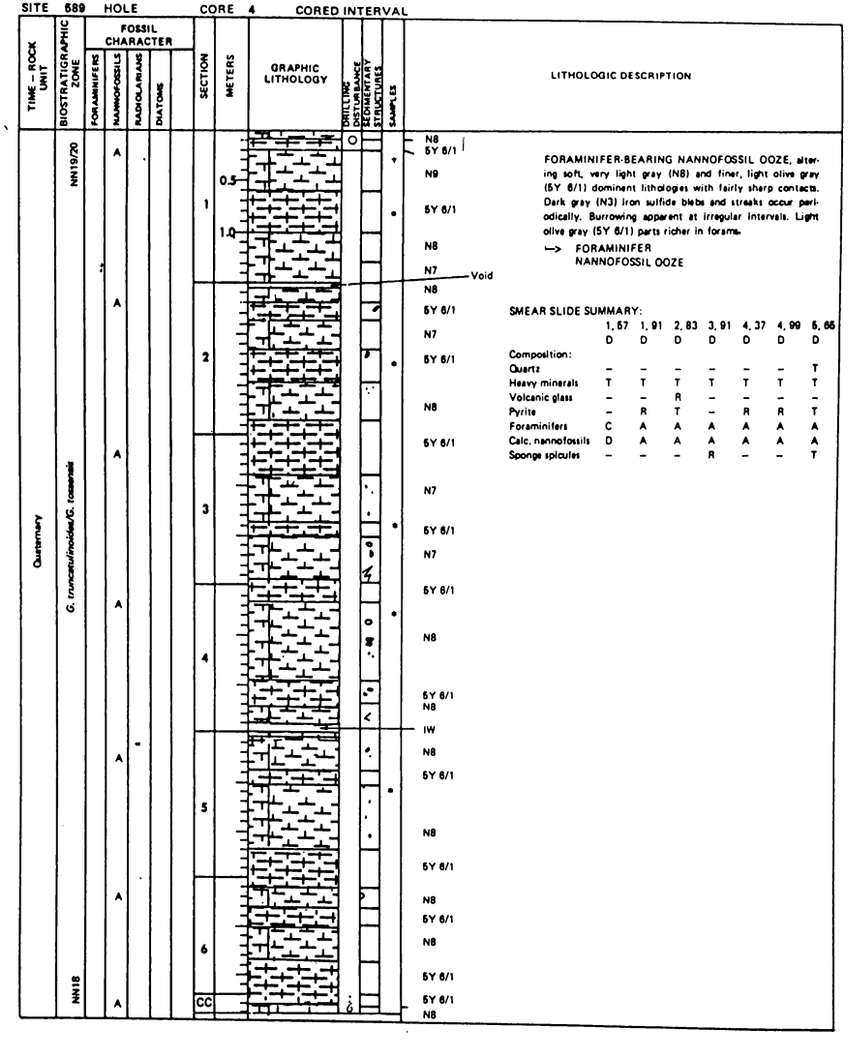

FORAMINIFER-BEARING NANNOFOSSIL OOZE, altering soft, very light gray (N8) and finer, light olive gray (5Y 6/1) dominent lithologies with fairly sharp contacts. Dark gray (N3) iron sulfide blebs and streaks occur periodically. Burrowing apparent at irregular intervals. Light olive gray (5Y 6/1) parts richer in forams.

⟷ FORAMINIFER NANNOFOSSIL OOZE

SMEAR SLIDE SUMMARY:

	1, 67 D	1, 91 D	2, 83 D	3, 91 D	4, 37 D	4, 99 D	5, 65 D
Composition:							
Quartz	–	–	–	–	–	–	T
Heavy minerals	T	T	T	T	T	T	T
Volcanic glass	–	–	R	–	–	–	–
Pyrite	–	R	T	–	R	R	T
Foraminifers	C	A	A	A	A	A	A
Calc. nannofossils	D	A	A	A	A	A	A
Sponge spicules	–	–	–	R	–	–	T

HOLE 590

Date occupied: 15 December 1982

Date departed: 15 December 1982

Time on hole: 13 hr.

Position: 31°10.02′S; 163°21.51′E

Water depth (sea level; corrected m, echo-sounding): 1299

Water depth (rig floor; corrected m, echo-sounding): 1309

Bottom felt (m, drill pipe): 1308

Penetration (m): 26.2

Number of cores: 3

Total length of cored section (m): 26.2

Total core recovered (m): 26.36

Core recovery (%): 100

Oldest sediment cored:
Depth sub-bottom (m): 26.2
Nature: Foraminifer-nannofossil ooze
Age: early Quaternary

Basement: Not reached

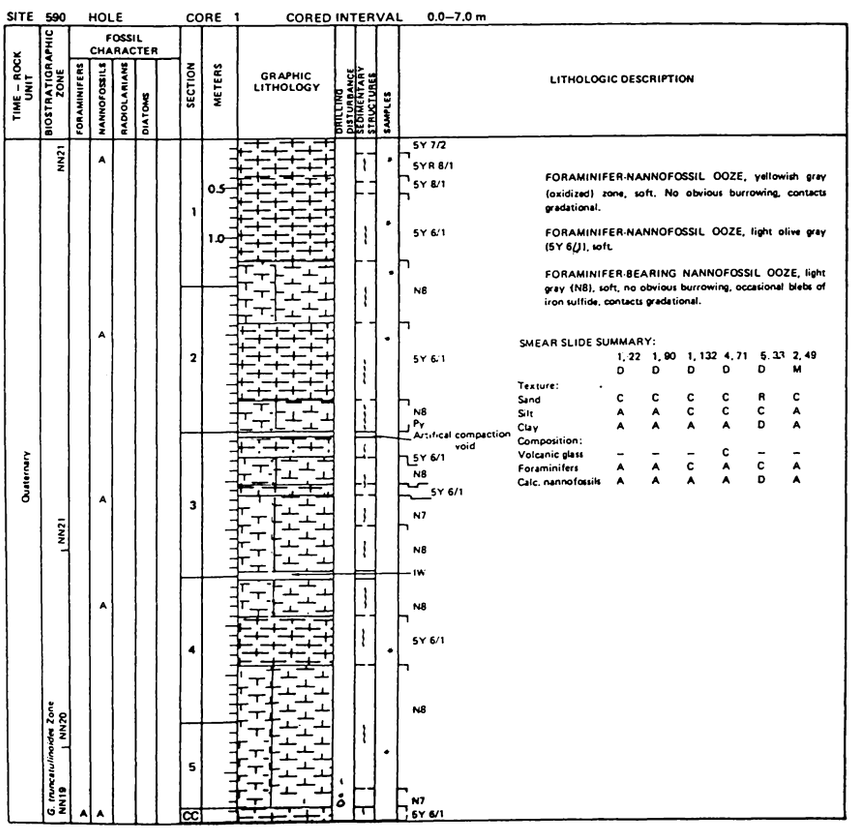

HOLE 591A

Date occupied: 20 December 1982

Date departed: 22 December 1982

Time on hole: 37 hr.

Position: 31°35.06'S; 164°26.92'E

Water depth (sea level; corrected m, echo-sounding): 2131

Water depth (rig floor; corrected m, echo-sounding): 2141

Bottom felt (m, drill pipe): 2142.9

Penetration (m): 284.6

Number of cores: 30

Total length of cored section (m): 284.6

Total core recovered (m): 233.15

Core recovery (%): 81.9

Oldest sediment cored:

Depth sub-bottom (m): 284.6
Nature: Nannofossil ooze
Age: Early late Miocene
Measured velocity (km/s): 1.656 km/s at 249 m
Shear strength: 145 g/cm^2 at 248 m;
greater than 250 g/cm^2 below

Basement: Not reached

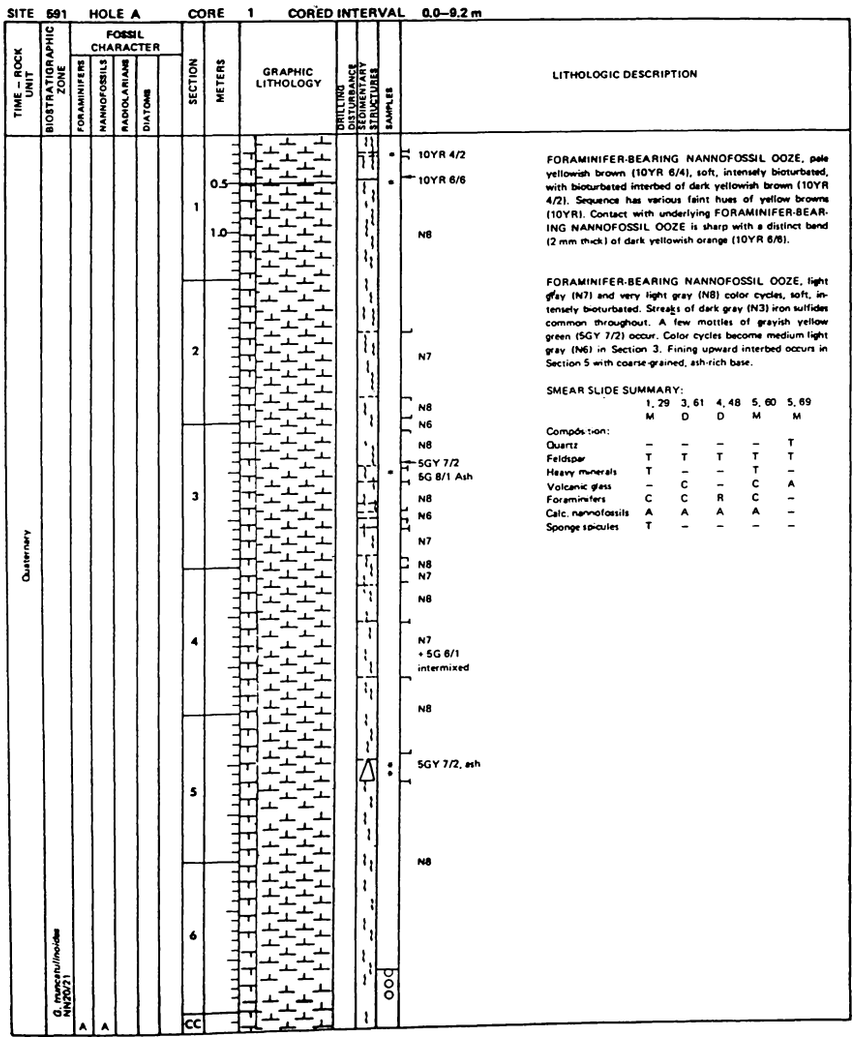

HOLE 592

Date occupied: 25 December 1982

Date departed: 27 December 1982

Time on hole: 46.5 hr.

Position: 36°28.40′S; 165°26.53′E

Water depth (sea level; corrected m, echo-sounding): 1088 m

Water depth (rig floor; corrected m, echo-sounding): 1098 m

Bottom felt (m, drill pipe): 1099

Penetration (m): 388.5

Number of cores: 41

Total length of cored section (m): 388.5

Total core recovered (m): 340.12

Core recovery (%): 87.5

Oldest sediment cored:
Depth sub-bottom (m): 388.5
Nature: Nannofossil chalk
Age: Middle late Eocene (Kaiatan Stage of New Zealand)
Measured velocity (km/s): 1.807 km/s at 383 m
Shear strength: 350 g/cm^2 at 353 m;
greater values below

Basement: Not reached

SITE 592 HOLE CORE 1 CORED INTERVAL 0.0–4.5 m

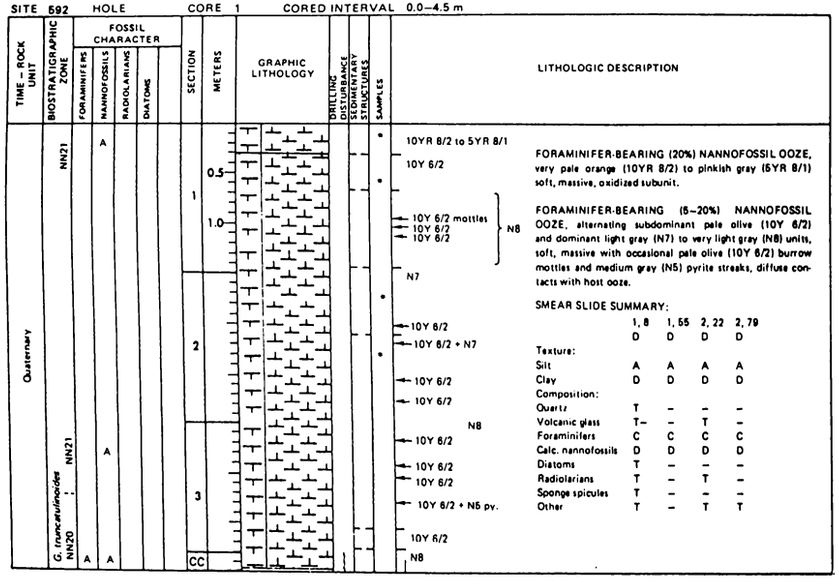

FORAMINIFER-BEARING (20%) NANNOFOSSIL OOZE, very pale orange (10YR 8/2) to pinkish gray (5YR 8/1) soft, massive, oxidized subunit.

FORAMINIFER-BEARING (5–20%) NANNOFOSSIL OOZE, alternating subdominant pale olive (10Y 6/2) and dominant light gray (N7) to very light gray (N8) units, soft, massive with occasional pale olive (10Y 6/2) burrow mottles and medium gray (N5) pyrite streaks, diffuse contacts with host ooze.

SMEAR SLIDE SUMMARY:

	1, 8 D	1, 55 D	2, 22 D	2, 79 D
Texture:				
Silt	A	A	A	A
Clay	D	D	D	D
Composition:				
Quartz	T	–	–	–
Volcanic glass	T–	–	T	–
Foraminifers	C	C	C	C
Calc. nannofossils	D	D	D	D
Diatoms	T	–	–	–
Radiolarians	T	–	T	–
Sponge spicules	T	–	–	–
Other	T	–	T	T

SITE 592 HOLE CORE 2 CORED INTERVAL 4.5–14.1 m

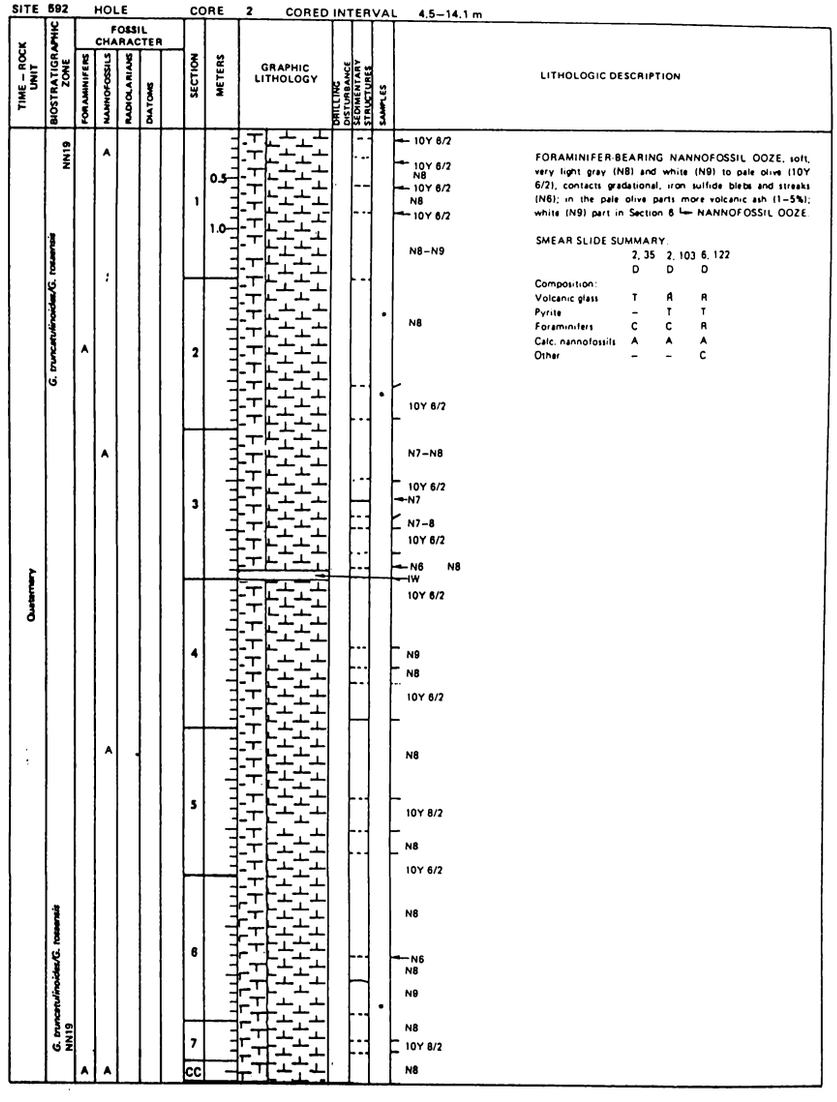

FORAMINIFER-BEARING NANNOFOSSIL OOZE, soft, very light gray (N8) and white (N9) to pale olive (10Y 6/2); contacts gradational, iron sulfide blebs and streaks (N6); in the pale olive parts more volcanic ash (1–5%); white (N9) part in Section 6 ← NANNOFOSSIL OOZE.

SMEAR SLIDE SUMMARY:

	2, 35 D	2, 103 D	6, 122 D
Composition:			
Volcanic glass	T	R	R
Pyrite	–	T	T
Foraminifers	C	C	R
Calc. nannofossils	A	A	A
Other	–	–	C

SITE 592 HOLE CORE 3 CORED INTERVAL 14.1–23.7 m

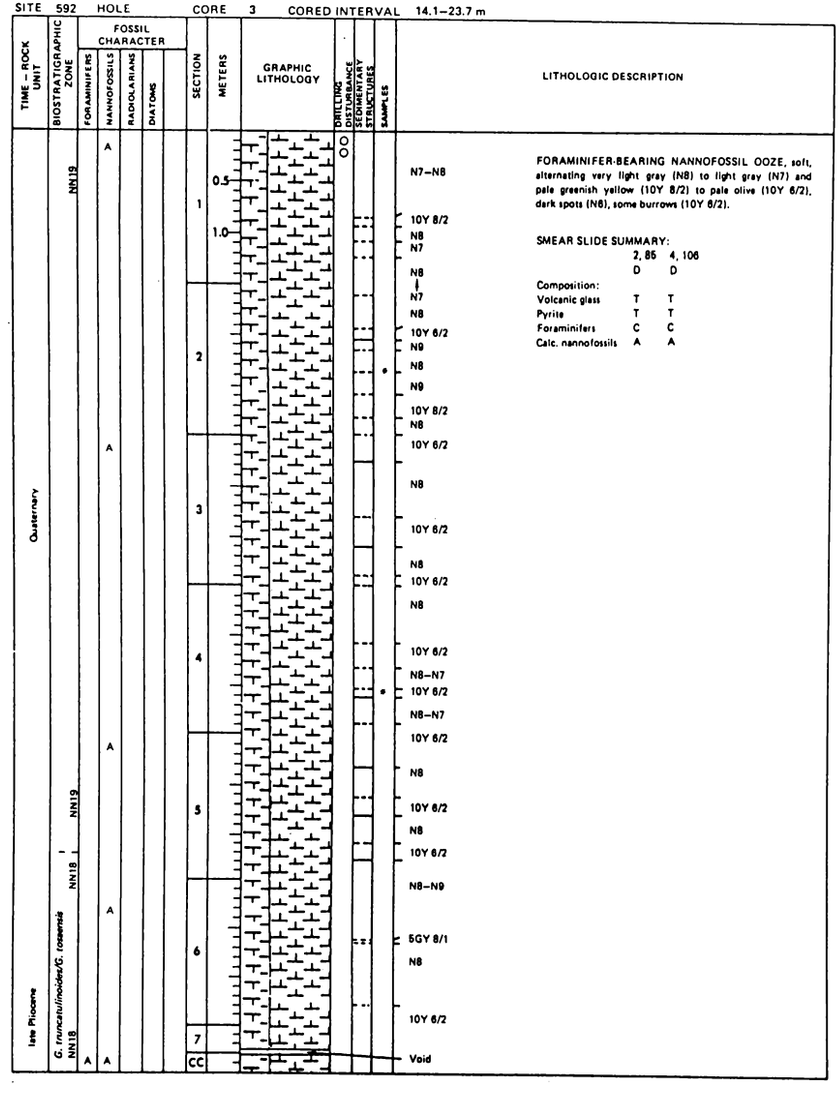

FORAMINIFER-BEARING NANNOFOSSIL OOZE, soft, alternating very light gray (N8) to light gray (N7) and pale greenish yellow (10Y 8/2) to pale olive (10Y 6/2), dark spots (N8), some burrows (10Y 8/2).

SMEAR SLIDE SUMMARY:

	2, 85	4, 106
	D	D
Composition:		
Volcanic glass	T	T
Pyrite	T	T
Foraminifers	C	C
Calc. nannofossils	A	A

HOLE 593

Date occupied: 28 December 1982

Date departed: 30 December 1982

Time on hole: 2 days, 16 hr.

Position: 40°30.47′S; 167°40.47′E

Water depth (sea level; corrected m, echo-sounding): 1068

Water depth (rig floor; corrected m, echo-sounding): 1078

Bottom felt (m, drill pipe): 1079

Penetration (m): 571.5

Number of cores: 60

Total length of cored section (m): 571.5

Total core recovered (m): 468.21

Core recovery (%): 81.9

Oldest sediment cored:
Depth sub-bottom (m): 571.5
Nature: Nannofossil chalk
Age: Late Eocene
Measured velocity (km/s): 2.340 km/s at 554 m

Basement: Not reached

SITE 593 HOLE CORE 1 CORED INTERVAL 0.0–5.1 m

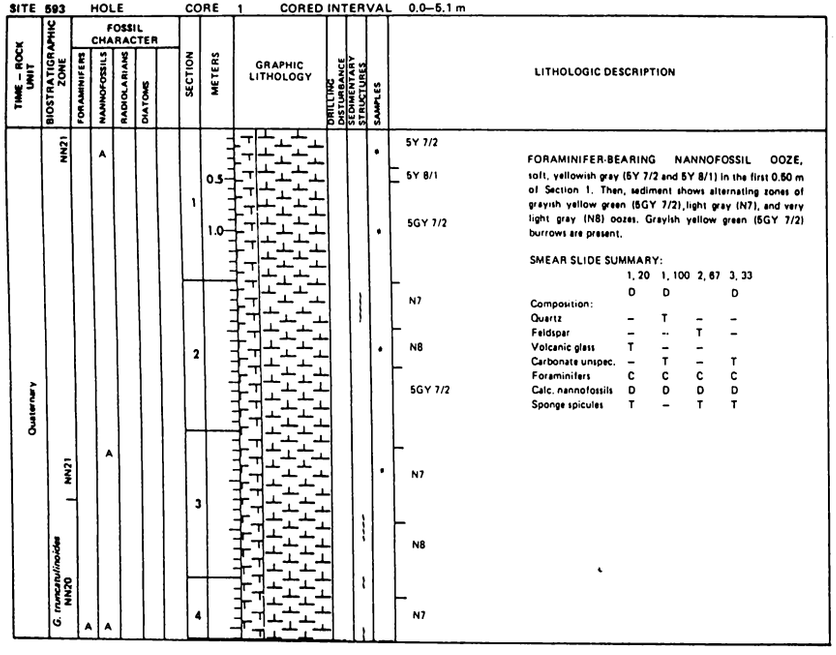

LITHOLOGIC DESCRIPTION

FORAMINIFER-BEARING NANNOFOSSIL OOZE, soft, yellowish gray (5Y 7/2 and 5Y 8/1) in the first 0.60 m of Section 1. Then, sediment shows alternating zones of grayish yellow green (5GY 7/2), light gray (N7), and very light gray (N8) oozes. Grayish yellow green (5GY 7/2) burrows are present.

SMEAR SLIDE SUMMARY:

	1, 20 D	1, 100 D	2, 67	3, 33 D
Composition:				
Quartz	–	T	–	–
Feldspar	–	--	T	–
Volcanic glass	T	–	–	
Carbonate unspec.	–	T	–	T
Foraminifers	C	C	C	C
Calc. nannofossils	D	D	D	D
Sponge spicules	T	–	T	T

SITE 593 HOLE CORE 2 CORED INTERVAL 5.1–14.7 m

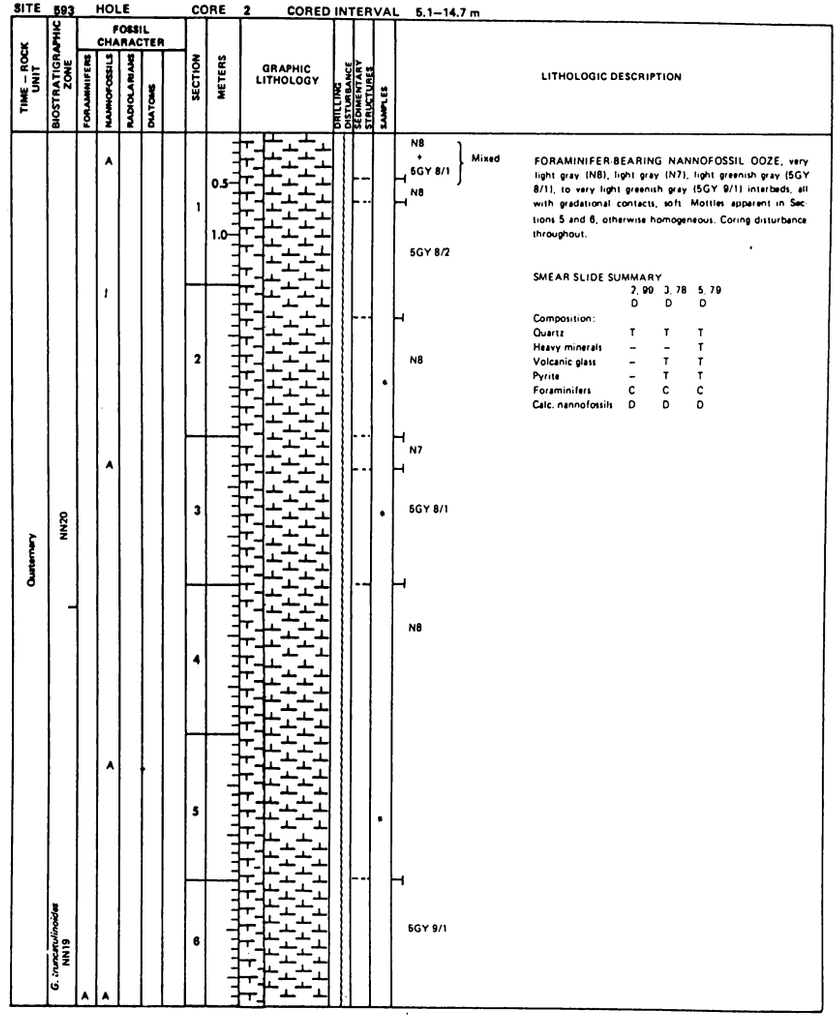

LITHOLOGIC DESCRIPTION

FORAMINIFER-BEARING NANNOFOSSIL OOZE, very light gray (N8), light gray (N7), light greenish gray (5GY 8/1), to very light greenish gray (5GY 9/1) interbeds, all with gradational contacts, soft. Mottles apparent in Sections 5 and 6, otherwise homogeneous. Coring disturbance throughout.

SMEAR SLIDE SUMMARY

	2, 99 D	3, 78 D	5, 79 D
Composition:			
Quartz	T	T	T
Heavy minerals	–	–	T
Volcanic glass	–	T	T
Pyrite	–	T	T
Foraminifers	C	C	C
Calc. nannofossils	D	D	D

SITE 593 HOLE CORE 3 CORED INTERVAL 14.7–24.3 m

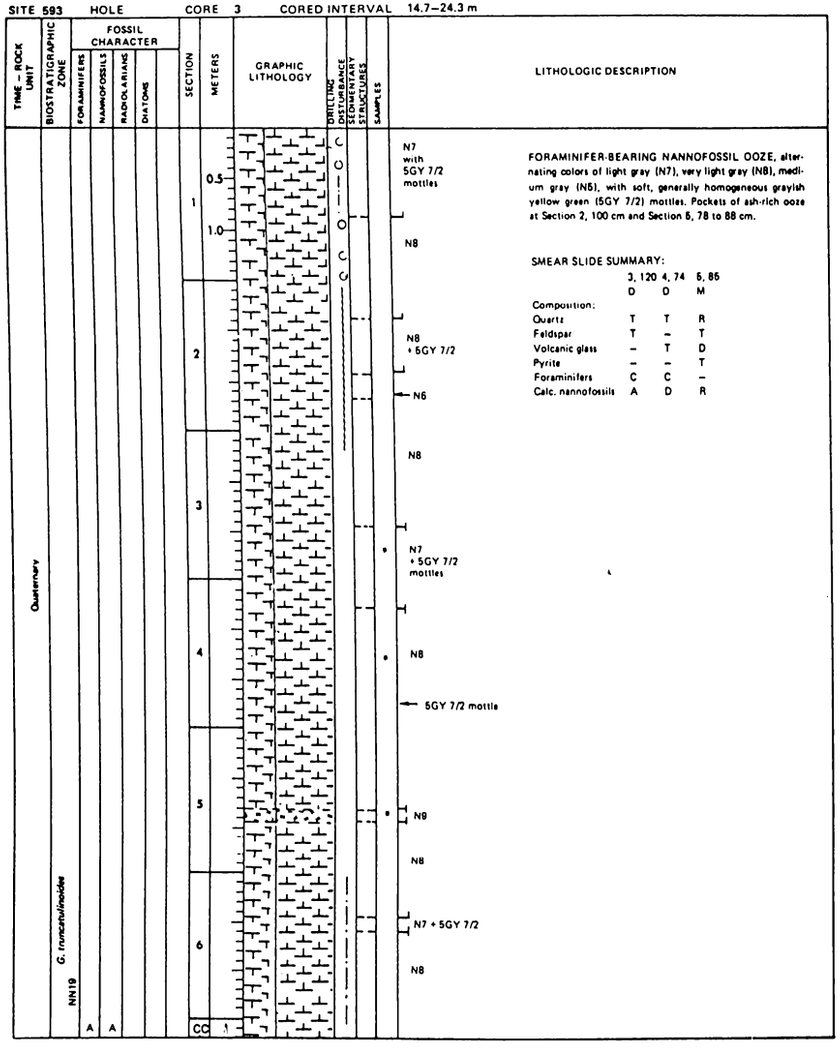

FORAMINIFER-BEARING NANNOFOSSIL OOZE, alternating colors of light gray (N7), very light gray (N8), medium gray (N5), with soft, generally homogeneous grayish yellow green (5GY 7/2) mottles. Pockets of ash-rich ooze at Section 2, 100 cm and Section 5, 78 to 88 cm.

SMEAR SLIDE SUMMARY:

	3, 120 D	4, 74 D	5, 85 M
Composition:			
Quartz	T	T	R
Feldspar	T	–	T
Volcanic glass	–	T	D
Pyrite	–	–	T
Foraminifers	C	C	–
Calc. nannofossils	A	D	R

SITE 593 HOLE CORE 4 CORED INTERVAL 24.3–33.7 m

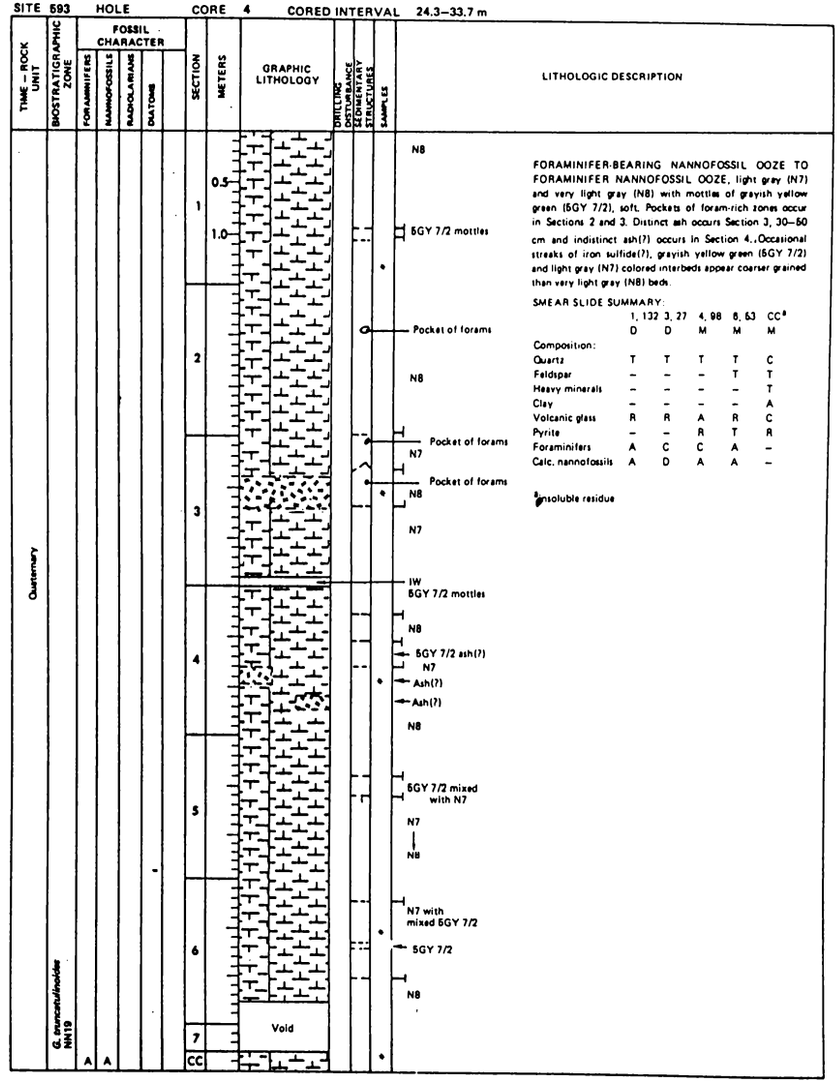

FORAMINIFER-BEARING NANNOFOSSIL OOZE TO FORAMINIFER NANNOFOSSIL OOZE, light gray (N7) and very light gray (N8) with mottles of grayish yellow green (5GY 7/2), soft. Pockets of foram-rich zones occur in Sections 2 and 3. Distinct ash occurs Section 3, 30–60 cm and indistinct ash(?) occurs in Section 4. Occasional streaks of iron sulfide(?), grayish yellow green (5GY 7/2) and light gray (N7) colored interbeds appear coarser grained than very light gray (N8) beds.

SMEAR SLIDE SUMMARY:

	1, 132 D	3, 27 D	4, 98 M	6, 63 M	CC[a] M
Composition:					
Quartz	T	T	T	T	C
Feldspar	–	–	–	T	T
Heavy minerals	–	–	–	–	T
Clay	–	–	–	–	A
Volcanic glass	R	R	A	R	C
Pyrite	–	–	R	T	R
Foraminifers	A	C	C	A	–
Calc. nannofossils	A	D	A	A	–

[a] Insoluble residue

SITE 593 HOLE CORE 5 CORED INTERVAL 33.9–43.5 m

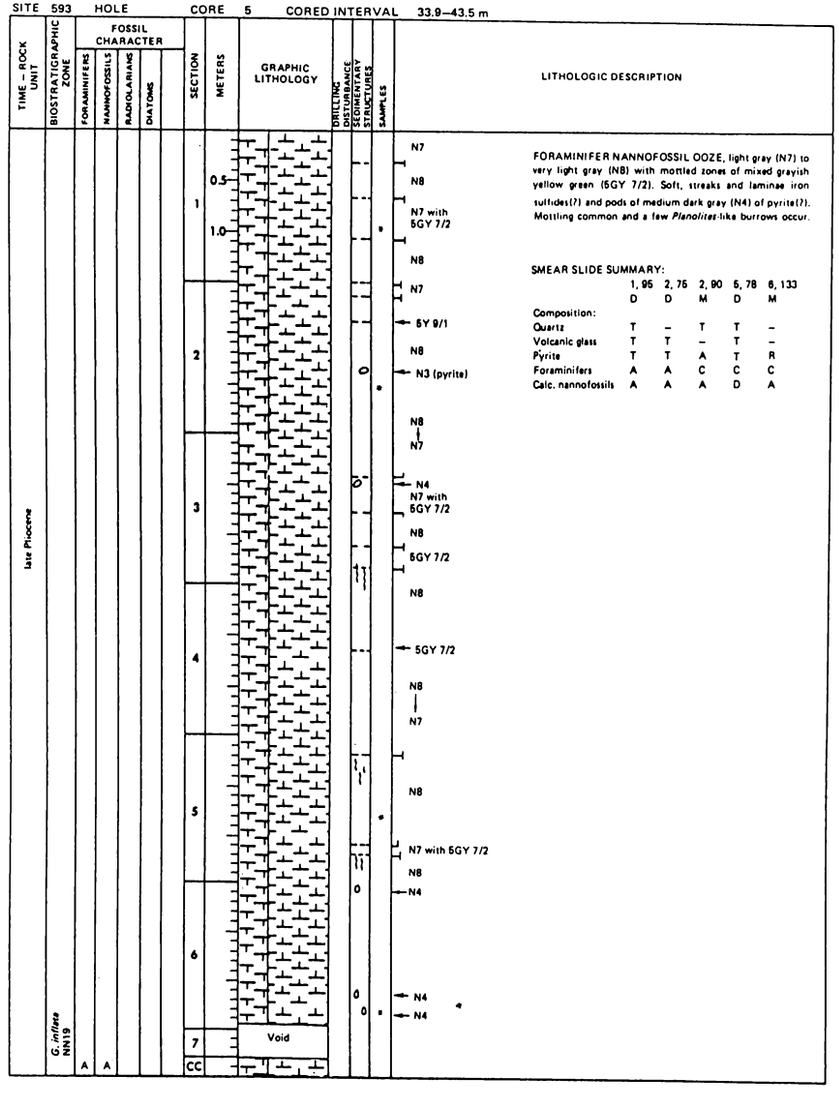

FORAMINIFER NANNOFOSSIL OOZE, light gray (N7) to very light gray (N8) with mottled zones of mixed grayish yellow green (5GY 7/2). Soft, streaks and laminae iron sulfides(?) and pods of medium dark gray (N4) of pyrite(?). Mottling common and a few *Planolites*-like burrows occur.

SMEAR SLIDE SUMMARY:

	1, 95 D	2, 75 D	2, 90 M	5, 78 D	6, 133 M
Composition:					
Quartz	T	–	T	T	–
Volcanic glass	T	T	–	T	–
Pyrite	T	T	A	T	R
Foraminifers	A	A	C	C	C
Calc. nannofossils	A	A	A	D	A

HOLE 594

Date occupied: 3 January 1983

Date departed: 5 January 1983

Time on hole: 52 hr.

Position: 45°31.41'S; 174°56.88'E

Water depth (sea level; corrected m, echo-sounding): 1204

Water depth (rig floor; corrected m, echo-sounding): 1214

Bottom felt (m, drill pipe): 1211

Penetration (m): 505.1

Number of cores: 53

Total length of cored section (m): 505.1

Total core recovered (m): 299.72

Core recovery (%): 59.3

Oldest sediment cored:
Depth sub-bottom (m): 505.1
Nature: Nannofossil ooze
Age: Late early Miocene
Measured velocity (km/s): 1.646 at 487 m

Basement: Not reached

SITE 594 HOLE CORE 1 CORED INTERVAL 0.0–5.9 m

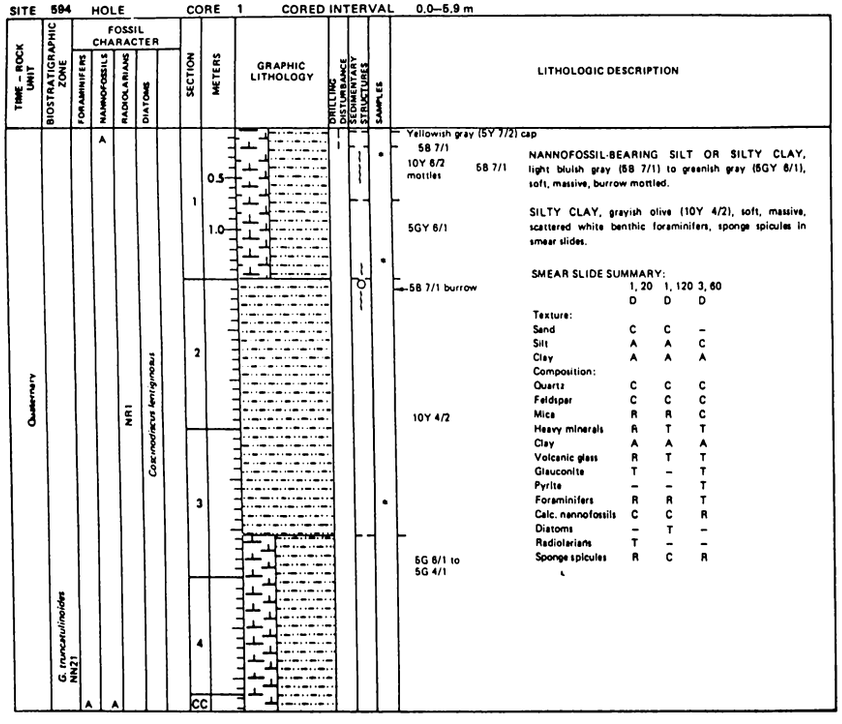

NANNOFOSSIL-BEARING SILT OR SILTY CLAY, light bluish gray (5B 7/1) to greenish gray (5GY 6/1), soft, massive, burrow mottled.

SILTY CLAY, grayish olive (10Y 4/2), soft, massive, scattered white benthic foraminifers, sponge spicules in smear slides.

SMEAR SLIDE SUMMARY:

	1, 20 D	1, 120 D	3, 60 D
Texture:			
Sand	C	C	–
Silt	A	A	C
Clay	A	A	A
Composition:			
Quartz	C	C	C
Feldspar	C	C	C
Mica	R	R	C
Heavy minerals	R	T	T
Clay	A	A	A
Volcanic glass	R	T	T
Glauconite	T	–	T
Pyrite	–	–	T
Foraminifers	R	R	T
Calc. nannofossils	C	C	R
Diatoms	–	T	–
Radiolarians	T	–	–
Sponge spicules	R	C	R

SITE 594 HOLE CORE 2 CORED INTERVAL 5.9–15.5 m

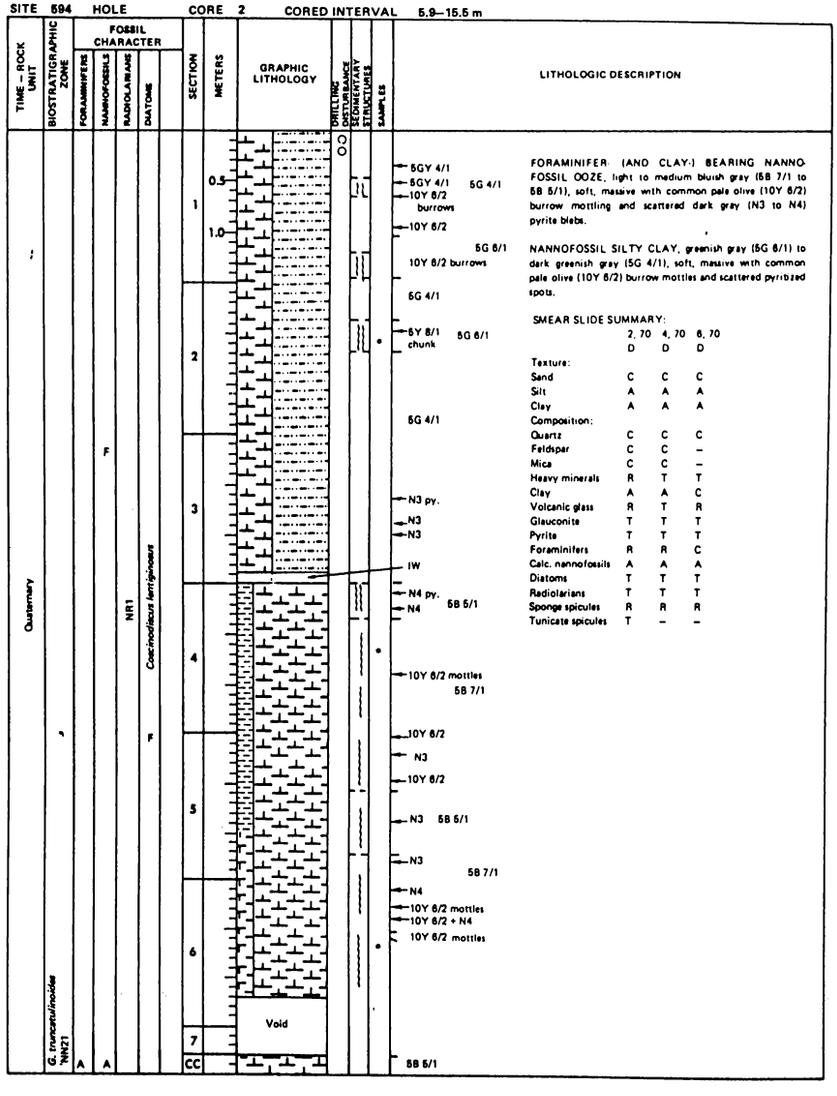

FORAMINIFER- (AND CLAY-) BEARING NANNOFOSSIL OOZE, light to medium bluish gray (5B 7/1 to 5B 5/1), soft, massive with common pale olive (10Y 6/2) burrow mottling and scattered dark gray (N3 to N4) pyrite blebs.

NANNOFOSSIL SILTY CLAY, greenish gray (5G 6/1) to dark greenish gray (5G 4/1), soft, massive with common pale olive (10Y 8/2) burrow mottles and scattered pyritized spots.

SMEAR SLIDE SUMMARY:

	2, 70 D	4, 70 D	6, 70 D
Texture:			
Sand	C	C	C
Silt	A	A	A
Clay	A	A	A
Composition:			
Quartz	C	C	C
Feldspar	C	C	–
Mica	C	C	–
Heavy minerals	R	T	T
Clay	A	A	C
Volcanic glass	R	T	R
Glauconite	T	T	T
Pyrite	T	T	T
Foraminifers	R	R	C
Calc. nannofossils	A	A	A
Diatoms	T	T	T
Radiolarians	T	T	T
Sponge spicules	R	R	R
Tunicate spicules	T	–	–

SITE 594 HOLE CORE 3 CORED INTERVAL 15.5–25.1 m

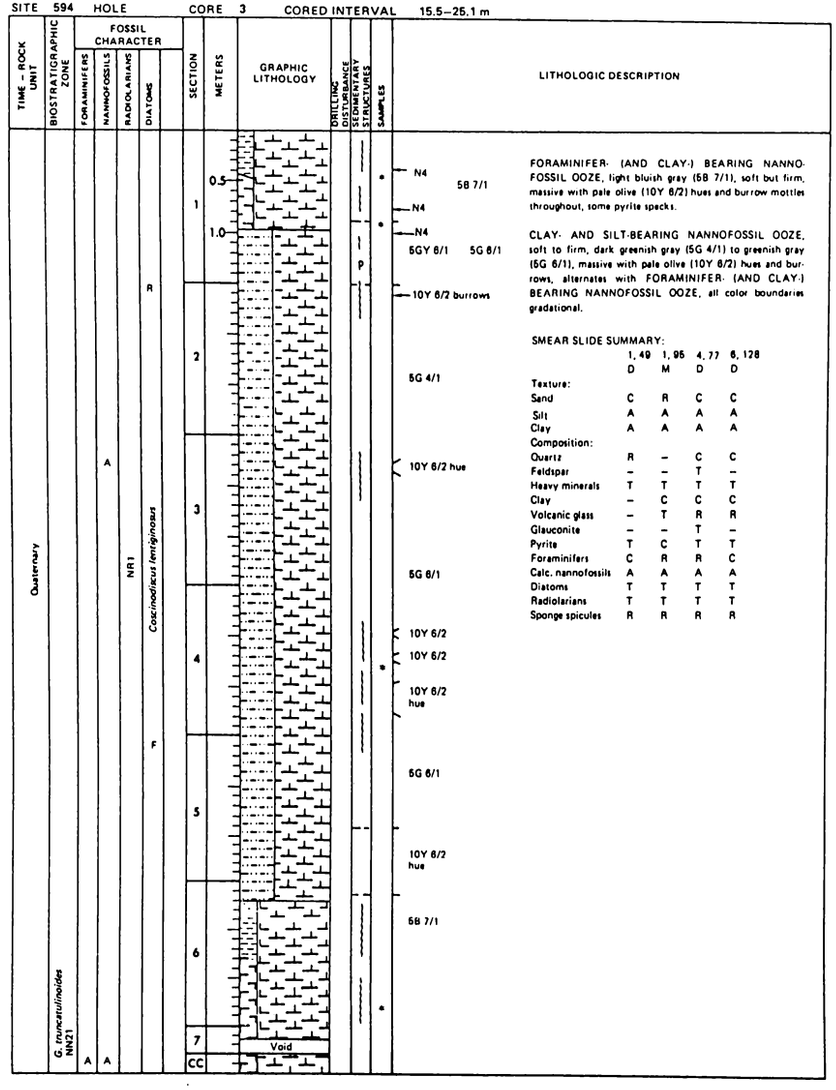

FORAMINIFER- (AND CLAY-) BEARING NANNOFOSSIL OOZE, light bluish gray (5B 7/1), soft but firm, massive with pale olive (10Y 8/2) hues and burrow mottles throughout, some pyrite specks.

CLAY- AND SILT-BEARING NANNOFOSSIL OOZE, soft to firm, dark greenish gray (5G 4/1) to greenish gray (5G 6/1), massive with pale olive (10Y 8/2) hues and burrows, alternates with FORAMINIFER- (AND CLAY-) BEARING NANNOFOSSIL OOZE, all color boundaries gradational.

SMEAR SLIDE SUMMARY:

	1, 49 D	1, 95 M	4, 77 D	6, 128 D
Texture:				
Sand	C	R	C	C
Silt	A	A	A	A
Clay	A	A	A	A
Composition:				
Quartz	R	–	C	C
Feldspar	–	–	T	–
Heavy minerals	T	T	T	T
Clay	–	C	C	C
Volcanic glass	–	T	R	R
Glauconite	–	–	T	–
Pyrite	T	C	T	T
Foraminifers	C	R	R	C
Calc. nannofossils	A	A	A	A
Diatoms	T	T	T	T
Radiolarians	T	T	T	T
Sponge spicules	R	R	R	R

Figure I.1. Photographs of core 594, showing distinct alternating colour sequences (discussed in Nelson et al., 1986).

LEG 90
SITE 594
15.9m - 25.1m
5.9m

LEG 90
SITE 594
5.9m - 15.9m

LEG 90
SITE 594
0 - 5.9m

HOLE 594B

Date occupied: 7 January 1983

Date departed: 7 January 1983

Time on hole: 8 hr., 8 min.

Position: 45°31.41'S; 174°56.88'E

Water depth (sea level; corrected m, echo-sounding): 1204

Water depth (rig floor; corrected m, echo-sounding): 1214

Bottom felt (m, drill pipe): 1212.2

Penetration (m): 42.9

Number of cores: 5

Total length of cored section (m): 42.9

Total core recovered (m): 34.18

Core recovery (%): 79.6

Oldest sediment cored:
Depth sub-bottom (m): 42.9
Nature: Hemipelagic ooze
Age: Quaternary
Measured velocity (km/s): 2.106 at 622 m

Basement: Not reached

Figure I.2. Photographs of Core 594B. Core number 2 was used in this study to fill the gap in 594 over stage 5e.

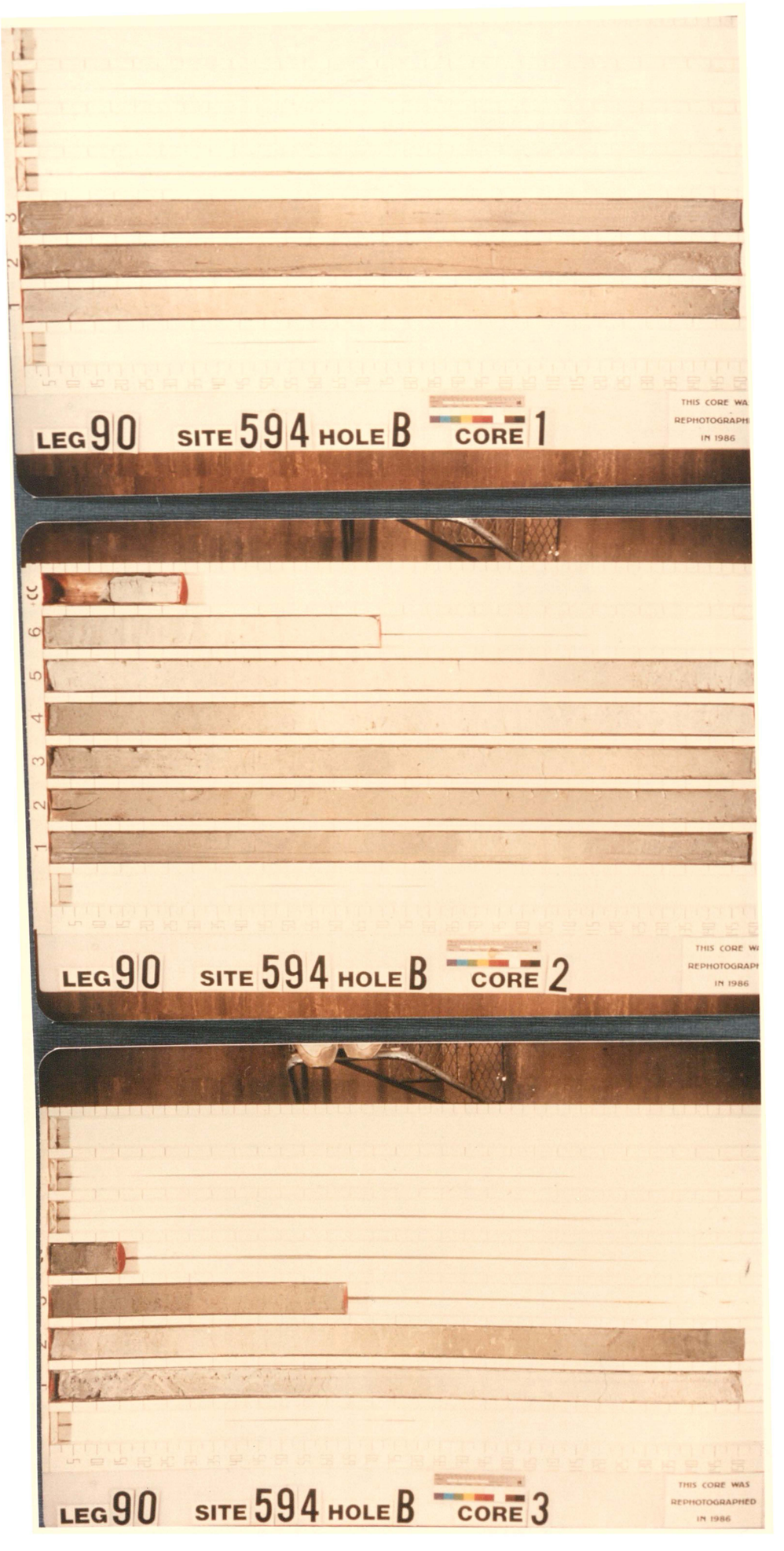
LEG 90 SITE 594 HOLE B CORE 1
THIS CORE WA
REPHOTOGRAPH
IN 1986
LEG 90 SITE 594 HOLE B CORE 2
THIS CORE WA
REPHOTOGRAPH
IN 1986
LEG 90 SITE 594 HOLE B CORE 3
THIS CORE WAS
REPHOTOGRAPHED
IN 1986

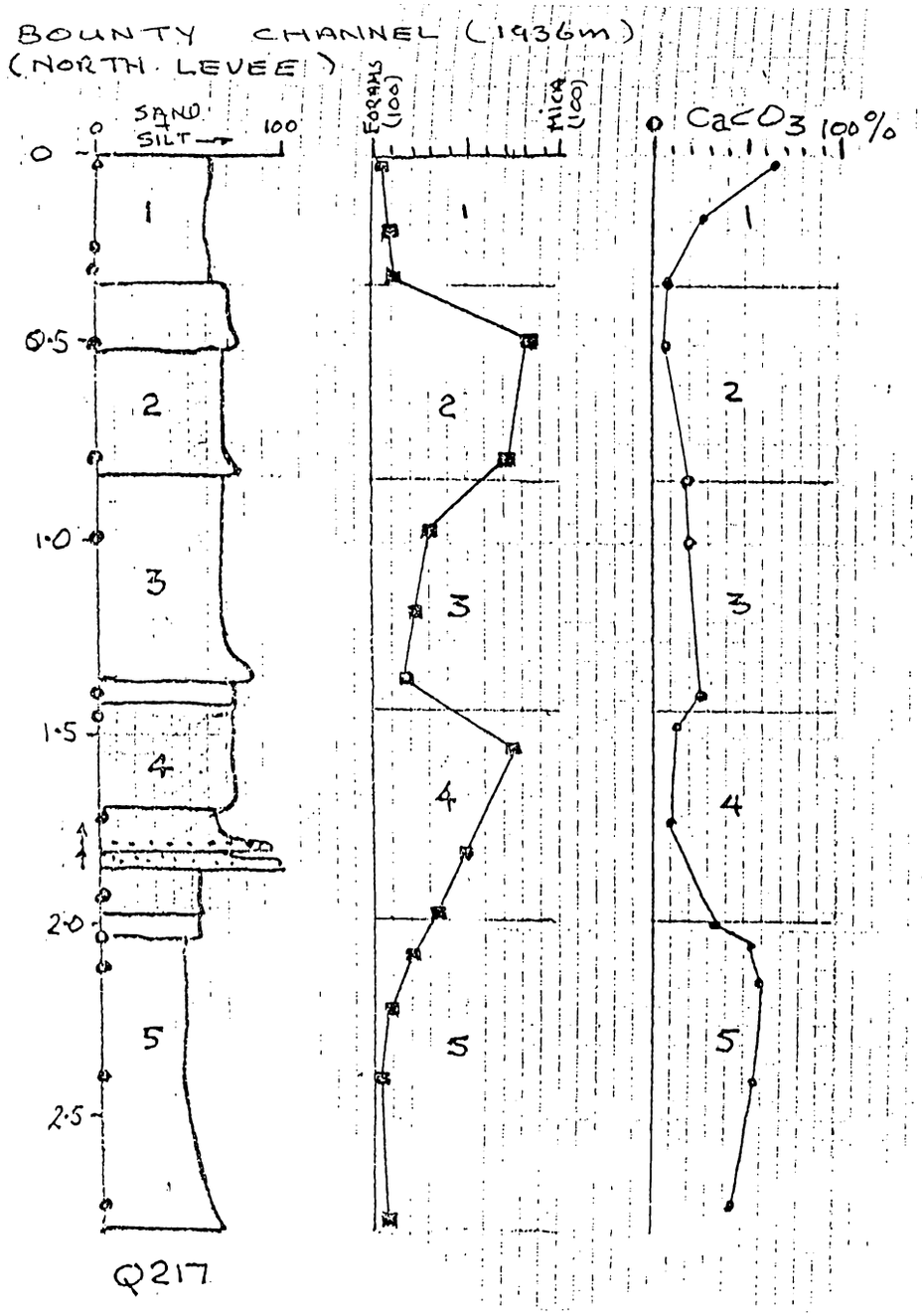
BOUNTY CHANNEL (1936m)
(NORTH LEVEE)
SAND + SILT
0
100
FORAMS (100)
MICA (100)
CaCO3
0
100%
0
0.5
1.0
1.5
2.0
2.5
1
2
3
4
5
Q217

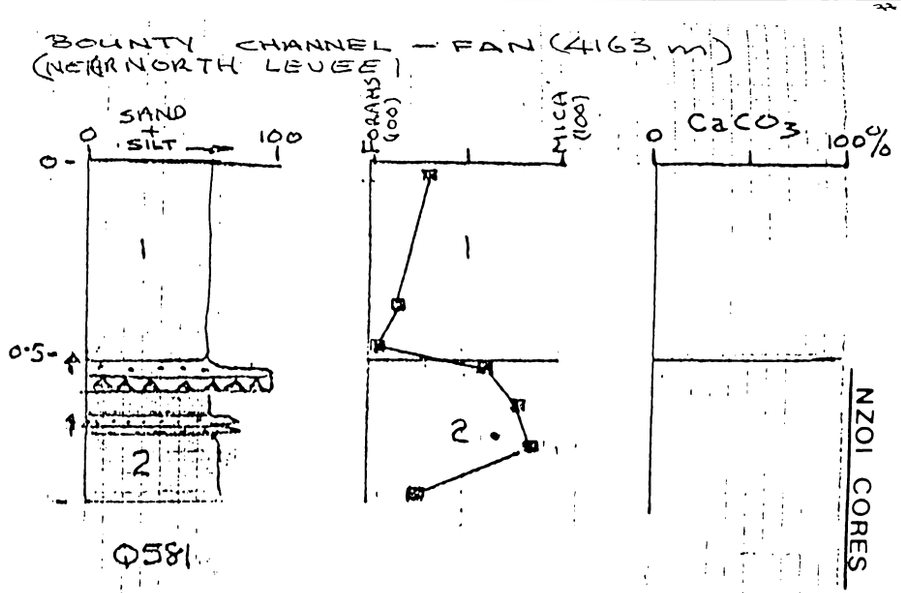
BOUNTY CHANNEL - FAN (4163 m)
(NEAR NORTH LEVEE)
SAND + SILT
0
100
FORAMS (100)
MICA (100)
CaCO3
0
100%
0.5
1
2
Q581
NZOI CORES

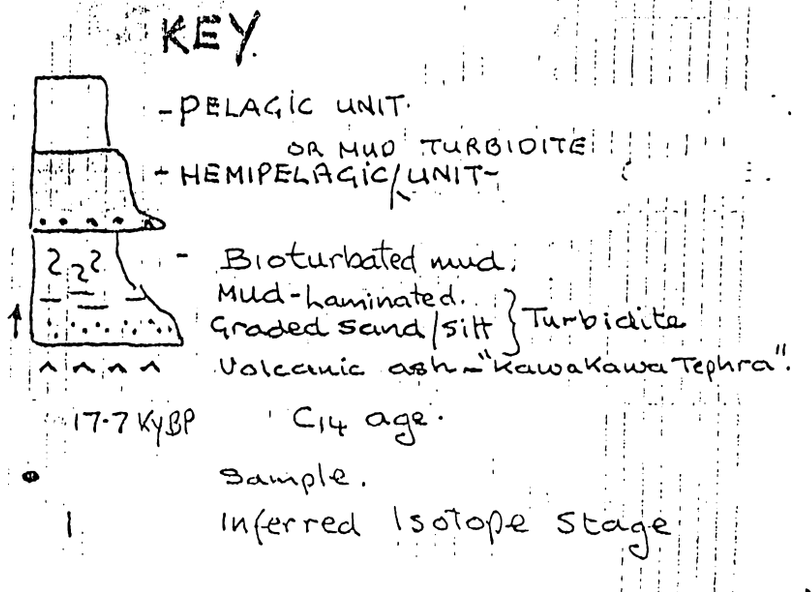
KEY
- PELAGIC UNIT
OR MUD TURBIDITE
- HEMIPELAGIC UNIT
- Bioturbated mud.
Mud-laminated.
Graded sand/silt } Turbidite
Volcanic ash - "Kawakawa Tephra".
17.7 KyBP C14 age.
Sample.
1 Inferred Isotope Stage

Q 580

0-29.5 cms	Light olive grey (5y 6/1) pelagic ooze; crudely & irregularly laminated, bioturbated.
29.5-77.0	Greenish grey (5gy 6/1), broadly and irregularly laminated; bioturbated. Fine sand turbidites at 48, 52. Sediment mainly pelagic ooze.
77-84	Greenish grey (5gy 5/1), hemipelagic ooze. Could be mud turbidite. Bioturbated.
84-117	Greenish grey (5gy 5/1), pelagic at top grading down to slightly hemiterrigenous at base. Fine sand turbidite at 104.
117-381	Medium bluish grey (5B 5/1), monotonous, faintly laminated hemiterrigenous mud; turbidite sand at 180-184.

Samples	NZOI	BIO
	2-4	0-2
	25-27	27-28.5
	29-31	31-33
	51-53	55-57
	53.5-55	73-75
	71.5-73	84.5-86
	86-88	119-121
	117-119	181.5-183
	179-181.5	273.5-276
	271.5-273.5	371-373
	373-375	
	189-190.5	190.5-192

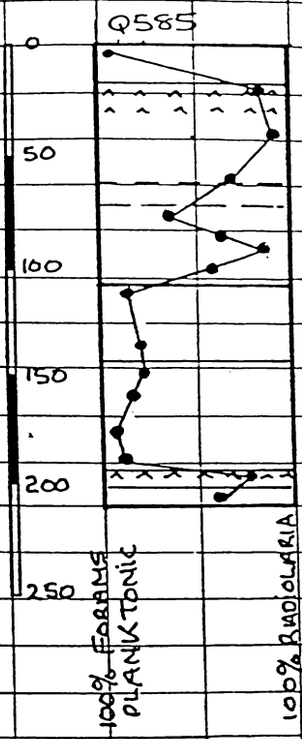

1 2 3 4 5 6

^ = ash.

alternating ⇒

Depth (cm)	Forams/Rad.	Lithology.
Q585 3·5 – 5·5	92 : 8	Light olive grey, pelagic mud
Contact 19 cm.		
20 – 22	19 : 81	Green grey hemipelagic mud
Ash @ 24 & 29 cm.		

Q585 (cont) Core depth (cm)	Forams/Rads	Lithology.
92 – 94	12 : 88	
133 – 135	74 : 26	
Contact @ 142 cm. Note the abundance of forams at 135 may be due to bioturbation.		
160 – 162·5	81 : 19	Yellow grey pelagic mud.
Contact @ 191 cm. ASH		
196·5 – 197·5	23 : 77	Green grey silt.
Contact @ 198·5		
201·5 – 203	42 : 58	Light blue grey clay.

Q585

Holocene.	0-19 cm	Yellowish brown (10 yR 5/2), mud-hemipelagic bioturbated and heavily mottled with light olive grey (5y 6/1) pelagic mud.
Last Glaciation	19-142	Greenish grey (5Gy 5/1) hemipelagic mud grading down core to greenish grey (5 gy 6/1). Faintly mottled. Thin, faint ash horizons at 24 cm, 29 cm.
Interglacial	142-191	Predominently yellowish grey (5y 8/1) foram ooze with beds and lenses of greenish grey (5 gy 5/1) hemipelagic mud with sharp contacts - may be mud turbidites. Hemipelagic horizons at 140-142; 167-168; 184-185, 187-191.
Glacial?	191-198.5	Massive greenish grey (5 gy 5/1) hemipelagic silt with lens of ash at 191.5-193.
	198.5-206.5	Light bluish grey (5 B 7/1) clay with medium bluish laminae at 199 & 205.

Samples	NZOI	BIO
	3.5-5.5	1.5-3.5
	20-22	22-23.5
Ash bearing with a few shards	24 Ash	60-63
	29 Ash	90.5-92
	92-94	131-133
	133-135	162.5-164.5
	160-162.5	185-187
	191-193 Ash only	188-190
	196.5-197.5	194.5-196.5
	201.5-203	199.5-201.5
	141-143	143-145.5

Core Q858 Length 1.905 m

0-70 mm	Medium yellowish brown (10 YR 5/2) mud with lt. ol. grey (5 y 6/1) lamination (9 m) 40-60 mm and dusky yellowish brown (10 YR 2/2) lamination at 30-35 mm. Laminae contacts diffuse and probably bioturbated.
70-845 mm	Lt. ol. grey (5 y 6/1) mud, mottled. At 120-130 mm, lt. grey ash horizon, bedded. At 215 mm dark grey inclusion, not bedded ash?? ? At 600-860 mm, diffuse lamination and probable thin, silty laminae.
845-1905 mm	Lt. Ol. grey (5 Y 5/2) massive mud. At 970 mm, lt grey ash horizon 5 mm thick. At 1270 mm, pumice granule.

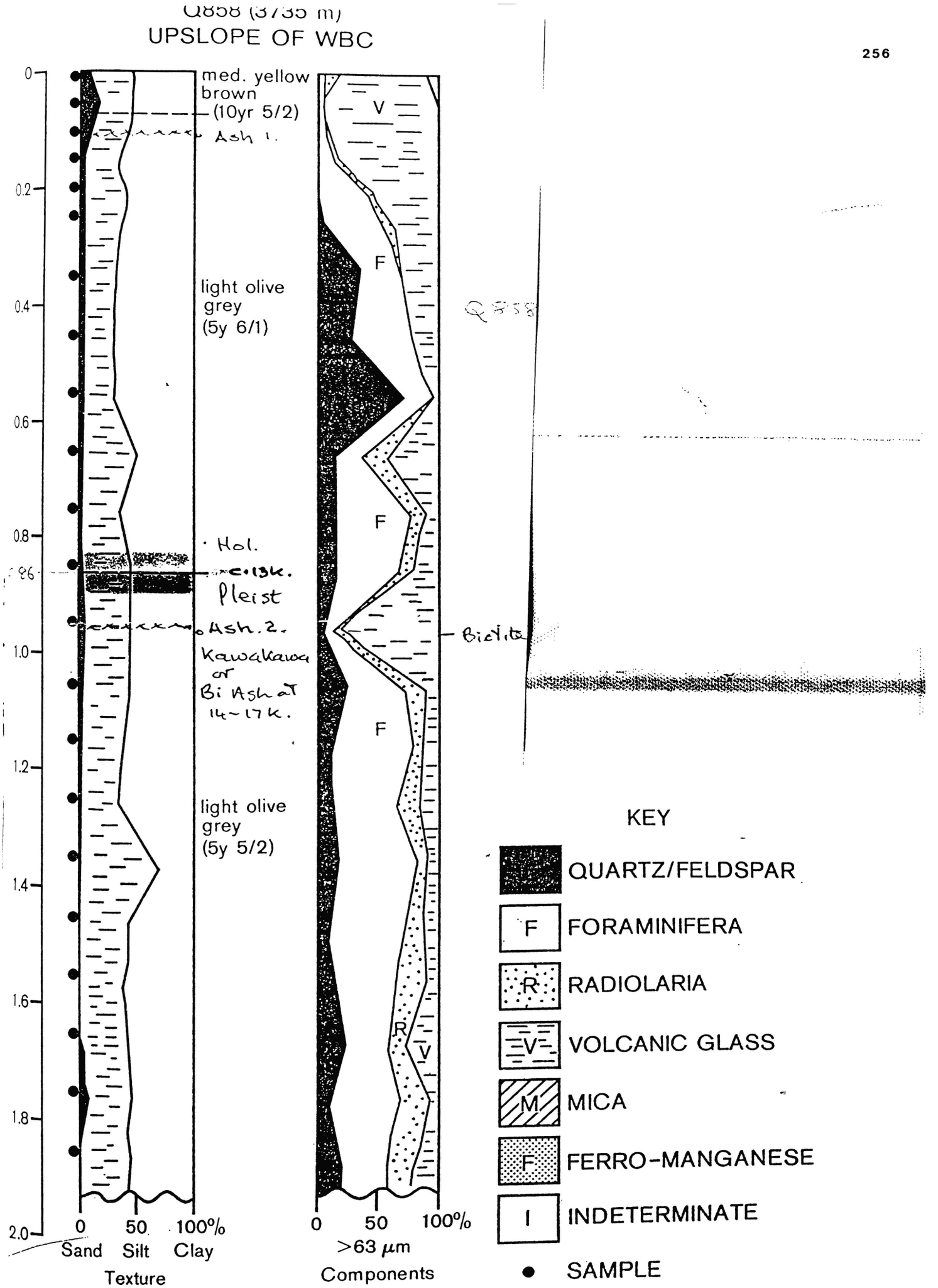
Q858 (3735 m)
UPSLOPE OF WBC
med. yellow brown (10yr 5/2)
Ash 1.
light olive grey (5y 6/1)
Hol.
c.13k.
Pleist
Ash.2.
Kawakawa or Bi Ash at 14~17k.
light olive grey (5y 5/2)
Biotite
Q858
0
0.2
0.4
0.6
0.8
1.0
1.2
1.4
1.6
1.8
2.0
0
50
100%
Sand Silt Clay
Texture
V
F
F
F
R
V
0
50
100%
>63 μm
Components
KEY
QUARTZ/FELDSPAR
F FORAMINIFERA
R RADIOLARIA
V VOLCANIC GLASS
M MICA
F FERRO-MANGANESE
I INDETERMINATE
SAMPLE

Foraminifera

Well-preserved tests of foraminifera, mostly planktonic species, make up most of the sand fraction in all subsamples of this core. The same planktonic species occur in subsamples 1–10, the most abundant being *Globorotalia inflata* (d'Orbigny), *Globorotalia truncatulinoides* (d'Orbigny), *Globorotalia crassula* Cushman & Stewart, *Globigerina pachyderma* Ehrenberg, *Globoquadrina dutertrei* (d'Orbigny), and *Orbulina universa* d'Orbigny. Specimens of *G. dutertrei* are most common in subsamples 1, 3, and 5 (13–19%). In all other subsamples it forms less than 10% of the total number of specimens. *Pulleniatina obliquiloculata* (Parker & Jones) occurs in every subsample and ranges from less than 1% to almost 8% of the total number of specimens. In subsamples 1, 3, 4, and 5 it is greater than 3% and in subsample 2 is 1%. In subsamples 6–10 it is less than 3%. *Globorotalia tumida* (Brady), although less common, has a similar percentage abundance curve to *P. obliquiloculata* (Fig. 10). It is most abundant in subsamples 3, 4, 5, and 8. The percentage abundance curve of *Globigerina pachyderma* is the reverse of that for *Globoquadrina dutertrei, P. obliquiloculata*, and *Globorotalia tumida*. It is less than 6% in subsamples 1–5 and, apart from subsample 8 (5%), subsamples 6–10 are greater than 10%.

Specimens of *Globorotalia truncatulinoides* are mostly right-coiled (97%–79%) in subsamples 1–8 and dominantly left-coiled (82% and 87%) in subsamples 9 and 10.

The foraminiferal fauna in subsample 11 consists mainly of specimens of *Globorotalia miotumida* Jenkins with fewer numbers of specimens of *Globigerina nepenthes* Todd, *Globorotalia merotumida* Banner & Blow, and *Sphaeroidinella subdehiscens* Blow. These species indicate a Middle to Upper Miocene age.

Discussion

The sediments of this core are typically pelagic in origin and have no terrigenous components. Based on percentage abundances of warm- and cold-water planktonic foraminifera, two zones may be recognised. The upper zone (0–175 cm) is characterised by relatively high percentages of *Globoquadrina dutertrei, P. obliquiloculata*, and *Globorotalia tumida* which indicate a climate similar to that of today. In the zone 175–318 cm these warm-water species are less common and there is an increase in percentage abundance of cold-water *Globigerina pachyderma* indicating a climate colder than that of the period represented by the upper zone. This change in climate is considered to correspond to the end of the last glacial period at approximately 11,000 years B.P.

Radiocarbon analyses at 2·5–7·5 cm and 306–312 cm give dates of 6,170 ± 75 and 34,700 ± 1,450 yr respectively, before 1950. Sedimentation rates have been calculated from these dates and the 11,000 yr B.P. date by the method used by Broecker *et. al.* (1958) (Table 8). The upper zone accumulated at an average rate of 35·2 ± 0·5 cm per 1,000 yr compared with 5·6 ± 0·3 cm per 1,000 yr for the lower zone. The high rate of sedimentation in the upper zone is considered to be related to the position of the core, viz., from the foot of the western slope of the Lord Howe Rise where sediment from spasmodic submarine slumps probably accumulates.

To summarise, the upper 175 cm is Holocene in age, the zone represented at 175–318 cm is uppermost Pleistocene (last glaciation); and the zone represented at 318–346 cm is Middle to Upper Miocene in age.

Z2108 Length of core: 421 cm Figs. 9, 10 Tables 9, 10

Sediments

Colour differences, although slight, are sufficient to distinguish between light olive grey layers alternating with yellowish grey layers. The boundaries are gradual and this to a great extent is caused by the activity of burrowing organisms. Worm burrows are present with few exceptions throughout the core and they all seem to have an orientation preference from horizontal to sub-horizontal.

TABLE 9—Locality Data and Sediment Parameters for Core Z2108
(symbols and abbreviations as in Table 1)

Core Z2108 (OPR 476-188)

Latitude	Longitude	Depth (m)	Length (cm)
33°23' S	161°37' E	1448	421

	Subsample	Sample cm	Colour	M_z	σ_I	Sk_I	K_G	%$CaCO_3$
0	1	0–2	5Y 7/2	5.71	3.38	0.05	1.00	93
	2	46–48	5Y 6/1	6.41	3.41	0.14	1.05	87
100	3	97–99	5Y 6/1	6.59	3.16	-0.01	0.86	87
	4	140–142	5Y 6/1	6.12	2.96	-0.22	1.02	84
200	5	190–192	5Y 7/1	6.92	3.50	0.11	0.83	91
	6	228–230	5Y 7/1	6.24	3.09	0.16	0.86	89
300	7	298–300	5Y 7/1	7.45	3.27	-0.04	0.91	80
	8	335–337	5Y 6/1	6.77	2.91	-0.09	0.94	89
	9	352–354	5Y 6/1	6.33	3.78	-0.04	0.87	87
400	10	393–395	5Y 6/1	6.47	3.14	-0.05	0.89	96
	11	419–421	5Y 8/1	5.87	2.31	-0.31	1.05	97

The sediment, a foraminiferal ooze to foraminiferal sand, falls entirely within the sandy pelite range, with silt/clay ratios of 0·7/1–3·1/1, but only two subsamples, 2 and 11, have ratios greater than 1·0/1, viz., 1·6/1 and 3·1/1 respectively. The proportion of sand, however, is fairly consistent throughout at 19%–29%, with the exception of a relatively finer zone between approximately 265 and 350 cm which has only 13% and 16% for subsamples 7 and 8 respectively. The mean diameters vary between 5·71ϕ and 6·92ϕ (19μm and 8μm; i.e., they fall within the finer silt grades). Subsample 7 with M_z = 7·45ϕ or 6μm is, however, on an average finer and falls nearer the clay range. The sorting of this core is again very poor, with standard deviations ranging from 2·31ϕ to 3·78ϕ. Skewness values vary between −0·31 and 0·16; the bottom of the core has the greatest asymmetric tendency and is strongly coarse skewed. Kurtosis values indicate the distributions to be dominantly near normal (Gaussian) to slightly flat curved. Carbonate content is high (84%–97%) and there is an indication that the lighter colour shades reflect relatively higher carbonate percentages. Two modes, respectively around 9ϕ and 4·5ϕ (2μm and 44μm) are persistent throughout the core, with a dominance of the clay mode over the silt mode, but subsamples 1, 4, 9, 10, and 11 have a subsidiary mode in the 250–350μm or medium sand range. Concentrated around the 350 cm mark, but also in a few other places, there are pockets of medium to coarse foraminiferal sand (faecal pellets?), whose uneven distribution is most likely related to the selective

Appendix Two

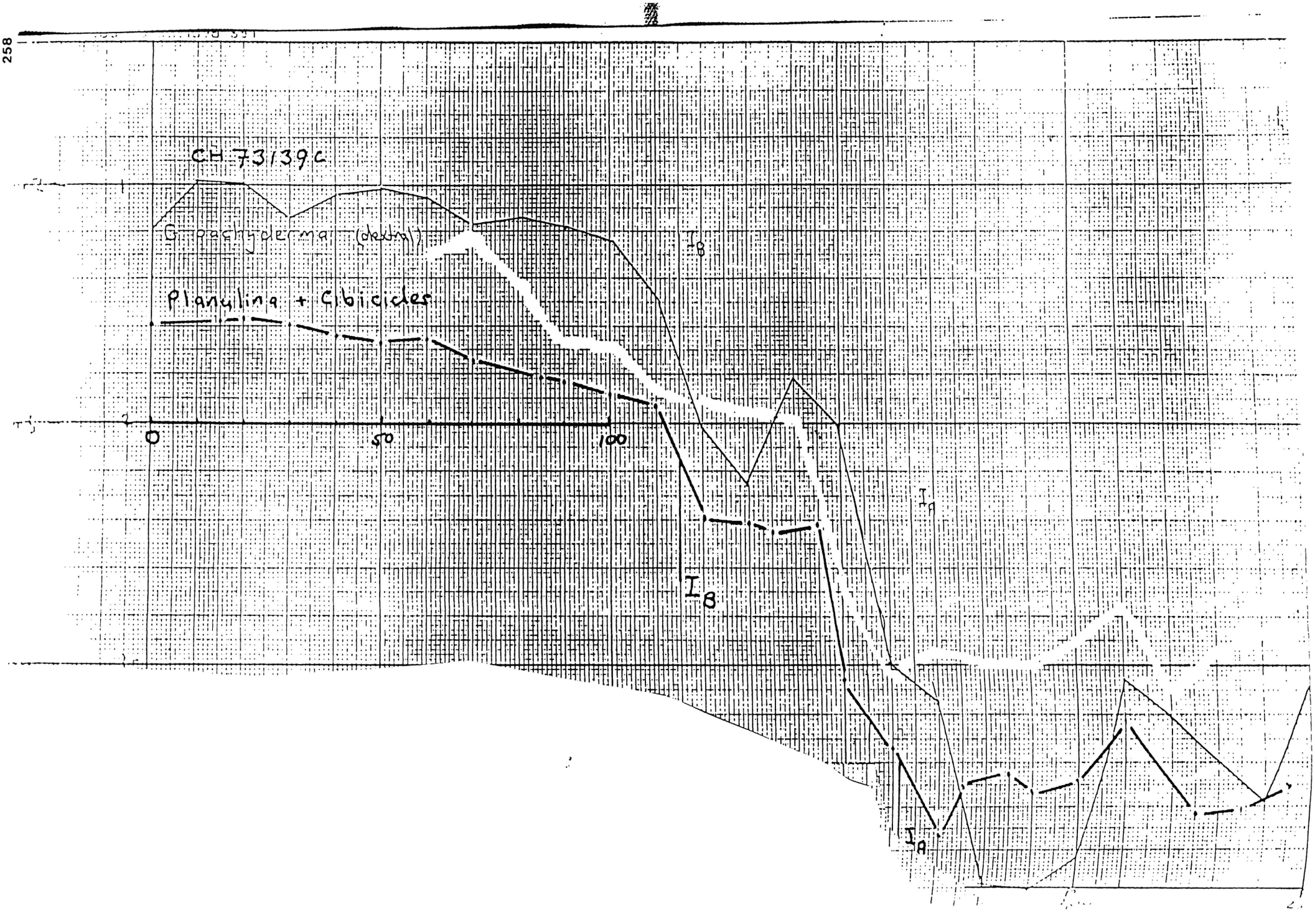
CH 73139c
Grachyderma (dextra)
Planulina + Cibicides
0
50
100
I_B
I_A

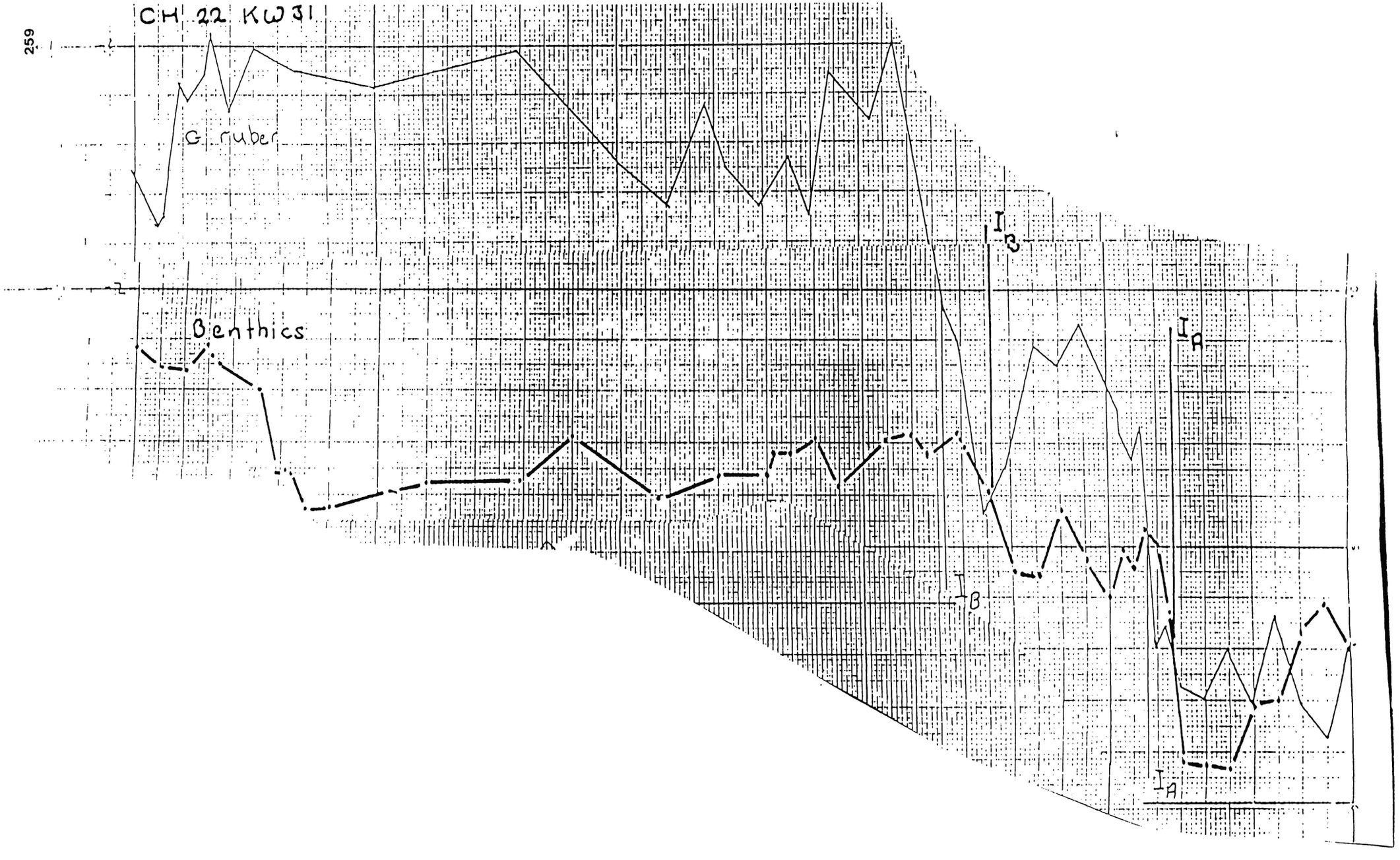
259
CH 22 KW 31
G ruber
Benthics
I_B
I_A
I_B
I_A

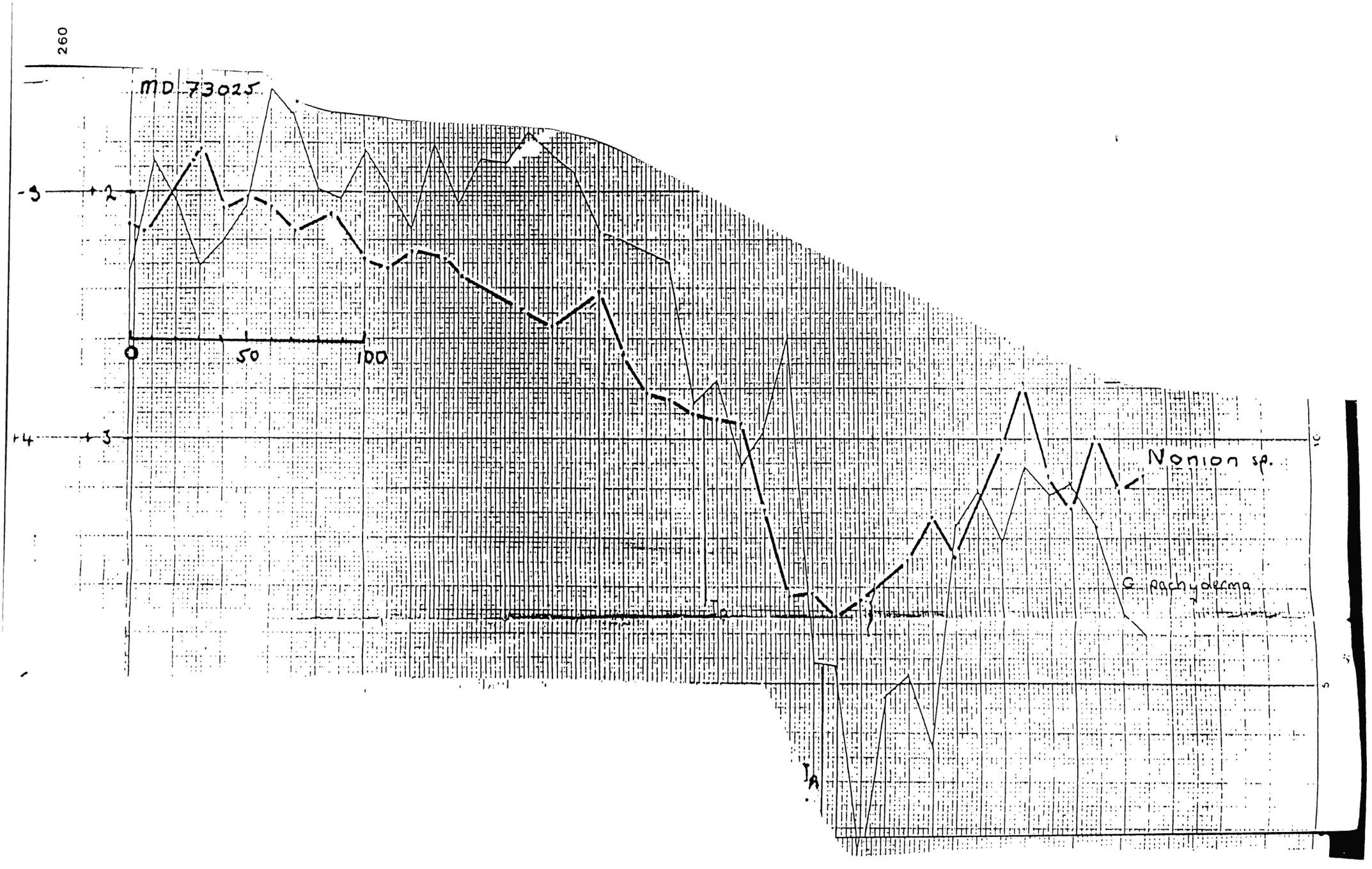
260
MD 73025
-3
+2
0
50
100
+4
+3
Nonion sp.
G. Pachyderma
I_A

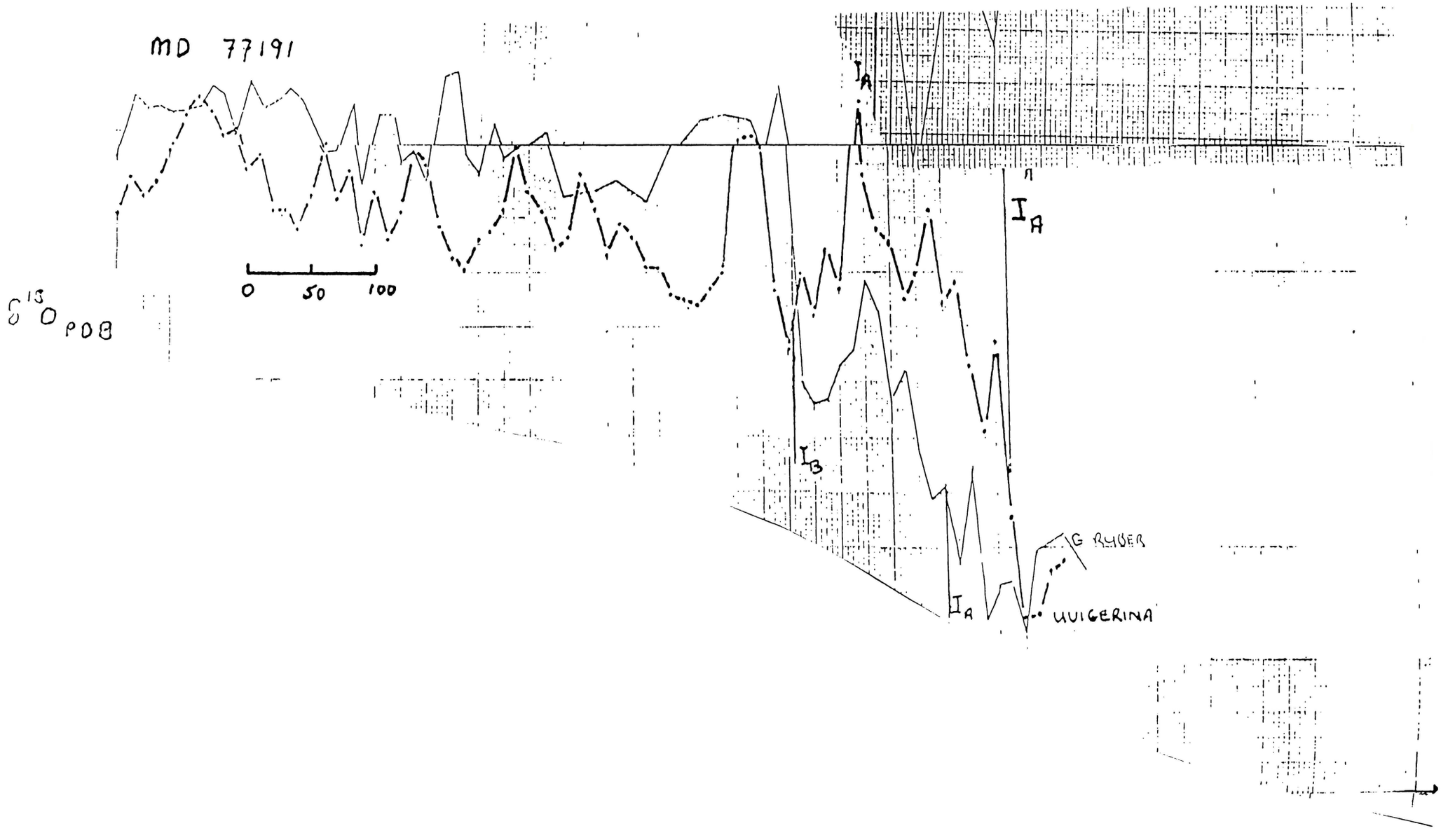
MD 77191
$\delta^{18}O_{PDB}$
0
50
100
I_A
I_B
G RUBER
UVIGERINA

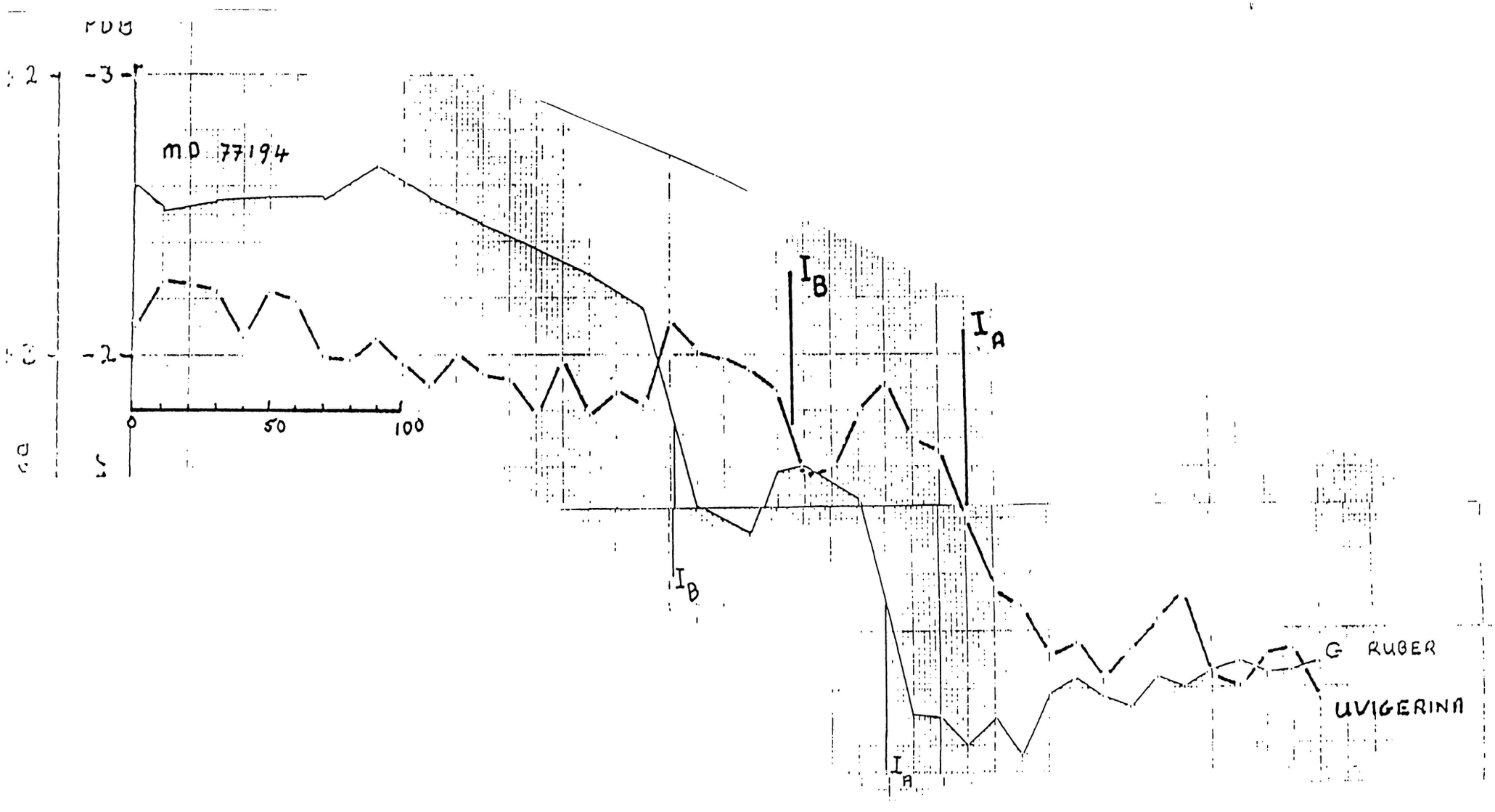
-3
-2
MD 77194
0
50
100
I_B
I_A
I_B
I_A
G RUBER
UVIGERINA

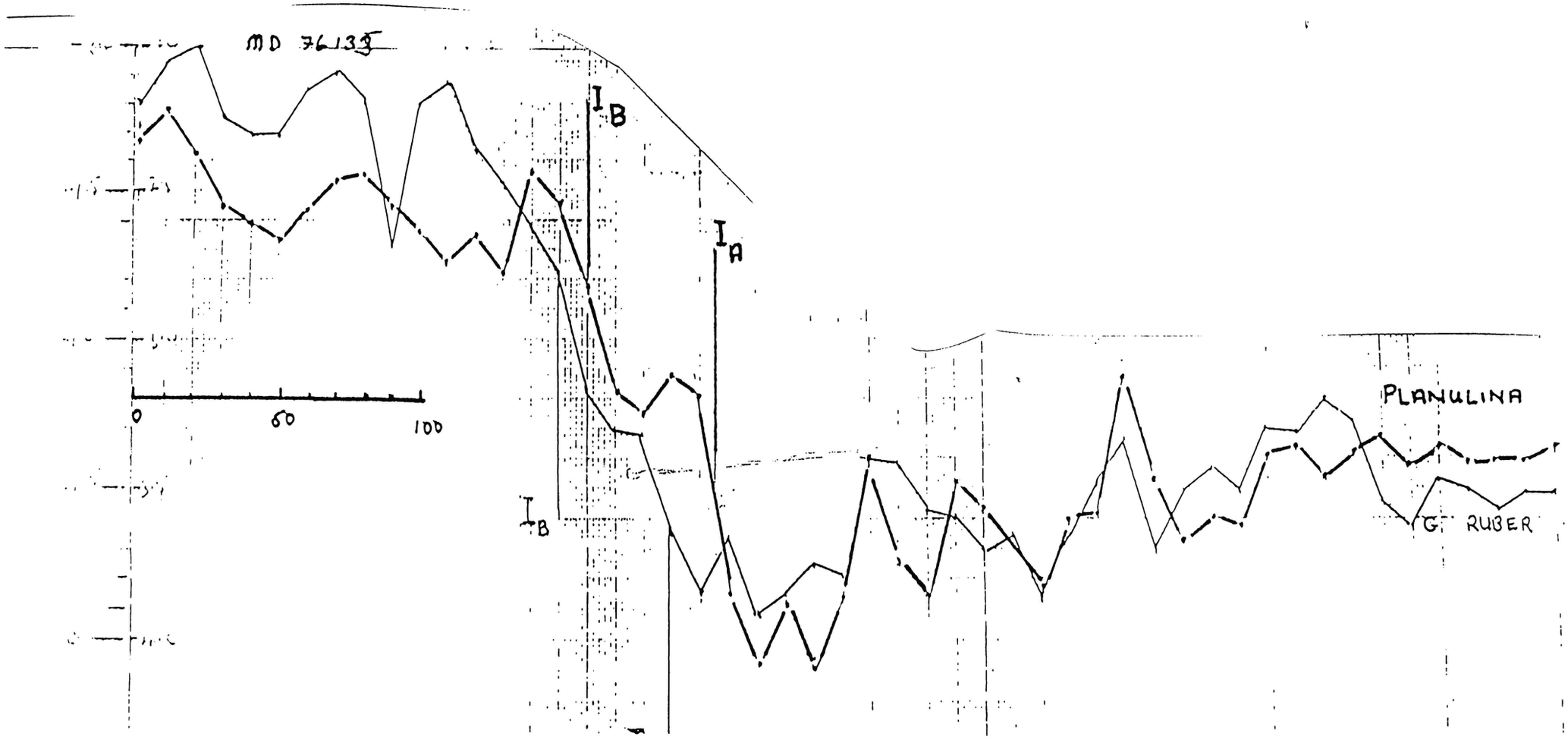
MD 76135
I_B
I_A
I_B
0
60
100
PLANULINA
G. RUBER

References

Anderson,N.R.; Malahoff,A. (Eds) (1977): The fate of fossil fuel in the oceans. Marine Science 6 Plenum Press, New York and London.

Andrews,J.C.; Lawrence,M.W.; Nilsson,C.S. (1980): Observations of the Tasman Front. Journal of Physical Oceanography 10 1854-1869.

Bard,E.; Arnold,M.; Maurice,P.; Duprat,J.; Moyes,J.; Duplessy,J.C. (1987): Retreat velocity of the North Atlantic polar front during the last deglaciation determined by ^{14}C accelerator mass spectrometry. Nature 328 (6133) 791-794.

Barker,P.H.; Kibblewhite,A.C. (1965): Physical oceanographic data from the *Tui* cruise. New Zealand Journal of Science 8 (4) 603-634.

Barton,C.E.; Bloemendal,J. (1986): Paleomagnetism of sediments collected during Leg 90, Southwest Pacific. In Kennett et al. (1986).

Bé,A.W.H. (1977): An ecological, zoogeographic and taxonomic review of recent planktonic foraminifera. In Ramsay (1977).

Berger,W.H. (1968): Planktonic foraminifera: Selective solution and palaeoclimatic interpretation. Deep-Sea Research 15 31-43.

Berger,W.H. (1971): Sedimentation of planktonic foraminifera. Marine Geology 11 325-358.

Berger,W.H. (1976): Biogenous deep-sea sediments: Production, preservation and interpretation. In Riley,J.P.; Chester,R. (Eds) Chemical Oceanography 5 265-288 Academic Press, New York.

Berger,W.H. (1982): On the definition of the Pleistocene/Holocene boundary in deep-sea sediments. In Ruddiman and Duplessy (1985).

Berger,W.H.; Killingley,J.S. (1982): The Worthington effect and the origin of the Younger Dryas. Journal of Marine Research 40 27-38.

Beu,A.G.; Edwards,A.R. (1984): New Zealand Pleistocene and Late Pliocene glacioeustatic cycles. Palaeogeography Palaeoclimatology Palaeoecology 46 119-142.

Blumenstock,D.I. (Ed.) (1966): Pleistocene and Post-Pleistocene climatic variations in the Pacific area Bishop Museum Press.

Bradford,J.M. (1980): New Zealand region, primary productivity, surface. NZOI Chart, Misc. Series #42.

Bradford,J.M.; Taylor,F.J. (1980): New Zealand region reactive phosphorus, surface. NZOI Chart, Misc. Series #46.

Brodie,J.W. (1965): Oceanography. In Hatherton,T. (Ed.) Antarctica Pub. Methuen, London.

Broecker,W.S. (1982): Glacial to interglacial changes in ocean chemistry. Progress in Oceanography 11 151-197.

Broecker,W.S.; Peng,T.-H. (1987): The oceanic salt pump.Does it contribute to the glacial-interglacial difference in atmospheric CO_2 content. Biogeochemical Cycles (submitted August, 1987).

Broecker,W.S,; Thurber,D.L.; Goddard,J.; Ku,T.; Mathews,R.K.; Mesolella,K.J. (1968): Milankovitch hypothesis supported by precise dating of coral reefs and deep-sea sediments. Science 159 297-300.

Broecker,W.S.; van Donk,J. (1970): Insolation changes, ice volumes and the ^{18}O record in deep-sea cores. Reviews of Geophysics and Space Physics 8 169-198.

Bryson,R.A. (1974): A perspective on climatic change. Science 184 753-760.

Burckle,L.H. (1983): Diatom-based paleoceanographic reconstruction in the Southern Ocean - Present and 18 000 B.P. Marine Micropalaeontology In Kennett (1983).

Burns,D.A. (1980): Aspects of the carbon and oxygen stable isotope geochemistry of some New Zealand Cenozoic calcareous sediments. Unpub. MSc Thesis University of Waikato, N.Z.

Carter,L.; Carter,R.M. (In press): Late Quaternary development of left-bank-dominant levees in the Bounty Trough, New Zealand.

Carter,L.; Herzer,R.H. (1979): The hydraulic regime and its potential to transport sediment on the Canterbury continental shelf. NZOI Memoir #83.

Carter,R.M.; Carter,L.; Johnson,D.P. (1986): Submergent shorelines in the Southwest Pacific: evidence for an episodic post-glacial transgression. Sedimentology 33 (5) 629-649.

Carter,R.M.; Carter,R.L.; Wiliams,J.J.; Landis,G.A. (1985): Modern and relict sedimentation on the South Otago continental shelf, New Zealand. NZOI Memoir #93.

Chappell,J; Shackleton,N.J. (1986): Oxygen isotopes and sea level. Nature 324 137-140.

CLIMAP Project Members (1976): The surface of the Ice-Age Earth. Science 191 (4232) 1131-1137.

CLIMAP Project Members (1982): Seasonal reconstructions of the Earth's surface at the last glacial maximum. In M^{c}Intyre,A.(1982): Geological Society of America Map and Chart Series 36.

CLIMAP Project Members (1984): The last interglacial ocean. Quaternary Research 21 123-224.

Cooke,P.J. (1988): The Late Quaternary stratigraphy and micro-palaeontology of DSDP Site 594, Southwest Pacific. Unpubl. MSc Thesis, University of Waikato (N.Z.).

Coplen,T.B.; Kendall,C; Hopple,J.(1983): Comparison of stable isotope reference samples. Nature 302 236-238.

Cox,A. (1969): Time scale for geomagnetic reversals. Science 163 237.

Craig,H. (1957): Geochimica et Cosmochimica Acta 12 133-149.

Craig,H. (1961): Standard for reporting concentrations of deuterium and oxygen-18 in natural waters. Science 133 1833-1834.

Craig,H.; Gordon,L.I. (1965): Deuterium and oxygen-18 variations in the ocean and the marine atmosphere. In Broecker and Peng (1987).

Crutzen,P.J.; Arnold,F. (1986): Nitric acid cloud formation in the cold Antarctic stratosphere: a major cause for the springtime 'ozone hole'. Nature 324 (6098) 651-655.

Curry,W.B.; Mathews,R.K. (1981): Paleo-oceanographic utility of oxygen isotopic measurements on planktonic foraminifera: Indian Ocean core top evidence. Palaeogeology Palaeoclimatology Palaeoecology 33 173-191.

Curry,W.B.; Lohman,G.P. (1982): Carbon isotopic changes in benthic foraminifera from the Western South Atlantic: Reconstruction of glacial abyssal circulation patterns. Quaternary Research 18 218-235.

Dansgaard,W. (1981): Palaeo-climatic studies on ice cores. In Berger,A. (Ed.) Climatic Variations and Variability: Facts and Theories D.Reidel Pub.

Dansgaard,W.; Johnson,S.J.; Clausen,H.B.; Langway,C.C. (1971): Climatic record revealed by Camp Century ice core. In Turekian,K.K. (Ed.) The Late Cenozoic Glacial Ages 37-56 Yale University Press.

Dansgaard,W.; Tauber,H. (1969): Glacier oxygen-18 content and Pleistocene ocean temperatures. Science 166 499.

Deacon,G.E.R. (1937): Hydrology of the Southern Ocean. In Heath (1973).

De Geer,E.H. (1957): Old and new datings of the Swedish ice lakes and the thermals of Bølling and Allerød. Geol. Föf. Stokh. Forh. 79 (1) 93-100. In Duplessy et al., 1981.

Delmas,R.J.; Ascencio,J.-M.; Legrand,M. (1980): Polar ice evidence that atmospheric CO_2 20 000yrs B.P. was 50% of present. Nature 284 155-157.

Denham,R.N.; Crooks,F.G. (1976): The Tasman Front. New Zealand Journal of Marine and Freshwater Research 10 (1) 15-30.

Denton,G.H.; Hughes,T.J. (1981): The last great ice sheets. Pub. Wiley Interscience, New York.

Dodge,R.E.; Fairbanks,R.G.; Benninger,L.K.; Maurasse,F. (1983): Science 219 1423-1425.

Dudley,W.C.; Nelson,C.S. (1988): The $\delta^{13}C$ content of calcareous nannofossils as an indicator of Quaternary palaeoproductivity in the southwest Pacific region. New Zealand Journal of Geology and Geophysics 31 (1) 111-116.

Duplessy,J.-C.; Cherrouard,L.; Vila,F. (1975): Weyl's theory of glaciation supported by isotopic study of Norwegian core K11. Science 188 1208-1209.

Duplessy,J.-C.; Delibrias, G.; Turon,J.L.; Pujol,C.; Duprat,J. (1981): Deglacial warming of the Northeastern Atlantic Ocean: Correlation with the paleoclimatic evolution of the Europeancontinent. Palaeogeology Palaeoclimatology Palaeoecology 35 121-144.

Duplessy,J.-C.; Lalou,C.; Vinot,A.C. (1970): Differential isotopic fractionation of benthic foraminifera and paleotemperatures reassessed. Science 168 250.

Duplessy,J.-C.; Mayes,J.; Pujol,C. (1980): Deep water formation in the North Atlantic Ocean during the last ice age. Nature 286 479-482.

Duplessy,J.-C.; Shackleton,N.J.; Mathews,R.K.; Prell,W.; Ruddiman,W.F.; Caralp,M.; Hendy,C.H.H. (1984): ^{13}C record of benthic foraminifera in the last interglacial ocean: Implications for the carbon cycle and the global deep water circulation. Quaternary Research 21 225-243.

Durazzi,J.T. (1981): Stable isotope studies of planktonic foraminifera in North Atlantic core tops. Palaeogeology Palaeoclimatology Palaeoecology 33 157-172.

Eade,J.V.; van der Linden,W.J.M. (1970): Sediments and stratigraphy of deep sea cores from the Tasman Basin. New Zealand Journal of Geology and Geophysics 13 228-268.

Edwards,A.R. (1987): An integrated biostratigraphy, magneto-stratigraphy and oxygen isotope stratigraphy for the Late Neogene of New Zealand. New Zealand Geological Record #23 D.S.I.R., Lower Hutt.

Embleton,C.; King,C.A.M. (1968): Glacial and Periglacial Geomorphology Pub. Arnold, London.

Emery,W.J. (1977): Antarctic polar frontal zone from Australia to the Deake Passage. Journal of Physical Oceanography 7 811-822.

Emiliani,C. (1954): American Journal of Science 252 149-158.

Emiliani,C. (1955): Pleistocene temperatures. Journal of Geology 63 538-573.

Emiliani,C. (1958): Paleotemperature analysis of Core 280 and Pleistocene correlations. Journal of Geology 66 264-275.

Emiliani,C. (1966): Paleotemperature analysis of Caribbean cores P6304-8 and P6304-9 and a generalised temperature curve for the last 425 000 years. Journal of Geology 74 109-123.

Emiliani,C. (1970): Pleistocene paleotemperatures. Science 189 1083-1088.

Emiliani,C.; Gartner,S.; Lidz,B.; Eldridge,K.; Elvey,D.K.; Huang,T.C.; Stipp,J.J.; Swanson,M.F. (1975): Science 189 1083-1088.

Epstein,S.; Buchsbaum,R.; Lowenstan,H.; Urey,H.C. (1951): Carbonate water isotopic temperature scale. Bulletin of the Geological Society of America 62 417.

Erez,J.; Honjo,S. (1981): Comparison of isotopic composition of planktonic foraminifera in plankton tows, sediment traps and sediments. Palaeogeology Palaeoclimatology Palaeoecology 33 129-156.

Ericson,D.B.; Wollin,G. (1954): Coiling direction of *Globorotalia truncatulinoides* in deep-sea cores. Deep-Sea Research 2 152-158.

Ericson,D.B.; Wollin,G. (1968): Pleistocene climates and chronology in deep sea sediments. Science 162 1227.

Fairbanks,R.G.; Mathews,R.K. (1978): The marine oxygen isotope record in Pleistocene coral, Barbados, West Indies. Quaternary Research 10 181-196.

Frakes,L.A. (1979): Climates Throughout Geologic Time Pub. Elsevier.

Frenzel, B. (1968): The Pleistocene vegetation of Northern Eurasia. Science 161 637-649.

Friedman,I.; O'Neil,J.R. (1977): Compilation of stable isotope fractionation factors of geochemical interest. U.S. Geological Survey Professional Paper #440-KK.

Fritz,P.; Fontes,J.C. (1966): In Gribben (1978).

Gabites,J.F. (1953a): Mean westerly wind flow in the upper levels over the New Zealand region. New Zealand Journal of Science and Technology B 34 384-390.

Gabites,J.F. (1953b): Temperatures in the troposphere and lower stratosphere over the New Zealand region. New Zealand Journal of Science and Technology B 35 213-224.

Gage,M. (1961): New Zealand glaciations and the duration of the Pleistocene. Journal of Glaciology 3 940-943.

Gage,M. (1965): Some characteristics of Pleistocene cold climates in New Zealand. Transactions of the Royal Society of New Zealand (Geology) 3 11-21.

Gage,M. (1966): The climate of New Zealand during cool phases of the Pleistocene. In Blumenstock(1966).

Gardner,J.V. (1982): High resolution carbonate and organic carbon stratigraphies for the Late Neogene and Quaternary from the Western Caribbean and eastern equatorial Pacific. In Prell,W.L.et al. (Eds) Initial Reports of the Deep Sea Drilling Project68 347-364.

Garlick,G.D. (1969): The stable isotopes of oxygen. In Wedepohl,K.H. (Ed.) Handbook of Geochemistry II/1.

Gilmour,A.E.; Cole,A.G. (1979): The subtropical convergence east of New Zealand. New Zealand Journal of Marine and Fresh Water Research 13 (4) 553-557.

Goldthwaite.R.P. (Ed.) (1975): Glacial Deposits Pub. Dowden, Hutchinson and Ross.

Gribben,J. (Ed.) (1978): Climatic Change Pub. Cambridge University Press.

Griggs,G.B.; Carter,L; Kennett, J.P.; Carter,R.V. (1983): Late Quaternary marine stratigraphy southeast of New Zealand. Geological Society of America Bulletin 94 791-797.

Grinstead,M.A. (1977): A study of the relationships between climate and stable isotope ratios in tree rings. Unpub. D.Phil. Thesis, University of Waikato, N.Z.

Hay,W.W. (1977): Calcareous nannofossils. In Ramsay (1977) 2 1055-1200.

Hays, J.D.; Imbrie,J.; Shackleton,N.J. (1976): Variations in the Earth's orbit: Pacemaker of the ages. Science 194 1121-1132.

Heath,G.R. (1974): Dissolved silica and deep-sea sediments. In Hay,W.W.(Ed.) Studies in Paleo-Oceanography SEPM #20.

Heath,R.A. (1972): The Southland current. New Zealand Journal of Marine and Freshwater Research 6 497-533.

Heath,R.A. (1973): Present knowledge of the oceanic circulation and hydrology around New Zealand - 1971) Tuatara 20 125140.

Heath,R.A. (1975): Oceanic circulation and hydrology off the southern half of South Island New Zealand. NZOI Memoir #72.

Heath,R.A. (1985): A review of the physical oceanography of the seas around New Zealand - 1982. New Zealand Journal of Marine and Freshwater Research 19 79-124.

Hecht,A.D. (Ed.) (1985): Palaeoclimate Analysis and Modelling Pub. Wiley Interscience.

Imbrie.J; Hays,J.D.; Martinson,D.G.; M^{c}Intyre,A.; Mix,A.C.; Morley,J.J.; Pisias,N.G.; Prell,W.L.; Shackleton,N.J. (1984): The orbital theory of Pleistocene climate: Suport from a revised chronology of the marine $\delta^{18}O$ record. In Berger,A.; Imbrie,J.; Hays,J.; Kukla,G.; Saltzman,B. (Eds). Milankovitch and Climate I 269-306 Pub. Dordrecht Reidel.

Hoefs,J. (1973): Stable Isotope Geochemistry Pub. Springer-Verlag.

Imbrie,J.; Imbrie,K.P. (1979): Ice Ages Pub. Einslow.

Imbrie,J.; Kipp,N.G. (1971): A new micro-paleontological method for quantitative paleoclimatology: Application to a Late Pleistocene Caribbean core. In Turekian,K.K.(Ed.) The Late Cenozoic Glacial Ages Pub. Yale University Press.

Imbrie,J.; van Donk,J.; Kipp,N.G. (1973): Palaeoclimatic investigation of a Late Pleistocene Caribbean deep-sea core: Comparison of isotopic and faunal methods. Quaternary Research 3 10-38.

Johnson,R.G.; Andrews,J.T. (1986): Glacial terminations in the oxygen isotope record of deep-sea cores: Hypothesis of massive Antarctic ice shelf destruction. Palaeogeology Palaeoclimatology Palaeoecology 53 107-138.

Johnson,S.J.; Dansgaard,W.; Clausen,H.B.; Langway,C.C. (1972): Oxygen isotope profiles through the Antarctic and Greenland ice sheets. Nature 235 429-434.

Kahn,M.I.; Williams,D.F. (1981): Oxygen and carbon isotopic composition of living planktonic foraminifera from the northeast Pacific Ocean. Palaeogeology Palaeoclimatology Palaeoecology 33 47-69.

Kamp,P.J.J. (1978): Stratigraphy and sedimentology of conglomerates in the Kidnappers Group, Hawke's Bay. Unpub. thesis, University of Waikato, N.Z.

Kennedy,T.F. (1974): A Descriptive Atlas of the Pacific Islands Pub. Reed.

Kennett,J.P. (1983): Paleo-oceanography: Global ocean evolution. Reviews of Geophysics and Space Physics 21 1258-1274.

Kennett,J.P.; Houtz,R.E. et al (1974): Initial Reports of the Deep Sea Drilling Project Vol. 29 U.S. Govt. Printing Office.

Kennett,J.P.; Shackleton,N.J. (1975): Science 188 147-150.

Kennett,J.P.; Shackleton,N.J.; Margolis, S.V.; Goodney,D.E.; Dudley,W.C.; Kroopnick,P.M. (1979): Late Cenozoic oxygen and carbon isotope history and volcanic ash stratigraphy: DSDP Site 284. South Pacific. American Journal of Science 279 52-69.

Kennett,J.P.; Srinivasan,M.S. (1983): Neogene Planktonic Foraminifera: a phylogenetic atlas.

Kennett,J.P.; von der Borsch,C.C. et al. (1986): Initial Reports of the Deep Sea Drilling Project Vol. 90 I and II. U.S. Govt. Printing Office.

Kershaw,A.P. (1973): Late Quaternary vegetation and climate in northeastern Australia. In Quaternary Studies. Ed. Suggate,R.P. and Cresswell,M.M. 181-187. The Royal Society of New Zealand.

Kidson,E. (1950): The elements of New Zealand's climate. In Garnier,B.J. (Ed.) New Zealand Weather and Climate. New Zealand Geographic Society. 45-83.

Köppen,W. (1900): Versuch einer Klassifikation der Klimate, vorsugsweise nach ihren Bezeihungen. In Hecht (1985).

Kroopnick,P. (1974): The dissolved O_2-CO_2-^{13}C system in the eastern equatorial Pacific. Deep Sea Research 21 211-227.

Kroopnick,P. (1980): The distribution of ^{13}C in the Atlantic Ocean. Earth and Planetary Science Letters 49 469-484.

Kroopnick,P.M.; Margolis,M.V.; Wong,C.S. (1977): $\delta^{13}C$ variations in marine carbonate sediments as indicators of the CO_2 balance between the atmosphere and the ocean. In Anderson and Malahoff (1977).

Labeyrie,L.D.; Duplessy,J.-C. (1985): Changes in the oceanic $^{13}C/^{12}C$ ratio during the lst 140 000years: high-latitude surface water records. Palaeogeography, Palaeoclimatology, Palaeoecology 50 217-240

Labeyrie,L.D.; Pichon,J.J.; Labracherie,M.; Ippolito,P.; Duprat,J.; Duplessy,J.-C. (1986): Melting history of Antarctica during the past 60 000 years. Nature 322 701-706.

Labeyrie,L.D.; Duplessy,J.-C.; Blanc,P.L. (1987): Variations in mode of formation and temperature of oceanic deep waters over the past 125 000 years. Nature 327 477-482.

Leventer,A.; Williams,D.F.; Kennett,J.P. (1982): Dynamics of the Laurentide ice sheet during the last deglaciation: Evidence from the Gulf of Mexico. Earth and Planetary Science Letters 59 11-17.

Li,V.H.; Takahashi,T.; Broecker,W.S. (1969): Degree of saturation of $CaCO_3$ in the oceans. Journal of Geophysical Research 74 (23) 5507-5525.

Lisitzin,A.P. (1972): Sedimentation in the world ocean. In Ramsay (1977).

Lorius,C. (1974): Antarctica: survey of near-surface isotope values. MIT Press.

Luz,B. (1977): Late Pleistocene paleoclimates of the South Pacific based on statistical analysis of planktonic foraminifera. Palaeogeology Palaeoclimatology Palaeoecology 22 61-78.

Malmgren,B.A.; Kennett,J.P. (1981): Phyletic gradualism in a Late Cenozoic planktonic foraminiferal lineage; DSDP Site 284, Southwest Pacific. Paleobiology 7 230-240.

Mankinen,E.A.; Dalrymple,G.B. (1979): Revised geomagnetic polarity time scale for the interval 0.5my B.P. Journal of Geophysical Research 84 615-626.

Manley,G. (1975): 1684:- The coldest winter in the English instrumental record. Weather 30 382.

Martinson,D.G.; Pisias,N.G.; Hays,J.D.; Imbrie,J.; Moore,T.C.(Jr); Shackleton,N.J. (1987): Age dating and the orbital theory of the ice ages: Development of a high resolution 0 to 300,000-year chronostratigraphy. Quaternary Research 27 (1) 1-29.

Mathews,R.K.; Curry,W.B.; Lohman,K.C.; Summer,M.A.; Poore,R.Z. (1980): Late Miocene palaeo-oceanography of the Atlantic: Oxygen isotope data on planktonic and benthic foraminifera. Nature 283 555-557.

Maunder,W. (1970): Climates of Australia and New Zealand. In Landsberg,H.E. (Ed.) World Survey of Climatology Vol. 13.

McCrea,J.M. (1950): On the isotopic chemistry of carbonates and a paleotemperature scale. Journal of Chemical Physics 18 (6) 849-857.

McGlone,M.S. (1985): Biostratigraphy of the last interglacial glacial cycle, southern North Island, New Zealand. In Pillans (1985).

McKinney,C.R.; McCrea,J.M.; Epstein,S.; Allen,H.A.; Urey,H.C. (1950): improvements in mass spectrometers for the measurements of small differences in isotopic abundance ratios. Review of Scientific Instruments 21 724.

Milankovitch,M. (1938): Die Chronologie des Pleistocene. In Broecker and van Donk (1970).

Mix,A.C.; Fairbanks,R.G. (1985): North Atlantic surface-ocean control of Pleistocene deep-ocean circulation. Earth and Planetary Science Letters 73 231-243.

Mix,A.C.; Ruddiman,W.F.(1984): Oxygen isotope analyses and Pleistocene ice volumes. Quaternary Research 21 1-20.

Mix,A.C.; Ruddiman,W.F. (1985): Structure and timing of the last deglaciation: Oxygen isotope evidence. Quaternary Science Reviews 4 59-108.

Mook,W.G. (1968): Geochemistry of the stable carbon and oxygen isotopes of natural waters in the Netherlands. Ph.D. Thesis, University of Groningen, Netherlands.

Moore,T.C.(Jr) (1978): The distribution of radiolarian assemblages in the modern ice-age Pacific. Marine Micropaleontology 3 229-266.

Moore,T.C.(Jr); Burckle,L.H.; Geitzenauer,K.; et al. (1980): The reconstruction of sea surface temperatures in the Pacific of 18 000B.P. Marine Micropaleontology 5 215-247.

Morley,J.J.; Hays,J.D. (1979): *Cycladophora davisiana*: A stratigraphic tool for Pleistocene North Atlantic and interhemispheric correlation. Earth and Planetary Science Letters 4 383-389.

Murphy,M.G.; Kennett,J.P. (1986): Development of latitudinal thermal gradients during the Oligocene: Oxygen-isotope evidence from the Southwest Pacific. In Kennett et al. (1986)

Murray,J. (1897): On the distribution of the pelagic foraminifera at the surface and on the floor of the ocean. In Ramsay (1977).

Neftel,A.; Oeschger,H.; Schwander,J.; Stauffer,B.; Zumbrunn,R. (1982): Ice core sample measurements give atmospheric CO_2 content during the past 40,000 years. Nature 295 220-223.

Nelson,C.S.; Hendy,C.H.H.; Cuthbertson,A.M.; Jarrett,G.R. (1986): Late Quaternary carbonate and isotope stratigraphy, subantarctic Site 594, Southwest Pacific. In Kennett et al. (1986).

Nelson,C.S.; Hendy,C.H.H.; Dudley,W.C. (1986): Quaternary isotope stratigraphy of hole 593, Challenger Plateau, South Tasman Sea: Preliminary observations based on foraminifera and calcareous nannofossils. In Kennett et al. (1986).

Nier,A.O.(1940): In Emiliani,C.(1966): Nature 54 851-857.

Nier,A.O.; Ney,E.P.; Inghram,M.G. (1947): Null method for the comparison of two ion currents in a mass spectrometer. Review of Scientific Instruments 18 294.

Niitsuma,N.; Ku,T.-L. (1977): What happened at the time of the Earth's magnetic field reversals? In Broecker (1982).

Okada,H.; M^{c}Intyre,A. (1977): Modern coccolithophores of the Pacific and North Atlantic Oceans. Micropaleontology 23 1-55.

Pastor,J.; Post,W.M. (1988): Response of northern forests to CO_2-induced climate change. Nature 334 (6177) 55-58.

Phillippi,E. (1910): Die grundproben der deutschen Südpolar expedition 1901 - 1903. Deutsche Südpolar Expd 2 (6) 411-416. In Ramsay (1977).

Pillans,B.J. (1983): Upper Quaternary marine terrace chronology and deformation, South Taranaki, New Zealand. Geology 11 292-297.

Pillans,B.J. (Ed.) (1985): Proceedings of the second CLIMANZ conference, held at Harihari, Westland, New Zealand, February 4-8, 1985. Pub. University of Victoria.

Pisias,N.G.; Martinson,D.G.; Moore,T.C.(Jr); Shackleton,N.J.; Prell,W; Hayes,J.; Boden,G. (1984): High resolution stratigraphic correlation of benthic oxygen isotopic records spanning the last 300,000 years. Marine Geology 56 (1/4) 119-136.

Prell,W.L. (1982): Oxygen and carbon isotope stratigraphy for the Quaternary of Hole 592B: Evidence for two modes of isotopic variability. In Prell,W.L.; Gardner,J.V. et al. (1982): Initial reports of the Deep Sea Drilling Project 68 455-464. U.S. Govt. Printing Office.

Prell,W.L. (1983): In Pisias et al. (1984), but not listed in references.

Prell,W.L.; Hutson,W.H.; Williams,D.G.; Bé,A.W.H.; Geitzenauer,K.; Molfino,B. (1980): Surface circulation of the Indian Ocean during the last glacial maximum, approximately 18 000yr B.P. Quaternary Research 14 309-336.

Pytkowicz,R.M. (1968): The carbon dioxide - carbonate system at high pressures in the oceans. Oceanographic Marine Biology Annual Review 6 83-135. In Ramsay (1977).

Ramsay,A.T.S. (Ed.) (1977): Oceanic Micropalaeontology Vol. 1 and 2. Academic Press London.

Ridgway,N.M. (1969): Temperature and salinity of sea water at the ocean floor in the New Zealand region. New Zealand Journal of Marine and Freshwater Research 3 57-72.

Ridgway,N.M. (1975): Hydrology of the Bounty Islands. NZOI Memoir #75.

Ridgway,N.M.; Heath,R.A.; Marott,C. (1979a): Southwest Pacific Ocean: Water temperature at the ocean floor. NZOI Chart, Misc. Series #32.

ibid (1979b): Southwest Pacific Ocean: Depth of the core of Antarctic Intermediate Water. NZOI Chart, Misc. Series #30.

ibid (1979c): Southwest Pacific Ocean: Salinity at the core of Antarctic Intermediate Water. NZOI Chart, Misc. Series #29.

ibid (1979d): Southwest Pacific Ocean: Salinity at 200m. NZOI Chart, Misc. Series #28.

ibid (1979e): Southwest Pacific Ocean: Temperature at 200m. NZOI Chart, Misc. Series #27.

Robertson,N.G. (1967): Climate of New Zealand. In New Zealand Official Year Book, 1967 15-20 Govt. Printer Wellington.

Romine,K. (1982): Late Quaternary history of atmospheric and oceanic circulation in the eastern equatorial Pacific. Marine Micropalaeontology 7 163-189.

Rubinson,H.; Clayton,R.N. (1969): Carbon 13 fractionation between aragonite and calcite. Geochimica et Cosmochimica Acta 33 997-1004.

Ruddiman,W.F.; Duplessy,J.-C. (1985): Conference on the last deglaciation: Timing and mechanism. Quaternary Research 23 1-17.

Ruddiman,W.F.; M^{c}Intyre,A. (1981): Oceanic mechanisms for amplification of the 23 000-year ice-volume cycle. Science 212 617-627.

Sackett,W.M.; Eckelman,W.R.; Bender,M.L.; Bé,A.W.H. (1965): Temperature dependence of carbon isotope composition in marine plankton and sediments. Science 148 235-237.

Schnitker,D. (1979): The deep waters of the western North Atlantic during the past 24 000 years, and the initiation of the Western Boundary Undercurrent. Marine Micropalaeontology 4 265-280.

Schott,W. (1935): Die foraminiferen in dem äquatorialen teil des Atlantischen Ozean. Deutche Atlantische Exped. *Meteor* 1925-1927. Wiss. Ergebn. 3 (3) 43-134. In Ramsay (1977).

Shackleton,N.J. (1965): The high-precision isotopic analysis of oxygen and carbon in CO_2. Journal of Scientific Instruments 42 689-692.

Shackleton,N.J. (1965a): Some variations in the technique for measuring carbon and oxygen isotope ratios in small quantities of calcium carbonate. In Burns (1980).

Shackleton,N.J. (1967): Oxygen isotope analyses and Pleistocene temperatures re-assessed. Nature 215 15-17.

Shackleton,N.J. (1974): Attainment of isotopic equilibrium between ocean water and benthonic foraminifera genus *Uvigerina*: Isotopic changes in the ocean during the last glacial. In Colloques Internationaux du CNRS #219. Les méthode quantitative d'étude des variations du climate au cours du Pléistocène, 203-209.

Shackleton,N.J. (1977): Tropical rainforest history and the equatorial Pacific carbonate dissolution cycles. In Anderson and Malahoff (Eds) (1977).

Shackleton,N.J. (1987): Oxygen isotopes, ice-volume and sea level. Quaternary Science Reviews 6 183-190.

Shackelton,N.J.; Hall,M.A.; Line,J.; Cang Shuxi (1983): Carbon isotope data in core V19-30 confirm reduced carbon dioxide concentration in the ice age atmosphere. Nature 306 (24) 319-322.

Shackleton,N.J.; Kennett,J.P. (1975): Paleotemperatue history of the Cenzoic and the initiation of Antarctic glaciation: Oxygen and carbon isotope analyses in DSDP Sites 277, 279 and 281. Initial Reports of the Deep Sea Drilling Project XXIX 743-755.

Shackleton,N.J.; Opdyke,N.D. (1973): Oxygen isotope and paleomagnetic stratigraphy of equatorial Pacific core V28-238: Oxygen isotope temperatures and ice volumes on a 10^5 year and 10^6 year scale. Quaternary Research 3 39-55.

Shackleton,N.J.; Opdyke,N.D. (1976): Oxygen isotope and palaeomagnetic stratigraphy of equatorial Pacific core V28-239, Late Pliocene to latest Pleistocene. Geological Society of America Memoir 145 449-464.

Shackleton,N.J.; Pisias,N.G. (1985): Atmospheric carbon dioxide, orbital forcing, and the climate. In The carbon cycle and atmospheric CO_2: Natural variations Archean to present. Geophysical Monograph 32.

Shackleton,N.J.; Wiseman,J.D.H.; Buckley,H.A. (1973): Non-equilibrium isotopic fractionation between sea water and planktonic foraminiferal tests. Nature 242 177-179.

Shaw,D.M.; Donn,W.L. (1968): Milankovitch radiation variations. A quantitative evaluation. Science 162 1270.

Shumskiy,P.A.; Krenke,A.N.; Zotikov,I.A. (1964): Ice and its changes. In Odishaw,H. (Ed.) Research in Geophysics 2 425-460. In Chorley,R.J. (Ed.) (1969): Water, Earth and Man Pub. Methuen.

Srinivasan,M.S.; Kennett,J.P. (1983): The Oligocene-Miocene boundary in the South Pacific. Geological Society of America Bulletin 94 798-812.

Stanton,B.R. (1973): Circulation along the eastern boundary of the Tasman Sea . In Fraser,R.(Ed.) Oceanography of the South Pacific 1972. New Zealand National Commission for UNESCO, Wellington, 141-147.

Stanton,B.R. (1979): The Tasman Front. New Zealand Journal of Marine and Freshwater Research 13 (2) 201-214.

Stein,R.; Sarnthein,M. (1984): Late Neogene events of atmospheric and ocean circulation offshore Northwest Africa: High resolution record from deep-sea sediments. In van Zinderen,E.M. (Ed.) Palaeoecology of Africa 16 9-36.

Streeter,S.S.; Shackleton,N.J. (1979): Paleocirculation of the deep North Atlantic: 150 000-year record of benthic foraminifera and oxygen-18. Science 203 168-203.

Stuiver,M.; Quay,P.D.; Ostlund,H.G. (1983): Abyssal water carbon-14 distribution and the age of the world's oceans. Science 219 849-851.

Suggate,R.P. (1985): Where have all the glaciations gone? In Pillans (1985).

Tchernia,P. (1980): Descriptive Regional Oceanography Pergammon Marine Series Vol. 3.

Thierstein,H.R.; Geitzenauer,K.R.; Molfino,B.; Shackleton,N.J. (1977): Global synchroneity of Late Quaternary coccolith datum levels: validation by oxygen isotopes. Geology 5 400-404.

UNESCO (1978): World Water Balance and Water Resources of the Earth UNESCO Press, Paris.

Urey,H.C. (1947): The thermodynamic properties of isotopic substances. Journal of the Chemical Society 562-581.

Valencia,M.J. (1977): Pacific Pleistocene paleoclimatic stratigraphy: A comparitive analysis of results. Quaternary Research 8 339-354.

Van Arx,W.S. (1962): An Introduction to Physical Oceanography Pub. Addison-Wesley.

Van Donk,J. (1970): Thesis, Columbia. In Hecht (1985), Shackleton et al. (1973) and others.

Vergnaud Grazzini,C. (1976): Non-equilibrium isotopic compositions of shells of planktonic foraminifera in the Mediterranean Sea. Palaeogeology Palaeoclimatology Palaeoecology 20 263-276.

Volat,J.-L.; Pastouret,L.; Vergnaud-Grazzini,C. (1980): Dissolution and carbonate fluctuations in Pleistocene deep-sea cores: A review. Marine Geology 34 1-28.

Wachter,E.A.; Hayes,J.M. (1985): Exchange of oxygen isotopes in carbon dioxide - phosphoric acid systems. Chemical Geology (Isotope Geoscience Section) 52 365-374.

Walters,L.J.; Claypool,G.E.; Choquette,P.W. (1972): Geochimica et Cosmochimica Acta 36 129-140.

Warme,J.E.; Douglas,R.G.; Winter,E.L. (Eds) (1981): The Deep Sea Drilling Project: A Decade of Progress. SEPM Publication.

Webb(III),T. (1982): Temporal resolution in Holocene pollen data. Proceedings of the 3^{d} North American Paleontol. Conv. 2 569-572. In Hecht (1985).

Willet,R.W. (1950): The New Zealand Pleistocene snowline, climatic conditions, and suggested biological effects. New Zealand Journal of Science and Technology 32B 18-48. In Blumenstock (1966).

Williams,D.F.; Thunell,R.C.; Tappa,E.; Rio,D.; Raffi,I. (1988): Chronology of the Pleistocene oxygen isotope record: 0-1.88m.y.B.P. Palaeogeology Palaeoclimatology Palaeoecology 64 221-240.

Wright, H.E.(Jr) (1984): Sensitivity and response times of natural systems to climatic change in the Late Quaternary. Quaternary Science Reviews 3 91-131.

Corrections and Additions to D.Phil. Thesis
Following Comment by the Examiners

Chapter One

p6 Diatoms: These are widespread, although not found in great abundance, and may be found throughout the Southern Indian, Atlantic and Pacific Oceans, as well as in the Southern Ocean (Lisitzin, 1972). In addition they have been found useful as palaeoceanographic tools (e.g. Burckle, 1983).

p9 4) By-product gases interfere with, rather than block, the detection of CO_2.

p16 Line 1 should refer to a sea depth, not level, of 3.8km.

p20 The numbering of the more recent stages by Williams et al. (1988) has been shown to be incorrect (Ruddiman, in prep.).

p22 It was not meant to imply that Milankovitch knew anything of the possible applications of his orbital theory to $\delta^{18}O$ results as he preceded them by nearly twenty years.

p28 Line 16/17 .....which modified the abyssal circulation through the Vema Channel into the Pacific.

Chapter Two

Figure 2.2. This represents only an idealised view of the structure of the oceans in the vicinity of New Zealand, but is useful for envisaging the relative positions of the water masses. An additional Figure (2.2a) extends this picture up to the Lord Howe Rise. Precise palaeoceanographic information was derived from charts.

It must be noted that Heath (1985) has stated that NADW is sufficiently modified to take on a new title of Pacific Deep Water (referred to as Deep Water in this thesis).

p47 Further additional references whose work provides useful background to the region of study, are those of:

Warren, B.A.(1973): Transpacific hydrographic sections at Lats. 43°S and 28°S. The SCORPIO Expedition II. Deep Sea Research 20 9-38.

Garner (1962): NZOI Memoir #9.

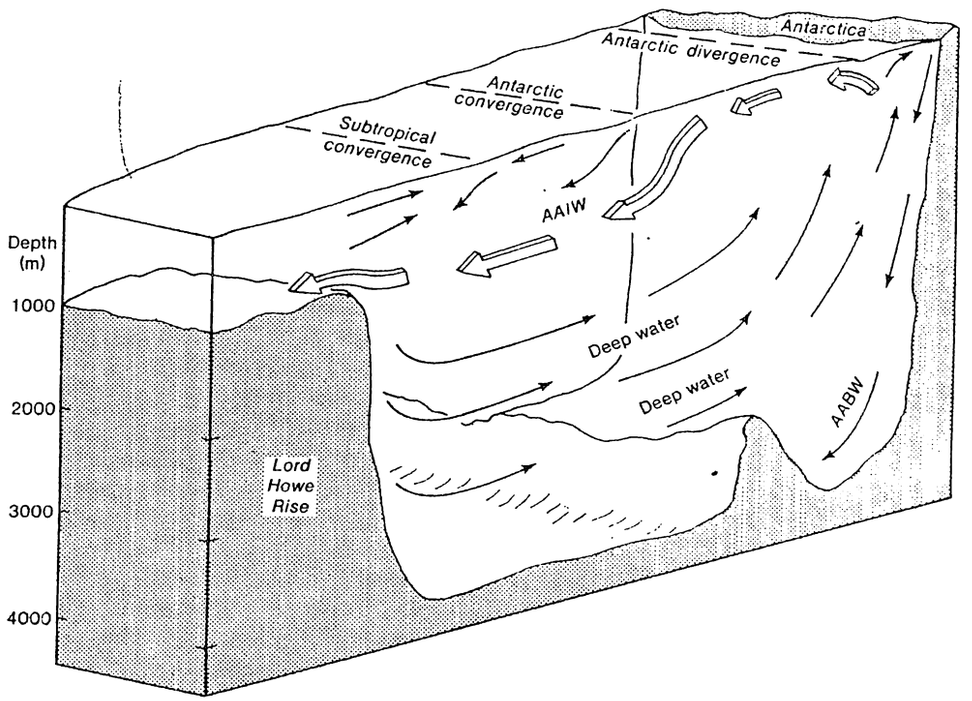

Figure 22a The generalized circulation of subsurface water masses in the southwest Pacific, showing the relationship between Antarctic Intermediate Water (AAIW) and the topographic expression of Lord Howe Rise (modified after Knox, 1970). FROM KENNETT ET AL. (1986) p1157 VOL II

p51 The original source of Figure 2.5 is: Stommel,H. (1958): The abyssal circulation (letter). Deep Sea Research 5 80-82. (figure 2), and is relevant to both deep water and bottom water circulation.

p53 Information from #4 and #5 was drawn from Heath (1985).

p67 The dates in Table 2.1 should be ignored. The ages of the New Zealand sub-stages relevant to this study are shown in the more recent Figure 2.15.

p68 No reference was made in the thesis to the work of Stewart and Neall (1984), who noted high accumulation rates of both quartz and carbonate during the last glacial, declining at 14 700y B.P. as the glacial westerly wind intensity decreased. They suggest accelerated fluvial transport from the mountains (and increased dust transport) before the decline of the polar westerlies from 14700 to 16200y B.P.

Their work centred on Core P69 off the east coast of North Island, slightly to the southwest of Q858 (in this study).

Increased wind erosion from arid regions during cold periods was proposed. Increased glacial upwelling (caused by the strong winds) was also suggested to result in increased glacial productivity (relative to interglacials).

p72 No outline of the sedimentaary environment has been made, and it was felt that this would have been helpful. The reader is referred to the NZOI Chart (1982) of the Bounty Trough (1;1,000,000), and to the rough figure included in these notes provided by Dr Lionel Carter (precise reference unknown). Dr Carter has pointed out that the positioning of 594 on a terrigenous-covered bathymetric bulge north of the Mernoo Saddle would suggest increased deposition at this site (compared to other Bounty Trough sites) as sediment moved through the Saddle.

Chapter Three

p80 Figure 3.1 Contour line marks 1000m.

Chapter Four

p127 Due to the presence of a gap of 1m in Core 594, it was necessary to request samples from the adjacent Hole 594B. A correlation between the two cores thus had to be made, in order to select the appropriate depth range in 594B which corresponded to the gap in 594. An initial rough correlation was done by Assoc. Prof.

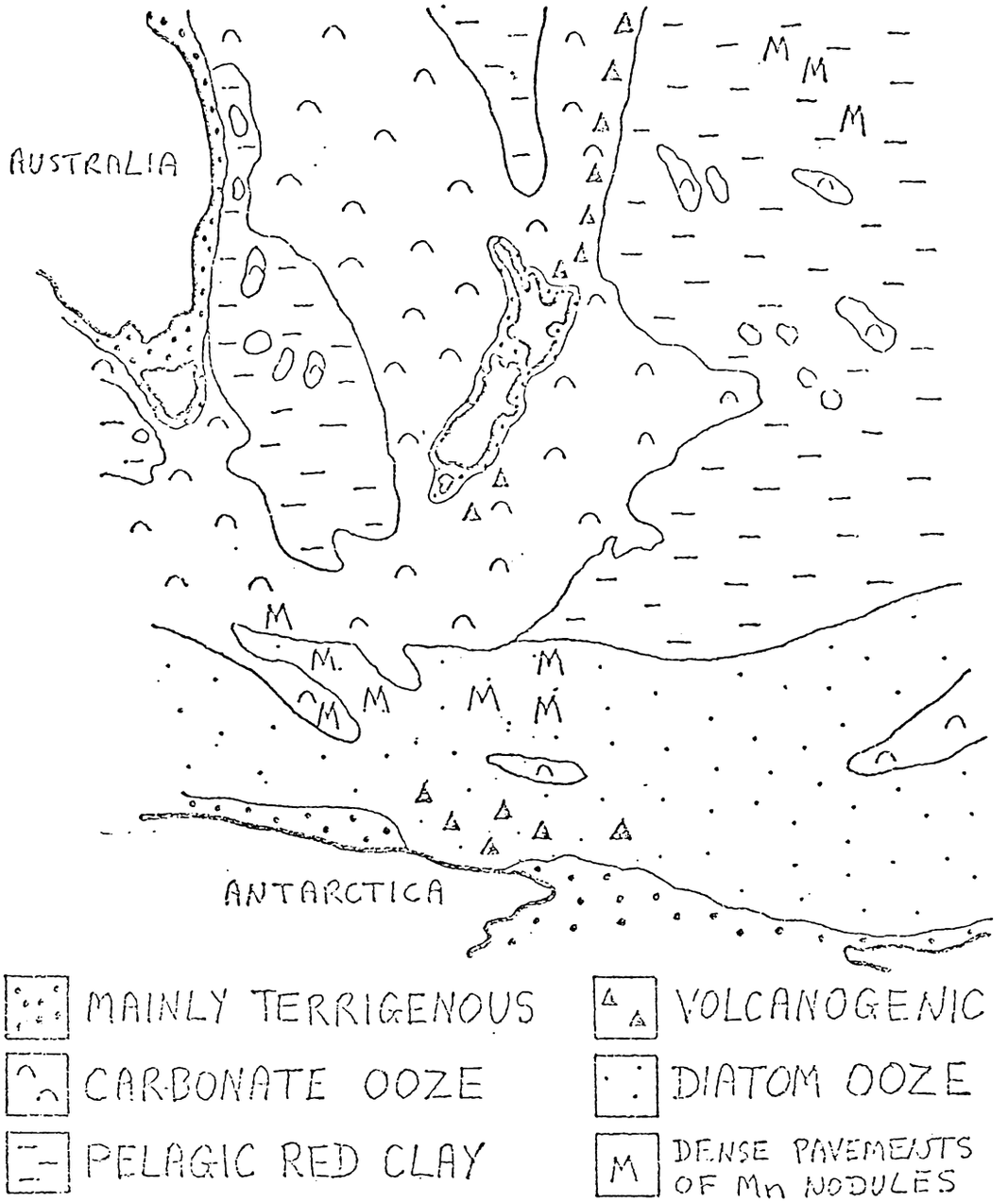

Figure 15 - Generalised distribution of surficial sediments in the ocean basins of the southwest Pacific (after Lisitzin, 1968).

C.S. Nelson, on the basis of similarity of colour stratigraphy (from the set of core photographs provided by the DSDP). Enough samples were requested to allow an overlap of the 594/594B samples, in order to permit further refinement of the alignment of the 594 and 594B samples.

The final positioning of the 594B samples relative to 594 was facilitated by the good overlap of the carbonate record. The figures produced by Cooke (1988) of the carbonate records off 594 and 594B are here presented. The Cooke figure 2.2 shows the 594 and 594B carbonate records which were combined to produce the Cooke composite figure 2.3. 594B samples have thus been used over the section 14.52-15..53m sub-bottom depth in the record from Site 594.

p115 During the course of analysis of Core 593 problems (probably instrumental) occurred with the analysis of planktonic foraminifera from the section of core from 6 to 15m sub-bottom depth. The first results obtained from this section were at variance with other cores of comparable age and location (extremely light $\delta^{18}O$), and consequently it was reanalysed twice. As the results of these last two analyses were in good agreement they were then averaged to give the value for planktonic $\delta^{18}O$ and $\delta^{13}C$ in Table 4.7 over the section of core in question.

p133 Some of the discussion in Chapter Five involves the mean values of the isotope ratios over the defined isotope stages (determined in Section 5.1.1). These mean values were determined by eye from the plots of the data presented in the tables of Chapter Four. Lines have been drawn on the duplicate plots in the back of the thesis to indicate the way in which the mean was determined. These lines give the value and the depth range of the means.

p160 Z2108 It must be noted that these stage boundaries are not consistent with those presented by Eade and van der Linden (1970) who examined the coiling ratios and species distributions of organisms from Z2108, and proposed the following scheme for the core:

Sub-bottom Depth(m)	0-0.15	0.15-2	2-2.6	2.6-4.1	4.1-4..21
Relative T	As modern	cooler	warmer	cooler	major warm
Sed. rate (cm/ky)	1.4	2.9		4.3	1.2

They noted increased deposition during glacial times. These boundaries between warm and cool periods are not entirely

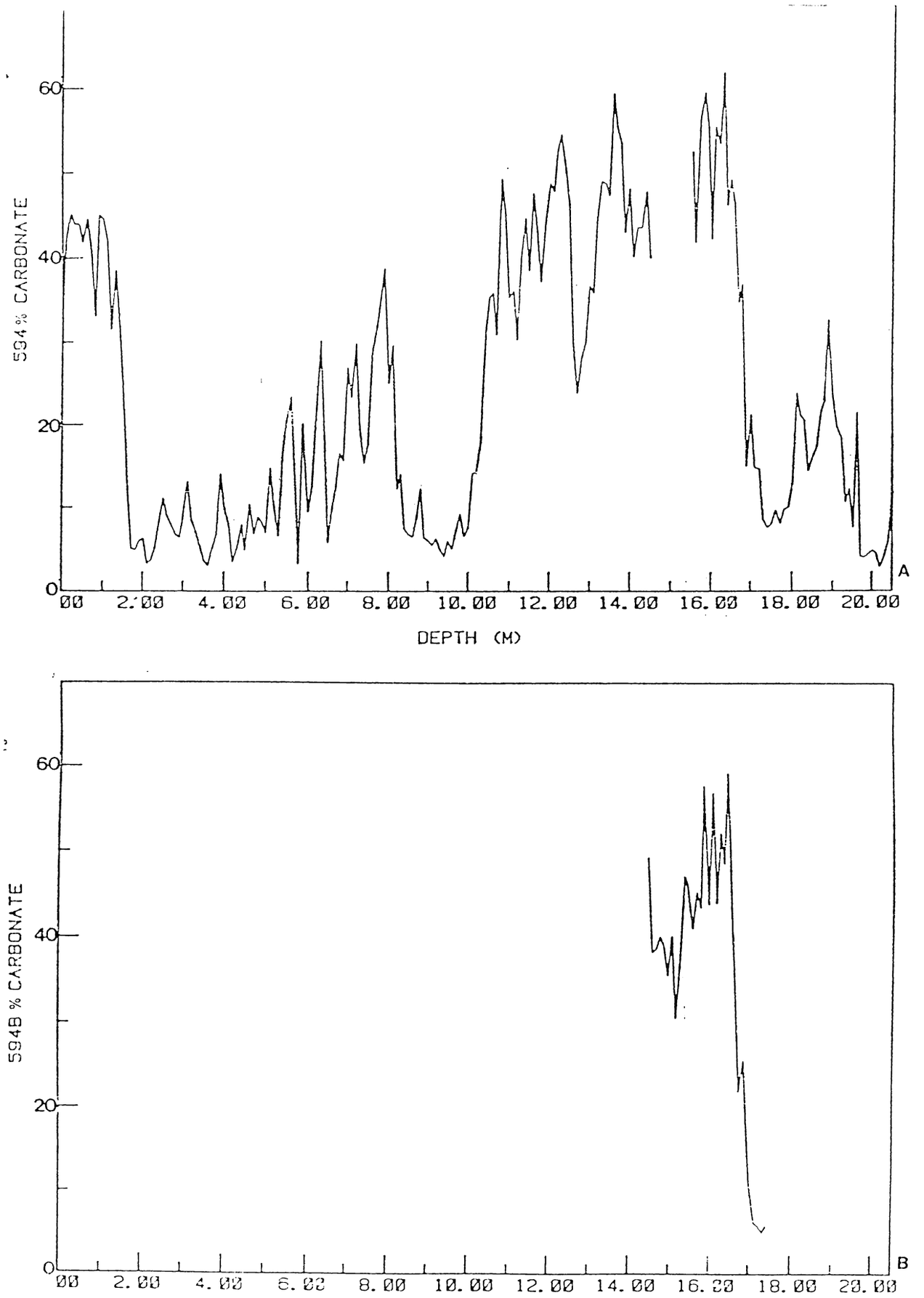

Figure 2.2 The carbonate curve generated using the Hole 594 data (A) and the carbonate curve generated using the Hole 594B data (B)

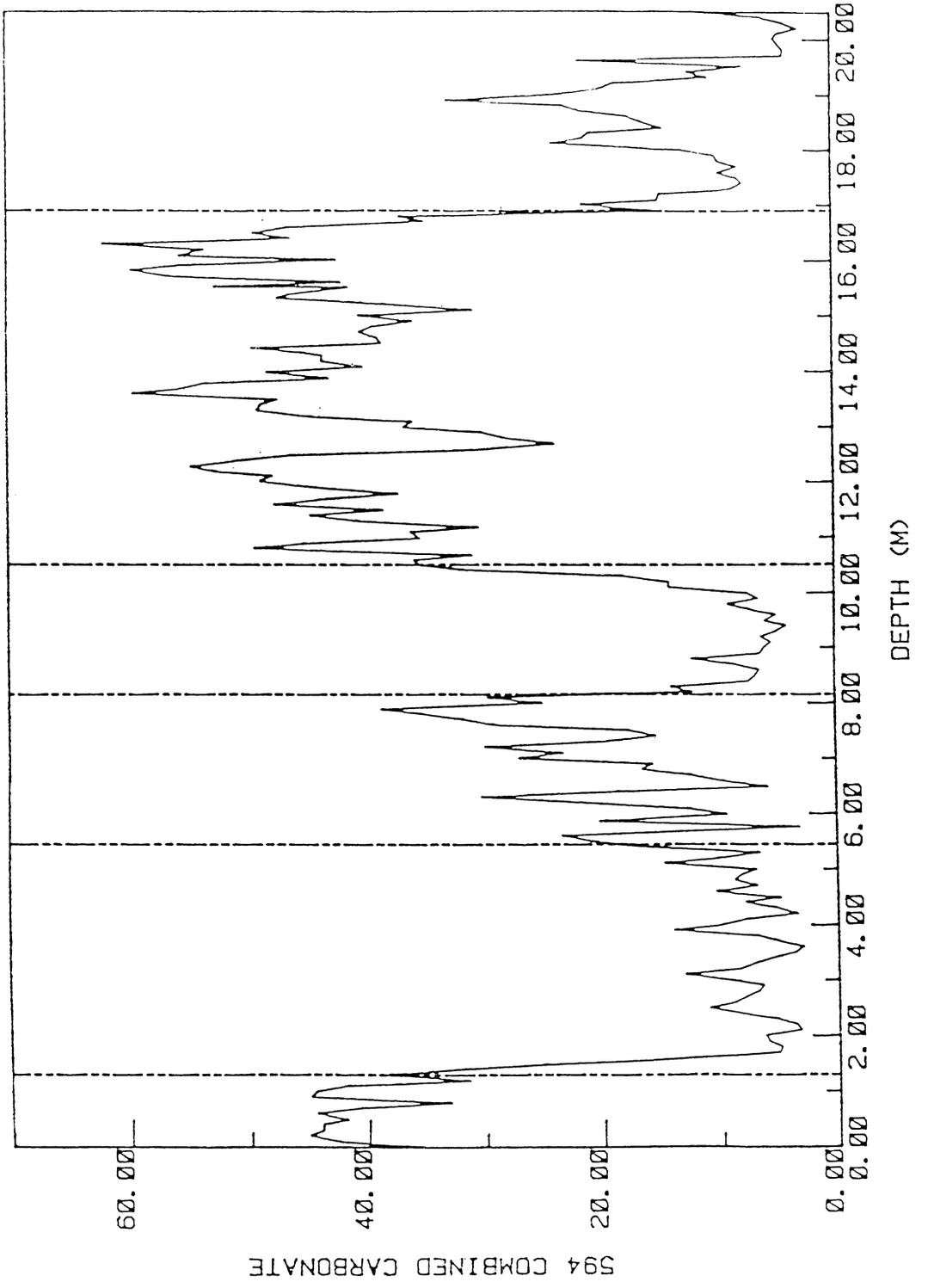

Figure 2.3 The composite carbonate curve for DSDP Site 594. Holes 594 and 594B.

consistent with the isotopic evidence, as the extremely light oxygen ratios of the planktonics, already evident above the 2m level would be in a cool period according to the above scheme. The 2.6m transition from cool to warm is consistent in both records, but isotope evidence suggests that it was the transition from a major warm period.

p165 Para.3 As the sediments to the west of New Zealand on the Lord Howe Rise have accumulated in a region separated from any terrestrial sources; it is not surprising that there is little glacial/interglacial variation in sedimentation rates. (Although Eade and van der Linden do propose a systematic increase in glacial, compared to interglacial, sed. rates. This is not the case if the stage boundaries for Z2108 are isotopically determined).

p196 A confusion of terminology arose at this point. The Tasman Sea sites should correctly be described as being located on the Lord Howe Rise (and not in the Tasman Basin).

p204 Line 13 .....global icesheet fluctuations.

p215 Table 5.23 footnotes 1 and 2 should refer to Bradford and not Bradley. In addition East and West are reversed.

p221 Line 9/10 .....increased upwelling in the eastern equatorial Pacific depressing the lysocline.

p222 Line 20 It is likewise not in agreement with Stewart and Neall (1984). Site P69 revealed higher glacial productivity (compared to interglacial) possibly related to the increased nutrient upwelling caused by the strong glacial winds. It is acknowledged that the Site 594 maximum productivity proposed for interglacial periods in this thesis is at odds with other literature. However, if Cooke (1988) is correct in her assertion of no evident dissolution at this Site, then no other suggestion may be put forward.

<u>The migration of the Subtropical Convergence</u>

A northwards migration of the Subtropical Convergence was suggested consistent with the lowering of surface temperatures in the vicinity of the Convergence. It has been pointed out that the lowering of temperatures could also be adequately explained by a compression of the isotherms against the Chatham Rise. This has

been noted for the Subtropical Convergence elsewhere (Hays,J.D.; Logano, J.A.; Shackleton,N.J.; Irving,G. (1976): Reconstruction of the Atlantic and Western Indian Ocean sectors of the 18000B.P. Antarctic Ocean). Hays et al. (1976) found the Antarctic Polar Front to be 7° further north 18000 B.P. compared to its modern position, but the position of the Subtropical Convergence was essentially unchanged, implying a narrower width of Subantarctic waters and a "bunching" of the isotherms. As the Chatham Rise serves to physically constrain the positioning of the front, this second explanation may be more feasible. A northwards migration is possible, however, in areas like the Mernoo Saddle where there would be less topographical constraint.

Criticism has been made of the assignment of water bodies (Table 5.14) at the core sites, and this is acknowledged as valid. Some suggestion is made in this thesis that changes in AABW would affect the sites. Although this may not directly be the case, changes in the flow of AABW must ultimately affect the overlying Deep Water. Many of the sites lie close to the AAIW/DW boundary, and thus are sensitive to changes in Deep Water flow and circulation.

Additions and Corrections to References

Anderson,T.F.; Steinmetz,J.C. (1983): Stable isotopes in calcareous nannofossils: potential applications to deep-sea paleoenvironmental reconstructions during the Quaternary. Utrecht Micropaleontological Bulletin 30 189-204.

Berger,W.H.; Killingley,J.S. (1977): Glacial-Holocene transitions in deep-sea carbonates: Selective dissolution and the stable isotope signal. Science 197 563-566.

Cuthbertson,A.M. (1985): Stable Isotope Studies of Deep Sea Cores. Unpubl. M.Sc. thesis. University of Waikato (N.Z.).

Epstein,S.; Buchsbaum,R.; Lowenstam,H.A.; Urey,H.C. (1953): Revised carbonate-water isotopic temperature scale. Geological Society of America Bulletin 64 1315-1326.

Gardner,J.V.; Hays,J.D. (1976): Responses of sea-surface temperature and circulation to global climatic change during the past 200,000 years in the east Equatorial Atlantic. Geological Society of America Bulletin. Memoir #145.

Hoefs (1973) is out of alphabetical order.

McCartney,M.S. (1977): Subantarctic mode water. In Angel,M. (Ed.) Deep-sea Research 24 (supplement) 103-119.

Nelson, Hendy, Dudley should be 1986a.

Stewart,R.B.; Neall,V.E. (1984): Chronology of palaeoclimatic change at the end of the last glaciation. Nature 311 47-48.

Suggate,R.P.(1978): Geology of New Zealand. Vols.I and II. N.Z. Govt. Printing Office.

Williams,D.F.; Moore,W.S.; Fillon R.H. (1981): Role of glacial Arctic Ocean ice sheets in Pleistocene oxygen isotope and sea level records. Earth and Planetary Science Letters 56 157-166.

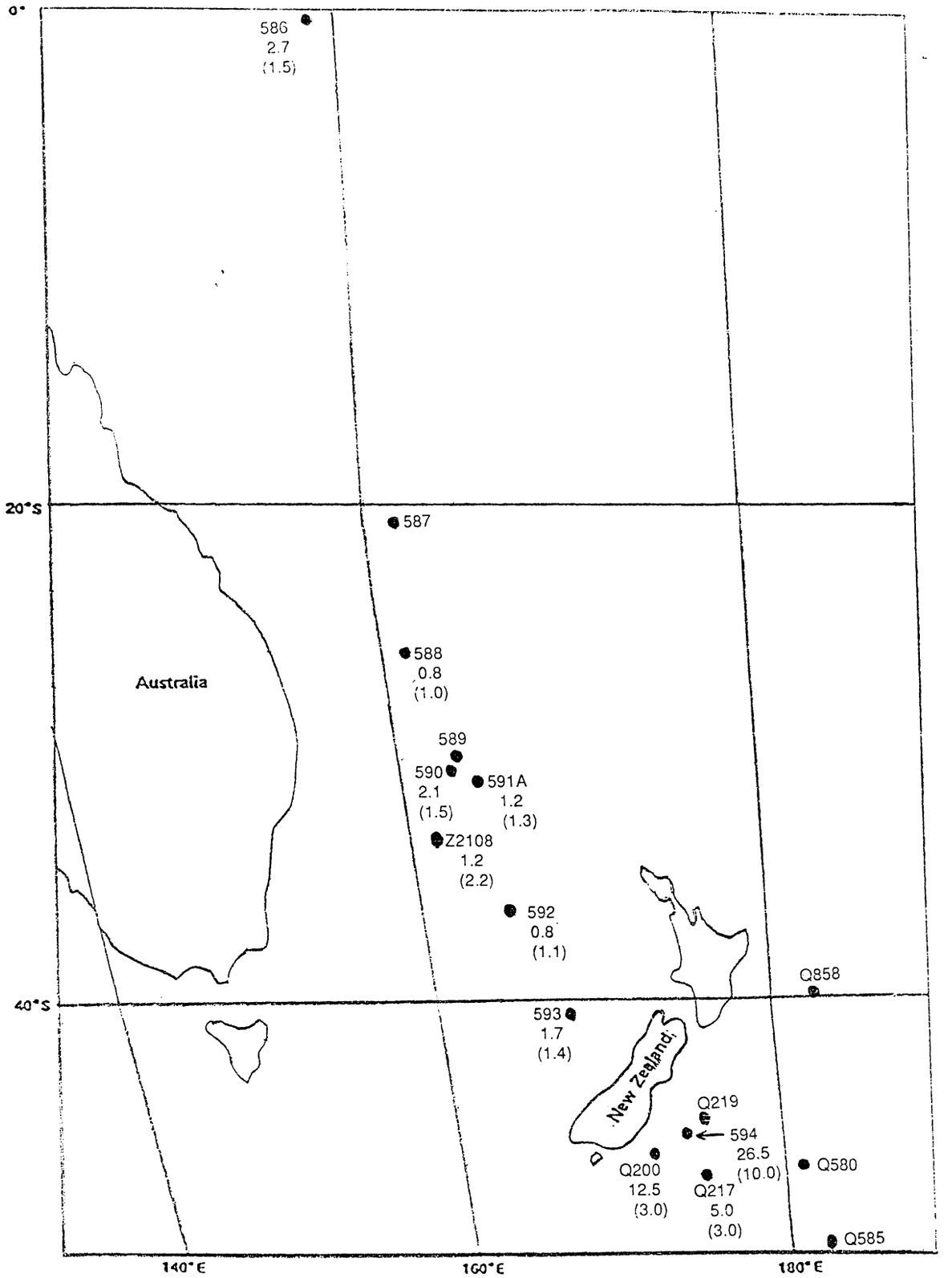

Figure 5.24. Mean glacial and interglacial (in brackets) sedimentation rates for the sites studied (where determinable) in cm/ky.

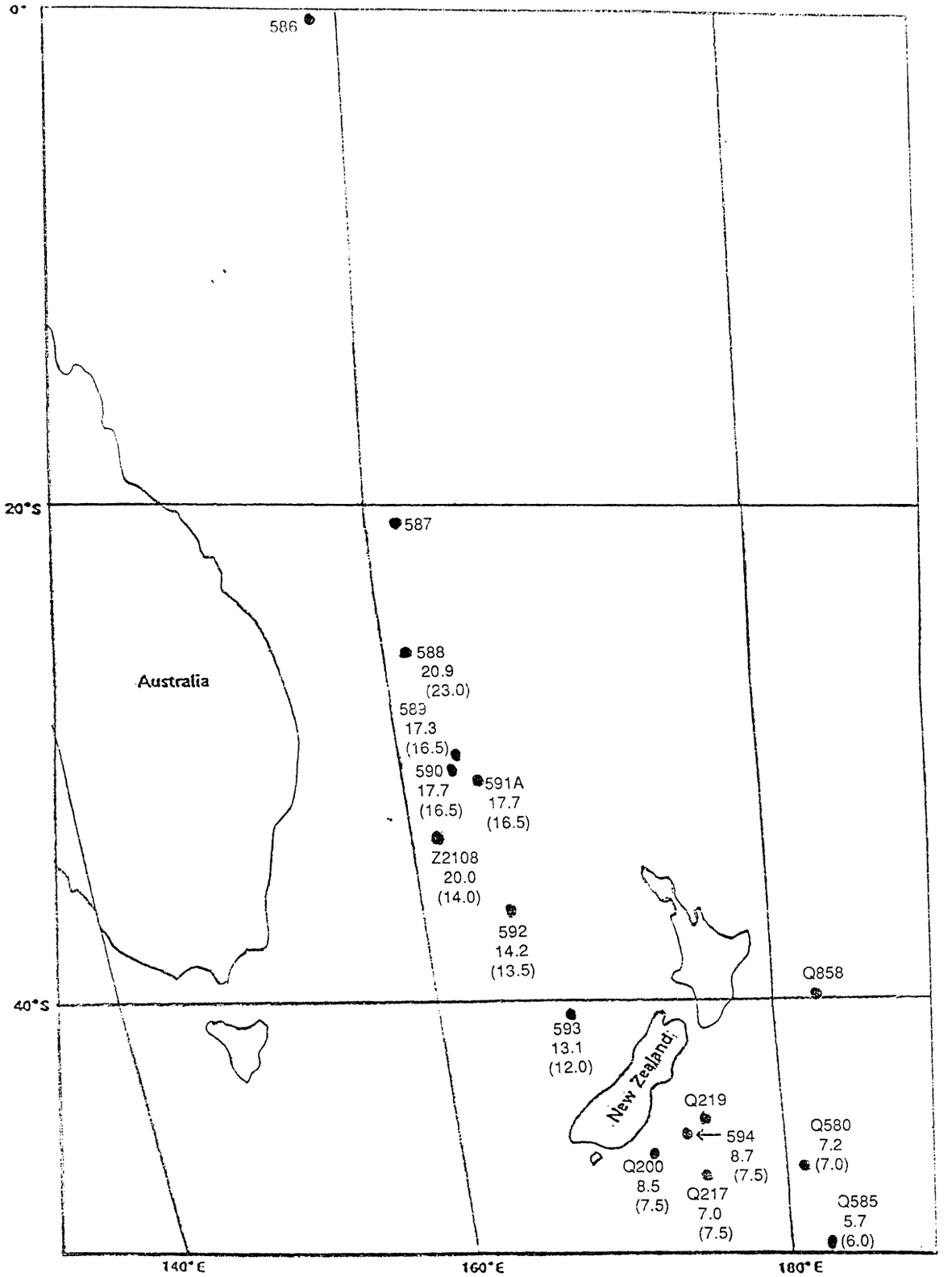

Figure 5.32. Map showing, where possible, isotopically derived Holocene surface water temperatures (deg. C.) at each of the sites studied. Modern measured temperatures are given in brackets.

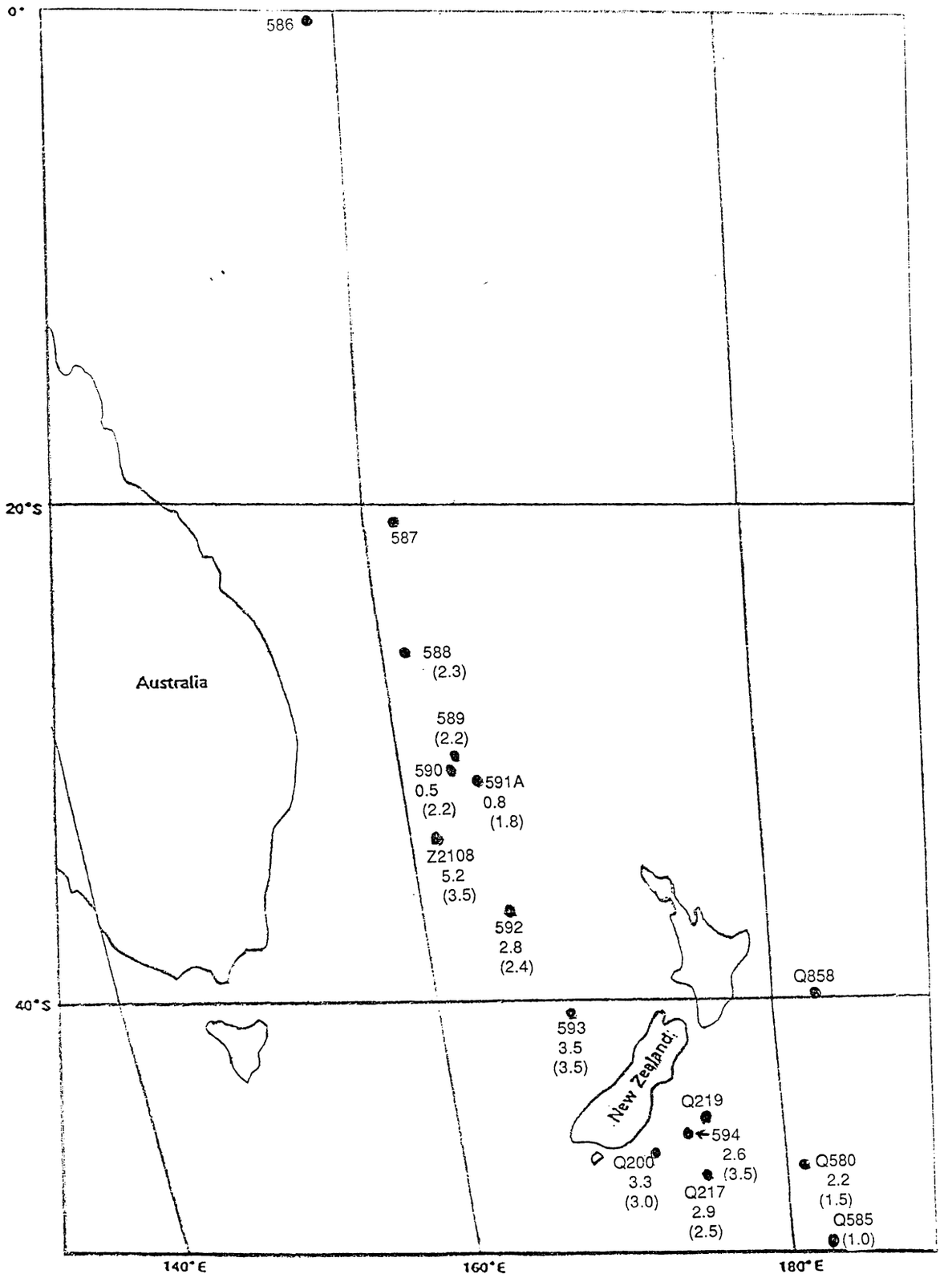

Figure 5.33. Map showing, where possible, isotopically derived Holocene bottom water temperatures (deg. C.) at each of the sites studied. Modern measured temperatures are given in brackets.

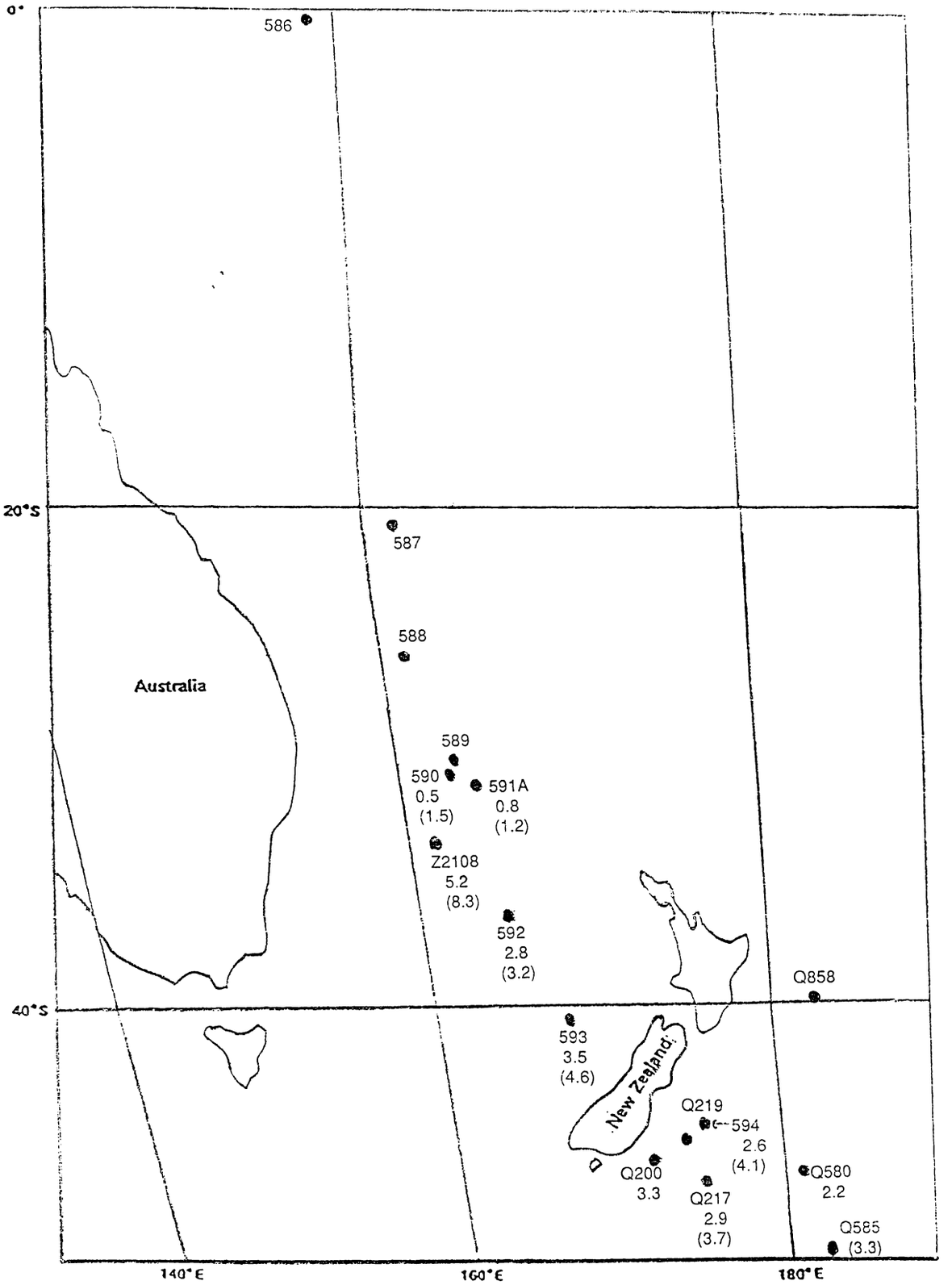

Figure 5.34. Stage 1 and Stage 5 (in brackets) bottom water temperatures derived from the benthic oxygen isotope ratio record.

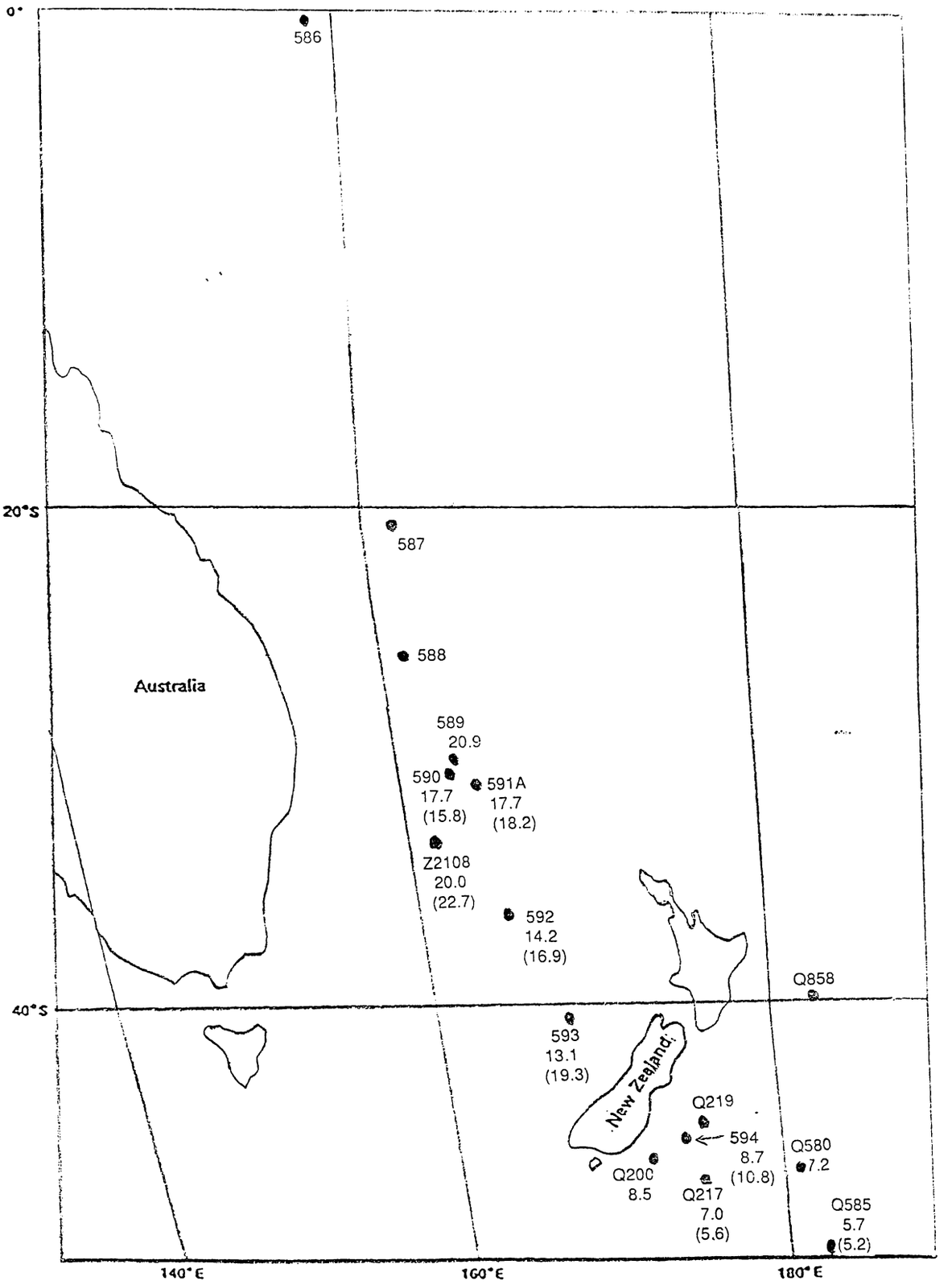

Figure 5.35. Stage 1 and Stage 5 (in brackets) surface water temperatures derived from the planktonic oxygen isotope ratio record.